



Universidade do Minho
Escola de Engenharia

Isabel Sofia Melo Pereira

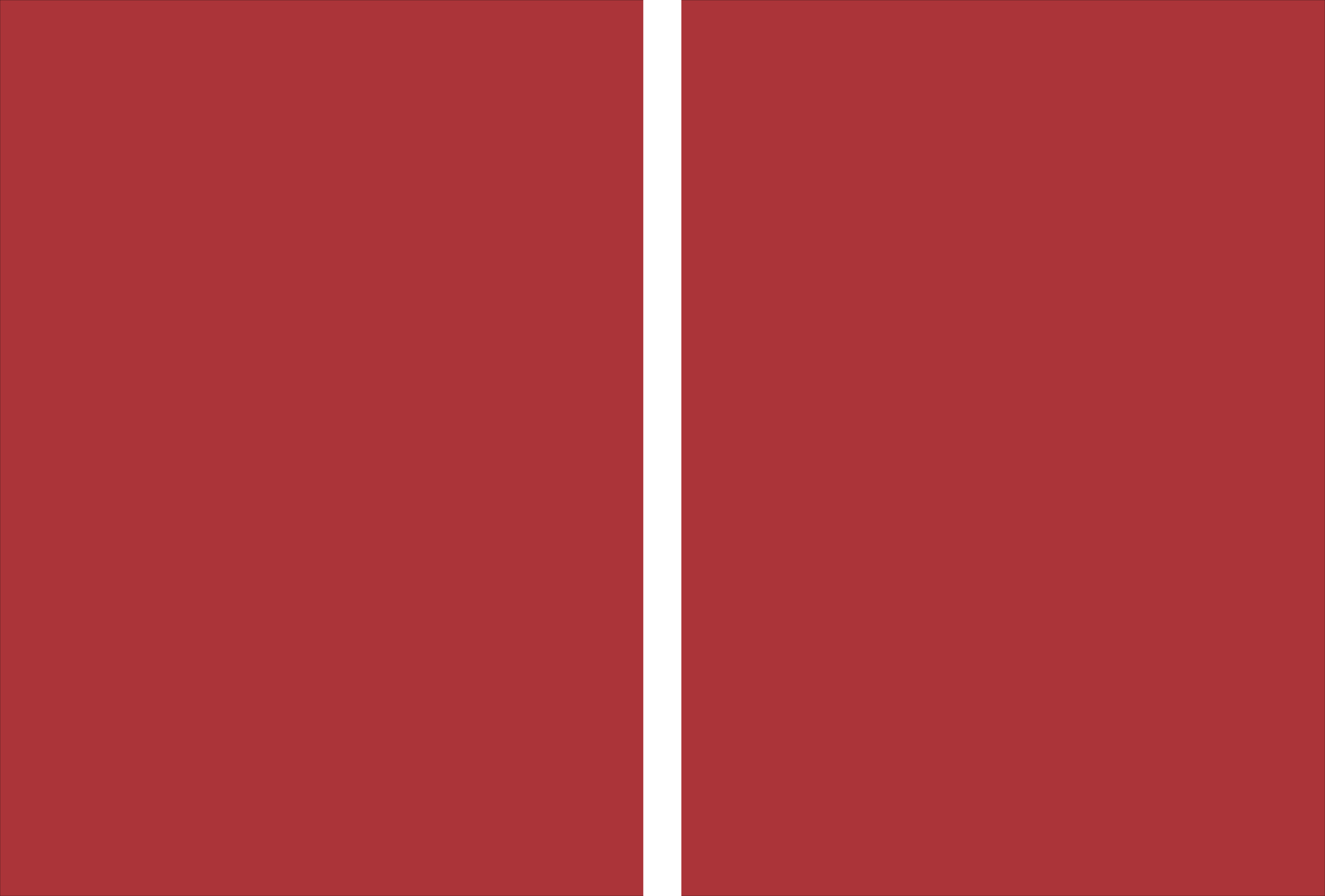
Dextrin injectable hydrogel for tissue healing and regeneration

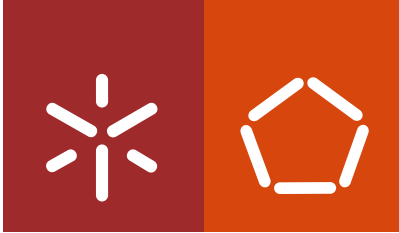
Isabel Sofia Melo Pereira | Dextrin injectable hydrogel for tissue healing and regeneration



UMinho | 2018

dezembro de 2018





Universidade do Minho
Escola de Engenharia

Isabel Sofia Melo Pereira

Dextrin injectable hydrogel for tissue healing and regeneration

Tese de Doutoramento
Doutoramento em Engenharia Biomédica

Trabalho efetuado sob a orientação do
Professor Doutor Francisco Miguel Portela da Gama

dezembro de 2018

DECLARAÇÃO

Nome: Isabel Sofia Melo Pereira

Endereço eletrónico: isabelsofia@ceb.uminho.pt

Cartão do Cidadão: 13612597

Título da tese: Dextrin injectable hydrogel for tissue healing and regeneration

Orientador: Professor Doutor Francisco Miguel Portela da Gama

Ano de conclusão: 2018

Designação do Doutoramento: Programa Doutoral em Engenharia Biomédica

É AUTORIZADA A REPRODUÇÃO PARCIAL DESTA TESE APENAS PARA EFEITOS DE INVESTIGAÇÃO,
MEDIANTE DECLARAÇÃO ESCRITA DO INTERESSADO, QUE A TAL SE COMPROMETE.

Universidade do Minho, 13 / 12 / 18

Assinatura: Isabel Sofia Melo Pereira

STATEMENT OF INTEGRITY

I hereby declare having conducted my thesis with integrity. I confirm that I have not used plagiarism or any form of falsification of results in the process of the thesis elaboration.

I further declare that I have fully acknowledged the Code of Ethical Conduct of the University of Minho.

University of Minho, 13 Dezembro de 2018

Full name: Isabel Sofia Melo Pereira

Signature: Isabel Sofia Melo Pereira

AGRADECIMENTOS / ACKNOWLEDGEMENTS

*“Where shall I begin, please your Majesty?” he asked. “Begin at the beginning” the king said, gravely,
“and go on till the end. Then, stop.”*

Alice’s Adventures in Wonderland, Lewis Carroll

Finda esta etapa, não posso deixar de lembrar todas as pessoas que se cruzaram comigo durante este longo percurso e que de alguma forma contribuíram e ajudaram na sua concretização.

Ao meu orientador, o professor Miguel Gama, pela imensa confiança depositada para a realização deste trabalho, disponibilidade e prontidão.

Aos professores Manuel A. Coimbra e Rosário Domingues do departamento de química da Universidade de Aveiro, por terem aceite colaborar neste trabalho, pela dedicação, pelas reuniões e pelas críticas construtivas. Agradeço também à Joana Simões, que me acompanhou durante todo o trabalho experimental. E, claro, um agradecimento especial à Cristina Ramos e à Fernanda Gandra pela companhia, partilha e boa disposição.

Ao professor João Paulo Rodrigues, por me ter aceite na unidade do ar e saúde ocupacional do Instituto Nacional de Saúde Dr. Ricardo Jorge (Porto). À Sónia agradeço a sua entrega, dedicação, incentivo, paciência, amizade, as longas conversas para discutir estratégias, protocolos, resultados, ... MUITO OBRIGADO! Um agradecimento a todas as meninas, pela simpatia, ajuda e jovialidade, em especial à Susana (a Boss), à Susana (a que não é “a Boss”) e às minhas fiéis companheiras da “Gruta”, Filipa e Raquel, pela companhia, partilha, apoio, e por terem aguentado o meu mau humor!

À equipa do biotério da Faculdade de Medicina da Universidade do Porto, nas pessoas da Dra. Luísa Guardão, da Dra. Joana Oliveira, do Dr. João Requicha e da Liliana. À professora Raquel e à Ilda, pelo enorme suporte técnico que deram na execução do ensaio de toxicidade sistémica.

Ao Departamento de Ciências Veterinárias da Universidade de Trás-os-Montes e Alto Douro (UTAD). Ao professor José Eduardo, pelo trabalho brutal que fez nas cabras, em conjunto com o Luís Maltez, o anestesista (cujo nome não me recordo, mas lembro-me que era alérgico ao feno!), as técnicas D. Leonor e D. Alda e aos assistentes voluntários. Foi um prazer trabalhar convosco! Um agradecimento especial ao professor José Eduardo, pelos conselhos, ajuda e dedicação.

A todos aqueles que passaram pelo LTEB. E foram muitos os que por lá passaram nos últimos anos! Agradeço a companhia, boa-disposição, companheirismo. Um agradecimento especial à Ana Cristina (aka Tina Maria), a única que permaneceu no LTEB nestes anos e grande companheira de PhD. Agradeço a sua amizade, carinho, companheirismo, os momentos bem passados e ajuda/desenrascanço! E, claro, não me poderia esquecer das meninas da “eterna” equipa passaporte (gêmea Catarina, gêmea Alexandra e Manuela)! Obrigado pela ajuda, dedicação, companheirismo e positivismo.

À Sofia da Biotecnómica, a minha comercial preferida! Agradeço a sua ajuda/desenrascanço com a aquisição dos materiais/reagentes, as conversas, os almoços, os bons momentos.

À equipa da IONISOS, na pessoa da Sophie Rouif pelo tratamento das amostras por irradiação.

À professora Justina Oliveira e ao Dr. Fernando Muñoz pelas análises histológicas.

Agradeço à Bioskin, Molecular and Cell Therapies, SA, nas pessoas da professora Ana Colette e professor José Domingos dos Santos pela colaboração ao longo deste trabalho.

E porque os amigos tornam tudo mais fácil não posso deixar de agradecer à Lapãozinho, Li, Maria Bea, Nat, PJ e Tchi pelos bons momentos! Um agradecimento adicional à Andreia, porque quis o destino que trabalhássemos juntas nos nossos PhDs.

Por fim, e não menos importante, agradeço aos meus pais, irmãs, cunhado e aos meus sobrinhos, pela compreensão, paciência e bons momentos de descontração. Agradeço também aos meus tios, que tão bem me acolheram em Aveiro e às suas princesinhas, que alegravam todos os meus finais de dia!

A todos, um grande e sincero OBRIGADO!



The work presented in this thesis was funded by the projects BioTecNorte (NORTE-01-0145-FEDER-000004), DEXGELERATION (project nº 003262), and iBone Therapies (Norte-07-0202-FEDER-038853). The author's PhD Grant (SFRH/BD/ 90066/2012) financed by FCT is also acknowledged.

RESUMO

A incidência de doenças/problemas ósseos tem aumentado mundialmente, principalmente devido ao envelhecimento da população. A falta de tratamentos eficazes tem impulsionado o desenvolvimento de novos substitutos ósseos sintéticos (SBSs). Os SBSs à base de cerâmicos comercialmente disponíveis apresentam limitações ao seu manuseamento. Por forma a contornar essa limitação e melhorar a aceitação clínica dessas formulações, os cerâmicos granulares têm sido associados a hidrogéis. Os hidrogéis, nomeadamente, aqueles que gelificam *in situ*, permitem a obtenção de formulações injetáveis capazes de alcançar áreas do corpo menos acessíveis, utilizando, para tal, procedimentos minimamente invasivos, e de preencherem perfeitamente os defeitos ósseo, que geralmente são irregulares. Além disso, os hidrogéis mimetizam a matriz extracelular e podem atuar como sistemas de entrega de células/fármacos.

O dextrino é um carboidrato de baixo peso molecular obtido a partir do amido. É uma matéria-prima de baixo custo, amplamente disponível e utilizada em variadas aplicações industriais, como adesivos na produção de fitas gomadas, têxteis e papel, e como agente hidratante em cosméticos. Contudo, é ainda pouco explorado na área biomédica. Em trabalho anterior desenvolvido no nosso grupo de investigação, foi desenvolvido um hidrogel de dextrino injetável e capaz de gelificar *in situ* com o intuito de ser uma matriz multifuncional, biocompatível e injetável capaz de transportar e estabilizar outros materiais e/ou células em procedimentos médicos. Para a produção do HG, o dextrino foi primeiramente oxidado com periodato de sódio e posteriormente reticulado com di-hidrazida de ácido adípico (ADH). A fim de demonstrar a biocompatibilidade e segurança do HG, foram neste trabalho realizados um conjunto de testes *in vitro* e *in vivo*, muitos deles em conformidade com as diretrizes internacionais (ISO e OECD). Assim, este trabalho teve como objetivo avaliar a biocompatibilidade e a segurança do HG para uso clínico e a sua aptidão como veículo e estabilizante dos grânulos de Bonelike® (BL), um SBS produzido pela Bioskin, SA, a fim de obter uma formulação com melhores propriedades de manuseamento, nomeadamente moldagem e injetabilidade, bem como bioatividade.

Dado que o HG foi concebido para uso clínico, foi testado e analisado um protocolo de esterilização para o dextrino oxidado (ODEX), usando a irradiação gama. As potenciais mudanças estruturais do material foram analisadas recorrendo a técnicas baseadas em espectrometria de massa. Os resultados mostraram que a irradiação gama não promoveu mudanças na estrutura química da ODEX e que pode ser usada como método de esterilização terminal seguro para o ODEX.

Foram efetuados testes de citotoxicidade *in vitro* em células linfoblásticas humanas, TK6, que revelaram que o HG apresenta uma citotoxicidade dependente da concentração causada pelo ODEX. O potencial genotóxico do HG e dos seus constituintes (ODEX e ADH) foi avaliado em células eucarióticas e procarióticas. Os resultados mostraram que o HG, bem como o ODEX e o ADH, não induziram danos genéticos ou cromossómicos.

A segurança e a biocompatibilidade *in vivo* do HG foram avaliadas pelos testes de toxicidade sistêmica subaguda e de sensibilização cutânea, usando modelos de roedores. Os resultados mostraram que o HG não induziu nenhum efeito sistêmico tóxico, dano genético nas células do sangue ou reações cutâneas, nem prejudicou o processo natural de reparação/regeneração óssea. O HG foi depois combinado, com sucesso, com os grânulos de BL (250-500 μm) para a obtenção um SBS moldável/injetável, que foi implantado em dois tipos de defeitos ósseos: defeitos críticos da calvária (14 mm) e fraturas da tíbia (4 mm), em cabras. Os resultados mostraram que o HG permitiu a estabilização dos grânulos no defeito, garantindo um manuseamento/moldagem fácil da formulação, sem, contudo, afetar as propriedades osteocondutoras do Bonelike[®], nem inibiu o processo de regeneração óssea. Os péptidos resultantes da degradação enzimática da matriz extracelular do intestino, o péptido pró-angiogénico LLKKK18 e as células estaminais do cordão umbilical também foram associadas ao hidrogel e BL com o intuito de melhorar a bioatividade das formulações.

ABSTRACT

The worldwide incidence of bone disorders is increasing, mainly due to ageing population. The lack of effective treatments stimulates the development of novel synthetic bone substitutes (SBSs). Ceramic based-SBSs commercially available display poor handling properties. Attempting to overcome this shortcoming improving the acceptance of these formulations, granular ceramics have been associated with hydrogels. Hydrogels, particularly, *in situ* gelling hydrogels, allow the production of injectable formulations which may be administered using minimally invasive procedures, able of perfect fitting to the irregularities of bone tissue defects. Moreover, hydrogels mimic the native extracellular matrix and can act as cell/drug delivery systems.

Dextrin is a low-molecular-weight carbohydrate obtained from starch. It is a low cost, broadly available raw material widely used in many industrial applications, such as adhesives in the manufacture of gummed tapes, textiles and paper, as moisturiser in cosmetics. However, as yet it is quite unexplored in the biomedical field.

An injectable and *in situ* gelation hydrogel based on dextrin (HG) was developed aiming to act as a multifunctional, biocompatible and injectable matrix able to carry and stabilize other materials and/or cells in medical procedures. To obtain the HG, dextrin was firstly oxidized with sodium periodate and then cross-linked with adipic acid dihydrazide (ADH). In order to demonstrate the biocompatibility and safety and of the newly produced hydrogel, a combination of *in vitro* and *in vivo* tests, many of them in compliance with international standard guidelines (ISO and OECD), were performed. Thus, this work aimed to assess the biocompatibility and safety of the HG for clinical utilization and its ability to act as a carrier and stabilizer for Bonelike® (BL) granules, a SBS produced by Bioskin, SA, in order to obtain a formulation with improved handling properties, such as mouldability and injectability, and bioactivity.

Since the HG is intended for usage as a vehicle for medical application, a sterilization protocol for oxidized dextrin (ODEX) by gamma irradiation was investigated. The potential structural changes of the material were analysed using mass spectrometry-based techniques. The results showed that gamma irradiation did not promote changes on the chemical structure of ODEX and can be used as suitable terminal sterilization method for ODEX.

In vitro cytotoxicity assays performed in human lymphoblastoid TK6 cells revealed that HG display concentration dependent cytotoxicity, which was assigned to ODEX. The genotoxic potential of the HG and its isolated components (ODEX and ADH) were assessed in eukaryotic and prokaryotic cells. The results revealed that HG, as well as ODEX and ADH, did not induce DNA or chromosomal damage.

The *in vivo* biocompatibility and safety of the HG was further assessed by subacute systemic toxicity and skin sensitization tests, using rodent models. The results showed that the HG did not induce any systemic toxic effect, DNA damage in blood cells or skin reactions, neither impaired the natural bone repair/regeneration process. Then, the HG was successfully combined with BL granules (250-500 µm) to

obtain a mouldable/injectable SBS and was implanted in two different bone defects: critical-sized calvarial defect (14 mm) and tibial fractures (4 mm) in goats. The results showed that HG allowed the stabilization of the granules into the defect, ensuring effective handling and moulding properties of the formulation and without affecting Bonelike[®] granules' osteoconductive properties neither impairing the bone repair/regeneration process. Peptides obtained by hydrolysis of extracellular matrix from small intestinal submucosa (SIS), LLKKK18, a pro-angiogenic peptide, and human mesenchymal stem cells (hMSCs) from umbilical cord were also combined with the HG and BL granules to improve the bioactivity of the formulations.

INDEX

AGRADECIMENTOS / ACKNOWLEDGEMENTS.....	v
RESUMO	vii
ABSTRACT	ix
LIST OF FIGURES	xvii
LIST OF TABLES	xxi
LIST OF ABBREVIATIONS AND ACRONYMS.....	xxiii
SCOPE AND AIMS.....	xxvii
SCIENTIFIC OUTPUT.....	xxix
CHAPTER 1 General introduction.....	1
1.1 Bone biology	3
1.1.1 Bone classification, gross anatomy and structure.....	3
1.1.2 Bone tissue	5
1.1.2.1 Bone matrix	5
1.1.2.2 Bone cells.....	5
1.1.3 Bone development	7
1.1.4 Bone remodeling	9
1.1.5 Fracture healing.....	10
1.2 Biomaterials for bone regeneration	10
1.2.1 Synthetic bone substitutes	12
1.2.1.1 Metallic biomaterials.....	12
1.2.1.2 Ceramics	13
1.2.1.3 Polymers.....	14
1.2.1.4 Composites	15
1.2.2 Ceramic-based injectable bone substitutes commercially available	15
1.2.2.1 Calcium phosphate bone cements	16
1.2.2.2 Injectable polymer-ceramic composites	17
1.2.3 Injectable bone substitutes based on hydrogels.....	18
1.2.3.1 <i>In situ</i> gelation hydrogels for injectable bone substitutes	20
1.2.3.2 Injectable bone substitutes based on hydrogels with additional bioactivity.....	21
1.3 Dextrin-based hydrogels for biomedical applications.....	28
1.3.1 Dextrin-based hydrogels for tissue engineering applications	29
1.3.2 Dextrin-based hydrogels for controlled release matrices.....	31
1.3.3 Dextrin-based nanogels for drug delivery	32

1.3.4 Dextrin-based hydrogels for bioadhesive applications	36
1.4 References	36
CHAPTER 2 Effects of gamma irradiation and periodate oxidation on the structure of dextrin assessed by mass spectrometry	45
2.1 Introduction	47
2.2 Experimental	48
2.2.1 Chemicals	48
2.2.2 Dextrin oxidation	49
2.2.3 Determination of bioburden and sterilization dose	49
2.2.4 Gamma irradiation	49
2.2.5 Sterility test	49
2.2.6 Sugars and linkage analyses	50
2.2.7 Size exclusion chromatography analysis	51
2.2.8 Enzymatic hydrolysis and chromatographic separation	51
2.2.9 Matrix-assisted laser desorption/ionization mass spectrometry (MALDI-MS)	51
2.2.10 Electrospray ionization mass spectrometry (ESI-MS) and tandem mass spectrometry (ESI-MS/MS)	52
2.3 Results and discussion	52
2.3.1 Determination of bioburden and sterility verification	52
2.3.2 Structural analysis of dextrin and ODEX	52
2.3.3 Fractionating of oligosaccharides and modified oligosaccharides obtained by partial enzymatic hydrolysis using LEX/SEC chromatography	54
2.3.4 Characterization of oligosaccharides from dextrin and ODEX samples by mass spectrometry	56
2.3.4.1 Neutral fractions from dextrin samples	57
2.3.4.2 Neutral fractions from ODEX samples	57
2.3.4.3 Identification of structural features in oligosaccharides by tandem mass spectrometry	62
2.4 Conclusions	64
2.5 References	65
CHAPTER 3 <i>In vitro</i> genotoxicity assessment of a dextrin-based hydrogel for biomedical applications	69
3.1 Introduction	71
3.2 Experimental	72

3.2.1 Chemicals.....	72
3.2.2 Material preparation	73
3.2.2.1 Dextrin oxidation	73
3.2.2.2 Preparation of the dextrin-based hydrogel.....	73
3.2.3 Cell culture.....	73
3.2.4 Cell exposure conditions.....	73
3.2.5 Assessment of the cellular viability	74
3.2.6 Assessment of the DNA damage	74
3.2.7 Assessment of the chromosomal damage	75
3.2.8 Assessment of mutagenicity.....	76
3.2.9 Statistical analysis.....	77
3.3 Results	77
3.3.1 Cellular viability	77
3.3.2 DNA damage.....	78
3.3.3 Chromosomal damage.....	79
3.3.4 AMES test for mutagenicity.....	80
3.4 Discussion	80
3.5 Conclusions.....	85
3.6 References.....	85

CHAPTER 4| *In vivo* systemic toxicity assessment of a dextrin-based hydrogel and its effectiveness as a carrier and stabilizer of granular synthetic bone substitutes 89

4.1 Introduction.....	91
4.2 Experimental.....	92
4.2.1 Chemicals.....	92
4.2.2 Material preparation	92
4.2.2.1 Dextrin oxidation	92
4.2.2.2 Preparation of dextrin-based hydrogel	93
4.2.2.3 Preparation of Bonelike® granules	93
4.2.2.4 Association of Bonelike® granules to dextrin-based hydrogel.....	93
4.2.3 Animals	93
4.2.4 Subacute systemic toxicity test	94
4.2.4.1 Genotoxicity assay.....	94
4.2.4.2 Histological processing	95
4.2.5 Skin sensitization test	95

4.2.6 Application of the Bonelike® granules combined to dextrin-based hydrogel in bone defects	96
4.2.6.1 Micro-computed tomography analysis	96
4.2.7 Statistical analysis	97
4.3 Results and discussion	98
4.3.1 Subacute systemic toxicity assessment	98
4.3.2 Genotoxicity assessment	102
4.3.3 Assessment of implanted site	103
4.3.4 Skin sensitization assessment	104
4.3.5 Association of Bonelike® granules to dextrin-based hydrogel	104
4.3.6 Assessment of the effectiveness of the dextrin-based hydrogel to mould and stabilize Bonelike® granules in bone defects	106
4.4 Conclusions	107
4.5 References	108

CHAPTER 5| The effect of the dextrin-based hydrogel associated with granular synthetic bone substitute and other bioactive agents in the regeneration of critical-sized defects, using a goat model

.....	113
5.1 Introduction	115
5.2 Experimental	117
5.2.1 Chemicals	117
5.2.2 Dextrin oxidation	117
5.2.3 Preparation of dextrin-based hydrogel	117
5.2.4 Preparation of Bonelike® granules	117
5.2.5 Enzymatic hydrolysis of small intestinal submucosa matrix	118
5.2.6 Human mesenchymal stem cells culture and characterization	118
5.2.7 Preparation of dextrin-based formulations	119
5.2.8 Surgical procedure	119
5.2.9 Micro-computed tomography analysis	120
5.2.10 Histological processing	121
5.2.11 Statistical analysis	121
5.3 Results	121
5.3.1 Mesenchymal stem cells characterization	121
5.3.2 Surgical and post-surgical observations	121
5.3.3 Performance of the dextrin-based hydrogel in bone regeneration of calvarial critical-sized defects	122

5.3.3.1 Micro-computed tomography analysis	122
5.3.2.2 Histological analysis.....	124
5.3.4 The effect of SIS, LLKKK18 and hMSCs on the performance of the hydrogel-based formulations in the regeneration of the calvarial critical-sized defects	125
5.3.4.1 Micro-computed tomography analysis	125
5.3.4.2 Histological analysis.....	126
5.4 Discussion	126
5.5 Conclusions.....	129
5.6 References	129
CHAPTER 6 Final remarks.....	133
6.1 General conclusions.....	135
6.2 Suggestions for future work	136

LIST OF FIGURES

CHAPTER 1|

- Figure 1.1:** Schematic representation of the main features of the bone tissue: **(A)** adult long bone with epiphyseal line, **(B1)** cancellous bone architecture, **(B2)** Transverse section of a trabecula from cancellous bone and **(C)** compact bone architecture (image adapted from ^{5,6}). 4
- Figure 1.2:** Endochondral ossification process: **(A)** mesenchymal cells differentiate, **(B)** the cartilage model of the future bone and the perichondrium form, **(C)** capillaries penetrate cartilage and the perichondrium transforms into periosteum; Periosteal collar and primary ossification center develop, **(D)** the cartilage and chondrocytes continue to grow at ends of the bone, **(E)** secondary ossification centers develop and (F) the cartilage remains at epiphyseal (growth) plate and at joint surface as articular cartilage (image adapted from ⁶). 8
- Figure 1.3:** Schematic representation of the different phases of the remodeling process (image adapted from ¹⁰). 9
- Figure 1.4:** Schematic representation of the fracture healing process in a long bone: **(A)** hematoma formation following a fracture, **(B)** the internal callus replaces the hematoma, while the external callus provides support, **(C)** woven, cancellous bone replaces the cartilage of the callus and **(E)** remodeling of the bone replaces the woven bone (image adapted from ⁵). 11
- Figure 1.5:** Chemical structure of dextrin (image adapted from ¹³⁵). 30

CHAPTER 2|

- Figure 2.1:** LEX/SEC chromatograms of the oligosaccharides obtained after partial enzymatic hydrolysis with α -amylase of the dextrin non-irradiated (A), irradiated at 10 kGy (B) and at 20 kGy (C), and of the ODEX non-irradiated (D) and irradiated at 20 kGy (E). 55
- Figure 2.2:** MALDI-MS spectra of the fraction that eluted at retention time of 14 minutes (F14) of dextrin non-irradiated (A), ODEX non-irradiated (B), and irradiated at 20 kGy (C). 58
- Figure 2.3:** ESI-MS spectra of the fraction eluted at 19 minutes (F19) of dextrin non-irradiated (A), ODEX non-irradiated (B), and irradiated at 20 kGy (C). 59
- Figure 2.4:** Periodate oxidation mechanism for different residues of dextrin, based on MS analysis. 61
- Figure 2.5:** ESI-MS/MS spectra and schematic fragmentation pathways of $[M+Na]^+$ ions identified after periodate oxidation of the dextrin: (A) $[Glc2-C2H4O2+Na]^+$; (B) $[Glc2-C2H4O2-2H+Na]^+$; (C) $[Glc2-C2H4O2-4H+Na]^+$ and (D) $[Glc3-C2H4O2-2H+Na]^+$ 63

CHAPTER 3 |

Figure 3.1: Chemical structures of oxidized dextrin (ODEX), adipic acid dihydrazide (ADH) and corresponding hydrogel (HG) formed after reticulation reaction between ODEX and ADH. 72

Figure 3.2: Effect of the different concentrations of the dilute hydrogel (HG_{dil}) and its isolated components – oxidized dextrin (ODEX) and adipic acid dihydrazide (ADH) – on TK6 cell viability as assessed by the MTT reduction assay. Cells were exposed to different concentrations (C1-C6) of the test agents for 24 h. Results were calculated as percentage of negative control (NC) and data are presented as mean ± SD of two independent experiments (n = 3 replicates per group). Data were analyzed by one-way ANOVA analysis followed by Dunnett’s post hoc test: * $p < 0.05$, ** $p < 0.01$ and *** $p < 0.001$ versus HG_{dil}. 78

Figure 3.3: Representative images (400x magnification) of the comet assay in TK6 cells after 24 h of exposure to negative control (NC) and to the highest concentration (C3) of the dilute hydrogel (HG_{dil}), oxidized dextrin (ODEX) and adipic acid dihydrazide (ADH) used. Methyl methanesulfonate (MMS, 40 µg/mL, 1 h) was used as positive control. 78

Figure 3.4: CBMN assay in TK6 cells exposed to different concentrations of the dilute hydrogel (HG_{dil}) and its isolated components – oxidized dextrin (ODEX) and adipic acid dihydrazide (ADH) – for 24 h. Mitomycin C (MMC, 0.04 µg/mL) was used as positive control. Columns: percentage of micronucleus (% MN) in binucleate cells; lines: % cytotoxicity. Results are presented as mean ± SD of two independent experiments (n = 2 replicates per group). Data were analysed by chi-square test: * $p < 0.001$ versus negative control (NC). 80

CHAPTER 4 |

Figure 4.1: Steps for creation of the bone defect in the diaphysis of the right tibia: (A) the holes were performed for inserting screws in the distal segment and placement of the 4 mm spacer, (B) fixation of the plate in the distal segment, (C) adjustment of the plate to the proximal side, (D) temporary fixation with forceps of the proximal segment, (E) the holes were performed in the proximal segment, (F) Bone defect realized and fixed with plate and screws, and (G) Filling of the bone defect with the HG + BL formulation. 97

Figure 4.2: Coefficients of organs in female (A) and male (B) rats treated with hydrogel (test group) and PBS (control group), at 3 weeks after surgery. Results are presented as mean ± SD (n = 5 replicates per group). Data were analysed by two-tailed t-test. No statistical significant difference from the respective control group was found. 100

Figure 4.3: Representative photographs of histopathologic examination, after haematoxylin and eosin staining, of kidneys, liver, lungs, pancreas and spleen of control and test groups of both genders, after 3 weeks after surgery.	101
Figure 4.4: Representative photographs of histologic images, after hematoxylin and eosin staining, from femur defect site of animal from control and test groups of both genders, after 3 weeks after surgery.....	104
Figure 4.5: Preparation of the injectable bone substitute: macroscopic evaluation of dextrin-based hydrogel (HG) with different concentrations of Bonelike® (BL) granules, after completely gelation reaction (A) and the results of the injectability test (B).....	106
Figure 4.6: Representative radiographic and microCT images of tibial fracture from control and test groups: (A) radiographic images of tibia after surgery (0 weeks) from control and test groups and (B) microCT images of tibia after 3 and 6 weeks, showing the whole sample and the hollow cylindrical region of interest within the whole sample.....	107

CHAPTER 5 |

Figure 5.1: Calvarial critical-sized defects performed in the animals filled with the dextrin-based hydrogel formulations without Bonelike® granules (A) or in presence of them (B). In each goat was performed a control defect (non-treated defect) marked with an asterisk.	120
Figure 5.2: Human umbilical cord Mesenchymal stem cells (hMSCs) characterization: (A) hMSCs from umbilical cord at passage 5 in standard culture conditions. (B) Chondrogenic, adipogenic and osteogenic, and differentiation visualized through Alcian Blue, Oil Red O, and Von Kossa and histochemical staining.....	122
Figure 5.3: Representative microCT reconstruction images of calvarial critical-sized defects, after 3, 6 and 12 weeks, for the different dextrin-based hydrogel (HG) formulations without Bonelike® (BL) granules (A) or in presence of them (B).	123
Figure 5.4: Results of microCT analysis for critical-sized calvarial defects, after 3, 6 and 12 weeks: quantification of the new bone volume formed in the defects treated with the dextrin-based hydrogel (HG) alone and loaded with 4 mg/ml of SIS (HG + SIS) or with 1 mg/mL of LLKKK18 (HG + LLKKK18) and the non-treated defect (control) (A); quantification of the total bone volume (new bone and granules volume) (B), the granules volume (C) and the new bone volume (D) in the defects treated with Bonelike (BL) granules alone or incorporated into HG matrix (HG + BL) and its combination with 4 mg/ml of SIS (HG + BL + SIS), 1 mg/mL of LLKKK18 (HG + BL + LLKKK18) or hMSCs (HG + BL + hMSCs). Data are presented as mean ± SD (<i>n</i> = 5 replicates per group) and were analysed by one-way ANOVA	

followed by Bonferroni's post hoc test: * $p < 0.05$, ** $p < 0.01$ and *** $p < 0.001$ vs HG + BL treatment, # $p < 0.05$ and ## $p < 0.01$ vs 3 weeks (intra group)..... 124

Figure 5.5: Haematoxylin and eosin stained histological sections from calvarial critical-sized defects of decalcified samples. BL, Bonelike® granules; NB, new bone; NV, new vessels; OB, osteoblasts; OC, osteoclasts; UM, unmineralized bone..... 125

Figure 5.6: Haematoxylin and eosin stained histological sections from calvarial critical-sized defects of decalcified samples. BL, Bonelike® granules; NB, new bone; NV, new vessels; OB, osteoblasts; OC, osteoclasts; UM, unmineralized bone..... 127

LIST OF TABLES

CHAPTER 1|

Table 1.1: Commercial calcium phosphate (CaP) cements and their clinical application.	16
Table 1.2: Injectable bone substitutes (IBSs) based on granular ceramic – polymer conjugation.	17
Table 1.3: Examples of injectable bone substitutes (IBSs) based on in situ gelation hydrogels.	23
Table 1.4: Glycosidic-linkage analysis of the dextrans (mol%) and estimated average degree of polymerization (DP) and percentage of branching of different commercial dextrans (adapted from ¹²³).	30

CHAPTER 2|

Table 2.1: Glycosidic-linkage analysis of irradiated (10 and 20 kGy) and non-irradiated (mol %) dextrin and oxidized dextrin (ODEX).	53
Table 2.2: Results on SEC analysis of ODEX samples before and after the gamma irradiation.	54
Table 2.3: Neutral oligosaccharide [M+Na] ⁺ ions from ODEX non-irradiated and irradiated at 20 kGy observed in the MALDI-MS (F14 products) and ESI-MS (F19 products) spectra, with the identification of the m/z value and the proposed assignments.	60

CHAPTER 3|

Table 3.1: Concentrations of the dilute dextrin-based hydrogel (HG _{dil}), oxidized dextrin (ODEX) and adipic acid dihydrazide (ADH) used in the cyto- and genotoxicity testing.	74
Table 3.2: Comet assay analysis of DNA damage in TK6 cells exposed to different concentrations of the dilute hydrogel (HG _{dil}) and its isolated components – oxidized dextrin (ODEX) and adipic acid dihydrazide (ADH) – for 24 h.	79
Table 3.3: Mutagenic potential of the different concentrations of the dilute hydrogel (HG _{dil}) assessed by the AMES test using different strains of <i>Salmonella typhimurium</i> and a combination of two <i>Escherichia coli</i> strains (<i>E. coli</i> combo mix), in absence of a metabolic activator (human S9 mix). ...	82
Table 3.4: Mutagenic potential of the different concentrations of the dilute hydrogel (HG _{dil}) assessed by the AMES test using different strains of <i>Salmonella typhimurium</i> and a combination of two <i>Escherichia coli</i> strains (<i>E. coli</i> combo mix), in presence of a metabolic activator (human S9 mix). ..	83

CHAPTER 4 |

Table 4.1: Body weight, in grams, of female and male rats exposed to the hydrogel (test group) and PBS (control group), at the beginning (0 th week) and 1 st and 3 rd weeks after surgery.	98
Table 4.2: Biochemical parameters in female and male rats treated with hydrogel (test group) and PBS (control group), at 3 weeks after surgery.	99
Table 4.3: Haematological parameters in female and male rats treated with hydrogel (test group) and PBS (control group), at 3 weeks after surgery.	100
Table 4.4: Comet assay analysis of DNA damage in whole-blood cells and PBMC of female and male rats exposed to hydrogel (test group) and PBS (control group), 3 weeks after surgery.....	103

LIST OF ABBREVIATIONS AND ACRONYMS**A**

ADH Adipic acid dihydrazide

ANOVA Analysis of variance

B

BCP Biphasic calcium phosphate

BG(s) bioactive glass(es)

BL Bonelike®

BMP(s) Bone morphogenetic protein(s)

C

CaF₂ Calcium fluoride

CaHPO₄ Calcium hydrogenphosphate

CaP Calcium phosphate

CaS Calcium sulfate

CBMN Cytokinesis-block micronucleus

CBPI Cytokinesis-block proliferation index

CFU Colony-forming units

cytoB Cytochalasin B

⁶⁰Co Cobalt-60

D

DBM Demineralized bone matrix

DMSO Dimethylsulfoxide

DNA Deoxyribonucleic acid

E

ECM Extracellular matrix

ESI-MS Electrospray ionization mass spectrometry

ESI-MS/MS
or ESI-MSⁿ Electrospray ionization tandem mass spectrometry

F

FCA Freund's complete adjuvant

FTIR Fourier transform infrared

G

GC Gas chromatography

Glc Glucose

GRAS Generally-recognized-as-safe

H

HA Hyaluronic acid

HAP Hydroxyapatite

HAPC Hydroxyapatite/collagen

HCl Hydrochloric acid

HE Hematoxylin and eosin

HG Dextrin-based hydrogel

HG_{dil} Dilute dextrin-based hydrogel

HPMC Hydroxypropylmethylcellulose

H₂O₂ Hydrogen peroxideH₂SO₄ Sulfuric acid**I**

IBS(s) Injectable bone substitute(s)

IO₄⁻ Periodate ion

ISO International organization for standardization

L

LEX/SEC Ligand-exchange/size exclusion chromatography

LMP Low melting point

M

MALDI-MS Matrix-assisted laser desorption/ionization mass spectrometry

microCT Micro-computed tomography

MMS Methyl methanesulfonate

MN Micronucleus

MS Mass spectrometry

MSC(s) Mesenchymal stem cell(s)

MTT	3-(4,5-dimethylthiazol-2-yl)-2,5-diphenyltetrazolium bromide
<i>M_w</i>	Molecular weight
<i>m/z</i>	Mass-to-charge ratio
N	
NaCl	Sodium chloride
NaIO ₄	Sodium periodate
NaNO ₃	Sodium nitrate
NaOH	Sodium hydroxide
Na ₂ CO ₃	Sodium carbonate
Na ₂ EDTA	Ethylenediaminetetraacetic acid disodium salt
NC	Negative control
NMP	Normal melting point
NMR	Nuclear magnetic resonance
O	
ODEX	Oxidized dextrin
OECD	Organisation for economic co-operation and development
P	
PBMC	Peripheral blood mononuclear cells
PBS	Phosphate buffered saline solution
PC	Positive control
PCL	Poly(ε-caprolactone)
PEG	Poly(ethylene glycol)
P _{FD} -5	Pro-Asp-(Phe-Asp) ₅ -Pro
PGA	Polyglycolic acid
PLA	Poly(lactic acid)
PLGA	Poly(lactic-co-glycolic) acid
PVA	Polyvinyl alcohol
P ₂ O ₅	Di-phosphorus penta-oxide
S	
SAL	Sterility assurance level
SBS(s)	Synthetic bone substitute(s)
SD	Standard deviation
SDS	Sodium dodecyl sulfate

SEC Size exclusion chromatography
Si-HPMC Silated hydroxypropylmethylcellulose

T

TCP Tricalcium phosphate
TG Test guideline
TSA Tryptic soy agar
TSB Tryptic soy broth
TTeC Tyramine–tetronic–grafted chitosan copolymer

U

UV Ultraviolet

3D Three-dimensional

SCOPE AND AIMS

Novel synthetic bone substitutes (SBSs) with improved handling properties and bioactivity are necessary to satisfy unmet clinical needs. Hydrogels may help in this endeavor by providing a three dimensional, hydrated, biocompatible environment, which resembles native extracellular matrix, and can act simultaneously as a carrier and stabilizer of bioactive agents. The combination of hydrogels with granular ceramic-based SBSs may yield injectable/mouldable bone substitutes able to stabilize the granules into the defect and modulate the bone healing process.

Dextrin is a low-molecular-weight and cheap carbohydrate obtained by partial hydrolysis of starch, that is already widely used in the cosmetic, textile and food industries but is quite yet unexplored in the biomedical field, despite presenting a set of advantages over other natural polymers. A dextrin-based hydrogel (HG) was designed to be a multifunctional, biocompatible and injectable matrix able to carry and stabilize other materials and/or cells in surgical procedures. To prepare the HG, dextrin was firstly oxidized with sodium periodate (NaIO_4) and then cross-linked with adipic acid dihydrazide (ADH).

This PhD work aims to assess the biocompatibility and safety of the HG for clinical utilization and its ability to act as a carrier and stabilizer for Bonelike® (BL) granules, a SBS produced by Bioskin, SA. The final goal consists in obtain a final formulation with improved handling properties (mouldability and injectability) and bioactivity. To achieve these goals a battery and a combination of *in vitro* and *in vivo* approaches, many of them in compliance with international standard guidelines (ISO and OECD), were performed and will be described along this thesis.

Chapter 1 presents a revision of the main subjects covered in this work, namely: i) bone biology, ii) biomaterials used in bone regeneration field, iii) the main approaches used to improve the handling properties of ceramic-based SBSs and iv) dextrin-based hydrogels for biomedical applications.

On Chapter 2, the effect of periodate oxidation and gamma irradiation on dextrin chemical structure was assessed by sugar and glycosidic-linkage analysis, SEC analysis, MALDI-MS and ESI-MSⁿ analysis. Particularly, MS based-techniques showed to be an advantageous tool for the identification and characterization of oxidized products and for validation of a sterilization protocol. This work was developed in collaboration with department of chemistry from university of Aveiro.

In chapter 3, a battery of *in vitro* genotoxicity tests employing eukaryotic and prokaryotic models is reported to determine the potential of HG and its isolated components (oxidized dextrin (ODEX) and ADH) to induce DNA or chromosomal damage. Cytotoxicity was also analysed. This work was developed in collaboration with environmental health department from National Institute of Health Dr. Ricardo Jorge (Porto).

Chapter 4 describes the *in vivo* biocompatibility and safety assessment to HG, using rodent models. For that, subacute systemic toxicity, genotoxicity, skin sensitization tests were performed, as well as bone histopathologic analysis. This work was developed in collaboration with Animal House Unit from

Faculty of Medicine of University of Porto and environmental health department from National Institute of Health Dr. Ricardo Jorge. In this chapter, the combination of HG with BL granules to obtain a mouldable/injectable SBS is also reported, as well as its effectiveness in the regeneration of tibial fractures, using a goat model. This work was developed in collaboration with the department of veterinary sciences from university of Trás-os-Montes e Alto Douro.

In chapter 5, the combination of HG with BL granules was tested in critical-sized calvarial defects, using a goat model. The effect on bone regeneration process of the incorporation of i) degraded products obtained by hydrolysis of extracellular matrix from small intestinal submucosa (SIS), ii) LLKKK18, a pro-angiogenic peptide and iii) human mesenchymal stem cells (hMSCs) from umbilical cord was also assessed. This work was developed in collaboration with the department of veterinary sciences from university of Trás-os-Montes e Alto Douro.

The final chapter 6 summarizes the main conclusions of this work and highlights future perspectives.

SCIENTIFIC OUTPUT

The overall work developed during this PhD thesis originated the following publications, as well as, the participation in several scientific meetings.

International journal publications

Pereira, I., Simões, J., Evtugin, D. V., Rouif, S., Coimbra, M. A., Domingues, M. R. M. & Gama M. Effects of gamma irradiation and periodate oxidation on the structure of dextrin assessed by mass spectrometry. *European Polymer Journal* 103, 158-169 (2018).

Pereira, I., Fraga, S., Silva, S., Teixeira, J. P. & Gama M. *In vitro* genotoxicity assessment of a dextrin-based hydrogel for biomedical applications. *Journal of Applied Toxicology* 1-11 (2018)

Pereira, I., Fraga, S., Maltez, L., Requicha, J., Guardão, L., Oliveira, J., Prada J., Alves, H., Santos, J.D., Teixeira, J. P., Santos, J. P., Pereira, J., Soares, R. & Gama, M. *In vivo* systemic toxicity assessment of a dextrin-based hydrogel and its effectiveness as a carrier and stabilizer of granular synthetic bone substitutes. (under preparation)

Pereira, I., Pereira, J., Maltez, L., Rodrigues, A., Rodrigues, C., Oliveira, M., Silva, D., Caseiro, R., Muñoz, F., Prada, J., Colette, A., Santos, J. D. & Gama, M. The effect of the dextrin-based hydrogel associated with granular synthetic bone substitute and other bioactive agents in the regeneration of a critical-sized defects, using a goat model. (under preparation)

Book chapter

Pereira, I., Rodrigues, A. C., Rodrigues, A., Oliveira, M. & Gama, F. M. Chapter 9 – Injectable hydrogels as a delivery system for bone regeneration in *Bioinspired Materials for Medical Applications* (ed. Rodrigues, L. & Mota, M.) 241-271 (Woodhead Publishing, 2017).

Abstracts in conference proceedings

Pereira, I., Simões, J., Fraga, S., Maltez, Evtugin, D. V., Domingues, R. M., Coimbra, M. A., Teixeira, J. P., Maurício, A. C., Santos, J. D., Muñoz, F., Pereira, J. & Gama, M. Dextrin-based hydrogel for the development of an injectable bone substitute. *Book of Abstracts of CEB Annual Meeting 2017*, 21. (ISBN: 978-989-97478-8-3)

Oral communications in scientific meetings

Pereira, I., Simões, J., Fraga, S., Maltez, L., Guardão, L., Soares, R., Evtuguin, D. V., Domingues, R. M., Coimbra, M. A., Teixeira, J. P., Maurício, A. C., Santos, J. D., Muñoz, F., Pereira, J. & Gama, M. Dextrin-based hydrogel for the development of an injectable bone substitute. *12^a Reunião do Grupo de Gúcidos – GLUPOR12*, 11-13th September 2017, Aveiro, Portugal.

Pereira, I., Simões, J., Fraga, S., Maltez, Evtuguin, D. V., Domingues, R. M., Coimbra, M. A., Teixeira, J. P., Maurício, A. C., Santos, J. D., Muñoz, F., Pereira, J. & Gama, M. Dextrin-based hydrogel for the development of an injectable bone substitute. *CEB Annual Meeting 2017*, 6th July 2017, Braga, Portugal.

Pereira, I. & Gama, M. Biomateriais injetáveis para regeneração óssea. *XI Congresso científico AEFUP: A nova era das ciências farmacêuticas*, 25 & 26th November 2016, Porto, Portugal.

Pereira, I., Simões, J., Evtuguin, D. V., Domingues, M. R., Coimbra, M. A. & Gama, M. Evaluation of the oxidation and irradiation effects on dextrin for biomedical purposes by mass spectrometry. *4th Workshop Mass spectrometry and Carbohydrates*, 13th May 2015, Aveiro, Portugal.

Poster communications in scientific meetings

Pereira, I., Oliveira, M., Rodrigues, A., Rodrigues, C., Maltez, L., Caseiro, A.R., Maurício, A. C., Santos, J.D., Muñoz, F., Pereira, J. & Gama, M. Dextrin-based hydrogel as an injectable carrier for macroporous bone graft granules and other bioactive agents. *5th International Conference on Multifunctional, Hybrid and Nanomaterials*, 6-10th March 2017, Lisbon, Portugal.

Pereira, I., Rodrigues, A., Rodrigues, A. C., Oliveira, O., Simões, J., Evtuguin, D. V., Domingues, M. R., Coimbra, M. A., Santos, J. D. & Gama, M. Characterization of a dextrin hydrogel for biomedical applications using mass spectrometry. *15th European Polymer Federation Congress*, 21-26th June 2015, Dresden, Germany.

CHAPTER 1

General introduction



Bone is a dynamic, highly vascularized tissue that remodels itself continuously. However, this regenerative capacity is limited and, as in the case of large bone defects, where the template for an orchestrated regeneration is absent, surgical procedures are needed. Simultaneously, the worldwide incidence of bone disorders is increasing, mainly due to ageing population. The lack of effective treatments is pushing the development of synthetic bone substitutes (SBSs). This chapter gives a brief description on bone biology and physiology. Also, it provides an overview of the currently available SBSs and describes the main advantages and limitations of commercially available ceramic-based injectable bone substitutes, IBSs (bone cements and polymer-ceramic composites – pastes and putties). The combination of injectable hydrogels and ceramic granules is emerging as a well-established trend, particularly based on the use of *in situ* gelling hydrogels. The recent progresses in the development and application of hydrogel-based IBS are presented in this chapter. Dextrin is an abundant resource, cheap, available in medical grade and with well-established safety for biomedical applications. During the last decade, dextrin has been explored for the design and fabrication of (nano)hydrogels suitable for drug delivery applications, tissue engineering scaffolds, excipient in tablets, bioadhesives or drug conjugates, which will be highlighted in this chapter.

1.1 | Bone biology

Bone is a hard, dense connective tissue of the structural elements of the skeleton. Bones provide structural support to the body, facilitate the movement and the locomotion, and protect internal organs¹. They also play several important roles in the homeostasis and maintenance of the metabolic systems, acting as homeostatic reservoir of i) minerals, such as calcium and phosphorous, ii) fat (yellow bone marrow) and iii) growth factors and cytokines; iv) provide the environment for hematopoiesis (red bone marrow), and v) take part in the acid–base balance^{1,2}. So that, pathologies of bone can be very serious, affecting a wide range of body functions and life's quality. Bone deficiencies can result from abnormal development, tumors or general trauma³.

Despite its inert appearance, bone constantly undergoes modeling (reshaping) during life in response to physiologic influences or mechanical forces, as well as, remodeling to remove old, microdamaged bone and its replacement with new one^{1,2}.

1.1.1 | Bone classification, gross anatomy and structure

Bones can be classified, according to shape, in long bones (such as femur), short bones (carpals), flat bones (skull) and irregular bones (vertebrae or facial bones)¹.

Long bones (**Figure 1.1 (A)**) can be divided into three physiologic sections: diaphysis, epiphysis and metaphysis. The diaphysis is the tubular shaft that runs between the proximal and distal ends of the bone. The hollow region in the diaphysis is called the medullary cavity, which is filled with yellow marrow. The walls of the diaphysis are composed of dense and hard compact bone. The wider section at each end of the bone is called the epiphysis, which is filled with cancellous bone. Red marrow fills the spaces in the cancellous bone. Each epiphysis meets the diaphysis at the metaphysis, the narrow area that contains the epiphyseal plate (growth plate), a layer of hyaline cartilage where the new bone growth takes place. When the bone stops growing in early adulthood (approximately 18–21 years), the hyaline cartilage is replaced by osseous tissue and the epiphyseal plate becomes an epiphyseal line. The medullary cavity has a delicate membranous lining called the endosteum. The outer surface of the bone is covered with a fibrous membrane called the periosteum. The periosteum contains blood vessels, nerves, and lymphatic vessels that nourish the compact bone. Tendons and ligaments also attach to bones at the periosteum. The periosteum covers the entire outer surface except where the epiphyses meet other bones to form joints. In this region, the epiphyses are covered with thin layer of articular cartilage that reduces friction and acts as a shock absorber^{1,3}.

The overall structure of bone can be divided into cancellous (trabecular, spongy) and compact (dense, cortical) bone (**Figure 1.1 (B) and (C)**). Long bones' diaphysis is composed primarily of compact bone, whereas the metaphysis and epiphysis are composed of cancellous bone surrounded by a relatively thin shell of compact bone¹. Flat bones consist in a cancellous bone layer between two compact bone layers. Short and irregular bones have a compact bone surface surrounding a cancellous bone center⁴.

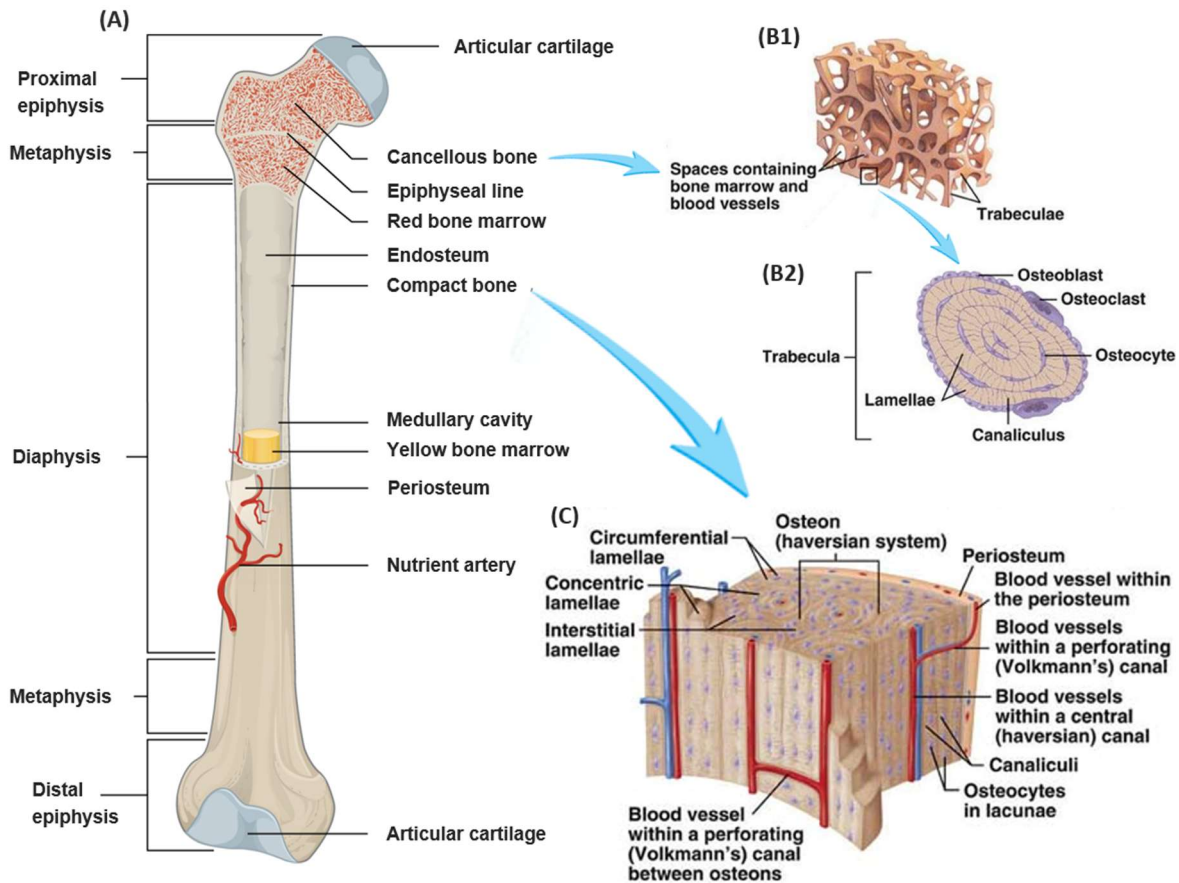


Figure 1.1: Schematic representation of the main features of the bone tissue: **(A)** adult long bone with epiphyseal line, **(B1)** cancellous bone architecture, **(B2)** Transverse section of a trabecula from cancellous bone and **(C)** compact bone architecture (image adapted from ^{5,6}).

The adult skeleton consists overall of 80% compact bone and 20% cancellous bone ¹. Both types of bones have the same matrix composition and cells, but different architectures, resulting in different mechanical properties. Compact bone is dense and solid and surrounds the marrow space, having a much higher resistance to torsional and bending forces; whereas cancellous bone is composed of a honeycomblike network of plates and rods called trabeculae (singular = trabecula) interspersed in the bone marrow compartment (**Figure 1.1 (B1)**), and provides greater resilience and shock absorption ^{1,4}. Cancellous bone generally has a higher metabolic rate and appears to respond quicker to changes in mechanical loading and unloading. Compact bone is composed of osteons or Haversian system ⁴ (**Figure 1.1 (C)**).

Microscopically, two major forms of bone can be identified: woven (or primary) and lamellar (or mature) bone ⁴. Woven and lamellar bone differ regarding formation, composition, organization, and mechanical properties ⁴, and both can be found in either cancellous or compact bone (Sikavitsas, 2001). Woven bone is characterized by a haphazard organization of collagen fibers. It occurs in all fetal bones and in locations where fast bone formation takes place, like in the growth plates and in fracture healing. Woven bone is replaced by lamellar bone via the process called remodeling. Woven bone is mechanically

weaker than lamellar bone and contains about four times more cells (osteocytes) per unit of volume ^{2,4}. Lamellar bone is generated slower than woven bone and is less mineralized. Collagen fibers are thicker and have a preferential orientation, which alternates between layers or lamellae (**Figure 1.1 (B2) and (C)**). These lamellae can be stacked if deposited on a flat surface or concentric if laid centered around a blood vessel. Collagen fibrils extend between lamellae, thus increasing the bone's strength. Haversian bone is the most complex of compact lamellar bone ⁴ (**Figure 1.1 (C)**). In this type of bone, the blood vessel is contained in a central canal, called the Haversian canal. Canaliculi extend outward from the central canal so that the canal can nourish the osteocytes. A central canal and its associated osteocytes are termed an osteon. The central canals branch and eventually join the Volkmann canals which run perpendicular to the central canals and connect them to the periosteal surface. A final stage of remodeling converts some concentric lamellar bone to Haversian systems (secondary osteons) ³.

1.1.2 | Bone tissue

The bone tissue consists of mineralized extracellular matrix with relatively small number of bone cells.

1.1.2.1 | Bone matrix

Bone matrix is a composite material consisting of an organic and an inorganic (mineral) component. The inorganic one contributes approximately with 65% of the wet weight of the bone, while the organic contributes with a little more than 20%, water accounting for approximately 10% ⁴. Bone mineral provides mechanical rigidity and load-bearing strength to bone, whereas the organic matrix provides elasticity and flexibility ¹.

The organic matrix contains collagenous proteins (90%), predominantly type I collagen, and noncollagenous proteins. Proteoglycans (e.g. decorin, biglycan, lumican, osteoaderin, and seric proteins) and glycoproteins (e.g. alkaline phosphatase, osteocalcin, osteonectin, osteopontin, fibronectin) are proportionally the most abundant constituents of the noncollagenous proteins in bone matrix. In minor amounts, there are also bone morphogenetic proteins (BMPs) and other growth factors ^{1,2,7}.

The inorganic fraction of bone consists predominantly of phosphate and calcium ions; however, significant amounts of bicarbonate, sodium, potassium, citrate, magnesium, carbonate, fluorite, zinc, barium, and strontium are also present. Calcium and phosphate ions nucleate to form the hydroxyapatite (HAP) crystals, which are represented by the chemical formula $\text{Ca}_{10}(\text{PO}_4)_6(\text{OH})_2$. Together with collagen, the noncollagenous matrix proteins form a scaffold for hydroxyapatite deposition and such association is responsible for the typical stiffness and resistance of bone tissue ⁷.

1.1.2.2 | Bone cells

Although bone cells represent a small amount of the bone volume, they are crucial for the bone formation, resorption and repair and for mineral homeostasis. Bone cells assume specialized forms and

may be distinguished according to morphology, function and location. They are originated from two cell lines: a mesenchymal stem cell (MSC) line and a hematopoietic stem cell line. From MSC line arise osteoblasts, bone lining cells and osteocytes, while from hematopoietic stem cell line arise osteoclasts⁴.

Osteoblasts are cells located at bone matrix surfaces in a side-by-side layer, which synthesize and secrete the organic component of the bone matrix and also participate in its mineralization. Phenotypically, active osteoblasts are cuboidal shaped and display characteristics of protein synthesizing cells, including abundant rough endoplasmic reticulum and prominent Golgi apparatus, as well as various secretory vesicles. As polarized cells, the osteoblasts start to secrete the osteoid (unmineralized matrix) toward the bone matrix⁷. The synthesis of bone matrix by osteoblasts occurs in two main steps: deposition of organic matrix and its subsequent mineralization. In the first step, osteoblasts secrete collagen proteins, proteoglycans and glycoproteins which form the organic matrix. In the mineralization step, osteoblasts release matrix vesicles, which bind to proteoglycans and other organic components with negative charge, to immobilize calcium ions that are stored within the matrix vesicles. When osteoblasts secrete enzymes that degrade the proteoglycans, the calcium ions are released from the proteoglycans and cross the calcium channels presented in the matrix vesicles membrane. On the other hand, phosphate-containing compounds are degraded by the alkaline phosphatase, releasing phosphate ions inside the matrix vesicles. Finally, the phosphate and calcium ions inside the vesicles nucleate, forming the HAP crystals⁷. Osteoblasts also produce growth factors in response to systemic hormones and local mechanical stress and regulate osteoclast activity⁷. Active osteoblasts may follow one of three fates: i) remain on the surface of the bone, decreasing their synthetic activity and assuming the flatter form of bone lining cells; ii) surround themselves with matrix and become osteocytes; iii) or undergo apoptosis⁴.

Bone lining cells are quiescent flat shaped osteoblasts that cover the bone surfaces, where neither bone resorption nor bone formation occurs. They are sometimes referred to as resting osteoblasts or surface osteocytes. Some of these cells show processes extending into canaliculi, gap junctions being also observed between adjacent bone lining cells and between these and osteocytes. The secretory activity of bone lining cells depends on the bone physiological status, whereby these cells can reacquire their secretory activity, enhancing their size and adopting a cuboidal appearance. Bone lining cells functions are not completely understood, but they have been shown to prevent the direct interaction between osteoclasts and bone matrix, when bone resorption should not occur, and also participate in osteoclast differentiation^{4,7}.

Osteocytes are terminally differentiated osteoblasts which comprise 90–95% of the total bone cells. They are the most abundant and long-lived cells, with a lifespan of up to 25 years. The osteocytes are located within lacunae surrounded by mineralized bone matrix, wherein they show a dendritic morphology. Whereas the osteocyte cell body is located inside the lacuna, its cytoplasmic processes (up

to 50 per each cell) cross tiny tunnels that originate from the lacuna space called canaliculi, forming the osteocyte lacunocanalicular system. These cytoplasmic processes are connected to other neighboring osteocytes processes by gap junctions, as well as to cytoplasmic processes of osteoblasts and bone lining cells on the bone surface, allowing communication between them. In addition, the osteocyte lacunocanalicular system is close to the vascular supply, whereby oxygen and nutrients achieve osteocytes. The osteocytes act as mechanosensors and as orchestrators of bone remodeling, through regulation of osteoblast and osteoclast activities ⁷.

Osteoclasts are the only cells that are known to be capable of resorbing bone during its growth and remodeling. Activated multinucleated osteoclasts are derived from mononuclear precursor cells of the monocyte-macrophage lineage ¹. When stimulated, the mononuclear osteoclast precursors proliferate and then fuse to form large multinucleated osteoclasts. Typically, osteoclasts have three to twenty nuclei and large numbers of mitochondria and lysosomes. Osteoclasts have an efficient method for destroying bone matrix. They first bind themselves to the surface of the bone, creating a sealed space between the cell and the bone matrix and then secrete hydrogen ions (H⁺) and matrix metalloproteinases, such as collagenases and cathepsin K. The pH is locally reduced to approximately 4, allowing the solubilization of mineral phase, whereas enzymes digest the organic matrix ^{1,4}.

1.1.3 | Bone development

The bone formation process is named ossification or osteogenesis. During fetal development, there are two types of ossification processes, intramembranous and endochondral, but bone is the same regardless of the pathway ². Intramembranous ossification is the mechanism for the formation of flat bones, as well as for the healing process of fractures treated by open reduction and stabilization by metal plate and screws ². Intramembranous ossification is characterized by invasion of capillaries into the mesenchymal connective tissue, and the emergence and differentiation of mesenchymal cells into osteoblasts. The osteoblasts secrete the osteoid, beginning the mineralization and form bone spicules. These spicules lengthen into trabeculae, and as the trabeculae increase in size and number they become interconnected forming woven bone ⁸. On the trabecular surfaces, the osteoblast zones will continue osteoid formation layer upon layer, a process called appositional bone formation. This process continues until sufficient bone density is obtained.

Endochondral ossification (**Figure 1.2**) is the mechanism for long bone formation and lengthening, as well as for the formation of most of the skeleton bones. It also occurs in the natural healing of bone fractures ^{2,8}. Endochondral ossification begins when MSCs differentiate into chondroblasts, which produce a hyaline cartilage with a similar shape to the future bone. Chondroblasts mature to chondrocytes as they become surrounded by cartilage matrix which they produce. The cartilage is covered with a dense fibrous layer known as perichondrium. Initially, lengthening is established by chondrocyte proliferation and matrix production, and widening is established by appositional growth

from the perichondrium⁹. Then, the ossification centers appear in each bone, first centrally at diaphyseal region (primary ossification centers) and later at the extremities (secondary ossification centers). The mostly primary ossification centers appear during fetal development, though a few short bones begin their primary ossification after birth. They are responsible for the formation of the diaphysis of the long bones, short bones, and certain parts of irregular bones. The secondary ossification centers are responsible for the formation of the epiphyses of the long bones and the extremities of irregular and flat bones². Before ossification, the chondrocytes enlarge (hypertrophy) and further mature, which results in increased intracellular calcium concentration. The thin cartilage matrix that surrounds the hypertrophied cells serves as a substrate for calcification that coincides with death (apoptosis) of the chondrocytes, resulting in a calcified scaffold for later bone apposition. Synchronously, the perichondrium is invaded by capillaries and differentiate into periosteum that delivers pre-osteoblasts. From the periosteum capillaries and osteogenic cells invade the calcified cartilage and start to produce woven bone⁹. Almost the entire bone is ossified except for the central canal of the diaphysis, where is located the medullary cavity, as well as in articular cartilage and epiphyseal plates (cartilaginous plates). Epiphyseal plates are responsible for the longitudinal bone elongation until adulthood, where cartilage in the plates is replaced by bone^{2,8}. During this time, same sequence of events (matrix calcification, death of chondrocytes, invasion of blood vessels from the periosteum, and seeding with osteogenic cells that become osteoblasts) occurs in the epiphyseal regions, and each of these centers of activity is referred to as a secondary ossification center. The point of union of the primary and secondary ossification centers is called the epiphyseal line, and the bone stops to grow².

The bones resulting from the two ossification processes are immature woven bones. These will be remodeled to form lamellar bone, which is more organized, gaining the most optimal shape and density

3.

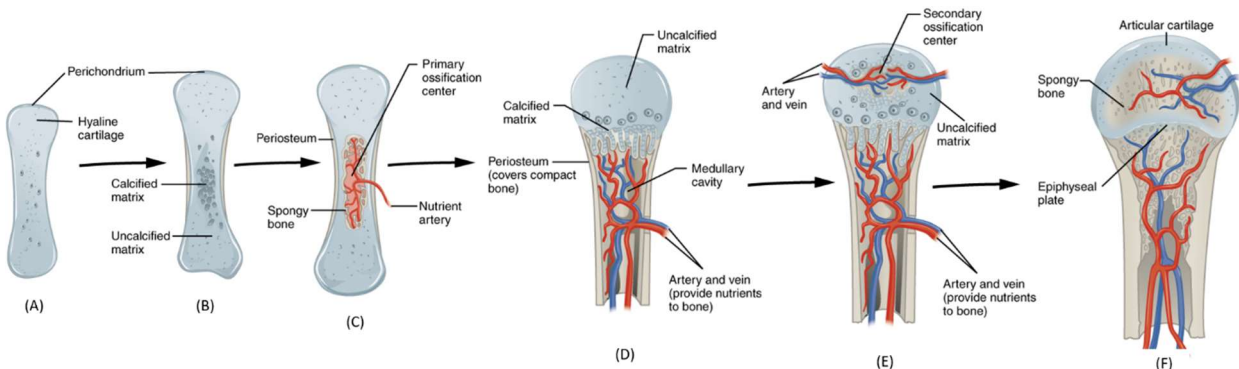


Figure 1.2: Endochondral ossification process: **(A)** mesenchymal cells differentiate, **(B)** the cartilage model of the future bone and the perichondrium form, **(C)** capillaries penetrate cartilage and the perichondrium transforms into periosteum; Periosteal collar and primary ossification center develop, **(D)** the cartilage and chondrocytes continue to grow at ends of the bone, **(E)** secondary ossification centers develop and **(F)** the cartilage remains at epiphyseal (growth) plate and at joint surface as articular cartilage (image adapted from⁶).

1.1.4 | Bone remodeling

Bone remodeling is a lifelong process responsible for replacing old bone as to maintain its strength and the mineral homeostasis, preventing the accumulation of bone microdamages. It is also the process by which lamellar bone is produced ¹⁻³. Bone remodeling process can be divided into five sequential phases: i) resting, ii) activation, iii) resorption, iv) reversal and v) formation.

- i) Resting phase corresponds to non-activated bone. The factors that initiate the remodeling process remain unknown ².
- ii) Activation phase consists in the recruitment and activation, due to hormonal or physical stimuli, of mononuclear monocyte-macrophage osteoclast precursors from the circulation, lifting of the endosteum that contains the bone lining cells off the bone surface, and its differentiation into osteoclasts ^{1,3}.
- iii) Resorption phase occurs when osteoclasts dissolve the mineral matrix and decompose the osteoid matrix. Osteoclastic resorption produces irregular scalloped cavities, named as Howship's lacunae, on the cancellous bone surface and in the Haversian canals of the compact bone ^{1,3}.
- iv) During the reversal phase, bone resorption reverts to bone formation. Osteoclasts disappear and mononuclear macrophage-like cells smooth the resorbed surface by depositing a cement-like substance that will bind new bone to old. Osteoblast precursors are recruited to initiate the new bone formation ^{2,3}.
- v) Formation phase consists on the osteoid deposition by osteoblasts and its further mineralization to substitute the removed old bone. In the end, the osteoblasts become resting lining cells that completely cover the newly formed bone surface and connect with the osteocytes in the bone matrix through a network of canaliculi, returning to resting/quiescent phase ².

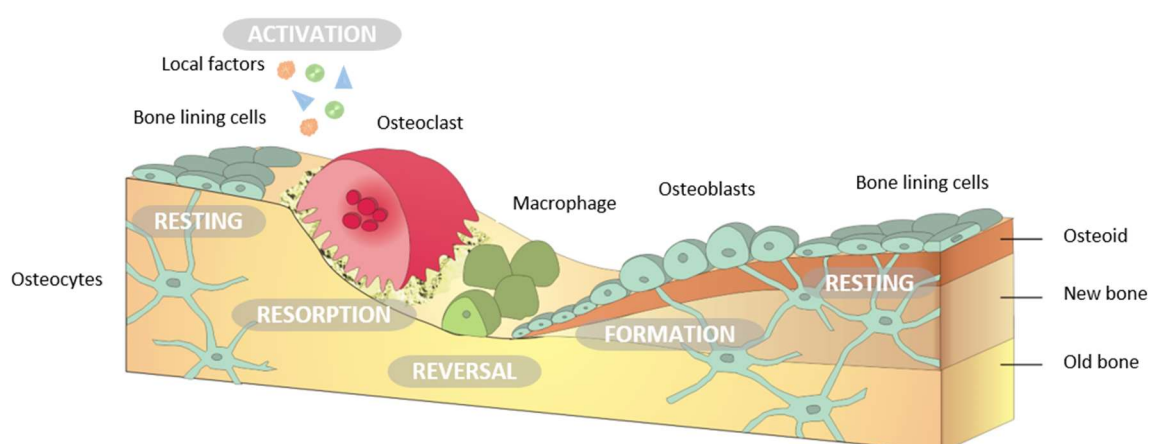


Figure 1.3: Schematic representation of the different phases of the remodeling process (image adapted from ¹⁰).

1.1.5 | Fracture healing

A fracture is a broken bone and the fracture healing process only aims a rapid stabilization of the broken bone parts with little commitment to anatomy ⁹. Fracture repair requires both of the above mechanisms of bone formation and involves four major steps: i) hematoma and ii) callus formation, iii) callus ossification and iv) bone remodeling.

- i) Hematoma formation (**Figure 1.4 (A)**): when a fracture occurs, blood flows from any vessel torn by the fracture, and a hematoma is formed. Usually the blood in a hematoma forms a clot, which consists of fibrous proteins that stop the bleeding. Inflammation and swelling of tissues around the bone often occur following the injury ⁵.
- ii) Callus formation (**Figure 1.4 (B)**): callus is a mass of tissue that forms at a fracture site and connects the broken ends of the bone. The internal callus is formed between the ends of the broken bone, and in the marrow cavity if the fracture occurs in the diaphysis of a long bone; the external callus is formed around the opposing ends of the bone fragments, and consists in a bone–cartilage collar that stabilizes the ends of the broken bone. Several days after the fracture, blood vessels grow into the clot. As the clot dissolves, macrophages clean up cell debris, osteoclasts break down dead bone tissue, and fibroblasts produce collagen and other extracellular components to form granulation tissue. Chondroblasts derived from osteochondral progenitor cells begin to produce cartilage in the fibrous network. As these events are occurring, osteochondral progenitor cells become osteoblasts and produce new bone ⁵. Simultaneously, intramembranous bone formation can be found depending on the local oxygen supply. Only when fracture is stable and with unchanged anatomy (like a crack) intramembranous repair alone will be enough ⁹.
- iii) Callus ossification (**Figure 1.4 (C)**): the internal and external calluses are ossified to become woven bone.
- iv) Bone remodeling (**Figure 1.4 (D)**): the woven bone is gradually resorbed and replaced with lamellar bone, and the excessive callus is resorbed ³.

1.2 | Biomaterials for bone regeneration

Although bone is able to heal and regenerate, to some extent, in the case of large bone defects - caused by significant trauma or systemic disease, pathological fractures (either because of metastasis or as part of a primary malignancy), bone infection or a compromised blood supply - this ability to adequately self-heal can fail and medical intervention may be needed. Bone injuries and diseases represent the main cause of pain and disability/incapacity ^{11,12}.

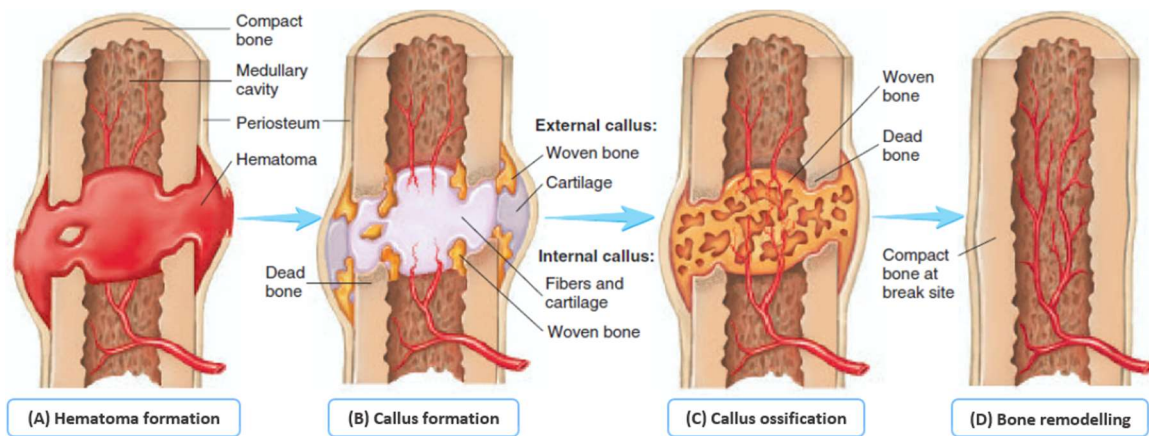


Figure 1.4: Schematic representation of the fracture healing process in a long bone: **(A)** hematoma formation following a fracture, **(B)** the internal callus replaces the hematoma, while the external callus provides support, **(C)** woven, cancellous bone replaces the cartilage of the callus and **(E)** remodeling of the bone replaces the woven bone (image adapted from⁵).

Currently, the standard procedure to treat bone defects is the autograft, which consists in harvesting small amount of bone tissue (usually from the iliac crest) from the patient and its transplantation to the defect site. Despite this procedure has the best clinical outcome, donor bone tissue availability is limited, the procedures are very expensive, and they may result in significant donor site injury and morbidity, deformity and scarring, being associated with surgical risks as well as bleeding, inflammation, infection and chronic pain^{12–14}.

Other approaches are available such as allografts or xenografts. The first one refers to the transplantation of bone tissue from other individuals (e.g. patients receiving a hip prosthesis) or corpses, and the second approach involves bone tissue from other species, usually pigs or bovines^{12–14}. Allografts must be processed within bone tissue banks. They are devitalized by freezing, and often additional procedures like sterilization are applied, with detrimental effects on mechanical properties of bone. In addition, there are concerns about the transmission of diseases (e.g. HIV) and immunogenicity, besides their limited availability. Allografts can be demineralized and deproteinized. During the demineralization process, the bone graft is chemically sterilized to preserve its extracellular matrix architecture and molecular signaling. Demineralized bone matrix (DBM) is a very popular bone graft substitute in the USA, and is generally used in the form of a mouldable paste (e.g. DBX[®] Putty, DePuy Synthes, Inc.). Other companies propose deproteinized human bone to decrease the biological risks associated with the presence of organic matter. Similar approaches have been applied with xenografts. They are usually commercialized as a calcified matrix (e.g. Bio-Oss[®], Geistlich Pharma North America Inc. and Endobon[®], Zimmer Biomet), which have given good results in dentistry^{15,16}.

Bone grafting frequency is indeed the second most frequent tissue transplantation worldwide, right after blood transfusion. Every year, roughly two million patients worldwide sustain a bone grafting procedure to repair bone defects¹⁶. The worldwide incidence of bone disorders and conditions has trended steeply upward, mainly due to baby boomer population, increased life expectancy and

democratization of high-risk sport ^{13,15}. The global market of bone graft substitute (allo-, xeno- and synthetic graft) is expected to reach \$ 5,031.0 million by the end of 2027 and this market is projected to grow at a compound annual growth rate (CAGR) of ~ 6.52 % during the forecast period 2017-2027 ¹⁷.

1.2.1 | Synthetic bone substitutes

The limitations of the traditional treatments for bone reconstruction and the prevalence of unmet clinical needs motivate the current trend in the development of synthetic bone substitutes (SBSs). The general concept for the development of SBSs consists in the designing of three-dimensional (3D) scaffolds, from biomaterials (natural or synthetic), which confers a temporary support for the regeneration of bone tissue, while the scaffold itself will be resorbed and replaced by newly formed tissue ^{12,18}. An improvement of the understanding of chemical and biological processes involved during the resorption of SBSs and during the concomitant bone formation should allow a better design of these biomaterials and eventually lead to superior performances ¹⁵.

Biomaterials can be defined as a “substance that has been engineered to take a form which, alone or as part of a complex system, is used to direct, by control of interaction with components of living systems, the course of any therapeutic or diagnostic procedure, in human or veterinary medicine” ¹⁹. Several biomaterials have been used for the development and improvement of SBSs, such as metallic, ceramics and polymers used alone or in combination (composites). They can be processed through different techniques such as solvent casting, particle leaching, freeze-drying, electrospinning, fiber meshing, sintering and rapid prototyping, in order to obtain 3D scaffolds with different shapes, microarchitectures and with suitable properties able to mimic the natural bone and facilitate its regeneration process ^{12,20}. Ideally, scaffolds for bone regeneration should be osteoinductive (promote the differentiation of primitive, undifferentiated and pluripotent cells to an osteoblastic lineage), should exhibit osteoconductivity (the process by which bone cells grow in the surface of a foreign material) and finally, should be capable of osseointegration (material’s integration by bone tissue without the formation of fibrous tissue at bone-material interface) ¹². Furthermore, they should display a set of characteristics such as: i) biocompatibility, ii) an internal porous structure with interconnected pore networks for cell in-growth and reorganization, iii) an appropriate surface chemistry that allows cell attachment, differentiation and proliferation, iv) adequate mechanical strength and v) a controllable degradation rate suitable for newly grown tissue replacement ¹⁸.

1.2.1.1 | Metallic biomaterials

To date, there are several biocompatible metallic materials that are frequently used as implanting materials in dental and orthopedic surgery to replace damaged bone or to provide support for healing bones or bone defects ²¹. Standard surgical implant biomaterials based on metals and metallic alloys include stainless steel, titanium, tantalum, magnesium, iron, cobalt and aluminum. They are especially

preferred for their usage in load-bearing applications due to their good mechanical properties^{15,20–22}. However, they have some limitations, such as (i) lack of biological recognition on the material surface or bioactivity, (ii) nonbiodegradability, (iii) release of toxic metallic ions and/or particles through corrosion or wear, which can lead to inflammatory cascades and allergic reactions, reducing its biocompatibility and causing tissue loss, and (iv) architecture control, since some metallic materials are too weak to be arranged into the desired architecture with a controlled porous structure and some metals are too stiff and would fracture when arranged into certain architectures^{21–23}. New strategies have been developed to overcome these limitations, including surface coating/modification to improve their *in vivo* performance^{21–23}.

1.2.1.2| Ceramics

Ceramics are inorganic solids, formed by action of heat and subsequent cooling, which may be composed by a crystalline, semi-crystalline or amorphous structure²⁴. Ceramics-based scaffolds are the best-studied SBS materials due to their chemical and structural similarity to the mineral phase of the bone tissue. Ceramic-based materials began to gain extreme popularity for biomedical applications in the late 1960s. The huge advance in knowledge and technology during the last 40 years has caused ceramics to be universally appreciated in terms of biocompatibility, osteoconductivity and bioactivity, and nowadays they are used in several applications in orthopaedic, craniofacial and dental surgery^{24–26}.

Ceramic-based products include materials such as calcium phosphate (CaP), bioactive glass (BG) and calcium sulfate (CaS) used alone or in combination with other materials. Among these materials, those based on CaP are the most attractive^{27–29}. CaP is bioactive, biodegradable and osteoconductive. In spite of these positive attributes, inherent brittleness and relatively slow degradation limit their clinical application as SBS materials. Moreover, they have no osteogenic or osteoinductive properties^{30,31}. Currently, the most common types of CaP ceramics used as SBSs are synthetic HAP, β -tricalcium phosphate (β -TCP), their derivatives or combination of both, such as biphasic calcium phosphate (BCP)^{32,33}. HAP is the most stable CaP at physiological conditions, thus displaying lower solubility and resorption, while β -TCP reabsorbs more quickly. For the same porosity, β -TCP scaffolds often exhibit lower mechanical strength than HAP scaffolds, limiting their use in the load-bearing applications^{20,23}. In this context, the combination of HAP and β -TCP (e.g. BCP) appears a strategy to achieve an optimum balance between mechanical strength/resorption and bone regeneration, by controlling TCP/HAP ratios¹⁶.

BG has long been established as biocompatible, biodegradable and highly bioactive materials. BG was designed as a bone graft for dental applications. Its use in orthopedic surgery seems to be limited by its brittleness, radiopacity (which compromises radiographic evaluation of bone healing) and prolonged resorption times³⁴. BGs are composed of $\text{SiO}_2\text{-CaO-Na}_2\text{O-P}_2\text{O}_5$ at specific ratios. Changes in stoichiometry, as well as in its microstructure and crystallinity, result in different resorption rates^{23,35}.

They have been shown to bond with bone more rapidly than other bioactive ceramics and to stimulate osteoblast cells, however they lag behind other bioactive ceramics in terms of commercial success. The bioactivity of these materials is related to the ion dissolution products (silica, calcium, sodium, phosphorous) and the formation of hydroxycarbonate apatite (HCA) layer on the surface of the glass, following initial glass dissolution. HCA is like bone mineral and is thought to interact with collagen fibrils to integrate (bond) with the host bone, promoting the osteointegration. Moreover, dissolution products of silicate-based glasses have been reported to up-regulate gene expression on osteoblasts and stimulate angiogenesis³⁵. One strategy that has been employed to improve the bioglasses bioactivity (and also CaP-based products) consists in its modification by incorporation of low amounts of biologically active ions, such as cerium, zinc, magnesium, cobalt, copper, strontium, among others³⁶. Such ions are known to be involved in the bone metabolism and to play a physiological role in angiogenesis and osteogenesis while providing antimicrobial properties and constitute an alternative approach to the use of expensive growth factors. Simultaneously, its incorporation in ceramic-based scaffolds allow to achieve products with a chemical composition closer to the mineral phase of the bone^{23,36}. BGs can also be associated to HAP to produce a glass-reinforced HAP^{37,38}, which display improved mechanical properties and enhanced bioactivity, comparing with HAP alone (e.g. Bonelike®, Bioskin, Molecular and Cell Therapies, S.A.)

CaS was the first material used as a bone graft substitute in clinical field, where it showed to be user-friendly, inexpensive, readily available and stable for filling-in bone defects, without a negative effect in bone healing. However, it presents fast absorption rates, leading to the loss of mechanical properties before equivalent new bone formation, a main disadvantage limiting its use in relevant clinical cases^{16,34}. In order to enhance the clinical outcome of CaS, it was combined with DBM (AlloMatrix™, Wright) to be used in dental guided bone regeneration³⁹.

1.2.1.3| Polymers

Polymers have physical, mechanical, and chemical properties quite different from other bone substitutes. The polymeric materials used in the biomedical field and particularly in bone regeneration applications may be of natural or synthetic origin. These, in turn, can be divided further into degradable and nondegradable¹⁶.

Natural polymers can be considered as the first biodegradable biomaterials used clinically. They can mimic the endogenous extracellular matrix, playing critical biological functions, e.g. display cell adhesion motifs or antimicrobial properties. On the other hand, the surrounding tissues can recognize and metabolize their degradation products through common pathways. Some of the most commonly used materials include chitosan, collagen, hyaluronic acid, fibrin, alginate, cellulose, gelatin and starch. However, some natural polymers can cause immunological responses, present variability among different supply sources, and may offer inferior mechanical properties to synthetic polymers⁴⁰⁻⁴².

Synthetic polymers, such as polyglycolic acid (PGA), polylactic acid (PLA) and their copolymer PLGA, poly(ϵ -caprolactone) (PCL) present a high versatility in their processing, generating a wide range of 3D scaffolds with different porosities, degradation times, surface and mechanical characteristics. They are often cheaper than biologic scaffolds, can be produced in large amounts with uniform and reliable properties and have a long shelf-time. Despite these advantages, they can lead to toxicity or chronic inflammation and exhibit lack of bioactivity⁴³⁻⁴⁷.

1.2.1.4 | Composites

The composites consist of a combination of materials of different properties (metals, ceramics and polymers) and might therefore use the individual advantages to optimize a new material and to achieve scaffolds that better mimic the natural bone^{12,22}. For instance, collagen and HAP composites (HAPC) have been designed to obtain scaffolds with improved mechanical properties and bioactivity (e.g. Healos®, DePuy Synthes, Inc.)¹⁶. As mentioned above, bone is mainly composed by collagen and carbonate substituted HAP, and such combination improves the tissue bonding, cell adhesion and cell differentiation. The ductile properties of collagen help to increase the poor fracture toughness of HAP, while the addition of CaP compounds to collagen sheets provide higher stability, increased resistance to 3D swelling compared to the collagen alone and enhanced mechanical 'wet' properties⁴⁸.

Organic and inorganic materials can also be combined to design composites with improved handling properties. Mouldable and/or injectable scaffolds are of paramount importance for the commercial success of SBSs, since they can extend their field of application, for instance for the treatment of bone fractures by minimally invasive techniques¹⁵.

1.2.2 | Ceramic-based injectable bone substitutes commercially available

Ceramic-based products are available mainly in granular/powder or as compact/porous forms (blocks). Nevertheless, as typical ceramics, they are hard and rigid, and therefore not easy to handle and to fit into the surgical sites, leaving empty spaces between bone tissues and the filling material. In fact, with ceramic granular bone substitutes it is very difficult to fill the defect cavities, namely in a bleeding situation, because the granules can be washed out by the blood stream and, consequently, migration of granular particles to the surrounding tissues occurs, which can cause adverse events. Also, sedimentation of the granules is yet another issue and, as a result, the distribution of the granules in the defect cavity is very irregular^{25,49,50}. In the case of ceramic blocks, they cannot be shaped intraoperatively, which means that they can only be worked into different forms to a limited extent. Moreover, they usually exhibit poor mechanical properties^{51,52}.

The limitations previously described suggest the need for various handling requirements to promote a reliable and safe clinical application. In fact, easy handling is of paramount importance for the commercial success of bone substitute materials. Thus, the current challenge to potentiate the clinical

application of the ceramic-based SBSs lies on the development of injectable bone substitutes (IBSs), in which a binder or gel is added to the granules.

Indeed, the development of IBSs has garnered great importance in the field of bone regeneration therapies, as a unique therapeutic method to reach areas of the body using minimally invasive procedures and showing the ability to conform to any shape irrespective of the defect geometry. Furthermore, IBSs can be used as fillers to reinforce the mechanical properties of diseased/injured bone and as a competent carrier of cells and therapeutic agents, such as drugs and growth factors^{53–55}.

With respect to ceramic-based IBSs, research and market has mainly focused on CaP cements and polymeric solutions with granules incorporated in order to obtain pastes/putties. These systems can be applied into the bone defects by using a syringe^{25,49,56}.

1.2.2.1 | Calcium phosphate bone cements

CaP cements are essentially mixtures of CaP powders and aqueous solutions. The powder and the liquid are mixed in an appropriate ratio prior to implantation to form a paste that subsequently hardens at body temperature within several minutes. Once injected, the CaP paste forms a low-crystallinity HAP that can be absorbed over time^{15,33,57}. Some commercial CaP cements available on the market are listed on **Table 1.1**.

Table 1.1: Commercial calcium phosphate (CaP) cements and their clinical application.

Commercial cement	Company	Application
Norian SRS®	Synthes Inc.	Bone fractures
ChronOs inject®	Synthes Inc.	Bone remodeling and cyst treatment
HydroSet®	Stryker Inc.	Bone void filler
BoneSource®	Stryker Inc.	Bone void filler for trauma and reconstructive surgery
Calcibon®	Biomet Inc.	Bone fractures
Callos®	Skeletal Kinetics LLC	Bone void filler

A very important handling property of the cements is their hardening rate, in addition to the denominated setting rate. This feature can directly affect the clinical procedure, because a fast setting reaction limits the period during which the surgeon can apply the cement, whereas a slow one prevents the surgeon to close the defect and therefore increase the overall procedure duration²⁵.

A few drawbacks associated with CaP cements have been identified, such as: i) a lack of paste cohesion may prevent setting and lead to negative *in vivo* reactions due to the release and migration of microparticles to the surrounding tissues^{15,25}; ii) inadequate hydraulic properties, that is, inability to flow easily under pressure through a cannula attached to the syringe^{15,58}, and iii) absence of adequate porosity, which compromise cell ingrowth⁵⁹.

Most of the presently available CaP cements are in the form of a powder and a liquid that are mixed immediately before use. In the clinical scenario, the ability of the surgeon to properly mix and inject the cement in the defect within the prescribed time is a crucial factor. In this context, pre-mixed cements have been described. However, these pre-mixed formulations tend to have poor mechanical properties and have a relatively short shelf-life^{60,61}.

1.2.2.2 | Injectable polymer-ceramic composites

Polymers are increasingly gaining interest for the development of injectable matrices for tissue engineering and regenerative medicine applications. Polymer injectable formulations, such as polymeric viscous solutions or hydrogels, provide the ability to conform to the cavity in which they are placed; therefore they can fill irregular defects⁶².

Polymer-ceramic composites have attracted much attention. In this approach, hydrosoluble polymers, such as hydroxypropylmethylcellulose (HPMC) and collagen, are considered to be merely carriers for ceramic granules, which are suspended in physiological fluids containing the polymer. Then, the viscous solution allows the injectability of the granules without phase separation¹⁵. Moreover, the combination of polymers and ceramic phases enhance the morphological and functional properties of the scaffolds: ceramic granules support bone healing by osteoconduction, while the polymer provides intergranular spaces for bone ingrowth and ensures the attachment of granules in the bone defect^{63,64}.

Usually, ceramic-only scaffolds are prepared via high temperature sintering to ensure strength and stability, crippling the incorporation of biochemical agents, such as drugs and/or growth factors, and hampers replication of any biomimetic process, such as co-deposition and co-precipitation that occurs in the physiological environment during natural bone regeneration⁶⁵. Their combination with hydrosoluble polymers can overcome such limitation. Some of pastes/putties based on granular ceramic-polymer conjugation available on the market are listed in **Table 1.2**.

Table 1.2: Injectable bone substitutes (IBSs) based on granular ceramic – polymer conjugation.

Company	Product	Composition	Commercial Form
ApaTech (UK)	Actifuse™	HAP, polymer and aqueous solution	Pre-mixed
Biomatlante (FR)	In'Oss™	BCP granules (60% HAP, 40% β -TCP; 80-200 m) and 2% HPMC	Pre-mixed
DePuy Spine (US)	Healos® Fx	HAP (20-30%) and collagen	<i>In situ</i> mixing
Therics (US)	Therigraft™ Putty	β -TCP granules and polymer	Pre-mixed
Integra LifeSciences (USA)	Integra Mozaik™ Putty	β -TCP granules and collagen	Pre-mixed

Regarding the application procedure, the IBS products may be divided into two main classes: the pre-mixed (ready-to-use) and *in situ* mixing formulations (the mixture occurs immediately before surgery). Pre-mixed products provide some advantages, namely simple application, because they do not require any mixing on transfer into an appropriate delivery system (ready-to-use formulations). However, they present limitations in clinical practice, including the low versatility, since the mixture composition is already pre-defined. For example, these products do not have the ability to incorporate other bioactive agents (osteogenic factors, cells) ¹⁵. In addition, pre-mixed formulations are presented in the form of "viscous pastes", which hampers the adjustment of its viscosity to targeted therapeutic procedures for each clinical condition.

In situ mixing formulations combine the powder(s) with the polymeric solution(s) just before use. This approach is more cumbersome, but also more versatile than the pre-mixed products since it allows the addition of various components (drugs, cells). Moreover, it is generally easier to process the liquid and the solid components individually. For instance, polymers and ceramics may require different sterilization methods, thus this kind of products overcome technical issues related to pre-mixed ones ²⁵.

Although current pastes and putties based on polymers have shown good biocompatibility and convenient rheological properties for injection, they are non-hardening (**Table 1.2**), which impairs the composite mechanical stability, so that the viscous suspension shows a tendency to flow after implantation *in vivo* ⁶⁶. Moreover, some pastes/putties, particularly pre-mixed formulations, are brittle and create string-like fragments, failing to fill the defect correctly. Therefore, self-hardening composites have been investigated to develop a new generation of IBSs. Hydrogels have been appointed as the best candidates to produce such formulations.

1.2.3 | Injectable bone substitutes based on hydrogels

Hydrogels are 3D, crosslinked networks of hydrophilic polymers swollen with a large amount of water or biological fluids, without dissolving. These can be produced through chemical or physical crosslinking of polymers. The chemically crosslinked hydrogels can be further divided into several types, according to the kind of reaction or catalyst used: radical polymerization, chemical reaction of complementary groups, high-energy irradiation and enzyme catalysed. Within the physically crosslinked hydrogels, we can find those stabilized through ionic interactions, crosslinked from amphiphilic blocks and graft copolymers. Hydrogel properties depend on the chemical composition, crosslinking density, and hydrophobicity ^{67,68}. Hydrogels can be formed from both natural and synthetic polymers, with advantages and disadvantages for each case, as well as, from hybrid combinations, which can mitigate some disadvantages of the individual components ^{69,70}.

Generally, hydrogels are biocompatible, biodegradable and mimic many of the properties of the native extracellular matrix (ECM), namely high-water content and viscoelastic mechanical properties, functional activity as provisional artificial support for cells and lack of mechanical strength. They display

porosity and interconnectivity, enabling the transport of nutrients, gas diffusion, and removal of metabolic wastes, they can also perform as carriers of growth factors or cells and as drug delivery systems. Moreover, hydrogels can be injectable, enabling less invasive clinical procedures, and can conform to the shape of the surface to which they are applied ^{67,68,71}.

The first goal when incorporating ceramics into a hydrogel is to ensure granules cohesiveness during injection and after its implantation into the bone defect. Hydrogels can also serve as space-holders to prevent granule packing and allow easier bone ingrowth ^{72,73}. In the last years, the ability of different types of injectable hydrogels to homogeneously incorporate various types of ceramics has been demonstrated (**Table 1.3**). For instance, Morais *et al.* ⁷⁴ developed an alginate-based hydrogel able to envelope and aggregate granules with 500-1000 μm , allowing a good handling and facile injectability. However, most reports use hydrogels as an injectable carrier of nanoceramics (**Table 4.3**). The crosslinking density of hydrogels is the main responsible for the maintenance of granules' cohesiveness and prevention of their washout in the biological fluids.

However, an equilibrium between crosslinking density, mechanical properties and hydrogel degradation should be found in order to achieve a better *in vivo* bone ingrowth. For instance, HPMC is currently used as a carrier of BCP granules (MBCP GelTM and In'OssTM) ^{64,75}. However, the viscous suspension shows a tendency to flow after implantation *in vivo*. The long-term flow was suppressed by using a silated HPMC (Si-HPMC), which resulted in a crosslinked hydrogel. The strength of the crosslinked Si-HPMC hydrogel was sufficient to maintain the BCP granules in the bone defects ⁷², since the use of silane improved the rheological and mechanical stability of the composite ⁶⁶. On the other hand, because of the higher density after reticulation, cell colonization followed by bone tissue ingrowth was delayed over time with Si-HPMC, as compared to the HPMC without gelation ^{63,64}.

Besides acting as binders for ceramic particles and providing injectability, hydrogels within these composites can contribute to obtain suitable scaffolds able to mimic the natural functions/structure of the bone. For example, the ceramics mimic bone's inorganic phase, providing mechanical properties (stiffness and mechanical strength) and nanotopographic features, while hydrogel provides toughness and elasticity, as the bone ECM, and creates intergranular spaces for fluid penetration, cell colonization and bone ingrowth. The interconnected pore structure, typical of hydrogels, is maintained intact after incorporation of ceramics, without significant changes in pore size ⁷⁶⁻⁸⁵.

Moreover, by combining the advantages of hydrogels and ceramics, synergetic effects are generated which, in the ideal case, are able to counteract individual materials' disadvantages. For instance, the combination of bioactive properties of ceramics with the elastomeric properties of hydrogels, results in composites with higher extensibilities, fracture stresses, compressive strengths, and toughness ^{80,86-91}. Killion *et al.* ⁸⁸ and Ni *et al.*, ⁹² by incorporation of BG and acellular bone matrix granules, were able to overcome the inherent brittleness typically associated with this kind of granules. The improved mechanical strength of the composites has been attributed to two factors: physical interaction between

polymer-ceramic and reduction in swelling degree^{86,88–90}. Besides the space-filling effect, ceramic particles can act as physical crosslinking points which reinforced the hydrogel and, consequently, reduce its swelling degree. However, high loadings of ceramics can disturb the crosslinked structure of hydrogel and negatively affect mechanical performance^{87,90}.

1.2.3.1 | *In situ* gelation hydrogels for injectable bone substitutes

One of the major advantages in using hydrogels to develop IBS is its ability to gel *in situ* in response to external physical or chemical stimuli, as temperature, pH or light (stimuli-responsive hydrogel). Thus, the *in situ* forming hydrogels with ceramics incorporated can be administered as flowable viscous liquids (sol state) into the bone defect and then turn into standing hydrogels (gel state). The mechanical stability and integrity are achieved by subsequent triggered network formation⁹³. Therefore, *in situ* gelation hydrogels facilitate the mixing/manipulation of granules and their injectability using minimally invasive methods, are able to mold perfectly to the shape of bone defects, suitable for delivery of cells and other bioactive agents, and can be prepared during surgery, under aseptic conditions. Since injectable and *in situ* crosslinking hydrogels can overcome the main drawbacks inherent to current IBSs (cements, pastes, putties), they have been intensively studied. **Table 1.3** summarizes the different *in situ* gelation systems investigated to incorporate diverse ceramics.

Thermosensitive hydrogels constitute an interesting system, since they avoid using any noxious substances as initiator of sol-gel transition (such as the pH adjustments, oxidants or UV light) owing to the sensitivity to the temperature. Currently, reported thermogelling systems include chitosan in presence of β -glycerophosphate, which is responsible for the chitosan solubility at neutral pH and room temperature^{80,94–101} and poly(ethylene glycol)-poly(ϵ -caprolactone)-poly(ethylene glycol) (PEG-PCL-PEG)^{77,78,83,92}. These hydrogels undergo sol-gel transition at body temperature.

Other authors have been testing photo-crosslinked hydrogels based on PEG^{86,88–90} and gelatin derivatives⁸⁵ (**Table 1.3**). The incorporation of di(meth)acrylate groups into the PEG chains and methacrylate groups into gelatin allows the formation of hydrogel network upon UV light. Photopolymerization has several advantages over conventional polymerization techniques, such as spatial and temporal control over polymerization, fast curing rates (less than a second to a few minutes) at room or physiological temperatures, and minimal heat production¹⁰². Furthermore, it can be carried out in the presence of cells and proteins/drugs without compromising its viability/bioactivity^{85,89,90}.

Chemical and ionic crosslinking hydrogels can also be formed *in situ*. As these types of hydrogels are generally composed by two components (polymer and crosslinking agent, or polymers modified with chemically complementary groups) they can easily be mixed by the surgeon under aseptic conditions and injected. In other words, initially there are two solutions and the ceramics can be dispersed in one or in both solutions; such solutions can be loaded into interconnected syringes^{103,104} or in into the separate chambers of a dual syringe system^{105,106} for mixing and posterior injection. Such devices are

available for this purpose and commercialized by, for example, MEDMIX® and Nordson Corporation. After mixing all the components of the formulation, the crosslinking process starts, the mixed solution becomes more viscous over time as it gels. The gelation process will finish *in situ*. Authors have reported gelling times from seconds to several minutes for this kind of composite hydrogels (**Table 1.3**). Surgeons generally advise 5–30 min as a suitable gelation time¹⁰⁷. This type of hydrogel can also be used as ready-to-use injectable formulations (as pastes or putties), however its properties can change over time.

In a subcutaneous assay, Stenfelt *et al.*¹⁰⁴ evaluated the effect of crosslinking period on mechanical and biological properties of hyaluronic acid (HA)-based hydrogel crosslinked via hydrazone linkage, loaded with HAP and BMP-2. Three pre-incubation times that resulted in slightly (1 min), moderately (5 h) and fully cured (3 days) hydrogels at the time of their injection were compared. It was observed that longer pre-incubation times gave rise to an increase in bone volume, corresponding to a lower bone density, and changed BMP-2 release profiles, as well as, its activity. The extrusion of 3 days incubated hydrogels through the needle, during injection, created thin string-like fragments, which fused together to form a compact scaffold, providing increased mechanical stability to these hydrogels. The authors suggested the use of different pre-incubations times according to the clinical requirements.

Alginate has been used to prepare *in situ* crosslinking hydrogels incorporating various types of ceramics in the presence of calcium ions (**Table 1.3**). Such ions can be provided by an extraneous calcium solution^{74,107–110} or from dissolution of ceramics^{87,105} in the presence of D-gluconic acid δ -lactone, which accelerates the release of calcium from ceramics. Amosi *et al.*,¹¹¹ developed a ionic crosslinking hydrogel based on synthetic acidic peptide Pro–Asp–(Phe–Asp)₅–Pro (P_{FD}-5) whose gelation is triggered by calcium ions. The authors reported an improvement in bone regeneration, due to its ability to maintain the calcium ions at the defect, where they are utilized in the new bone formation, and control their availability and release.

pH-sensitive hydrogels have also been reported for the development of new IBS, particularly Si-HPMC^{72,73,112,113} (**Table 1.3**). Dissolution of Si-HPMC takes place in a strong basic medium. Hydrogel formation occurred by adding an acidic buffer to achieve both final physiological osmotic pressure and pH.

1.2.3.2| Injectable bone substitutes based on hydrogels with additional bioactivity

Hydrogels can also modulate cell colonization, as well as the healing process, since they can act as scaffolds and carriers of bioactive agents and cells. This is the case of, mainly, *in situ* crosslinking hydrogels. Although ceramic particles provide osteoconductivity to the composite, the hydrogel may incorporate other biomaterials/particles allowing to develop IBSs with improved cell adhesion, osteoinductivity and osteointegration, as well as, with antimicrobial properties (**Table 1.3**).

One strategy to improve the hydrogel's cell adhesion relies on the use of naturally derived polymer with cell adhesion sites, particularly ECM components (proteins/peptides, HA). For instance, in order to improve cell adhesion and protein adsorption in an alginate-based hydrogel, Morais *et al.*^{74,109}

associated chitosan or hyaluronate to alginate. Besides providing cell adhesion cues, natural polymers display other biological functions. HA, for example, is a non-sulfated glycosaminoglycan present in ECM, which is involved in many biological processes, such as the embryonic development, morphogenesis, tissue organization, wound healing, cell signaling¹¹⁴, and inhibition of osteoclast differentiation¹¹⁵. Many chemical modifications have been introduced on the HA chain in order to form crosslinking-based hydrogels, and it has been demonstrated that its bioactivity can be conserved^{114,116}.

The incorporation of BMP-2 into composite hydrogels has been carried out in order to improve osteoinduction (**Table 1.3**). Hydrogels can often be combined with proteins without inducing denaturation, providing protection from degradation and allowing for prolonged release. Besides HAP, BG, and other ceramic materials, especially nanosized particles, are known to be specifically prone to protein adsorption, and may thus perform as carriers of therapeutic proteins¹¹⁷.

Successful outcomes have been reported in preclinical assays, resulting from combination of injectable hydrogel with nanoHAP and BMP-2. Martínez-Sanz *et al.*¹¹⁸ studied HA-based hydrogel containing nanoHAP and BMP-2 to achieve mandibular bone augmentation in rats, using a minimally invasive method. The hydrogel worked not only as a ceramic and BMP-2 carrier, but also as an expander that defines the space to be substituted by newly formed bone. The conventional approaches used for mandibular bone augmentation involve screws, plates, incisions, dissections, graft exposure and sutures. In this study, the authors mixed the components of the hydrogel with BMP-2 and nanoHAP into syringes; the composite was injected subperiosteally through needles 25-gauge into the innate mandibular diastema. The injection procedure was quick, bloodless and resulted in fast healing with no sign of inflammation, distress or discomfort. After 8 weeks, newly formed bone was observed and the bone volume was dependent on the concentration of BMP-2 incorporated within the hydrogel. Martínez-Álvarez *et al.*¹⁰³ used HA-based hydrogel commercially available (AuxiGel™) containing nanoHAP and BMP-2 (250 µg/mL) to develop a new technique to treat congenital cleft palate, named injection/adhesion technique, which consists in two steps: i) injection of the composite at the cleft palate margins and ii) direct closure of the cleft. Cleft lip and palate remains the most prevalent major facial malformation. It has major clinical implications, requiring multidisciplinary treatment throughout childhood and the current treatments (e.g. palatoplasty) display adverse effects such as impaired mid-facial growth, with alveolar arch collapse, midface retrusion, and malocclusion. The composite hydrogel was injected into the dogs' cleft palate margins, using a needle 18-gauge. The procedure took about 30 min and was bloodless. After 4 weeks, the tested formulation had caused the cleft palate margins to reach the midline and a direct closure was done by surgeon. The observed bone augmentation was primarily attributed to the swelling of the hydrogel by the hydrolytic cleavage of some of its crosslinks and by the underlying bone formation later on. In comparison with two-flap palatoplasty, the new technique based on injectable composite hydrogel was easier, reduced trauma and pain, and overlapping or bending of palatal bone did not occur¹⁰³.

Table 1.3: Examples of injectable bone substitutes (IBSs) based on in situ gelation hydrogels.

Network formation	Hydrogel components	Ceramic filler	Other bioactive agents	Additional information	Ref.
Thermally induced crosslinking	-Chitosan - β -glycerophosphate	nanoHAP	Zinc sulphate	-Gelation <i>in situ</i> at body temperature in 10 min -Zinc ions provide antimicrobial activity -Accelerates bone formation <i>in vivo</i> (critical-sized bone defects in rat tibia)	76
		HAP: $d = 55$ nm	-Dexamethasone -BMP-2	-Dexamethasone and BMP-2 loaded on the HAP through the soak-absorbed method	80
		BG: $d = 40$ -100 nm		-Gelation temperature around 37 °C: it decreases with increasing of BG content -Composites, even with 40% of BG, workable in the liquid state -BG nanoparticles form well dispersed agglomerates, between 5 and 10 μ m in size	96
		BG: $d = 87 \pm 5$ nm	Collagen	-Injectable by an insulin syringe with ultra-fine 6 mm needle -Show proper viscous behavior and flow smoothly and evenly through the needle opening	82
		NanoHAPC	MSCs	-Injectable by a syringe with a 26-gauge needle -Gelation around 31 °C -nanoHAPC uniformly disperse in the chitosan matrix -Strong and stable composite, partially thermoreversible -Show some features of natural bone both in main composition and hierarchical structure -Able to load MSC homogeneously and provide a biocompatible environment for MSC survival <i>in vivo</i>	94,95,98-100,119

			-MSC improve the biocompatibility and enhance new bone formation <i>in vivo</i> (cancellous bone defects in rabbit femurs)	
	-PEG-PCL-PEG	Acellular bone matrix: the shape and size of granules were irregular (1-20 μm)	-Composite sterilization by ^{60}Co gamma rays -Gelation <i>in situ</i> at body temperature in a few minutes -Reinforced hydrogel due to hydrogen bonds between polymer and acellular bone matrix -Present mild cytotoxicity to MSCs (<i>in vitro</i>) and good biocompatibility in subcutaneous assays (mice) -Display enhanced bone regeneration guidance in rabbit calvarial defects	83,92
		HAP: $d = 20\text{-}40\text{ nm}$, $l = 80\text{-}120\text{ nm}$	-Collagen -Composite sterilization by ^{60}Co gamma rays -Gelation at body temperature -Hydrogen-bond formation between polymer and HAP -Enhanced cell-material interaction due to collagen -Good degradability and biocompatibility -Good performance in guided bone regeneration (rabbit calvarial defect)	77,78
Photo-crosslinking	-PEG diacrylate -Photoinitiator: Irgacure [®] 2959	HAP: $d = 20\text{-}70\text{ nm}$	-Relative low viscosities of the precursor solutions -Strong physical crosslinking between PEG diacrylate and HAP	79
	-PEG dimethacrylate -Photoinitiator: Irgacure [®] 2959	BG: $d < 45\text{ }\mu\text{m}$	-Photopolymerisation time: 10 min -Physical crosslinking between PEG dimethacrylate and BG -Do not display the inherent brittleness typically associated with BG -Suitable for cancellous bone defects, or low load bearing orthopaedic applications such as bone defect filler and coating-agent onto metallic bioimplants	120

	HAP: $d < 45 \mu\text{m}$	-Dexamethasone -Vancomycin	-Strong physical crosslinking between PEG dimethacrylate and HAP -Suitable for cancellous bone defects, or low load bearing defects -Vancomycin provides antimicrobial activity	89
	β -TCP powder	Vancomycin	-Photopolymerisation time: 10 min -Physical crosslinking between PEG dimethacrylate and β -TCP -Incorporation of β -TCP accelerates vancomycin release profile. -Suitable for cancellous bone defects, or low load bearing orthopaedic applications such as bone defect filler	90
	-Gelatin methacrylate -Photoinitiator: Irgacure® 2959	HAP: $d \approx 60 \text{ nm}$	-Improved mechanical strength -Encapsulated preosteoblasts readily elongated, proliferated, and formed a 3D interconnected network -Suitable for low load-bearing applications	85
Hydrazone crosslinking	-Aldehyde-HA -Hydrazide-Polyvinyl alcohol	-Clods of HAP: $d > 100 \mu\text{m}$ -HAP: $d = 1-50 \mu\text{m}$ -nanoHAP: $d \approx 20 \text{ nm}$ - β -TCP: $d \approx 45 \text{ nm}$	BMP-2 -A dual compartment syringe system (MiniMix™) was used -The hydrogel containing nanoHAP and BMP-2 induced ectopic bone formation with a higher density compared with the other groups	106
		HAP: $d \approx 3.39 \mu\text{m}$,	BMP-2 -Injectable by a syringe with a 21-gauge needle -Evaluation of biological effects in hydrogels with different crosslinking duration	104
	-Aldehyde-HA -Hydrazide-HA	HAP: $d \approx 30 \text{ nm}$	BMP-2 -Gelling time: 1 min -Injected after 1 h, using 25-gauge needle -Successful bone mandibular augmentation (rats)	121

				-The increase of bone volume depends on BMP-2 concentration	
Chemical Crosslinking	-AuxiGel™ (HA-based hydrogel)	HAP: $d \approx 30$ nm	BMP-2	-Hydrogel components mixture using two interconnected syringes -Gelling time: 1 min -Composite injected after 3 h -Successful development of a minimally invasive procedure to treat congenital cleft palate (facial malformation)	103
Ionic crosslinking	-Alginate -Calcium chloride	Glass-reinforced HAP: $d = 500-1000$ μm	-HA -Cerium (III) nitrate	-Polyelectrolyte complex formation between HA and alginate using cations as intermediate agents -Injectable using low extrusion forces -Cerium ions enhance antimicrobial activity	74,109
		Glass-reinforced HAP: $d = 500-1000$ μm	- Chitosan	-Polyelectrolyte complex formation between chitosan and alginate -Injectable with low extrusion forces	74
	-Alginate -Calcium sulfate	NanoHAPC		-Promote proliferation and differentiation of MSC	81
	-Alginate -Calcium sulfate -Trisodium phosphate	HAPC: $d = 50 \pm 6.6$ μm		-Trisodium phosphate avoids an abrupt gelation process: the gelling time increases with increasing of sodium (3-47 min) -Injectability of the system tunable -Good degradability and biocompatibility	107,110
	-Alginate - D-gluconic acid δ -lactone	CaS: $d = 100-150$ μm		-Gelling time can be controlled, from about 30 s to 10 min, by varying the amounts of CS and D-gluconic acid δ -lactone -Not suitable for load-bearing applications	87
	-Alginate -Glycerol	Crystalline CaP nanoparticles:		-Dual syringe system (MEDMIX®, L-system, 2.5 mm chamber, mixing tip 25 mm) used	105

	- D-gluconic acid δ -lactone	i) Monetite ii) HAP (VPP132, AAP Biomaterials)		-Gelling time controlled from seconds to 10 min by varying the solubility of the CaP phase (HAP vs monetite) or the amount of D-gluconic acid δ -lactone -Composite display biocompatibility (subcutaneous assay) and osteocompatibility (rabbit femoral condyle) -Composites disintegrate upon implantation in subcutaneous or bone tissue -Not suitable for load-bearing conditions	
	-P _{FD} -5 -Calcium chloride	Two types of 150–500 μ m β -TCP particles: i) non-porous (TCP DENTAL, Kasios) ii) 65% porous (Cerasorb M, Curasan AG)		-Peptide hydrogel itself induce better bone regeneration in comparison to non-treated defects -The hydrogel and the ceramics act synergistically to enhance bone regeneration (rat femur defect) - Superior <i>in vivo</i> regeneration with hydrogels loaded with porous β -TCP -Hydrogel accelerates β -TCP dissolution and acts as a reservoir for calcium and phosphate ions	111
pH induced crosslinking	-Si-HPMC	BCP: $d = 40\text{--}80 \mu\text{m}$	MSCs	-Sol-gel transition in about 30 min -Injectable using a syringe with a 18-gauge needle -Good biocompatibility (subcutaneous and intramuscular assays) -Support bone healing process (critically sized femoral defect in rabbits)	72,73
Enzyme induced crosslinking	-TTeC -Horseradish peroxidase -Hydrogen peroxide	BCP: $d = 60\text{--}100 \text{ nm}$		-Gelling times within a few seconds -Strong physical interactions between chitosan and BCP surface	122

Abbreviation: d – diameter; l – length; TTeC – tyramine–tetronic–grafted chitosan copolymer.

1.3 | Dextrin-based hydrogels for biomedical applications

Dextrins are a class of low molecular weight carbohydrates produced by partial hydrolysis of starch and glycogen. They are composed by a linear ($\alpha 1 \rightarrow 4$)-D-glucose residues backbone, branched with ($\alpha 1 \rightarrow 4,6$)-linked-D-glucose residues containing terminal or ($\alpha 1 \rightarrow 4$)-D-glucose oligomers (**Figure 1.5**). Some dextrins also present ($\alpha 1 \rightarrow 6$)-D-glucose residues in small percentage ^{123,124}. **Table 1.4** presents structural features of some dextrins commercially available.

Partial hydrolysis of starch can be accomplished by means of heat and acid, specific enzymatic treatments, or combined acid and enzyme hydrolysis ¹²⁵. Dextrin produced by heat is also known as pyrodextrins and they are obtained by the combinations of depolymerization (hydrolysis) and transglycosylation (molecular rearrangement). Transglycosylation produces more highly branched structures and forms glycosidic linkages not found in native starches ¹²⁶. The main enzymes used are α -amylase from *Bacillus subtilis* and pullulanase. The α -amylase is an endoenzyme that cleaves ($\alpha 1 \rightarrow 4$) bonds in amylose, while pullulanase is specific for ($\alpha 1 \rightarrow 4$) bonds, and therefore acts as a debranching enzyme ¹²⁵. Generally, acid hydrolysates contain larger amounts of residual high molar mass oligomers than their enzymatic counterparts. In summary, any dextrin is a mixture of polyglucose molecules of different chain lengths, containing an assortment of branched and linear oligosaccharides ¹²⁷.

The extent of hydrolysis is expressed in terms of “dextrose equivalent” (DE) ¹²⁸, which is a measure of the fraction of reducing sugars expressed on a dry weight basis, taking the reducing power of glucose as reference. Therefore, a dextrin with a high DE has been subjected to a larger degree of hydrolysis ¹²⁵. Depending on the source of the native starch, as well as on the hydrolysis conditions, and therefore DE, several types of dextrins can be obtained, displaying different physicochemical properties, such as viscosity, fermentability, solubility, hygroscopicity, freezing point depression, and osmolality ¹²⁸. Thus, different dextrins can be tailored for specific applications.

Dextrin is a low cost, broadly available raw material widely used in a variety of applications. Dextrin forms a strongly adherent paste mixed with water, being used as adhesive in the manufacture of gummed tapes, textiles and paper ¹²⁷. Moreover, it is used as moisturiser in cosmetics and it is accepted in nutritional products, like sports energy drinks, as a generally-recognized-as-safe (GRAS) ingredient ^{124,128}. In biomedical applications, dextrin is still relatively unexplored compared with other polysaccharides ¹²⁹. Dextrin has been clinically used as a peritoneal dialysis solution that can also perform as a drug delivery solution ^{130–133}, and as wound dressing agent ¹³⁴. Dextrin displays clinical tolerability due to its biocompatibility and non-immunogenicity, degradability by amylases, easy elimination by renal pathway, avoiding tissue accumulation due to repeated administration ^{129,135}. Therefore, dextrin is available in medical grade. During the last decade, due to its properties, which include solubility in both water and dimethylsulfoxide (DMSO) and availability of hydroxyl groups, dextrin has been explored for the design and fabrication of (nano)hydrogels suitable for drug delivery applications, tissue engineering scaffolds, excipient in tablets, bioadhesives or drug conjugates.

1.3.1| Dextrin-based hydrogels for tissue engineering applications

Carvalho *et al.*¹³⁶ developed a dextrin-based hydrogel as scaffold for biomedical applications. Soluble dextrin was modified by transesterification with vinyl acrylate (VA) in anhydrous DMSO. Hydrogels were obtained by free radical polymerization of dextrin-VA with ammonium persulfate (APS) and N,N,N',N'-tetramethylethylenediamine (TEMED), in water. This method allowed the production of dextrin with different concentrations of grafted acrylate groups (degree of substitution from ca. 10% to 70%). Then, the potential of the dextrin-VA hydrogels as a controlled release system was evaluated by accessing the diffusion of two different molecules (glucose and bovine serum albumin) from the hydrogel matrix, in the presence and absence of amyloglucosidase¹³⁷. The enzyme was used to modulate the release of proteins entrapped in the hydrogel by accelerating the hydrolysis of the dextrin-VA hydrogel. This study showed that by regulating the degree of substitution and the enzyme concentration it was possible to control the release rate, from days (low degree of substitution, higher enzyme) to months (higher degree of substitution, no enzyme).

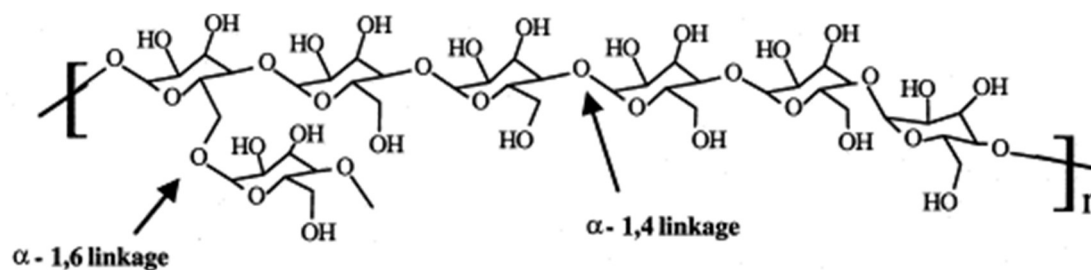
The same research group also developed a new class of dextrin-based hydrogel by derivatizing dextrin with hydroxyethyl methacrylate ester (HEMA) followed by radical polymerization in water¹³⁸. An *in vitro* comparative study performed with both dextrin hydrogels - Dextrin-VA and Dextrin-HEMA - revealed that only the later were effectively hydrolysed under physiologic conditions. In terms of biocompatibility, both hydrogels revealed negligible cell toxicity, allowing cell adhesion and proliferation¹³⁸. The *in vivo* studies confirmed the results obtained *in vitro*: the dextrin-VA hydrogels are non-degradable while the dextrin-HEMA ones are degradable; both were biocompatible, as none of them induced necrosis, immunotoxicity, nor damage to muscle tissue¹³⁹.

In order to improve the cell adhesion and surface spreading of dextrin-VA hydrogels, Moreira *et al.*¹⁴⁰ functionalized the hydrogels, using a recombinant fusion protein containing a C-terminal starch binding module (SBM) and a N-terminal Arg-Gly-Asp (RGD) sequence. The RGD sequence, present in several ECM proteins, is considered the major motif for cell adhesions. The recombinant RGD-SBM protein improved by more than 30% the adhesion and spreading of fibroblasts on the dextrin-VA hydrogel surface enhancing its biocompatibility and consequently widening its potential for biomedical application.

Ramos *et al.*¹⁴¹, developed a hydrogel by reticulation of chitosan with dextrin-VA, without crosslinking agents. It was possible to obtain hydrogels with different properties (charge, porosity, mechanical strength) by varying the ratio of chitosan to dextrin-VA, and the dextrin-VA degree of substitution. These hydrogels were simple to produce and presented interconnected micro- and macropores that made them interesting for cell and tissue culture.

Table 1.4: Glycosidic-linkage analysis of the dextrans (mol%) and estimated average degree of polymerization (DP) and percentage of branching of different commercial dextrans (adapted from ¹²³).

Dextrin	w28	w60	D4894	w35	w80	Tackidex	Icodextrin	Koldex 60
Company	Avebe	Avebe	Sigma	Avebe	Avebe	Roquette	Baxter	Tate & Lyle
T-Glcp	25.3 ± 1.2	9.9 ± 0.3	17.2 ± 2.4	12.9 ± 0.5	14.8 ± 0.3	14.4 ± 1.2	19.1 ± 2.1	11.2
(1→4)- Glcp	64.9 ± 1.7	86.2 ± 0.6	79.1 ± 1.1	84.7 ± 0.7	80.3 ± 0.9	73.7 ± 1.9	68.7 ± 3.9	85.3
(1→6)- Glcp	-	-	-	-	-	3.3 ± 0.5	0.3 ± 0.1	-
(1→4,6)- Glcp	9.8 ± 2.9	3.9 ± 0.3	3.7 ± 0.5	2.4 ± 0.2	4.9 ± 1.2	8.6 ± 0.8	11.9 ± 1.6	3.5
DP	6	17	7	10	10	16	13	13
Branching (%)	11	4	4	2	5	9	13	14

**Figure 1.5:** Chemical structure of dextrin (image adapted from ¹³⁵).

Molinos *et al.*¹⁴² described a fully resorbable and injectable dextrin-based hydrogel, produced without using chemical initiators. Dextrin was firstly oxidized with sodium periodate and then cross-linked with adipic acid dihydrazide, a non-toxic crosslinking molecule. The oxidized dextrin (ODEX) hydrogel showed good mechanical properties and biocompatibility, allowing the proliferation of mouse fibroblasts 3T3 cells on top of the gel. It was biodegradable and presented a 3D network with continuous porous structure, an important feature for gas and metabolites exchanges¹⁴². The combination of the ODEX hydrogel with nanogels and urinary bladder matrix was achieved without compromising the mechanical properties or microstructure. The encapsulation of cells, preserving its viability, confirmed the biocompatibility of the injectable hydrogels¹²³. *In vivo* biocompatibility study was performed using subcutaneous implantation in a rat model, showing that the hydrogel is a biodegradable and a non-irritant biomaterial¹⁴³. In the same study, the ODEX hydrogel was associated with granular ceramics, enabling their stabilization in the implant site. It was also shown that hMSCs carried within the hydrogel survived to the reticulation process and participated favourably on inflammatory response. In summary, the authors demonstrated that ODEX-based hydrogel is a biocompatible multifunctional matrix for minimally invasive biomedical procedures, including orthopedic surgeries when associated with bone substitutes and also as a possible encapsulation matrix for cell-based therapies¹⁴³.

1.3.2| Dextrin-based hydrogels for controlled release matrices

Pal and his research group synthesized and characterized new classes of crosslinked dextrin-based hydrogels for the preparation of tablets for the controlled release of ornidazole and ciprofloxacin, antibiotics used for the treatment of colon related disorders, via oral route administration. These novel classes of biodegradable crosslinked hydrogels are composed by dextrin grafted with i) HEMA^{144,145}, ii) polylactic acid (PLA)¹⁴⁶ or iii) *poly* (*N*-isopropylacrylamide) (NIPAm) monomers¹⁴⁷, crosslinked with *N,N'*-methylene bisacrylamide (MBA) by free-radical polymerization, in the presence of a chemical initiator – potassium persulfate (KPS) - respectively yielding the i) Dxt-g-p(HEMA), ii) Dxt-g-PLA and iii) c-Dxt/pNIPAm hydrogels. The administration of these controlled releases systems via oral route should prevent the attack of enzymes, as well as the effect of pH gradients along the gastrointestinal transit (3–16 h) from mouth to caecum. Resistance to acidic pH and enzymes along with sustained release profiles are essential features for a promising oral drug delivery matrix in controlled release system¹⁴⁷. All hydrogels displayed pH responsive behavior, biocompatibility and biodegradability. Concerning to drug release, the new hydrogel-based tablets showed more sustained release features than conventional ones (dextrin and HPMC). Moreover, the tested drugs displayed an excellent stability in the tablet formulation (close to 100 %) for up to 3 months (1 month for Dxt-g-PLA). The authors considered these delivery systems as excellent alternatives for controlled release of ornidazole and ciprofloxacin for colon drug delivery applications.

More recently, the same research group developed a dextrin and vinyl acetate-based graft copolymer (Dxt-g-pVAc) through “graft from” approach¹⁴⁸. In the first step, the macroinitiator (Dxt-Br) was prepared using 2-bromopropionyl bromide and pyridine. Then, grafting of vinyl acetate on macroinitiator was carried out in the presence of CuBr/bpy activators. Reaction parameters were varied as to achieve the graft copolymer with higher molecular weight and lower polydispersity index. The obtained hydrogel displayed biodegradability in presence of hen egg lysozyme.

In order to obtain a hydrogel with higher mechanical strength, elasticity and water absorption capacity, Guilherme *et al.*¹⁴⁹ used montmorillonite (MMT), an inorganic nanoparticle, as a crosslinking agent. For that purpose, the maltodextrin (malt-dex) and MMT were modified to incorporate carbon-carbon π -bonds (malt-dex- π and MMT- π , respectively); then, the nanocomposite copolymer hydrogel was obtained via radical crosslinking reaction of malt-dex- π with MMT- π in the presence of dimethylacrylamide. An excellent dispersion of MMT- π at the interior of the matrix was achieved, even after swelling of the nanocomposite hydrogel. It was reported that the nanocomposite hydrogel was a stable device suitable for pharmaceutical formulations where the release of solutes is dependent on a diffusional process.

1.3.3 | Dextrin-based nanogels for drug delivery

Dextrin allows the preparation of amphiphilic derivatives through conjugation with hydrophobic chains. Hydrophobized dextrans in aqueous environment self-assemble, originating hydrophobic domains able to solubilize by complexation of different type of hydrophobic molecules. Moreover, to obtain stability of the complex upon dilution in the body fluids, the amphiphilic domains must bear multiple intermolecular interactions (hydrophobic interactions), stabilizing the self-assembled structure upon dilution and allowing a low critical micelle concentration¹²⁷.

Gonçalves *et al.* modified dextrin with long alkyl chains to produce an amphiphilic molecule. Dextrin-VA-SC₁₆ (dexC₁₆) has a hydrophilic dextrin backbone with grafted acrylate groups (VA), substituted with hydrophobic 1-hexadecanethiol (SC₁₆). A versatile synthetic method was developed allowing control of the dextrin degree of substitution with the hydrophobic chains. Upon dispersion in water, dexC₁₆ self-assembled through association of the hydrophobic alkyl chains, originating spherical nanoparticles (nanogels), with high colloidal stability with a critical micelle concentration around 0.001 g/dL¹⁵⁰. Size distribution obtained by dynamic light scattering (DLS) showed two distinct populations, with 25 and 150 nm, the former being the predominant one¹⁵¹. As the uptake of nanogels by cells of the mononuclear phagocytic system limits its use as colloidal drug carriers, reducing the blood circulation time and the ability to reach biological targets, the interaction between dexC₁₆ nanogels and murine bone marrow-derived macrophages was evaluated *in vitro*¹⁵². The results showed that the nanogels were not cytotoxic and did not stimulate the production of nitric oxide by macrophages. Moreover, the nanogels were phagocytosed by macrophages and detected inside the cells, concentrated in cellular organelles. The

blood clearance was studied in BALB/c mice and it was verified that the blood removal of the nanogels occurred with a more pronounced rate in the first 3 h after administration, remaining about 30% of the material in systemic circulation at this stage¹⁵². The authors also assessed the tissue distribution of the nanogels, after intravenous injection in Wistar rats, using for that functionalized nanogels with a 1,4,7,10-tetraazacyclododecanetetraacetic acid (DOTA) metal chelator and subsequently labelled with the γ -emitting $^{153}\text{Sm}^{3+}$ radioisotope¹⁵³. The blood clearance rate and organ biodistribution of radioactively labelled nanogels were analyzed, using materials both with and without PEG surface coating. The radioactivity of the dexC₁₆ nanogels were mainly located in the organs of the mononuclear phagocyte system - liver and spleen. The functionalization of the nanogels with PEG 5,000 improved their circulation time in the bloodstream and reduced the accumulation in the liver and spleen. In order to explore the ability of dexC₁₆ nanogels as a drug carrier, curcumin was used as a model hydrophobic drug. The release profile, using sink conditions, showed that dextrin nanogel may perform as a suitable carrier for the controlled release of curcumin, overcoming the limited bioavailability of curcumin after *in vivo* administration, without using organic solvents¹⁵⁴. Further improvements on this system led to the development of nanomagnetogels, consisting of superparamagnetic iron oxide nanogels ($\gamma\text{-Fe}_2\text{O}_3$) stabilized by hydrophobic dextrin nanogel, with great potential as magnetic resonance imaging contrast agent¹⁵⁵. The loading of $\gamma\text{-Fe}_2\text{O}_3$ nanoparticles (4 nM of iron) within dexC₁₆ nanogel structure allowed iron oxide stabilization, avoiding aggregation at physiological pH, while maintaining its magnetic properties and the nanomagnetogel integrity. The biodistribution and stability of dextrin nanomagnetogels were evaluated in a mice model, using systems with and without PEGylated dextrans¹⁵⁶. The introduction of PEG chains did not affect the magnetic properties of the nanomagnetogels, inducing lower levels of spleen accumulation. Dextrin nanomagnetogels presented high stability after intravenous administration and a higher blood half-life than the commercial available formulations, which makes them attractive systems for the delivery of contrast agents.

A similar nanogel obtained by self-assembling of hydrophobized dextrin-based nanogel (Dextrin-MVA-SC₁₆ – MVA: vinyl methacrylate; SC₁₆: alkyl chain) was able to incorporate, stabilize, and enable the release over time of the Interleukin-10 (IL-10), an anti-inflammatory cytokine¹⁵⁷. The release profile of IL-10 and its biological activity were also evaluated *in vivo*, in C57 BL/6 mice¹⁵⁸. The results showed that although able to maintain a stable concentration of IL-10 for at least 4 hours in the serum of mice, the amount of protein released was rather low. Despite this, the amount of IL-10 released from the nanogels was biologically active, inhibiting tumor necrosis factor α (TNF- α) production, *in vivo*, after lipopolysaccharide (LPS) challenge. The authors concluded that additional effort is necessary to develop an effective delivery system for this cytokine, able to release active protein over longer periods of time. Nevertheless, the good biocompatibility, the protein stabilization effect and the ability to perform as a carrier with controlled release suggested that self-assembled dextrin nanogels may be useful protein delivery systems¹⁵⁸.

Another kind of nanoformulations using amphiphilic dextrin was described by Senanayake and co-workers for the treatment of drug-resistant tumors by oral delivery of nanogel-drug conjugates. Their work reported the use of nucleoside analogs (NA), such as, 5-fluoro-2'-deoxyuridine (FdU) and gemcitabine, through the conjugation with a modified dextrin nanogel. For that, dextrin was first modified with cholesterol, a hydrophobic molecule, which in an aqueous environment promoted the formation of a nanogel with a hydrophobic core, which conferred protection to the NA and also facilitated the transport of these molecules across cellular membranes, two major issues in NAs resistance. The conjugation of FdU was achieved by grafting in the hydroxyl groups of modified dextrin through a biodegradable tetraphosphate linker. The cytotoxic effect of polymeric-FdU conjugate was accessed in human prostate adenocarcinoma, breast carcinoma, hepatic carcinoma, gemcitabine-resistant follicular lymphoma and cytarabin-resistant T-lymphoma cell lines. The conjugate potentiated an increased toxicity and a lower IC_{50} value when compared to free FdU in all the cell lines, including the resistant ones, while the modified dextrin nanogel alone was not toxic ¹⁵⁹. The same research group tested the conjugation of an acylated gemcitabine in dextrin-cholesterol nanogels for the treatment of resistant tumor by oral delivery ¹⁶⁰. Such nanogel-drug conjugates were fairly stable in gastric conditions and able to actively penetrate through the gastrointestinal barrier, according to permeability studies in Caco-2 cell model. In tumor xenograft models of several drug-resistant human cancers, the authors observed an efficient inhibition of tumor growth and extended the life-span of the animals by 4 times that of the control with orally treated Gemcitabine- or Floxuridine-nanogel conjugates. In summary, the authors have demonstrated the potential of therapeutic dextrin-based nanogel conjugates with the activated and stabilized Gemcitabine as a successful oral drug delivery system against Gemcitabine-resistant and other drug-resistant tumors.

Orienti *et al.* ¹⁶¹ reported the preparation of several amphiphilic dextrans and their evaluation as complexing agents for anti-tumor hydrophobic drugs such as fenretinide, paclitaxel, etoposide, and camptothecin. Low molecular weight dextrin (Mw 1670 Da) was linked to different acyl hydrocarbon chains by direct ester bond formation. The aqueous solubility of amphiphilic dextrans, containing saturated hydrocarbon chains, decreased with increasing molecular weight of the chain. Upon dissolution, the modified dextrin induces formation of nano-aggregates endowed with hydrophobic inner cores able to host hydrophobic drugs by complexation (physical interaction). Complexation raised hydrophobic drugs aqueous solubility, the best results being obtained with fenretinide. Regarding the biological effects, the cytotoxicity of complexed fenretinide towards HTLA-230 neuroblastoma (NB) cell line was always higher than that of the free drug, suggesting that complexation increased drug bioavailability ¹⁶². In another study, fenretinide-loaded amphiphilic dextrin, in comparison with fenretinide alone, was studied both *in vitro* (human NB cells) and *in vivo* (pseudometastatic NB models). Fenretinide-loaded amphiphilic dextrin exerted a more potent cytotoxic activity on NB cells and significantly increased the proportion of sub-G1 cells, with respect to free drug. Dextrin derivatives

showed no haemolytic activity, indicating their suitability for parenteral administration. Conjugates increased the lifespan and the long-term survival of treated mice over controls. The analysis of drug plasma levels indicated that the complexed drug has a higher area under the concentration–time curve due to a reduced clearance from the blood. Thus, the dextrin injectable formulation seemed to be a good carrier for fenretinide, able to improve drug aqueous solubility and bioavailability¹⁶³.

Other approaches for chemical modifications to develop covalently crosslinked nanogels have been used. For instance, Manchun and colleagues described a nanoemulsion method to prepare dextrin nanogels sensitive to pH, followed by glyoxal crosslinking¹⁶⁴. In this method, nanoemulsion templates were prepared by high power ultrasonication in a mixture of *n*hexane/surfactants with an aqueous solution containing dextrin. The crosslinking reaction then followed, under sonication process, in presence of glyoxal. The resulted pH-sensitive linkages became attractive tools for drug delivery, especially of chemotherapy agents, targeted to tumors where the tissue pH is more acidic. Doxorubicin was used as drug model to evaluate the behavior of the dextrin pH responsive nanogels¹⁶⁵, without inducing cytotoxic side effects described for the free drug^{166,167}. *In vivo* assays demonstrated that doxorubicin-nanogel group prevented the formation of tumors in mice model, suggesting that these dextrin nanogels are effective drug carriers for inhibition of tumor growth¹⁶⁸.

Das and colleagues also reported two types of chemically crosslinked, pH responsive and biocompatible nanogels derived from dextrin as doxorubicin carrier for targeted release. The first one (*n*-Dxt-p(lactide)) was synthesized from dextrin and poly(lactide) by *in-situ* crosslinking with MBA via free radical polymerization¹⁶⁹. The second one was obtained through michael-type addition reaction using dextrin, the crosslinker MBA, acrylic acid as monomer and KPS as initiator¹⁷⁰. Both types of nanogels could efficiently encapsulate doxorubicin hydrochloride (Dox). Intracellular uptake experiment demonstrated that both were able to cross the cell membrane.

The same research group also developed a dextrin and poly(methyl methacrylate) (PMMA) based chemically crosslinked amphiphilic nanogel (*c*-Dxt/pMMA) through conventional radical polymerization with KPS initiator and MBA crosslinker for dual drugs carrier of the antibiotics ciprofloxacin and ornidazole¹⁷¹. Field emission scanning electron microscopy (FESEM) analysis confirmed that microgels have spherical shape within the range of 100 nm, whereas DLS study demonstrated that the hydrodynamic diameter of the microgel was 115-230 nm. The microgels could efficiently encapsulate both ciprofloxacin and ornidazole. The *in vitro* results of cytotoxicity assays revealed that the crosslinked microgel is non-toxic to hMSCs. Hemocompatibility study showed the safety of the nanogel for intravenous administration.

Zhang *et al.*¹⁷² developed a redox-responsive dextrin nanogel platform for targeting CXCR4, chemokine receptor, for treating of metastasis of breast cancer. The nanogel was composed by carboxylated dextrin and thiolated dextrin. The bio-reducible crosslinked dextrin nanogel (DNG) coated with AMD3100, an FDA-approved CXCR4 antagonist, was then designed to possess multiple functions,

including CXCR4 chemokine targeting, inhibition of tumor metastasis, and reduction-responsive intracellular release of doxorubicin (DOX) to reduce the cells proliferation. *In vivo* imaging and biodistribution assays revealed that AMD3100-coated DOX-DNG achieved superior accumulation in tumors because of the targeting property of AMD3100. Furthermore, the nanogel possessed remarkable anticancer activity and antimetastatic effects in 4T1 tumor-bearing Balb/C mice.

1.3.4 | Dextrin-based hydrogels for bioadhesive applications

Serrero *et al.*¹⁷³ developed hydrogels composed by maltodextrin previously oxidized by sodium periodate crosslinked with chitosan via imine linkage (Schiff Base). Its application as an adhesive of biological tissues was assessed¹⁷⁴. The study revealed that chitosan alone did not provide any significant adhesion, however, a system comprising chitosan and oxidized maltodextrin promoted the cell adhesion. Mixtures of these polysaccharides form either viscoelastic solutions or hydrogels, depending on various experimental parameters (chitosan concentration, maltodextrin degree of oxidation, molar ratio between amine and aldehyde functions, pH). The rheological behavior of each formulation was correlated to its adherence, and it was found that optimum adhesion is obtained for systems exhibiting an intermediate behavior between the viscoelastic solution and the gel.

1.4 | References

1. Clarke, B. Normal bone anatomy and physiology. *Clin. J. Am. Soc. Nephrol.* **3**, S131–S139 (2008).
2. Kini, U. & Nandeesh, B. N. in *Radionuclide and hybrid bone imaging* (eds. Fogelman, I., Gnanasegaran, G. & van der Wall, H.) 29–57 (Springer Berlin Heidelberg, 2012). doi:10.1007/978-3-642-02400-9_2
3. Sikavitsas, V. I., Temenoff, J. S. & Mikos, A. G. Biomaterials and bone mechanotransduction. *Biomaterials* **22**, 2581–2593 (2001).
4. Buckwalter, J. A.; Glimcher, M. J.; Becker, R. R. Bone Biology. *J. Bone Jt. Surg.* **77**, 1256–1275 (1995).
5. Seeley, R., Stephens, T. & Tate, P. in *Anatomy and Physiology* 166–196 (McGraw-Hill Companies, 2004). at <<https://www.zuj.edu.jo/download/seeley-anatomy-and-physiology-6th-ed-pdf/>>
6. OpenStax College. in *Anatomy & Physiology* 207–242 (OpenStax College, 2013). at <<http://cnx.org/content/col11496/latest/>>
7. Florencio-Silva, R., Sasso, G. R. da S., Sasso-Cerri, E., Simões, M. J. & Cerri, P. S. Biology of bone tissue: structure, function, and factors that influence bone cells. *Biomed Res. Int.* **2015**, 1–17 (2015).
8. Kanczler, J. & Oreffo, R. Osteogenesis and angiogenesis: The potential for engineering bone. *Eur. Cells Mater.* **15**, 100–114 (2008).
9. Gaalen, S. van *et al.* in *Tissue Engineering* (ed. Clements van Blitterswijk) 559–610 (Elsevier, 2008). doi:10.1016/B978-0-12-370869-4.00019-7
10. OsteoCord project. Bone remodelling. *Biomedical Tissue Research, University of York* (2005). at <<https://www.york.ac.uk/res/bonefromblood/background/boneremodelling.html>>
11. Tang, D. *et al.* Biofabrication of bone tissue: approaches, challenges and translation for bone regeneration. *Biomaterials* **83**, 363–382 (2016).
12. Stevens, M. M. Biomaterials for bone tissue engineering. *Mater. Today* **11**, 18–25 (2008).

13. Amini, A. A. & Nair, L. S. Injectable hydrogels for bone and cartilage repair. *Biomed. Mater.* **7**, 024105 (2012).
14. Shekaran, A. & García, A. J. Extracellular matrix-mimetic adhesive biomaterials for bone repair. *J. Biomed. Mater. Res. Part A* **96A**, 261–272 (2011).
15. Bohner, M. Resorbable biomaterials as bone graft substitutes. *Materials Today* **13**, 24–30 (2010).
16. Campana, V. *et al.* Bone substitutes in orthopaedic surgery: from basic science to clinical practice. *J. Mater. Sci. Mater. Med.* **25**, 2445–2461 (2014).
17. Medgadget. Bone graft substitute market - 2018 global analysis, growth, trends and opportunities research report forecasting to 2027. *2nd may* (2018). at <<https://www.medgadget.com/2018/05/bone-graft-substitute-market-size-statistics-growth-analysis-and-industry-facts-at-a-cagr-of-6-52-global-forecast-to-2027-marketresearchfuture-com.html>>
18. Stevens, B., Yang, Y., Mohandas, A., Stucker, B. & Nguyen, K. T. A review of materials, fabrication methods, and strategies used to enhance bone regeneration in engineered bone tissues. *J. Biomed. Mater. Res. Part B Appl. Biomater.* **85B**, 573–582 (2007).
19. Williams, D. F. On the nature of biomaterials. *Biomaterials* **30**, 5897–5909 (2009).
20. Prakasam, M., Popescu, M., Piticescu, R. & Largeteau, A. in *Scaffolds in tissue engineering - materials, technologies and clinical applications* (ed. Baino, F.) 3–30 (InTech, 2017). doi:10.5772/intechopen.70707
21. Alvarez, K. & Nakajima, H. Metallic scaffolds for bone regeneration. *Materials (Basel)*. **2**, 790–832 (2009).
22. Matassi, F., Nistri, L., Chicon Paez, D. & Innocenti, M. New biomaterials for bone regeneration. *Clin. cases Miner. bone Metab.* **8**, 21–4 (2011).
23. Amin, A. M. M. & Ewais, E. M. M. in *Scaffolds in tissue engineering - materials, technologies and clinical applications* (ed. Baino, F.) 49–74 (InTech, 2017). doi:10.5772/intechopen.70194
24. Dorozhkin, S. Calcium orthophosphate-based bioceramics. *Materials (Basel)*. **6**, 3840–3942 (2013).
25. Bohner, M. Design of ceramic-based cements and putties for bone graft substitution. *Eur. Cells Mater.* **20**, 1–12 (2010).
26. El-Ghannam, A. Bone reconstruction: from bioceramics to tissue engineering. *Expert Rev. Med. Devices* **2**, 87–101 (2005).
27. Heini, P. & Berlemann, U. Bone substitutes in vertebroplasty. *Eur. Spine J.* **10**, 205–213 (2001).
28. Schnürer, S., Gopp, U., Kühn, K. & Breusch, S. Bone substitutes. *Orthopade* **32**, 2–10 (2003).
29. Vaccaro, A. R. & Madigan, L. Spinal applications of bioabsorbable implants. *J. Neurosurg.* **97**, 407–412 (2002).
30. Eniwumide, J., Yuan, H., Cartmell, S., Meijer, G. & De Bruijn, J. Ectopic bone formation in bone marrow stem cell seeded calcium phosphate scaffolds as compared to autograft and (cell seeded) allograft. *Eur. Cells Mater.* **14**, 30–38 (2007).
31. Gupta, A. *et al.* Bone graft substitutes for spine fusion: A brief review. *World J. Orthop.* **6**, 449–56 (2015).
32. Dorozhkin, S. Bioceramics of calcium orthophosphates. *Biomaterials* **31**, 1465–1485 (2010).
33. Navarro, M., Michiardi, A., Castaño, O. & Planell, J. Biomaterials in orthopaedics. *J. R. Soc. Interface* **5**, 1137–1158 (2008).
34. Pinho, P. O. *et al.* in *Scaffolds in tissue engineering - materials, technologies and clinical applications* (ed. Baino, F.) 95–127 (InTech, 2017). doi:10.5772/intechopen.70341
35. Jones, J. R. Review of bioactive glass: from hench to hybrids. *Acta Biomater.* **9**, 4457–4486 (2013).
36. Hoppe, A., Güldal, N. S. & Boccaccini, A. R. A review of the biological response to ionic dissolution products from bioactive glasses and glass-ceramics. *Biomaterials* **32**, 2757–2774 (2011).

37. Lopes, M. ., Knowles, J. ., Santos, J. ., Monteiro, F. . & Olsen, I. Direct and indirect effects of P2O5 glass reinforced-hydroxyapatite composites on the growth and function of osteoblast-like cells. *Biomaterials* **21**, 1165–1172 (2000).
38. Atayde, L. M. *et al.* Morphology effect of bioglass-reinforced hydroxyapatite (Bonelike®) on osteoregeneration. *J. Biomed. Mater. Res. Part B Appl. Biomater.* **103**, 292–304 (2015).
39. Kim, Y.-K., Lee, J.-Y., Kim, S.-G. & Lim, S.-C. Guided bone regeneration using demineralized allogenic bone matrix with calcium sulfate: case series. *J. Adv. Prosthodont.* **5**, 167 (2013).
40. Laurencin, C., Khan, Y. & Veronick, J. in *Bone Graft Substitutes and Bone Regenerative Engineering, 2nd Edition* (eds. Laurencin, C. T. & Jiang, T.) 1–9 (ASTM International, 2014). doi:10.1520/MONO62013002501
41. Nair, L. & Laurencin, C. Biodegradable polymers as biomaterials. *Prog. Polym. Sci.* **32**, 762–798 (2007).
42. Yannas, I. in *An Introduction to Materials in Medicine* (eds. Ratner, B. D., Hoffman, A. S., Schoen, F. J. & Lemons, J. E.) (Elsevier Academic Press, 2004). at <<http://www.efn.uncor.edu/escuelas/biomedica/Plandeestudios/materias completas/biomateriales/Biomaterials Science - An Introduction to Materials in Medici.pdf>>
43. Gunatillake, P., Mayadunne, R. & Adhikari, R. *Recent developments in biodegradable synthetic polymers. Biotechnology Annual Review* **12**, (2006).
44. Liu, Y., Lim, J. & Teoh, S. H. Review: development of clinically relevant scaffolds for vascularised bone tissue engineering. *Biotechnol. Adv.* **31**, 688–705 (2013).
45. Ma, P. Scaffolds for tissue fabrication. *Materials Today* **7**, 30–40 (2004).
46. Okamoto, M. & John, B. Synthetic biopolymer nanocomposites for tissue engineering scaffolds. *Prog. Polym. Sci.* **38**, 1487–1503 (2013).
47. Stevens, M. Biomaterials for bone tissue engineering. *Mater. Today* **11**, 18–25 (2008).
48. Wahl, D. A. & Czernuszka, J. T. Collagen-hydroxyapatite composites for hard tissue repair. *Eur. Cell. Mater.* **11**, 43–56 (2006).
49. Bongio, M., van den Beucken, J. J. J. P., Leeuwenburgh, S. C. G. & Jansen, J. A. Development of bone substitute materials: from ‘biocompatible’ to ‘instructive’. *J. Mater. Chem.* **20**, 8747 (2010).
50. Navarro, M., Michiardi, A., Castaño, O. & Planell, J. A. Biomaterials in orthopaedics. *J. R. Soc. Interface* **5**, 1137–1158 (2008).
51. Bohner, M. *et al.* Synthesis and characterization of porous beta-tricalcium phosphate blocks. *Biomaterials* **26**, 6099–105 (2005).
52. Chow, L. Next generation calcium phosphate-based biomaterials. *Dent. Mater. J.* **28**, 1–10 (2009).
53. Ifkovits, J. & Burdick, J. Review: photopolymerizable and degradable biomaterials for tissue engineering applications. *Tissue Eng.* **13**, 2369–2385 (2007).
54. Kretlow, J., Klouda, L. & Mikos, A. Injectable matrices and scaffolds for drug delivery in tissue engineering. *Adv. Drug Deliv. Rev.* **59**, 263–273 (2007).
55. Temenoff, J. & Mikos, A. Injectable biodegradable materials for orthopedic tissue engineering. *Biomaterials* **21**, 2405–2412 (2000).
56. Bongio, M., van den Beucken, J. J. J. P., Leeuwenburgh, S. C. G. & Jansen, J. A. Preclinical evaluation of injectable bone substitute materials. *J. Tissue Eng. Regen. Med.* doi: **10.10**, (2012).
57. Khan, Y., Yaszemski, M., Mikos, A. & Laurencin, C. Tissue engineering of bone: material and matrix considerations. *J. Bone Joint Surg. Am.* **90 Suppl 1**, 36–42 (2008).
58. Low, K. L. *et al.* Calcium phosphate-based composites as injectable bone substitute materials. *J. Biomed. Mater. Res. - Part B Appl. Biomater.* **94**, 273–286 (2010).
59. Gauthier, O., Bouler, J. M., Aguado, E., Pilet, P. & Daculsi, G. Macroporous biphasic calcium phosphate ceramics: Influence of macropore diameter and macroporosity percentage on bone ingrowth. *Biomaterials* **19**, 133–139 (1998).
60. Carey, L., Xu, H., Simon, C., Takagi, S. & Chow, L. Premixed rapid-setting calcium phosphate

- composites for bone repair. *Biomaterials* **26**, 5002–14 (2005).
61. Xu, H., Carey, L. & Simon, C. Premixed macroporous calcium phosphate cement scaffold. *J. Mater. Sci. Mater. Med.* **18**, 1345–1353 (2007).
 62. Liu, X. & Ma, P. Polymeric scaffolds for bone tissue engineering. *Ann. Biomed. Eng.* **32**, 477–486 (2004).
 63. Daculsi, G., Uzel, A. P., Weiss, P., Goyenvalle, E. & Aguado, E. Developments in injectable multiphasic biomaterials. The performance of microporous biphasic calcium phosphate granules and hydrogels. *J. Mater. Sci. Mater. Med.* **21**, 855–61 (2010).
 64. Daculsi, G., Uzel, A. P., Cursolle, J. C., Goyenvalle, E. & Aguado, E. Scaffold effects of microporous biphasic calcium phosphate granules and role of HPMC hydrogels in injectable multiphasic bone substitute developments. *Bioceram. Dev. Appl.* **1**, 1–4 (2011).
 65. Sarkar, S. & Lee, B. Hard tissue regeneration using bone substitutes: an update on innovations in materials. *Korean J. Intern. Med.* **30**, 279–293 (2015).
 66. Fatimi, A., Tassin, J. F., Quillard, S., Axelos, M. & Weiss, P. The rheological properties of silylated hydroxypropylmethylcellulose tissue engineering matrices. *Biomaterials* **29**, 533–543 (2008).
 67. Geckil, H., Xu, F., Zhang, X., Moon, S. & Demirci, U. Engineering hydrogels as extracellular matrix mimics. *Nanomedicine* **5**, 469–484 (2010).
 68. Hoare, T. & Kohane, D. Hydrogels in drug delivery: Progress and challenges. *Polymer (Guildf)*. **49**, 1993–2007 (2008).
 69. Kim, M. *et al.* Polymeric scaffolds for regenerative medicine. *Polym. Rev.* **51**, 23–52 (2011).
 70. Zhu, J. & Marchant, R. Design properties of hydrogel tissue-engineering scaffolds. *Expert Rev. Med. Devices* **8**, 607–626 (2011).
 71. Drury, J. & Mooney, D. Hydrogels for tissue engineering: Scaffold design variables and applications. *Biomaterials* **24**, 4337–4351 (2003).
 72. Fellah, B. H. *et al.* Bone repair using a new injectable self-crosslinkable bone substitute. *J. Orthop. Res. Off. Publ. Orthop. Res. Soc.* **24**, 628–35 (2006).
 73. Trojani, C. *et al.* Ectopic bone formation using an injectable biphasic calcium phosphate/Si-HPMC hydrogel composite loaded with undifferentiated bone marrow stromal cells. *Biomaterials* **27**, 3256–3264 (2006).
 74. Morais, D. S. *et al.* Development and characterization of novel alginate-based hydrogels as vehicles for bone substitutes. *Carbohydr. Polym.* **95**, 134–142 (2013).
 75. Seris, E., Borget, P., Durand, M., Daculsi, C. & Daculsi, G. Bone regeneration at the expense of Bioceramic/Hydrogel composite: Clinical evidence. *IRBM* **34**, 342–345 (2013).
 76. Dhivya, S., Saravanan, S., Sastry, T. & Selvamurugan, N. Nanohydroxyapatite-reinforced chitosan composite hydrogel for bone tissue repair in vitro and in vivo. *J. Nanobiotechnology* **13**, 40 (2015).
 77. Fu, S. *et al.* Injectable biodegradable thermosensitive hydrogel composite for orthopedic tissue engineering. 1. Preparation and characterization of nanohydroxyapatite/ poly(ethylene glycol)-poly(ϵ -caprolactone)-poly(ethylene glycol) hydrogel nanocomposites. *J. Phys. Chem. B* **113**, 16518–16525 (2009).
 78. Fu, S. *et al.* Injectable and thermo-sensitive PEG-PCL-PEG copolymer/collagen/n-HA hydrogel composite for guided bone regeneration. *Biomaterials* **33**, 4801–4809 (2012).
 79. Gaharwar, A., Dammu, S., Canter, J., Wu, C.-J. & Schmidt, G. Highly Extensible, Tough, and Elastomeric Nanocomposite Hydrogels from Poly(ethylene glycol) and Hydroxyapatite Nanoparticles. *Biomacromolecules* **12**, 1641–1650 (2011).
 80. Gao, C., Cai, Y., Kong, X., Han, G. & Yao, J. Development and characterization of injectable chitosan-based hydrogels containing dexamethasone/rhBMP-2 loaded hydroxyapatite nanoparticles. *Mater. Lett.* **93**, 312–315 (2013).
 81. Liu, X. *et al.* The preparation and in vitro evaluations of a nanoscaled injectable bone repair material. *J. Nanomater.* **2015**, 1–8 (2015).

82. Moreira, C., Carvalho, S., Mansur, H. & Pereira, M. Thermogelling chitosan-collagen-bioactive glass nanoparticle hybrids as potential injectable systems for tissue engineering. *Mater. Sci. Eng. C. Mater. Biol. Appl.* **58**, 1207–16 (2016).
83. Ni, P.-Y. *et al.* Synthesis and characterization of injectable, thermosensitive, and biocompatible acellular bone matrix/poly(ethylene glycol)-poly(ϵ -caprolactone)-poly(ethylene glycol) hydrogel composite. *J. Biomed. Mater. Res. A* **100**, 171–9 (2012).
84. Niranjana, R. *et al.* A novel injectable temperature-sensitive zinc doped chitosan/ β -glycerophosphate hydrogel for bone tissue engineering. *Int. J. Biol. Macromol.* **54**, 24–9 (2013).
85. Sadat-Shojai, M., Khorasani, M.-T. & Jamshidi, A. 3-Dimensional cell-laden nano-hydroxyapatite/protein hydrogels for bone regeneration applications. *Mater. Sci. Eng. C. Mater. Biol. Appl.* **49**, 835–43 (2015).
86. Gaharwar, A. K., Dammu, S. A., Canter, J. M., Wu, C.-J. & Schmidt, G. Highly Extensible, Tough, and Elastomeric Nanocomposite Hydrogels from Poly(ethylene glycol) and Hydroxyapatite Nanoparticles. *Biomacromolecules* **12**, 1641–1650 (2011).
87. Han, Y., Zeng, Q., Li, H. & Chang, J. The calcium silicate/alginate composite: preparation and evaluation of its behavior as bioactive injectable hydrogels. *Acta Biomater.* **9**, 9107–17 (2013).
88. Killion, J. A. *et al.* Hydrogel/bioactive glass composites for bone regeneration applications: synthesis and characterisation. *Mater. Sci. Eng. C. Mater. Biol. Appl.* **33**, 4203–12 (2013).
89. Killion, J. A., Geever, L. M., Devine, D. M. & Higginbotham, C. L. Fabrication and in vitro biological evaluation of photopolymerisable hydroxyapatite hydrogel composites for bone regeneration. *J. Biomater. Appl.* **28**, 1274–83 (2014).
90. Killion, J. A., Geever, L. M., Devine, D. M., Farrell, H. & Higginbotham, C. L. Compressive Strength and Bioactivity Properties of Photopolymerizable Hybrid Composite Hydrogels for Bone Tissue Engineering. *Int. J. Polym. Mater. Polym. Biomater.* **63**, 641–650 (2014).
91. Nguyen, T. P., Doan, B. H. P., Dang, D. V., Nguyen, C. K. & Tran, N. Q. Enzyme-mediated in situ preparation of biocompatible hydrogel composites from chitosan derivative and biphasic calcium phosphate nanoparticles for bone regeneration. *Adv. Nat. Sci. Nanosci. Nanotechnol.* **5**, 015012 (2014).
92. Ni, P. *et al.* Injectable thermosensitive PEG-PCL-PEG hydrogel/acellular bone matrix composite for bone regeneration in cranial defects. *Biomaterials* **35**, 236–48 (2014).
93. He, C., Kim, S. & Lee, D. In situ gelling stimuli-sensitive block copolymer hydrogels for drug delivery. *J. Control. Release Off. J. Control. Release Soc.* **127**, 189–207 (2008).
94. Chen, Y. *et al.* In vitro biocompatibility and osteoblast differentiation of an injectable chitosan/nano-hydroxyapatite/collagen scaffold. *J. Nanomater.* **2012**, 1–6 (2012).
95. Chen, Y. *et al.* Noninvasive evaluation of injectable Chitosan/Nano-Hydroxyapatite/Collagen scaffold via ultrasound. *J. Nanomater.* **2012**, 1–7 (2012).
96. Couto, D., Hong, Z. & Mano, J. Development of bioactive and biodegradable chitosan-based injectable systems containing bioactive glass nanoparticles. *Acta Biomater.* **5**, 115–123 (2009).
97. Dhivya, S., Saravanan, S., Sastry, T. P. & Selvamurugan, N. Nanohydroxyapatite-reinforced chitosan composite hydrogel for bone tissue repair in vitro and in vivo. *J. Nanobiotechnology* **13**, 40 (2015).
98. Huang, Z., Feng, Q., Yu, B. & Li, S. Biomimetic properties of an injectable chitosan/nano-hydroxyapatite/collagen composite. *Mater. Sci. Eng. C* **31**, 683–687 (2011).
99. Huang, Z. *et al.* In situ-forming chitosan/nano-hydroxyapatite/collagen gel for the delivery of bone marrow mesenchymal stem cells. *Carbohydr. Polym.* **85**, 261–267 (2011).
100. Huang, Z. *et al.* In vivo bone regeneration with injectable chitosan/hydroxyapatite/collagen composites and mesenchymal stem cells. *Front. Mater. Sci.* **5**, 301–310 (2011).
101. Moreira, C. D. F., Carvalho, S. M., Mansur, H. S. & Pereira, M. M. Thermogelling chitosan-collagen-bioactive glass nanoparticle hybrids as potential injectable systems for tissue engineering. *Mater. Sci. Eng. C. Mater. Biol. Appl.* **58**, 1207–16 (2016).

102. Nguyen, K. & West, J. Photopolymerizable hydrogels for tissue engineering applications. *Biomaterials* **23**, 4307–4314 (2002).
103. Martínez-Álvarez, C. *et al.* Injection and adhesion palatoplasty: a preliminary study in a canine model. *J. Surg. Res.* **183**, 654–62 (2013).
104. Stenfelt, S. *et al.* Pre-incubation of chemically crosslinked hyaluronan-based hydrogels, loaded with BMP-2 and hydroxyapatite, and its effect on ectopic bone formation. *J. Mater. Sci. Mater. Med.* **25**, 1013–23 (2014).
105. Cardoso, D. *et al.* Gelation and biocompatibility of injectable alginate-calcium phosphate gels for bone regeneration. *J. Biomed. Mater. Res. Part A* **102**, 808–817 (2014).
106. Hulsart-Billström, G. *et al.* Calcium phosphates compounds in conjunction with hydrogel as carrier for BMP-2: A study on ectopic bone formation in rats. *Acta Biomater.* **7**, 3042–3049 (2011).
107. Tan, R., Niu, X., Gan, S. & Feng, Q. Preparation and characterization of an injectable composite. *J. Mater. Sci. Mater. Med.* **20**, 1245–53 (2009).
108. Liu, X. *et al.* The Preparation and In Vitro Evaluations of a Nanoscaled Injectable Bone Repair Material. *J. Nanomater.* **2015**, 1–8 (2015).
109. Morais, D. S. *et al.* Biological evaluation of alginate-based hydrogels, with antimicrobial features by Ce(III) incorporation, as vehicles for a bone substitute. *J. Mater. Sci. Mater. Med.* **24**, 2145–2155 (2013).
110. Tan, R. *et al.* In vitro and in vivo degradation of an injectable bone repair composite. *Polym. Degrad. Stab.* **95**, 1736–1742 (2010).
111. Amosi, N. *et al.* Acidic peptide hydrogel scaffolds enhance calcium phosphate mineral turnover into bone tissue. *Acta Biomater.* **8**, 2466–2475 (2012).
112. Sohier, J., Corre, P., Weiss, P. & Layrolle, P. Hydrogel/calcium phosphate composites require specific properties for three-dimensional culture of human bone mesenchymal cells. *Acta Biomater.* **6**, 2932–2939 (2010).
113. Struillou, X. *et al.* Treatment of periodontal defects in dogs using an injectable composite hydrogel/biphasic calcium phosphate. *J. Mater. Sci. Mater. Med.* **22**, 1707–17 (2011).
114. Burdick, J. & Prestwich, G. Hyaluronic acid hydrogels for biomedical applications. *Adv. Mater.* **23**, 41–56 (2011).
115. Chang, E.-J. *et al.* Hyaluronan inhibits osteoclast differentiation via Toll-like receptor 4. *J. Cell Sci.* **120**, 166–176 (2007).
116. Collins, M. & Birkinshaw, C. Hyaluronic acid based scaffolds for tissue engineering - A review. *Carbohydr. Polym.* **92**, 1262–1279 (2013).
117. Utech, S. & Boccaccini, A. A review of hydrogel-based composites for biomedical applications: enhancement of hydrogel properties by addition of rigid inorganic fillers. *J. Mater. Sci.* **51**, 271–310 (2016).
118. Martínez-Sanz, E. *et al.* Minimally invasive mandibular bone augmentation using injectable hydrogels. *J. Tissue Eng. Regen. Med.* **6 Suppl 3**, s15-23 (2012).
119. Huang, Z., Tian, J., Yu, B., Xu, Y. & Feng, Q. A bone-like nano-hydroxyapatite/collagen loaded injectable scaffold. *Biomed. Mater.* **4**, 055005 (2009).
120. Killion, J. *et al.* Hydrogel/bioactive glass composites for bone regeneration applications: synthesis and characterisation. *Mater. Sci. Eng. C. Mater. Biol. Appl.* **33**, 4203–12 (2013).
121. Martínez-Sanz, E. *et al.* Minimally invasive mandibular bone augmentation using injectable hydrogels. *J. Tissue Eng. Regen. Med.* **6 Suppl 3**, s15-23 (2012).
122. Nguyen, T., Doan, B. H. P., Dang, D., Nguyen, C. & Tran, N. Enzyme-mediated in situ preparation of biocompatible hydrogel composites from chitosan derivative and biphasic calcium phosphate nanoparticles for bone regeneration. *Adv. Nat. Sci. Nanosci. Nanotechnol.* **5**, 015012 (2014).
123. Silva, D. M. *et al.* Structural analysis of dextrans and characterization of dextrin-based biomedical hydrogels. *Carbohydr. Polym.* **114**, 458–466 (2014).

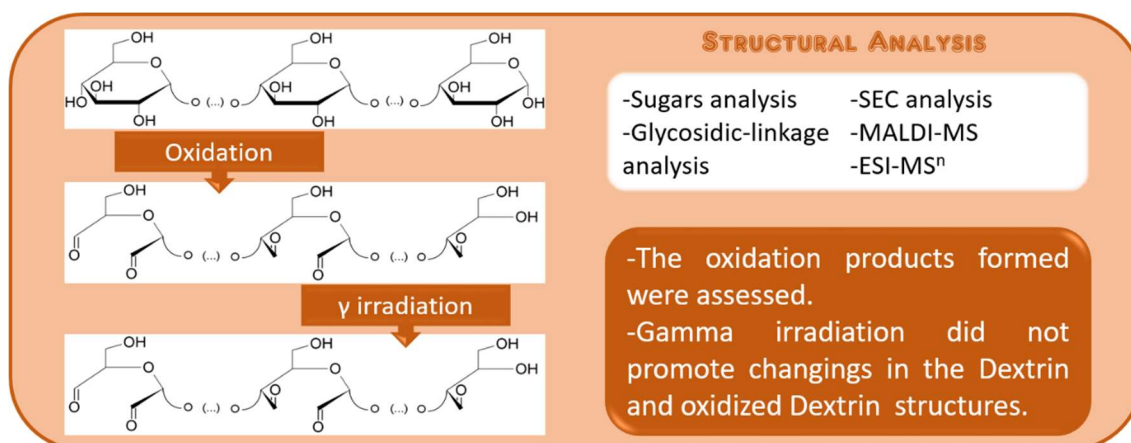
124. Tomasik, P., Wiejak, S. & Pałasiński, M. in *Advances in Carbohydrate Chemistry and Biochemistry* **47**, 279–343 (1989).
125. Chronakis, I. S. On the molecular characteristics, compositional properties, and structural-functional mechanisms of maltodextrins: a review. *Crit. Rev. Food Sci. Nutr.* **38**, 599–637 (1998).
126. BeMiller, J. N. in *Encyclopedia of Food Sciences and Nutrition* (ed. Benjamin Caballero) 1773–1775 (Elsevier, 2003). doi:10.1016/B0-12-227055-X/00331-X
127. Gonçalves, C., Moreira, S. M., Carvalho, V., Silva, D. M. & Gama, M. in *Encyclopedia of Biomedical Polymers and Polymeric Biomaterials* (ed. Mishra, M.) 2634–2649 (Taylor & Francis, 2016).
128. Hofman, D. L., van Buul, V. J. & Brouns, F. J. P. H. Nutrition, health, and regulatory aspects of digestible maltodextrins. *Crit. Rev. Food Sci. Nutr.* **56**, 2091–2100 (2016).
129. Das, D. & Pal, S. Modified biopolymer-dextrin based crosslinked hydrogels: application in controlled drug delivery. *RSC Adv.* **5**, 25014–25050 (2015).
130. Peers, E. & Gokal, R. Icodextrin provides long dwell peritoneal dialysis and maintenance of intraperitoneal volume. *Artif. Organs* **22**, 8–12 (1998).
131. Takatori, Y. *et al.* Icodextrin technique survival rate in peritoneal dialysis patients with diabetic nephropathy by improving body fluid management: a randomized controlled trial. *Clin. J. Am. Soc. Nephrol.* **6**, 1337–1344 (2011).
132. Treetharnmathurot, B. *et al.* Dextrin–trypsin and ST-HPMA–trypsin conjugates: Enzyme activity, autolysis and thermal stability. *Int. J. Pharm.* **373**, 68–76 (2009).
133. Kerr, D. J. *et al.* Prolonged intraperitoneal infusion of 5-fluorouracil using a novel carrier solution. *Br. J. Cancer* **74**, 2032–5 (1996).
134. DeBusk, A. O. V. & Alleman, T. Method for preparing medical dressings. (2006).
135. Hreczuk-Hirst, D., Chicco, D., German, L. & Duncan, R. Dextrins as potential carriers for drug targeting: tailored rates of dextrin degradation by introduction of pendant groups. *Int. J. Pharm.* **230**, 57–66 (2001).
136. Carvalho, J., Gonçalves, C., Gil, A. M. & Gama, F. M. Production and characterization of a new dextrin based hydrogel. *Eur. Polym. J.* **43**, 3050–3059 (2007).
137. Carvalho, J. M., Coimbra, M. A. & Gama, F. M. New dextrin-vinylacrylate hydrogel: Studies on protein diffusion and release. *Carbohydr. Polym.* **75**, 322–327 (2009).
138. Carvalho, J., Moreira, S., Maia, J. & Gama, F. M. Characterization of dextrin-based hydrogels: Rheology, biocompatibility, and degradation. *J. Biomed. Mater. Res. Part A* **9999A**, 398–399 (2009).
139. Moreira, S. *et al.* In Vivo Biocompatibility and Biodegradability of Dextrin-based Hydrogels. *J. Bioact. Compat. Polym.* **25**, 141–153 (2010).
140. Moreira, S. M., Andrade, F. K., Domingues, L. M. & Gama, M. Development of a strategy to functionalize a dextrin-based hydrogel for animal cell cultures using a starch-binding module fused to RGD sequence. *BMC Biotechnol.* **8**, 78 (2008).
141. Ramos, R., Carvalho, V. & Gama, M. Novel hydrogel obtained by chitosan and dextrin-VA copolymerization. *Biotechnol. Lett.* **28**, 1279–1284 (2006).
142. Molinos, M., Carvalho, V., Silva, D. M. & Gama, F. M. Development of a Hybrid Dextrin Hydrogel Encapsulating Dextrin Nanogel As Protein Delivery System. *Biomacromolecules* **13**, 517–527 (2012).
143. Silva, D. M. *et al.* Inflammatory response to dextrin-based hydrogel associated with human mesenchymal stem cells, urinary bladder matrix and Bonelike[®] granules in rat subcutaneous implants. *Biomed. Mater.* **11**, 065004 (2016).
144. Das, D. & Pal, S. Dextrin/poly (HEMA): pH responsive porous hydrogel for controlled release of ciprofloxacin. *Int. J. Biol. Macromol.* **72**, 171–178 (2015).
145. Das, D. *et al.* Dextrin cross linked with poly(HEMA): a novel hydrogel for colon specific delivery of ornidazole. *RSC Adv.* **3**, 25340 (2013).

146. Das, D., Das, R., Mandal, J., Ghosh, A. & Pal, S. Dextrin crosslinked with poly(lactic acid): A novel hydrogel for controlled drug release application. *J. Appl. Polym. Sci.* **131**, 40039 (2014).
147. Das, D. *et al.* Stimulus-responsive, biodegradable, biocompatible, covalently cross-linked hydrogel based on dextrin and poly(N -isopropylacrylamide) for in vitro/in vivo controlled drug release. *ACS Appl. Mater. Interfaces* **7**, 14338–14351 (2015).
148. Das, D. *et al.* Synthesis and characterization of biodegradable copolymer derived from dextrin and poly(vinyl acetate) via atom transfer radical polymerization. *RSC Adv.* **6**, 9352–9359 (2016).
149. Guilherme, M. R. *et al.* Porous nanocomposite hydrogel of vinylated montmorillonite-crosslinked maltodextrin-co-dimethylacrylamide as a highly stable polymer carrier for controlled release systems. *Eur. Polym. J.* **46**, 1465–1474 (2010).
150. Gonçalves, C. & José A. Martins, F. M. G. Self-Assembled Nanoparticles of Dextrin Substituted with Hexadecanethiol. *Biomacromolecules* **8**, 392–398 (2007).
151. Gonçalves, C. & Gama, F. M. Characterization of the self-assembly process of hydrophobically modified dextrin. *Eur. Polym. J.* **44**, 3529–3534 (2008).
152. Gonçalves, C. *et al.* Dextrin nanoparticles: Studies on the interaction with murine macrophages and blood clearance. *Colloids Surfaces B Biointerfaces* **75**, 483–489 (2010).
153. Gonçalves, C. *et al.* Studies on the biodistribution of dextrin nanoparticles. *Nanotechnology* **21**, 295103 (2010).
154. Gonçalves, C. Self-assembled dextrin nanogel as curcumin delivery system. *J. Biomater. Nanobiotechnol.* **03**, 178–184 (2012).
155. Gonçalves, C. *et al.* New dextrin nanomagnetogels as contrast agents for magnetic resonance imaging. *J. Mater. Chem. B* **1**, 5853 (2013).
156. Gonçalves, C. *et al.* Dextrin-based nanomagnetogel: in vivo biodistribution and stability. *Bioconjug. Chem.* **26**, 699–706 (2015).
157. Carvalho, V. *et al.* Biological activity of heterologous murine interleukin-10 and preliminary studies on the use of a dextrin nanogel as a delivery system. *Int. J. Pharm.* **400**, 234–242 (2010).
158. Carvalho, V. *et al.* Self-assembled dextrin nanogel as protein carrier: Controlled release and biological activity of IL-10. *Biotechnol. Bioeng.* **108**, 1977–1986 (2011).
159. Senanayake, T. H., Warren, G. & Vinogradov, S. V. Novel anticancer polymeric conjugates of activated nucleoside analogues. *Bioconjug. Chem.* **22**, 1983–1993 (2011).
160. Senanayake, T. H., Warren, G., Wei, X. & Vinogradov, S. V. Application of activated nucleoside analogs for the treatment of drug-resistant tumors by oral delivery of nanogel-drug conjugates. *J. Control. Release* **167**, 200–209 (2013).
161. Orienti, I. *et al.* Enhancement of oleyl alcohol anti tumor activity through complexation in polyvinylalcohol amphiphilic derivatives. *Drug Deliv.* **14**, 209–217 (2007).
162. Orienti, I., Zuccari, G., Carosio, R. & G. Montaldo, P. Improvement of aqueous solubility of fenretinide and other hydrophobic anti-tumor drugs by complexation with amphiphilic dextrans. *Drug Deliv.* **16**, 389–398 (2009).
163. Carosio, R. *et al.* Enhanced anti-neuroblastoma activity of a fenretinide complexed form after intravenous administration. *J. Pharm. Pharmacol.* **64**, 228–236 (2012).
164. Manchun, S., Dass, C. R. & Sriamornsak, P. Designing nanoemulsion templates for fabrication of dextrin nanoparticles via emulsion cross-linking technique. *Carbohydr. Polym.* **101**, 650–655 (2014).
165. Manchun, S., Dass, C. R. & Sriamornsak, P. Stability of freeze-dried pH-responsive dextrin nanogels containing doxorubicin. *Asian J. Pharm. Sci.* **11**, 648–654 (2016).
166. Manchun, S., Cheewatanakornkool, K., Dass, C. R. & Sriamornsak, P. Novel pH-responsive dextrin nanogels for doxorubicin delivery to cancer cells with reduced cytotoxicity to cardiomyocytes and stem cells. *Carbohydr. Polym.* **114**, 78–86 (2014).
167. Manchun, S., Dass, C. R. & Sriamornsak, P. Cytotoxicity of pH-responsive dextrin nanogels against

- human osteosarcoma 143B cells. *Adv. Mater. Res.* **1060**, 227–230 (2014).
168. Manchun, S., Dass, C. R., Cheewatanakornkool, K. & Sriamornsak, P. Enhanced anti-tumor effect of pH-responsive dextrin nanogels delivering doxorubicin on colorectal cancer. *Carbohydr. Polym.* **126**, 222–230 (2015).
 169. Das, D. *et al.* Dextrin and poly(lactide)-based biocompatible and biodegradable nanogel for cancer targeted delivery of doxorubicin hydrochloride. *Polym. Chem.* **7**, 2965–2975 (2016).
 170. Das, D. *et al.* Biocompatible nanogel derived from functionalized dextrin for targeted delivery of doxorubicin hydrochloride to MG 63 cancer cells. *Carbohydr. Polym.* **171**, 27–38 (2017).
 171. Das, D. *et al.* Biocompatible amphiphilic microgel derived from dextrin and poly(methyl methacrylate) for dual drugs carrier. *Polymer (Guildf)*. **107**, 282–291 (2016).
 172. Zhang, F. *et al.* CXCR4-Targeted and redox responsive dextrin nanogel for metastatic breast cancer therapy. *Biomacromolecules* **18**, 1793–1802 (2017).
 173. Serrero, A. *et al.* Polysaccharide gels based on chitosan and modified starch: structural characterization and linear viscoelastic behavior. *Biomacromolecules* **11**, 1534–1543 (2010).
 174. Serrero, A. *et al.* Polysaccharide-based adhesive for biomedical applications: correlation between rheological behavior and adhesion. *Biomacromolecules* **12**, 1556–1566 (2011).

CHAPTER 2

Effects of gamma irradiation and periodate oxidation on the structure of dextrin assessed by mass spectrometry



Sterilization of biomaterials by gamma irradiation should not change its structure, since this may affect also its bioactivity. In this work, dextrin and periodate-oxidized dextrin (ODEX), both irradiated and non-irradiated, were hydrolysed by α -amylase and the obtained oligosaccharides were fractionated by ligand-exchange/size exclusion chromatography and analyzed by matrix-assisted laser desorption/ionization (MALDI-MS) and electrospray ionization (ESI-MSⁿ) mass spectrometry. This allowed the identification of structures formed during partial periodate oxidation, which displayed aldehyde groups in different positions of dextrin backbone, according to the type of residue which was oxidized. Importantly, gamma irradiation did not structurally change either dextrin or ODEX, showing that it can be used as suitable terminal sterilization method of these materials for biomedical applications. To our best knowledge, this is the first report using MS-based techniques to evaluate the effects of partial periodate oxidation and of gamma irradiation on polysaccharides and, in particular, on dextrin and its oxidized form.

2.1 | Introduction

Dextrins are low-molecular-weight carbohydrates produced by partial hydrolysis of glycogen or starch obtained under acidic and/or enzymatic conditions¹. They are composed by a linear ($\alpha 1 \rightarrow 4$)-D-glucose residues backbone, branched with ($\alpha 1 \rightarrow 4,6$)-linked-D-glucose residues containing terminal or ($\alpha 1 \rightarrow 4$)-D-glucose oligomers. Some dextrins also present ($\alpha 1 \rightarrow 6$)-D-glucose residues in small percentage^{2,3}.

Dextrin is a low cost, broadly available raw material widely used in many industrial applications, such as adhesives in the manufacture of gummed tapes, textiles and paper, as moisturiser in cosmetics and accepted in food applications as a generally-recognized-as-safe (GRAS) ingredient^{1,3}. Regarding biomedical applications, dextrin is still relatively unexplored, being clinically used as a peritoneal dialysis solution that can also perform as a drug delivery solution⁴⁻⁶, and as wound dressing agent⁷. During last decade, due to its properties, which include the solubility in both water and DMSO, availability in medical grade, and availability of hydroxyl groups, dextrin has been explored for the design and fabrication of (nano)hydrogels suitable for controlled release applications, tissue engineering scaffolds, excipient in tablets, bioadhesives or drug conjugates. Such applications have been extensively reviewed by Gonçalves *et al.*¹ and by Das and Pal⁸.

Dextrin was used by our research group to develop a fully resorbable and injectable hydrogel. Dextrin was firstly oxidized (ODEX) with sodium periodate (NaIO_4) and then cross-linked with adipic acid dihydrazide, a non-toxic cross-linking molecule. The cross-linked ODEX is an *in situ* gelling hydrogel, able to incorporate nanogels, cells, biomolecules, and granular ceramics for bone regeneration applications^{2,9,10}.

Periodate oxidation (“glycol cleavage” oxidation) is a simple and effective method for introduction reactive groups in polysaccharide backbones. It is a catalysis-free aqueous reaction, where periodate ion (IO_4^-) attacks vicinal diols to cleave the carbon-carbon bond, leading to the formation of two aldehyde groups¹¹. Initially, this method was routinely used in the characterization and elucidation of the polysaccharide structure through complete oxidation¹¹. In later years, low and mild periodate oxidations have been used to functionalize polysaccharides: the aldehyde groups along the backbone serve as reactive chemical anchors for further reactions with nucleophilic molecules, allowing the immobilization/stabilization of drugs/biomolecules¹²⁻¹⁴ and the formation of hydrogels^{9,15,16}.

Partial periodate oxidation has been extensively investigated in many polysaccharides, such as cellulose^{17,18}, alginate^{16,19,20}, hyaluronate²¹, starch^{22,23}, pectin²⁴, chitosan²⁵, and dextran^{15,26,27}. Such works have been mainly focused on the characterization of physico-chemical properties of the oxidized derivatives, such as molecular weight (M_w), radius of gyration (R_G), persistence length, intrinsic viscosity, rheology, thermal properties, crystallinity, and reaction kinetics. Fourier transform infrared (FTIR) spectroscopy, ^1H and/or ^{13}C nuclear magnetic resonance (NMR) and colorimetric titrations have been used to detect and/or quantify the aldehydes produced, which form hydrated, hemiacetals or hemialdal

structures^{11,15,27}, allowing to determine the oxidation degree of the polysaccharides. However, published data still lacks comprehensive characterization on the polysaccharides structural modifications during partial periodate oxidation.

Sterilization is a fundamental step for the manufacturing of biomaterials and implantable medical devices. However, many sterilization procedures have been shown to deeply affect polymer properties. Ionizing sterilization is the most popular procedure for medical devices sterilization²⁸⁻³¹. No chemicals are needed, there is no additional processing and there is no waste. The main sources of radiation used in sterilization process are electron beam (e-beam) generated from electron accelerators, and gamma irradiation from radioactive sources, mainly ⁶⁰Co³⁰. Gamma irradiation has been the most used sterilization technique, while e-beam is a newer and promising process for the sterilization of medical devices. Gamma irradiation has the advantages to display a higher penetration ability, inducing homogeneous dose delivery in thick products or large batches³⁰⁻³². Nevertheless, ionizing irradiation may produce free radicals, resulting from the radiolysis of water molecules, which can react with the polysaccharide sugar residues and modify its chemical structure and molecular weight^{31,33,34}. In this context, it is relevant performing detailed studies on chemical structure of the oxidized dextrin after irradiation.

The main goal of this work was to evaluate the effect of partial periodate oxidation followed by gamma irradiation on dextrin chemical structure for biomedical applications. The sugars and glycosidic-linkage composition were analysed before and after oxidation and irradiation. Mass spectrometry (MS), namely matrix-assisted laser desorption/ionization mass spectrometry (MALDI-MS), electrospray ionization mass spectrometry (ESI-MS) and tandem mass spectrometry (ESI-MS/MS) was used to identify and characterize the structural modifications induced by oxidation and irradiation processes. For this, the samples were hydrolysed with α -amylase and further fractionated by semi-preparative ligand-exchange/size exclusion chromatography (LEX/SEC). MS has been used for the structural characterization of polysaccharides and oligosaccharides³⁵⁻³⁷, including the oxidation of oligosaccharides³⁸⁻⁴⁰. Biomolecules, and namely polysaccharides (cellulose, dextran, dextrin, etc), are being increasingly used in the field of biomedicine. Thus, the assessment of the effects of irradiation, commonly used to sterilize biomaterials, must be comprehensively carried out, in order to understand whether significant changes occur, potentially compromising functionality/bioactivity.

2.2 | Experimental

2.2.1 | Chemicals

All chemicals used were of laboratory grade from Sigma-Aldrich, unless stated otherwise. Dextrin was from Tackidex B 167 (batch E 1445), generously provided by Roquette (Lestrem, France). Its structural characterization was done in a previous study².

2.2.2 | Dextrin oxidation

Dextrin oxidation was performed as described by Molinos et al. ⁹, with some modifications. Aqueous solutions of dextrin (14 g; 2% w/v) were oxidized in the dark with 7,39 g of sodium *m*-periodate, to yield a theoretical degree of oxidation of 40%, at room temperature and with stirring. After 20 h, the oxidation reaction was stopped by adding drop wise 3,32 mL of diethylene glycol under stirring for 0,5 h to reduce any unreacted periodate. Sodium *m*-periodate and diethylene glycol were removed by ultrafiltration, using a membrane with a molecular weight cut-off of 1,000 Da (Merk Millipore, Billerica, MA, USA), and then the oxidized dextrin (ODEX) was lyophilized. The yield was about 69,5 % ± 3,3 of ODEX in each batch (n = 12 batches).

2.2.3 | Determination of bioburden and sterilization dose

The initial bioburden (initial microbiological contamination) of non-sterilized ODEX was determined using conventional microbiological techniques and according to ISO 11737-1 guidelines ⁴¹. Briefly, ODEX solutions using sterile phosphate buffered saline solution (PBS) with pH 7.4 were prepared at concentration 30% w/v, and allowed to stir for complete dissolution of ODEX and microorganisms' extraction (seven batches were used). Then, ODEX solution was plated on tryptic soy (TSA) medium (3 plates/batch) for growing of fastidious microorganisms and incubated at 30 °C. After 7 days, colony-forming units (CFU) were counted and the average bioburden determined. The obtained value was used to determine the irradiation dose necessary to obtain a sterility assurance level (SAL) of at least 10⁻⁶, using for that the tabulated values depicted in ISO 11137-2 ⁴².

2.2.4 | Gamma irradiation

Gamma irradiation was performed by IONISOS (Dagneux, France). Dextrin and ODEX were dissolved 30% w/v in PBS with pH 7.4 and irradiated using a ⁶⁰Co source, at 20 kGy (average dose rate of 2 kGy/h), at room temperature. The dextrin was also irradiated at 10 kGy (2 kGy/h) for comparison of the irradiation effects on the polysaccharide's structure.

2.2.5 | Sterility test

The efficacy of gamma irradiation sterilization for ODEX samples was evaluated by a sterility test based on conventional microbiological techniques and described in ISO 11737-2 ⁴³ with slight modifications. Briefly, after the sterilization processes, samples were transferred to test tubes containing tryptic soy broth (TSB) medium for growing of fastidious microorganisms and incubated under agitation, at 30 °C for 3 weeks. Culture medium alone served as negative control, whereas non-irradiated ODEX served as positive control. The turbidity of the broth indicated contamination and inefficient sterilization, while a clear, uncontaminated broth indicated efficient sterilization, producing a sterile solution. Sterility tests were carried out in triplicate.

2.2.6 | Sugars and linkage analyses

Neutral sugars were determined by gas chromatography (GC) as alditol acetates⁴⁴. The pre-hydrolysis was performed with 72 % of sulfuric acid (H₂SO₄) at room temperature for 3 h followed by hydrolysis for 1 h in H₂SO₄ 2 M at 120 °C. Monosaccharides were reduced with NaBH₄ (15% in NH₃ 3 M) for 1 h at 30 °C and subsequently acetylated with acetic anhydride (3 mL) in the presence of 1-methylimidazole (450 µL) for 30 min at 30 °C. Alditol acetate derivatives were separated with dichloromethane and analysed by GC with a FID detector and equipped with a 30 m column DB-225 (J&W Scientific, Folsom, CA, USA) with i.d. and film thickness of 0.25 mm and 0.15 µm, respectively. The following oven temperature program used: the initial temperature was set at 200 °C and increased at a rate of 40 °C /min until 220 °C; then it was kept constant for 7 min and again increased at a rate of 20 °C/min until 230 °C; then, the temperature was kept constant for 1 min. The injector and detector temperatures were, respectively, 220 and 230 °C. The flow rate of the carrier gas (H₂) was set at 1.7 mL/min.

Uronic acids were determined colorimetrically according to a modification⁴⁴ of the method of Blumenkrantz and Asboe-Hansen⁴⁵. Samples were prepared by pre-hydrolysis in 0.2 mL of 72 % H₂SO₄ for 3 h at room temperature followed by hydrolysis for 1 h in H₂SO₄ 1M at 100 °C. A calibration curve was made with D-galacturonic acid.

Linkage analysis was carried out by methylation as described by Ciucanu and Kerek⁴⁶ with modifications. Dextrin samples (1–2 mg) were dissolved in 1 mL of anhydrous dimethylsulfoxide (DMSO). Sodium hydroxide (NaOH) pellets were ground with a pestle in a dry mortar to get a fine powder in a N₂ atmosphere; then, powdered NaOH (about 40 mg) was added and the samples were methylated with CH₃I (80 µL) during 20 min. The samples were dissolved in 3 mL of chloroform:methanol (1:1, v/v) and dialyzed against water:ethanol (1:1, v/v) using a membrane with a molecular weight cut-off of 1000 Da. The methylated fractions were also carboxyl-reduced by a modification of the method described by Nunes *et al.*³⁷. The partially methylated alditol acetates (PMAA) were separated and analyzed by gas chromatography with mass spectrometry detector (GC–MS) on a Shimadzu GC-MS-QP2010 Plus (Kyoto, Japan). The GC was equipped with a DB-1 (J&W Scientific, Folsom, CA, USA) capillary column (30 m length, 0.25 mm of internal diameter and 0.15 µm of film thickness). The samples were injected in split less mode (time of split less 5 min), with the injector operating at 220 °C, and using the following temperature program: 45 °C for 5 min with a linear increase of 10 °C /min up to 140 °C, and standing for 5 min at this temperature, followed by linear increase of 0.5 °C /min up to 170 °C, and standing for 1 min at this temperature, followed by linear increase of 15 °C /min up to 280 °C, with further 5 min at 280 °C. The carrier gas was helium with a flow rate of 1.7 mL/min and a column head pressure of 2.8 psi. The GC was connected to an Agilent 5973 mass quadrupole selective detector operating with an electron impact mode at 70 eV and scanning the range *m/z* 40–500 in a 1 s cycle in a full scan mode acquisition.

2.2.7 | Size exclusion chromatography analysis

About 4-5 mg of ODEX was dissolved in 500 μL of 0.1 M of sodium nitrate (NaNO_3) aqueous solution at room temperature, during 180 min reaching a sample concentration of ca. 1%. The size exclusion chromatography (SEC) analysis was carried out using two PL aquagel-OH MIXED 8 μm 300 x 7.5 mm columns protected by a PL aquagel-OH Guard 8 μm pre-column on a PL-GPC 110 system (Polymer Laboratories, UK). The columns, injector system, and the detector (RI) were maintained at 36 $^\circ\text{C}$ during the analysis. The eluent (0.1 M NaNO_3) was pumped at a flow rate of 0.9 mL/min. The injected volume was 100 μL . The columns were calibrated with pullulans (Polymer Laboratories, UK) in the range 0.7-48.0 kDa, allowing the determination of an estimated value of molecular weight (M_w), designated as apparent M_w .

2.2.8 | Enzymatic hydrolysis and chromatographic separation

Dextrin and ODEX (2-3 mg) were hydrolyzed with an α -amylase (EC 3.2.1.1) from *Bacillus subtilis* (Fluka, 625 U/mg) in 1 mL ammonium hydrogen carbonate (5 mM, pH 7.0). The enzymatic hydrolysis was performed during 24 h, at 37 $^\circ\text{C}$ with continuous stirring.

The resulting oligosaccharides were separated by semi-preparative LEX/SEC on a high-performance liquid chromatograph equipped with a Shodex sugar KS 2002 column (300 mm of length and 20 mm of internal diameter) from Showa Denko K. K. (Tokyo, Japan). The column was maintained at 30 $^\circ\text{C}$, the injected sample volume was 500 μL and ultrapure water was used as eluent at a flow rate of 2.80 mL/min. A refractive index detector (Knauer K-2401, Berlin, Germany) was used. All collected fractions were dried, then neutral fractions were redissolved in 100 μL of ultrapure water, while acidic fractions were redissolved in 50 μL and kept frozen at -20 $^\circ\text{C}$ until analysis by MS. Before MS analysis, acidic fractions were decationized being incubated with AG 50W-X8 cation exchange resin (Bio-Rad Laboratories, Hercules, CA) for 15 min at room temperature.

2.2.9 | Matrix-assisted laser desorption/ionization mass spectrometry (MALDI-MS)

Samples preparation for MALDI analysis was performed by mixing 4 μL of each sample, previously dissolved in water, to 4 μL of 2,5-dihydroxybenzoic acid matrix (10 mg/mL in methanol). From this mixture, 0.5 μL were deposited on the MALDI plate, allowed to dry at ambient conditions. MALDI-MS spectra were acquired using a MALDI-TOF/TOF Applied Biosystems 4800 Proteomics Analyzer (Applied Biosystems, Framingham, MA) instrument equipped with a nitrogen laser emitting at 337 nm and operating in a reflectron mode. Full-scan mass spectra ranging from m/z 500 to 4000 were acquired in the positive mode.

2.2.10| Electrospray ionization mass spectrometry (ESI-MS) and tandem mass spectrometry (ESI-MS/MS)

The ESI-MS and ESI-MS/MS experiments were carried out in the positive mode in a LXQ linear ion trap (LIT) mass spectrometer (ThermoFinnigan, San Jose, CA). Samples were diluted in methanol/water (1:1) containing formic acid 0.1% (v/v) and introduced into the electrospray source at a flow rate of 8 μ L/min. The ESI conditions were as follows: nitrogen sheath gas 30 psi, spray voltage 5 kV, capillary temperature, 275 °C, capillary voltage 1 V, and the tube lens voltage, 40 V. Nitrogen was used as nebulizing and drying gas. ESI-MS spectra were acquired scanning the mass range from m/z 100 to 1500. In the MS/MS experiments, the collision energy used was set between 15 and 40 of normalized values. The data were processed using an Xcalibur data system (version 2.0).

2.3| Results and discussion

2.3.1| Determination of bioburden and sterility verification

The average bioburden (microbiological contamination) of ODEX before sterilization was 10.3 ± 7.5 CFU/g. A gamma irradiation dose of 20 kGy ensures the achievement of a SAL of at least 10^{-6} of the product. To confirm that such dose was enough, a sterility test after ODEX irradiation was performed. After 3 weeks of incubation in TSB, the samples were visually checked for turbidity. Sterile TSB, and irradiated ODEX were clear. At the same time, contamination evidenced by a cloudy aspect, was observed for the non-irradiated ODEX samples. Hence the results suggested that gamma irradiation at 20 kGy (2 kGy/h) effectively sterilizes ODEX solutions. The investigation of the eventual post-sterilization changes in the structure of polymers becomes fundamental, since such alterations can compromise their functionality/bioactivity.

2.3.2| Structural analysis of dextrin and ODEX

The dextrin used in this work, Tackidex, is a medical grade dextrin obtained by thermal and acidic hydrolysis of potato starch. A structural characterization of this material has been performed in a previously study², that is now extended to the oxidized and irradiated dextrin. Sugar analyses revealed that all samples of dextrin and ODEX are composed only by glucose, as confirmed by glycosidic-linkage analysis (**Table 2.1**). The oxidation process reduced the glucose amount by 44.4 % (**Table 2.1**), while gamma irradiation of ODEX did not change its amount of glucose.

Table 2.1: Glycosidic-linkage analysis of irradiated (10 and 20 kGy) and non-irradiated (mol %) dextrin and oxidized dextrin (ODEX).

Linkages	Dextrin			ODEX	
	0 kGy	10 kGy	20 kGy	0 kGy	20 kGy
T-Glcp	15.8	16.6	16.4	28.1	27.0
4-Glcp	77.0	77.3	76.3	62.2	62.5
6-Glcp	3.2	3.2	3.3	4.8	4.7
4,6-Glcp	4.0	2.8	4.1	5.3	5.8
Glucose loss %	-	-	-	44.4	44.5

In the dextrin samples, glucose occurs mainly as (1→4)-linked residues with small amounts of (1→4,6)- and (1→6)-linked residues (**Table 2.1**), as observed previously². Similar results were obtained for the ODEX samples, with a slightly higher relative amount of branched, 6-Glcp and terminally linked residues, corresponding to a lower relative amount of 4-Glcp. Nevertheless, a high loss of glucose occurred in the oxidation process, as could be expected (**Table 2.1**). Shorter and oxidized residues likely formed during the oxidation reactions, such as glyoxal and D-erythrose⁴⁷, was not detected by methylation analysis due to the higher volatility of their alditol acetates. The linkage analysis showed that gamma irradiation and oxidation processes did not induce the formation of new glycosidic bonds. The formation of new glycosidic bonds during oxidation process was not expected, since periodate ion is a highly selective glycol-cleaving oxidant¹¹. However, it is known that the aldehyde groups formed during oxidation react with nearby hydroxyl groups, forming hemiacetals or hemialdals, in water. These transitory events could be either intra or inter-residue and, in certain situations, may interfere with the oxidation evolution, the polysaccharide stability/degradability, and with the determination of oxidation degree^{11,27,48,49}. Irradiation seems not to change substantially the relative frequencies of the different linkages. It is known that gamma irradiation generates free radicals, in a dose dependent manner, which are capable of cleaving glycosidic bonds, leading to depolymerization of the polysaccharides, including starch and its derivatives⁵⁰⁻⁵⁴. The depolymerization reaction is dependent of many factors, such as atmosphere (e.g. presence or absence of O₂), temperature/phase and dose rate used during irradiation process^{30,34}. Generally, higher irradiation dose levels and/or higher dose rates promote greater depolymerization^{50-52,55-59}. The origin and type of polysaccharide are also relevant. For instance, it has been reported that alginates depolymerize even under lower doses of gamma irradiation (0,5–10 kGy)⁶⁰⁻⁶³. It is possible that the presence of carboxyl groups in alginate residues increases the production of radical species, leading to further depolymerization⁶⁴. Moreover it has been demonstrated that guluronic acid/mannuronic acid ratio is an important factor for controlling the degradation rate of sodium alginate^{62,63}. Concerning to dextrin, only one report was found⁵². In that work, dextrin (0,8–70 kDa) in solid state was irradiated at dose range between 5-100 kGy, at higher dose rate (6,316 kGy/h), and a reduction of dextrin viscosity was observed already for 5 kGy. In this work, a very small degradation

was detected in dextrin solutions irradiated 20 kGy: according to linkage analysis, dextrin displayed an increase of terminally-linked Glc residues of only 0,6% (mol) (**Table 2.1**). The concentration of the solutions was 30 % (w/v), while most works use dilute solutions (below 10 %) to study the effect of gamma irradiation^{30,65}. It has been reported that degradation decreases with increasing polysaccharide concentration (1-4 % w/v)⁵⁷⁻⁵⁹. Additionally, SEC analysis were performed to confirm whether gamma irradiation affect the oxidized dextrin. The results (**Table 2.2**) revealed that the apparent *M_w* of ODEX before (3610 Da) and after (3790 Da) gamma irradiation were very similar, as well as the polydispersity (*M_w/M_n*) – 2.11 for ODEX non-irradiated and 2.23 for ODEX irradiated at 20 kGy. The SEC results, together with the linkages analysis, suggest that gamma irradiation did not alter the length of ODEX chains or its hydrodynamic volume. It may be hypothesized that the low *M_w* of the dextrin used in this work (4,5 kDa)² makes it difficult the detection of depolymerization. Further studies should be performed, e.g. using MALLS or viscosity analysis, to evaluate the effect of the concentration of dextrin, as well as the impact of *M_w* on the depolymerisation reaction. Nevertheless, the evidences obtained point towards a very low depolymerisation under the conditions used in this work.

To our best knowledge, this is the first report that study the effect gamma irradiation on low molecular polysaccharides containing dialdehydes groups. The obtained results show that gamma irradiation can be used as a terminal sterilization process of dextrin and aldehyde-modified dextrin for biomedical applications, since it does not induce major structural modifications. Although gamma irradiation has been the most used sterilizing technique, e-beam irradiation is attracting more attention recently for the sterilization of polymeric-based medical devices³¹. Generally, e-beam irradiation causes less radiolysis than gamma irradiation, and less polymer degradation is the result of shorter processing times with higher irradiation dose rates. While gamma irradiation delivers a certain dose over a period of minutes to hours to a large volume of product, e-beam irradiation delivers the same dose in a few seconds but to a very small volume. Generally, similar radicals are formed when irradiating the materials by gamma irradiation and e-beam³². Therefore, it can be hypothesized that applying the same dose (20 kGy) of e-beam irradiation, no major structural modifications should occur. However, further studies should be performed to confirm this assumption.

Table 2.2: Results on SEC analysis of ODEX samples before and after the gamma irradiation.

Sample	<i>M_w</i> , Da	<i>M_n</i> , Da	<i>M_w/M_n</i>
ODEX	3610	1705	2.11
ODEX 20 kGy	3790	1700	2.23

2.3.3| Fractionating of oligosaccharides and modified oligosaccharides obtained by partial enzymatic hydrolysis using LEX/SEC chromatography

Dextrin and ODEX samples were selectively hydrolyzed by α -amylase, an endoglucanase which cleaves (α 1 \rightarrow 4)-D-glucose linkages. This selective hydrolysis yields oligosaccharides of low molecular

weight, allowing their separation by LEX/SEC and simplifying further MS spectra analyses. LEX/SEC provides an effective separation of acidic and neutral products, as well as the fractionation of neutral oligosaccharides according to their size^{39,40,66}.

The LEX/SEC chromatograms of dextrin and ODEX (irradiated and non-irradiated samples) are shown in **Figure 2.1**. According to previous studies³⁸⁻⁴⁰, the peak with the lowest elution time (10 min) was assigned to oligosaccharides bearing acidic residues, the one at 12 min was attributed to the enzyme, and the other peaks at 13-20 min were assigned to the neutral oligosaccharides.

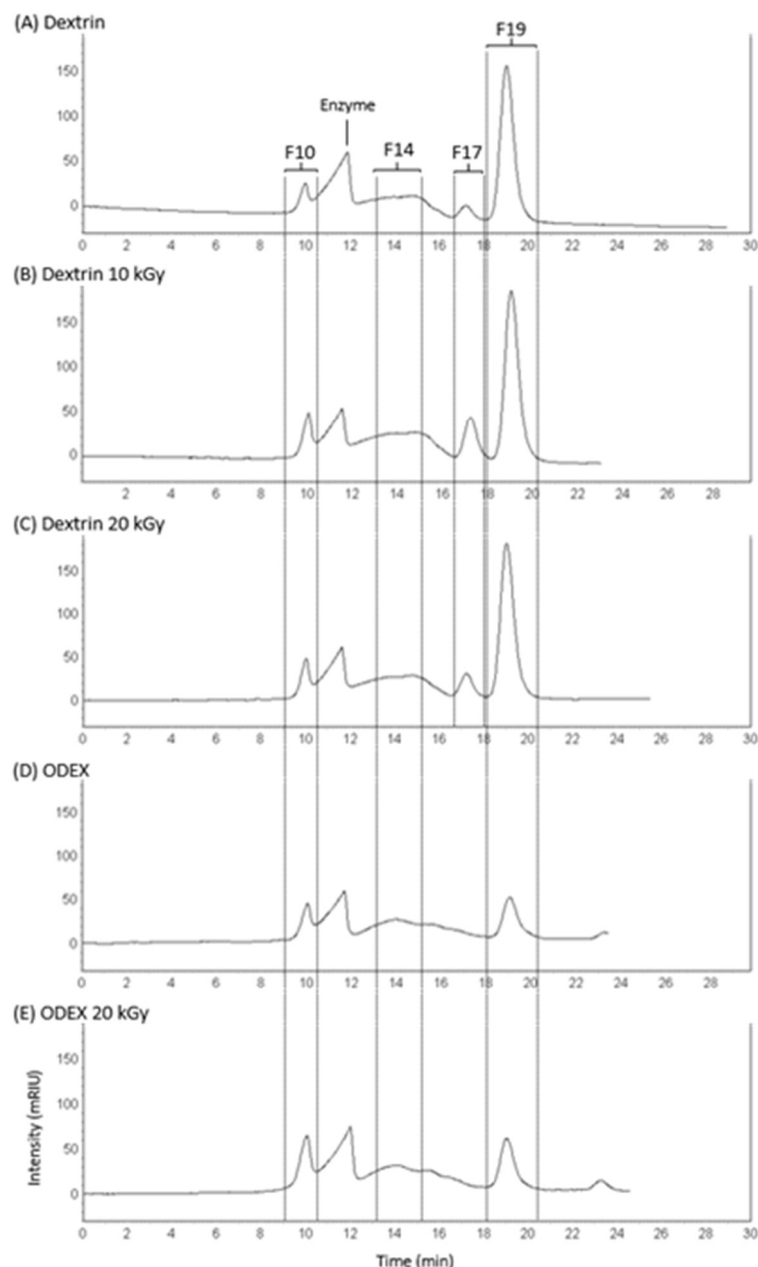


Figure 2.1: LEX/SEC chromatograms of the oligosaccharides obtained after partial enzymatic hydrolysis with α -amylase of the dextrin non-irradiated **(A)**, irradiated at 10 kGy **(B)** and at 20 kGy **(C)**, and of the ODEX non-irradiated **(D)** and irradiated at 20 kGy **(E)**.

The fractions eluted at 10 min (F10), 14 min (F14), 17 min (F17) and 19 min (F19) were selected to be analyzed by MALDI-MS, ESI-MS, and ESI-MS/MS. MS analyses allowed to assign F14, present in all samples, mainly to oligosaccharides with higher molecular weight, containing 4 to 9 residues, modified or not. The F17 observed only in dextrin samples (**Figure 2.1 (A-C)**), was assigned to oligosaccharides containing 2 and 5 residues. F19 corresponded mainly to mono-, di- and trisaccharides, also with or without modifications. The di- and trisaccharides thus eluted in fractions F17 and F19. In ODEX samples (**Figure 2.1 (D) and (E)**), the peak corresponding to F19 decreased significantly in relation to the other ones, probably due to the loss of glucose during the oxidation process. These results allowed to confirm that sodium periodate oxidation promoted structural modifications to dextrin. Comparing the chromatograms of the irradiated and non-irradiated samples, the LEX/SEC profile was similar, thus suggesting that gamma irradiation did not affect the structure of dextrin or ODEX, as observed by linkage analysis.

All samples displayed a peak at 10 min assigned to acidic oligosaccharides. However, it is possible that such peak does not correspond exclusively to acidic OS, since the analysis performed by *m*-phenylphenol, a colorimetric assay specific for uronic acids was negative for all samples. In addition, ESI-MS and MALDI-MS spectra revealed very few acidic oligosaccharides possessing carboxylic or carbonyl groups in hemiacetal form, present in trace amounts. It is known that the aldehyde groups formed during oxidation react with neighbour hydroxyl groups, forming hemiacetals, in water. These transitory events could be either intra or inter-residue^{11,27,48,49}. As the dextrin and ODEX samples were dissolved in PBS buffer, such ions interacted with the LEX/SEC matrix, eluting at the same retention time as the acidic OS. Therefore, only the MS spectra of the neutral fraction will be discussed in detail.

2.3.4| Characterization of oligosaccharides from dextrin and ODEX samples by mass spectrometry

The structural changes of dextrin associated to partial periodate oxidation and gamma irradiation were studied by MS using different ionization techniques: ESI and MALDI-MS. Analyses of oligosaccharides fractions with higher molecular weight were performed by MALDI-MS, since usually it generates only monocharged ions for larger molecules, unlike ESI-MS where multiple charged ions are commonly observed in this case⁶⁷. Thus, the fractions F14 were analyzed by MALDI-MS. On the contrary, fractions F19 were analyzed only by ESI-MS and not by MALDI-MS due to the interference of the ions formed during the matrix ionization in the observation of low molecular weight oligosaccharides (DP lower than 3). Finally, fractions F17 were analyzed by MALDI- and ESI-MS. The oligosaccharides were observed in a positive mode as $[M+Na]^+$ ions; as Glc was the only sugar detected by sugar and methylation analysis, the hexoses detected were all attributed to glucose.

2.3.4.1 | Neutral fractions from dextrin samples

The selected fractions collected from LEX/SEC chromatography of dextrin non-irradiated and irradiated at 10 kGy and at 20 kGy were analyzed, for further comparison with the oxidized ones, as well as to study the impact of gamma irradiation. The neutral series of ions observed in the fractions F14, F17, and F19 of the dextrin samples were analysed. For each fraction, the MS spectra acquired were similar among all dextrin samples (irradiated and non-irradiated ones), confirming that gamma irradiation, under the tested conditions, did not affect the chemical structure of dextrin.

In all spectra of F14, F17, and F19, the major ions observed in dextrin (irradiated and non-irradiated samples) can be attributed to the sodium adducts of a series of hexose oligosaccharides (Glc_n), bearing from one to nine glucose residues ($[\text{Glc}_n+\text{Na}]^+$, $n=[1-9]$). Small ions were also observed that may be attributed to Glc_n with less 18 Da, correspondent to dehydrated derivatives, $[\text{Glc}_n-\text{H}_2\text{O}+\text{Na}]^+$ ($n=[2-8]$). A representative MALDI-MS spectrum for F14 is presented in **Figure 2.2 (A)** and a representative ESI-MS spectrum for F19 in **Figure 2.3 (A)**, both corresponding to non-irradiated dextrin.

The ions belonging to $[\text{Glc}_n+\text{Na}]^+$ series are in accordance with that expected from the action of α -amylase on dextrin samples, and corroborate the sugar and linkage analyses. The minor series observed, $[\text{Glc}_n-\text{H}_2\text{O}+\text{Na}]^+$, as reported by Moreira *et al.*^{67,68}, which also observed dehydration products using MS-based techniques for carbohydrate analysis, may be attributed to the presence of the anomeric carbon at the reducing terminal.

2.3.4.2 | Neutral fractions from ODEX samples

For the oxidized samples (ODEX), the fractions F14 and F19 were analyzed by MALDI-MS and ESI-MS, respectively. The neutral oxidation series of ions observed of both ODEX samples and the proposed assignments were summarized in **Table 2.3**. These fractions, mainly F14, allowed to identify chemical modifications resultant from partial periodate oxidation. The MS spectra of ODEX non-irradiated (**Figure 2.2 (B)** and **2.3 (B)**) were very similar to those of the irradiated ones (**Figure 2.2 (C)** and **2.3 (C)**), displaying the same series of ions, also corroborating that gamma irradiation did not promote additional chemical modifications on ODEX structure. These results are very relevant, since as aldehydes are very reactive groups, it was hypothesized that irradiation could promote the formation of oxygen reactive species that could originate new chemical species by reacting with ODEX. For instance, some studies performed in carbohydrates subjected to oxidation with HO^\bullet generated under Fenton reaction conditions ($\text{Fe}^{2+}/\text{H}_2\text{O}_2$) demonstrated the formation of new chemical species resulted from insertion of oxygen, and the occurrence of oxidative ring scission³⁸⁻⁴⁰. However, the formations of such chemical species after ODEX irradiation was not observed in MS spectra, by comparison with ODEX non-irradiated spectra.

In the MALDI-MS spectra of the ODEX samples (**Figure 2.2 (B)** and **(C)**), it was possible to observe that the relative abundance of ions of unmodified oligosaccharides ($[\text{Glc}_n+\text{Na}]^+$ series) decreased significantly as compared to dextrin (**Figure 2.2 (A)**), and several new ions were observed. Relating to $[\text{Glc}_n-\text{H}_2\text{O}+\text{Na}]^+$

series in dextrin samples, only the ions at m/z 347 were observed in ESI-MS spectrum (Table 2.3), assigned as $[\text{Glc}_2\text{-H}_2\text{O}+\text{Na}]^+$. The new ions observed in MALDI- and ESI-MS could be attributed to oxidized oligosaccharides resulting from partial periodate oxidation process and will be described below.

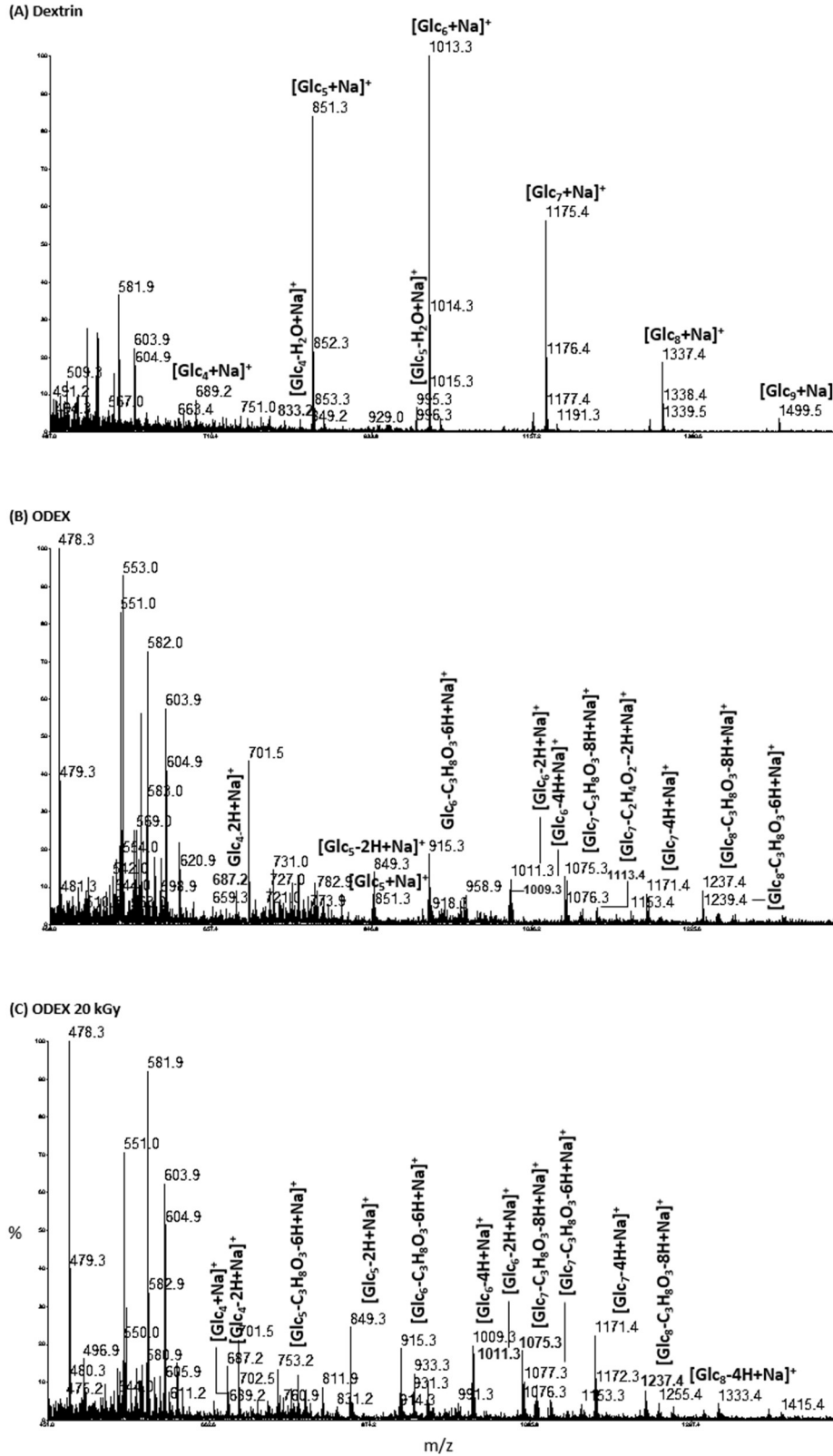


Figure 2.2: MALDI-MS spectra of the fraction that eluted at retention time of 14 minutes (F14) of dextrin non-irradiated (A), ODEX non-irradiated (B), and irradiated at 20 kGy (C).

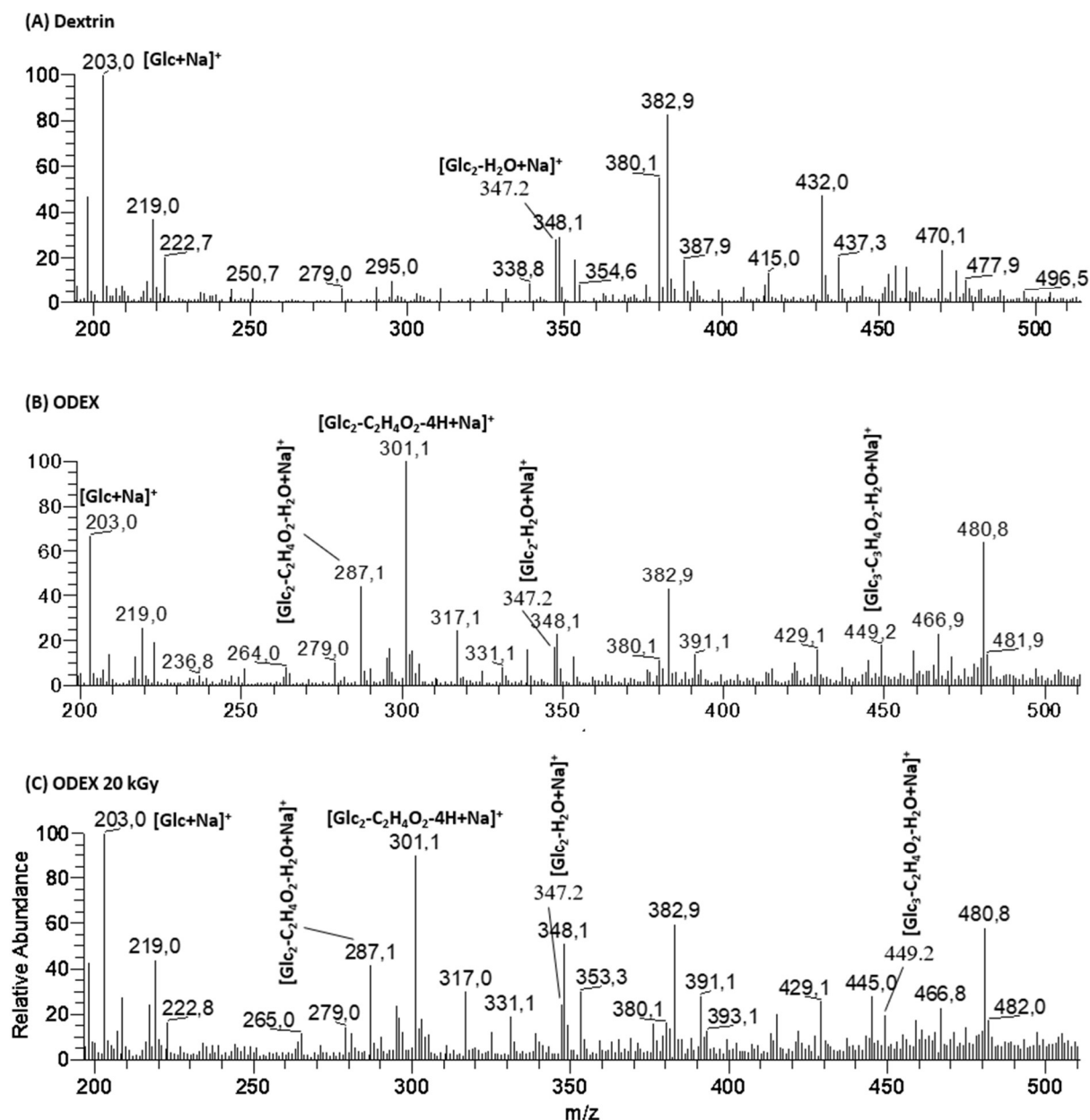


Figure 2.3: ESI-MS spectra of the fraction eluted at 19 minutes (F19) of dextrin non-irradiated (A), ODEX non-irradiated (B), and irradiated at 20 kGy (C).

The new ions observed in MALDI- and ESI-MS spectra of both ODEX samples allowed to identify ions belonging to the series with less 2 Da, 4 Da and 6 Da than the $[\text{Glc}_n+\text{Na}]^+$ series, assigned, respectively, as $[\text{Glc}_n-2\text{H}+\text{Na}]^+$, $[\text{Glc}_n-4\text{H}+\text{Na}]^+$ ($n=[4-8]$) and $[\text{Glc}_n-6\text{H}+\text{Na}]^+$ ($n=[7-8]$). These products must correspond to the oxidation of one, two or three residues of glucose of the oligosaccharides, respectively. Periodate oxidation occurs by the attack of periodate ion (IO_4^-) specifically to vicinal diols, breaking the carbon-carbon bond and yielding two aldehyde groups¹¹. As dextrin is mainly composed by (1→4)-Glc, it only contains a vicinal diol at C2-C3, which in turn can be attacked by one periodate ion, forming aldehyde groups at C2 and C3 with loss of two hydrogens (-2H) per oxidized hexose (**Figure 2.4 (A)**). For instance, the product ions at m/z 1011 and 1009 present in the F14 of ODEX spectra (**Figure 2.2 (B)** and **(C)**) resulted from the formation of two ($[\text{Glc}_6-2\text{H}+\text{Na}]^+$) or four ($[\text{Glc}_6-4\text{H}+\text{Na}]^+$) aldehydes groups,

corresponding to the oxidation of one and two (1→4)-linked residues of the oligosaccharides, respectively. It was also identified dehydrated oligosaccharides with loss of 2 Da ($[\text{Glc}_n\text{-H}_2\text{O-2H+Na}]^+$, $n=[4-7]$), 4 Da ($[\text{Glc}_n\text{-H}_2\text{O-4H+Na}]^+$, $n=[5-7]$), and one ion (m/z 1151) with loss of 6 Da, assigned as $[\text{Glc}_7\text{-H}_2\text{O-6H+Na}]^+$.

Table 2.3: Neutral oligosaccharide $[\text{M+Na}]^+$ ions from ODEX non-irradiated and irradiated at 20 kGy observed in the MALDI-MS (F14 products) and ESI-MS (F19 products) spectra, with the identification of the m/z value and the proposed assignments.

n	(*)	1	2	3	4	5	6	7	8	9
Glc_n	(0)	203[#]	365	-	689	851	1013	-	-	-
$\text{Glc}_n\text{-2H}$	(-2)	-	-	-	687	849	1011	1173	1335 ^a	-
$\text{Glc}_n\text{-4H}$	(-4)	-	-	-	685 ^b	847	1009	1171	1333 ^a	-
$\text{Glc}_n\text{-6H}$	(-6)	-	-	-	-	-	-	1169 ^a	1331 ^a	-
$\text{Glc}_n\text{-H}_2\text{O}$	(-18)	-	347	-	-	-	-	-	-	-
$\text{Glc}_n\text{-H}_2\text{O-2H}$	(-20)	-	-	-	669 ^a	831 ^a	993	1155	-	-
$\text{Glc}_n\text{-H}_2\text{O-4H}$	(-22)	-	-	-	-	829 ^a	991 ^a	1153	-	-
$\text{Glc}_n\text{-H}_2\text{O-6H}$	(-24)	-	-	-	-	-	-	1151 ^a	-	-
$\text{Glc}_n\text{-CH}_4\text{O}$	(-32)	-	-	-	-	819 ^b	981 ^a	-	-	-
$\text{Glc}_n\text{-CH}_4\text{O-2H}$	(-34)	-	-	-	-	-	979	-	-	-
$\text{Glc}_n\text{-CH}_4\text{O-8H}$	(-40)	-	-	-	-	-	-	1135 ^a	-	-
$\text{Glc}_n\text{-CH}_4\text{O-10H}$	(-42)	-	-	-	-	-	-	1133 ^a	-	-
$\text{Glc}_n\text{-C}_2\text{H}_4\text{O}_2$	(-60)	-	305	-	629 ^a	-	953 ^b	1115 ^b	-	-
$\text{Glc}_n\text{-C}_2\text{H}_4\text{O}_2\text{-2H}$	(-62)	-	303	465	627	-	951	1113	1275	-
$\text{Glc}_n\text{-C}_2\text{H}_4\text{O}_2\text{-4H}$	(-64)	-	301	-	-	-	949	1111	1273	-
$\text{Glc}_n\text{-C}_2\text{H}_4\text{O}_2\text{-6H}$	(-66)	-	-	-	-	-	-	1009 ^a	1271	-
$\text{Glc}_n\text{-C}_2\text{H}_4\text{O}_2\text{-8H}$	(-68)	-	-	-	-	-	-	-	1269 ^b	-
$\text{Glc}_n\text{-C}_2\text{H}_4\text{O}_2\text{-H}_2\text{O}$	(-78)	-	287	449	611	-	-	1097 ^a	-	-
$\text{Glc}_n\text{-C}_2\text{H}_4\text{O}_2\text{-H}_2\text{O-2H}$	(-80)	-	-	-	609 ^a	771	933	1095	1257	-
$\text{Glc}_n\text{-C}_2\text{H}_4\text{O}_2\text{-H}_2\text{O-4H}$	(-82)	-	-	445	-	-	931 ^a	1093	1255	-
$\text{Glc}_n\text{-C}_2\text{H}_4\text{O}_2\text{-H}_2\text{O-6H}$	(-84)	-	-	443	-	-	-	1091	1253	-
$\text{Glc}_n\text{-C}_3\text{H}_8\text{O}_3$	(-92)	-	-	-	597 ^a	-	-	-	-	-
$\text{Glc}_n\text{-C}_3\text{H}_8\text{O}_3\text{-4H}$	(-96)	-	-	-	593 ^b	755	917	1079	1241	-
$\text{Glc}_n\text{-C}_3\text{H}_8\text{O}_3\text{-6H}$	(-98)	-	-	-	-	753	915	1077	1239	1401 ^a
$\text{Glc}_n\text{-C}_3\text{H}_8\text{O}_3\text{-8H}$	(-100)	-	-	-	-	-	913	1075	1237	1399 ^a
$\text{Glc}_n\text{-C}_3\text{H}_8\text{O}_3\text{-10H}$	(-102)	-	-	-	-	-	-	-	1235 ^a	1397 ^a

*Values in brackets are the m/z value differences compared to the $[\text{Glc}_n\text{+Na}]^+$ ions

[#] The ions in bold were also observed in all dextrin samples

^aNot observed in ODEX non-irradiated spectrum

^bNot observed in ODEX irradiated at 20 kGy spectrum

Other series of neutral oxidation products were identified as resulting from oxidative ring scissions reactions on terminal and branched residues. Non-reducing and reducing terminals, as well as, (1→4,6)-

Glc residues, contain hydroxyl groups on each of three adjacent carbon atoms, which can be oxidized by 2 periodate ions, with the release of formic acid (HCOOH) ¹¹. Thus, the ions observed with less 60 Da than the $[\text{Glc}_n+\text{Na}]^+$ series, revealed by the ions at m/z 305, 629, 953 and 1115, were assigned to $[\text{Glc}_n-\text{C}_2\text{H}_4\text{O}_2+\text{Na}]^+$ ($n=2,4,6-7$) and resulted from the oxidation of the reducing terminal of dextrin. At this terminal, C1-C2 and C2-C3 bonds could be attacked by two periodate ions, with the formation of an aldehyde at C3 position ^{11,69}, leading to the formation of $(\text{Glc}_n-\text{C}_2\text{H}_4\text{O}_2)$ species (**Figure 2.4 (B)**). Oxidized oligosaccharides formed by carbon-carbon cleavage at reducing terminal can also display oxidative cleavages between C2-C3 at (1→4)-Glc $[\text{Glc}_n-\text{C}_2\text{H}_4\text{O}_2-m\text{H}+\text{Na}]^+$; $n=[2-8]$; $m=[2-8]$). For example, the ion at m/z 1113, observed in the MALDI-MS spectra of ODEX, can be attributed to oligosaccharide modified at the reducing terminal ($-\text{C}_2\text{H}_4\text{O}_2$) and with other modification in another glucose residue (-2H), leading to $[\text{Glc}_7-\text{C}_2\text{H}_4\text{O}_2-2\text{H}+\text{Na}]^+$.

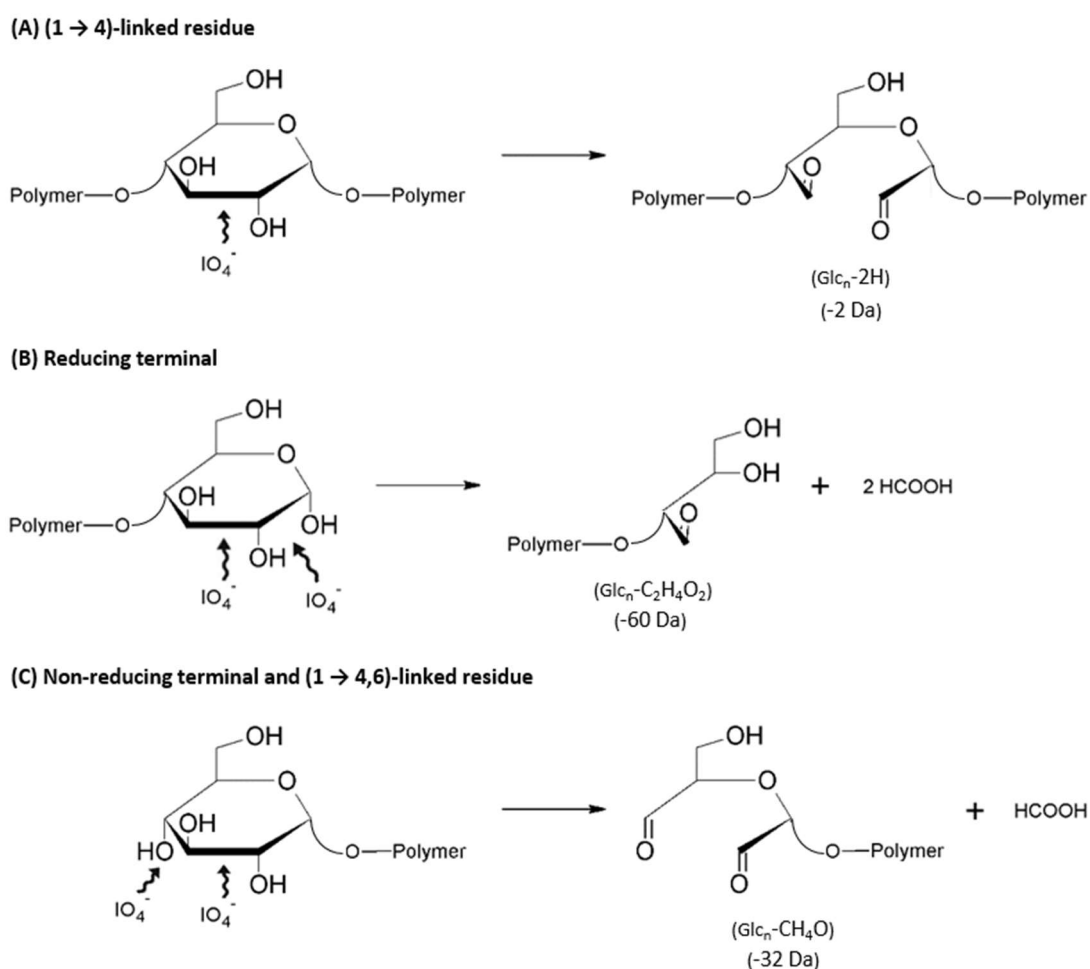


Figure 2.4: Periodate oxidation mechanism for different residues of dextrin, based on MS analysis.

The ion series with less 32 Da than the $[\text{Glc}_n+\text{Na}]^+$ series were assigned to $[\text{Glc}_n-\text{CH}_4\text{O}+\text{Na}]^+$ ($n=5-6$) and could be attributed to the oxidation of the non-reducing terminal or the (1 → 4,6)-Glc. At these residues, two periodate ions can attack the hydroxyl groups between C3–C4 and C2–C3 bonds. During these reactions occur the formation of aldehyde groups at C2 and C4 positions, and C3 is eliminated as

formic acid ^{11,70}, generating (Glc_n-CH₄O) species (**Figure 2.4 (C)**). For this series, the possibility of additional oxidation of other glucose residues was also observed, by the oxidative cleavage between C2-C3 of one (-2 Da), four (-8 Da) or five (-10 Da) residues, as revealed by the ions at *m/z* 979, 1135 and 1133, respectively.

An ion series with less 92 Da than the [Glc_n+Na]⁺ was observed and could be attributed to the oxidation of both terminal residues by periodate ions. For instance, the ion with *m/z* 597, observed in the MALDI-MS spectrum of ODEX irradiated at 20 kGy, can arise from oligosaccharides modified at the reducing (-C₂H₄O₂) and non-reducing (-CH₄O) terminals, leading to [Glc₄-C₃H₈O₃+Na]⁺. Oligosaccharides with both oxidized terminals can also present oxidative cleavages between C2-C3 at (1→4)-Glc ([Glc_n-C₃H₈O₃-mH+Na]⁺; n=[4-9]; m=[4-10]).

2.3.4.3 | Identification of structural features in oligosaccharides by tandem mass spectrometry

In order to confirm the structural features based on the MS spectra, all the oligosaccharides observed in ESI-MS from F19 were also analyzed by ESI-MS/MS. In this fraction, the only ions observed as a result of partial periodate oxidation process are belonging to series Glc_n-C₂H₄O₂, Glc_n-C₂H₄O₂-2H and Glc_n-C₂H₄O₂-4H, whose product ion spectra (ESI-MS/MS) will be described in detailed.

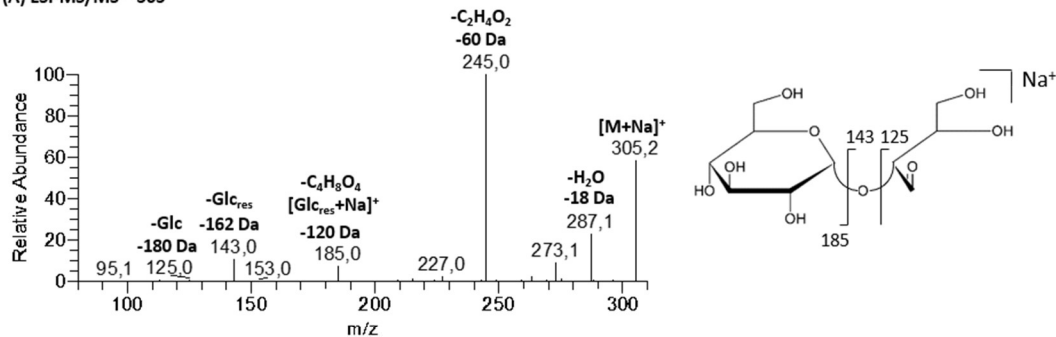
Previous studies performed on the fragmentation of [M+Na]⁺ ions of hexose oligosaccharides under ESI-MS/MS conditions exhibited a characteristic predominant loss of water (-18 Da), and loss of a hexose residue (here represented as Glc_{res}, -162 Da), due to glycosidic bond cleavage ^{38,67}. Additionally, the cross-ring cleavages (cleavage of two bonds within the sugar ring) with loss of 60 Da (-C₂H₄O₂), typical for (1→4)-linked Glc units, were also detected ³⁶.

The ion at *m/z* 305 observed in the ESI-MS/MS of ODEX samples (irradiated and non-irradiated), may correspond to [Glc₂-C₂H₄O₂+Na]⁺. The formation of this product can be attributed to the oxidation of the reducing terminal. The ESI-MS/MS spectrum (**Figure 2.5 (A)**) showed the product ion at *m/z* 185, assigned to [Glc_{res}+Na]⁺, formed due to the loss of 120 Da, indicating that this oligosaccharide bears an unmodified glucose and a tetrose (C₄H₈O₄). The presence of the tetrose resulted from the oxidative ring scission between C2 and C3 of the reducing terminal (loss of C₂H₄O₂), promoted by periodate. The product ions at *m/z* 125 and 143 are due to the loss of a Glc and Glc_{res}, respectively, confirming also that this oligosaccharide is composed by a glucose linked to a tetrose.

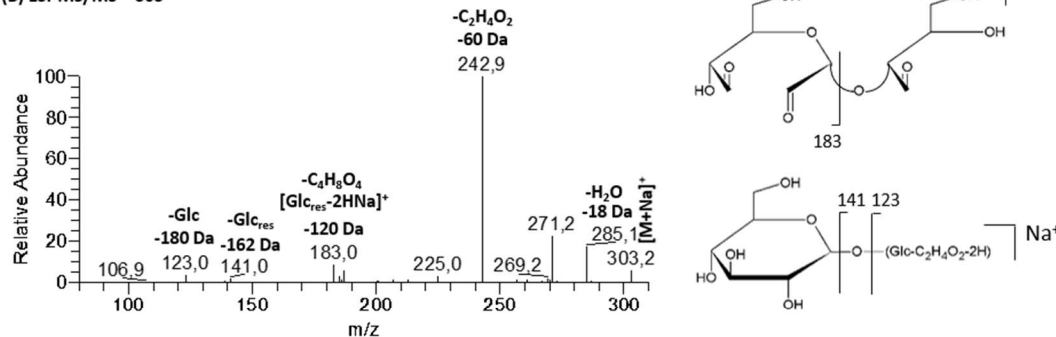
The product ion at *m/z* 303 ([Glc₂-C₂H₄O₂-2H+Na]⁺) is present in small abundance in ESI-MS spectra of the ODEX samples (irradiated and non-irradiated). The ESI-MS/MS spectrum of this ion (**Figure 2.5 (B)**) showed the product ion at *m/z* 183, assigned to [Glc_{res}-2H+Na]⁺ due to loss of 120 Da, indicating the presence of an oxidized hexose (-2H). The loss of 120 Da (-C₄H₈O₄) from the precursor ion allows to infer also that this oligosaccharide bears a tetrose at the reducing terminal, resulting from the oxidation (-C₂H₄O₂) of the initial glucose, promoted by periodate. However, the ions identified at *m/z* 123 (-Glc) and 141 (-Glc_{res}) indicate the presence of another isomer with one intact glucose, so that the loss of 2H may

occur at the reducing terminal (tetrose-2H). The trace abundance of these ions can indicate that such isomer might be present in smaller abundance, and it is possible that the reducing terminal of dextrin was already oxidized before the periodate oxidation reaction performed.

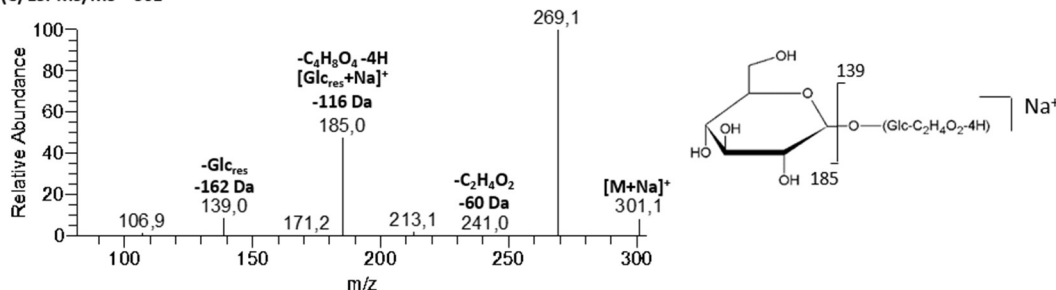
(A) ESI-MS/MS – 305



(B) ESI-MS/MS – 303



(C) ESI-MS/MS – 301



(D) ESI-MS/MS – 465

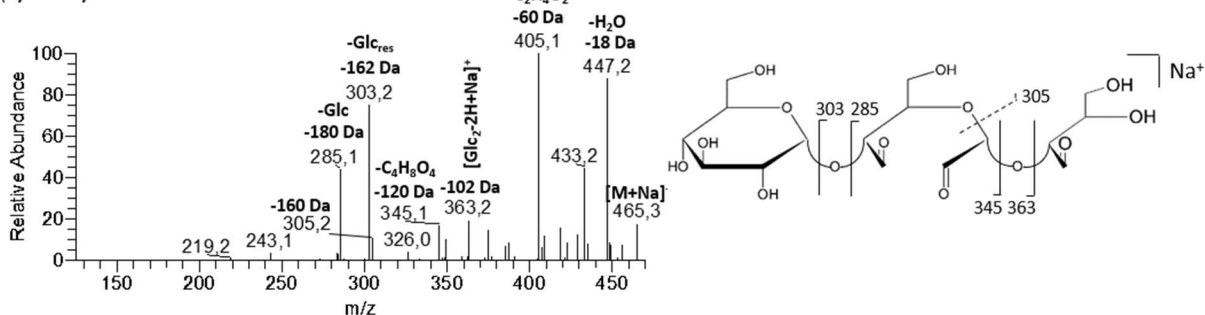


Figure 2.5: ESI-MS/MS spectra and schematic fragmentation pathways of $[M+\text{Na}]^+$ ions identified after periodate oxidation of the dextrin: (A) $[\text{Glc}_2\text{-C}_2\text{H}_4\text{O}_2+\text{Na}]^+$; (B) $[\text{Glc}_2\text{-C}_2\text{H}_4\text{O}_2\text{-}2\text{H}+\text{Na}]^+$; (C) $[\text{Glc}_2\text{-C}_2\text{H}_4\text{O}_2\text{-}4\text{H}+\text{Na}]^+$ and (D) $[\text{Glc}_3\text{-C}_2\text{H}_4\text{O}_2\text{-}2\text{H}+\text{Na}]^+$.

The ion at m/z 301 is one of the most prominent ions in the ESI-MS spectra of the ODEX samples (irradiated and non-irradiated) and can be attributed to $[\text{Glc}_2\text{-C}_2\text{H}_4\text{O}_2\text{-}4\text{H}+\text{Na}]^+$. The ESI-MS/MS spectrum

(**Figure 2.5 (C)**) showed the product ions at m/z 139 ($-\text{Glc}_{\text{res}}$) and 185 ($[\text{Glc}+\text{Na}]^+$) which confirm the presence of an intact glucose residue. The loss of 116 Da from the precursor ion suggests that this oligosaccharide bears a modified tetrose at the reducing terminal (tetrose-4H). However, the absence of other peaks hinders the identification of the exact locations of the loss of 4H.

The ion at m/z 465 is present in ESI-MS spectra of the ODEX samples (irradiated and non-irradiated) in residual abundance and was assigned to an oligosaccharide bearing a tetrose as a result of oxidation of the reducing terminal, and with one (1 \rightarrow 4)-Glc residue oxidized ($[\text{Glc}_3-\text{C}_2\text{H}_4\text{O}_2-2\text{H}+\text{Na}]^+$). The ESI-MS/MS spectrum (**Figure 2.5 (D)**) showed the ion at m/z 363, assigned to $[\text{Glc}_2-2\text{H}+\text{Na}]^+$, indicating that one glucose suffered an oxidative ring scission at C3-C4 bond. The ions at m/z 303 (-162 Da) and at m/z 285 (-180 Da), formed by loss of a Glc_{res} and Glc, respectively, indicate that the non-reducing terminal is composed by an unmodified glucose and the oxidative ring scission occurred in the middle of the oligosaccharide, originating aldehyde groups at C2 and C3, as confirmed by ion at m/z 305. The products ions at m/z 345 and 363, corresponding to the loss of 120 Da and 102 Da respectively, confirm that oligosaccharide contains a tetrose ($\text{C}_4\text{H}_8\text{O}_4$) at the reducing terminal caused by oxidative ring scission between C2 and C3 (loss of $\text{C}_2\text{H}_4\text{O}_2$) promoted by periodate.

2.4 | Conclusions

In this study, different MS-based techniques (MALDI-MS, ESI-MS and ESI-MS/MS) were used, for the first time, for identification and characterization of dextrin structural modifications related to partial periodate oxidation. The results obtained confirmed that periodate ion is a glycol-cleaving oxidant highly selective, leading to formation of aldehydes groups. The results showed that during periodate oxidation reaction three major series of oxidation products are formed, according to the type of residue of the dextrin backbone which is attacked by periodate ion: i) the oxidation of (1 \rightarrow 4)-Glc residues leads to the formation of ($\text{Glc}_n\text{-mH}$; $n=[4-8]$; $m=[2-6]$) species; ii) the oxidation of reducing terminal residues, leads to the formation of ($\text{Glc}_n\text{-C}_2\text{H}_4\text{O}_2$; $n=[5-7]$) species, and iii) the oxidation of non-reducing terminal or (1 \rightarrow 4,6)-Glc residues produces ($\text{Glc}_n\text{-CH}_4\text{O}$; $n=[2-8]$) species. Oxidation products containing more than one type of residue oxidized were also identified.

Gamma irradiation is a commonly used method to sterilize biomaterials for biomedical applications. However, the impact of this sterilization procedure on the biomaterial structure/functionality has not been sufficiently addressed, in particular in the case of biological materials such as oxidized polysaccharides. In this study, it was demonstrated that gamma irradiation can be used as suitable terminal sterilization method for ODEX and dextrin related biomaterials. Indeed, sugars and glycosidic-linkage, as well as MS analysis showed that sterilizing gamma irradiation, under the tested conditions, did not promote changes on the chemical structure of dextrin or ODEX. It can be hypothesized that gamma irradiation will also not impact significantly the structure of other polysaccharides relevant in biomedicine, such as pullulan, alginate, cellulose and dextran.

2.5 | References

1. Gonçalves, C., Moreira, S. M., Carvalho, V., Silva, D. M. & Gama, M. in *Encyclopedia of Biomedical Polymers and Polymeric Biomaterials* (ed. Mishra, M.) 2634–2649 (Taylor & Francis, 2016).
2. Silva, D. M. *et al.* Structural analysis of dextrans and characterization of dextrin-based biomedical hydrogels. *Carbohydr. Polym.* **114**, 458–466 (2014).
3. Tomasik, P., Wiejak, S. & Pałasiński, M. in *Advances in Carbohydrate Chemistry and Biochemistry* **47**, 279–343 (1989).
4. Peers, E. & Gokal, R. Icodextrin provides long dwell peritoneal dialysis and maintenance of intraperitoneal volume. *Artif. Organs* **22**, 8–12 (1998).
5. Takatori, Y. *et al.* Icodextrin Increases Technique Survival Rate in Peritoneal Dialysis Patients with Diabetic Nephropathy by Improving Body Fluid Management: A Randomized Controlled Trial. *Clin. J. Am. Soc. Nephrol.* **6**, 1337–1344 (2011).
6. Treetharnmathurot, B. *et al.* Dextrin–trypsin and ST-HPMA–trypsin conjugates: Enzyme activity, autolysis and thermal stability. *Int. J. Pharm.* **373**, 68–76 (2009).
7. DeBusk, A. O. V. & Alleman, T. Method for preparing medical dressings. (2006).
8. Das, D. & Pal, S. Modified biopolymer-dextrin based crosslinked hydrogels: application in controlled drug delivery. *RSC Adv.* **5**, 25014–25050 (2015).
9. Molinos, M., Carvalho, V., Silva, D. M. & Gama, F. M. Development of a Hybrid Dextrin Hydrogel Encapsulating Dextrin Nanogel As Protein Delivery System. *Biomacromolecules* **13**, 517–527 (2012).
10. Silva, D. M. *et al.* Inflammatory response to dextrin-based hydrogel associated with human mesenchymal stem cells, urinary bladder matrix and Bonelike[®] granules in rat subcutaneous implants. *Biomed. Mater.* **11**, 65004 (2016).
11. Perlin, A. S. in *Advances in Carbohydrate Chemistry and Biochemistry* **60**, 183–250 (2006).
12. Takei, T., Sato, M., Ijima, H. & Kawakami, K. In Situ Gellable Oxidized Citrus Pectin for Localized Delivery of Anticancer Drugs and Prevention of Homotypic Cancer Cell Aggregation. *Biomacromolecules* **11**, 3525–3530 (2010).
13. Xiao, S. *et al.* Dialdehyde starch nanoparticles as antitumor drug delivery system: An in vitro, in vivo, and immunohistological evaluation. *Chinese Sci. Bull.* **57**, 3226–3232 (2012).
14. Ragothaman, M., Palanisamy, T. & Kalirajan, C. Collagen–poly(dialdehyde) guar gum based porous 3D scaffolds immobilized with growth factor for tissue engineering applications. *Carbohydr. Polym.* **114**, 399–406 (2014).
15. Maia, J., Ferreira, L., Carvalho, R., Ramos, M. A. & Gil, M. H. Synthesis and characterization of new injectable and degradable dextran-based hydrogels. *Polymer (Guildf)*. **46**, 9604–9614 (2005).
16. Gomez, C. G., Rinaudo, M. & Villar, M. A. Oxidation of sodium alginate and characterization of the oxidized derivatives. *Carbohydr. Polym.* **67**, 296–304 (2007).
17. Potthast, A., Kostic, M., Schiehsler, S., Kosma, P. & Rosenau, T. Studies on oxidative modifications of cellulose in the periodate system: Molecular weight distribution and carbonyl group profiles. *Holzforschung* **61**, 662–667 (2007).
18. Rinaudo, M. Periodate Oxidation of Methylcellulose: Characterization and Properties of Oxidized Derivatives. *Polymers (Basel)*. **2**, 505–521 (2010).
19. Vold, I. M. N., Kristiansen, K. A. & Christensen, B. E. A Study of the Chain Stiffness and Extension of Alginates, in Vitro Epimerized Alginates, and Periodate-Oxidized Alginates Using Size-Exclusion Chromatography Combined with Light Scattering and Viscosity Detectors. *Biomacromolecules* **7**, 2136–2146 (2006).
20. Kristiansen, K. A., Tomren, H. B. & Christensen, B. E. Periodate oxidized alginates: Depolymerization kinetics. *Carbohydr. Polym.* **86**, 1595–1601 (2011).
21. Kristiansen, K. A., Dalheim, M. Ø. & Christensen, B. E. Periodate oxidation and macromolecular compaction of hyaluronan. *Pure Appl. Chem.* **85**, 1893–1900 (2013).

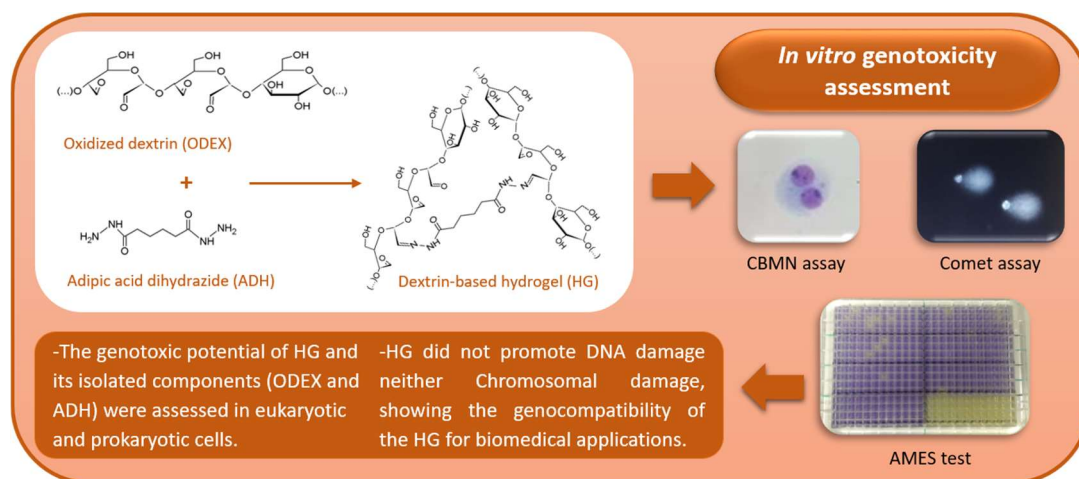
22. Fiedorowicz, M. & Para, A. Structural and molecular properties of dialdehyde starch. *Carbohydr. Polym.* **63**, 360–366 (2006).
23. Veelaert, S., Polling, M. & De Wit, D. Structural and Physicochemical Changes of Potato Starch Along Periodate Oxidation. *Starch - Stärke* **47**, 263–268 (1995).
24. Gupta, B., Tummalapalli, M., Deopura, B. L. & Alam, M. S. Functionalization of pectin by periodate oxidation. *Carbohydr. Polym.* **98**, 1160–1165 (2013).
25. Christensen, B. E., Vold, I. M. N. & Vårum, K. M. Chain stiffness and extension of chitosans and periodate oxidised chitosans studied by size-exclusion chromatography combined with light scattering and viscosity detectors. *Carbohydr. Polym.* **74**, 559–565 (2008).
26. Maia, J. *et al.* Ocular injectable formulation assessment for oxidized dextran-based hydrogels. *Acta Biomater.* **5**, 1948–1955 (2009).
27. Maia, J., Carvalho, R. A., Coelho, J. F. J., Simões, P. N. & Gil, M. H. Insight on the periodate oxidation of dextran and its structural vicissitudes. *Polymer (Guildf)*. **52**, 258–265 (2011).
28. Clough, R. . High-energy radiation and polymers: A review of commercial processes and emerging applications. *Nucl. Instruments Methods Phys. Res. Sect. B Beam Interact. with Mater. Atoms* **185**, 8–33 (2001).
29. Kanjickal, D., Lopina, S., Evancho-Chapman, M. M., Schmidt, S. & Donovan, D. Effects of sterilization on poly(ethylene glycol) hydrogels. *J. Biomed. Mater. Res. Part A* **87A**, 608–617 (2008).
30. Al-Assaf, S. *et al.* *The Radiation Chemistry of Polysaccharides*. (International Atomic Energy Agency, 2016). at <http://www-pub.iaea.org/MTCD/Publications/PDF/P1731_web.pdf>
31. Silindir, M. & Özer, A. Y. Sterilization methods and the comparison of e-beam sterilization with gamma radiation sterilization. *FABAD J. Pharm. Sci* **34**, 43–53 (2009).
32. Silindir, M. & Ozer, Y. The Effect of Radiation on a Variety of Pharmaceuticals and Materials Containing Polymers. *PDA J. Pharm. Sci. Technol.* **66**, 184–199 (2012).
33. Sharpatyi, V. A. Radiation Chemistry of Polysaccharides: 1. Mechanisms of Carbon Monoxide and Formic Acid Formation. *High Energy Chem.* **37**, 369–372 (2003).
34. von Sonntag, C. in *Advances in Carbohydrate Chemistry and Biochemistry* **37**, 7–77 (1980).
35. Asam, M. R. & Glish, G. L. Tandem mass spectrometry of alkali cationized polysaccharides in a quadrupole ion trap. *J. Am. Soc. Mass Spectrom.* **8**, 987–995 (1997).
36. Simões, J. *et al.* Identification of Anomeric Configuration of Underivatized Reducing Glucopyranosyl-glucose Disaccharides by Tandem Mass Spectrometry and Multivariate Analysis. *Anal. Chem.* **79**, 5896–5905 (2007).
37. Nunes, C. *et al.* Occurrence of cellobiose residues directly linked to galacturonic acid in pectic polysaccharides. *Carbohydr. Polym.* **87**, 620–626 (2012).
38. Tudella, J. *et al.* Oxidation of mannosyl oligosaccharides by hydroxyl radicals as assessed by electrospray mass spectrometry. *Carbohydr. Res.* **346**, 2603–2611 (2011).
39. Moreira, A. S. P. *et al.* Neutral and acidic products derived from hydroxyl radical-induced oxidation of arabinotriose assessed by electrospray ionisation mass spectrometry. *J. Mass Spectrom.* **49**, 280–290 (2014).
40. Simões, J. *et al.* Oxidation of amylose and amylopectin by hydroxyl radicals assessed by electrospray ionisation mass spectrometry. *Carbohydr. Polym.* **148**, 290–299 (2016).
41. ISO 11737-1. Sterilization of medical devices -- Microbiological methods -- Part 1: Determination of a population of microorganisms on products. (2006). at <<https://www.iso.org/standard/38711.html>>
42. ISO 11137-2. Sterilization of health care products -- Radiation -- Part 2: Establishing the sterilization dose. (2012). at <<https://www.iso.org/standard/51238.html>>
43. ISO 11737-2. *Sterilization of medical devices — Microbiological methods — Part 2: Tests of sterility performed in the definition, validation and maintenance of a sterilization process*. (2009). at

- <http://www.benebion.com/docs/cer/iso_11737-2_2009-en.pdf>
44. Coimbra, M. A., Delgadillo, I., Waldron, K. W. & Selvendran, R. R. in 19–44 (Springer Berlin Heidelberg, 1996). doi:10.1007/978-3-642-60989-3_2
 45. Blumenkrantz, N. & Asboe-Hansen, G. New method for quantitative determination of uronic acids. *Anal. Biochem.* **54**, 484–489 (1973).
 46. Ciucanu, I. & Kerek, F. A simple and rapid method for the permethylation of carbohydrates. *Carbohydr. Res.* **131**, 209–217 (1984).
 47. Jackson, E. L. & Hudson, C. S. The Structure of the Products of the Periodic Acid Oxidation of Starch and Cellulose 1. *J. Am. Chem. Soc.* **60**, 989–991 (1938).
 48. Sulaeva, I. *et al.* Determination of molar mass distributions of highly oxidized dialdehyde cellulose by size exclusion chromatography and asymmetric flow field-flow fractionation. *Cellulose* **22**, 3569–3581 (2015).
 49. Kristiansen, K. A., Potthast, A. & Christensen, B. E. Periodate oxidation of polysaccharides for modification of chemical and physical properties. *Carbohydr. Res.* **345**, 1264–1271 (2010).
 50. Kamal, H. *et al.* Controlling of Degradation Effects in Radiation Processing of Starch. *J. Macromol. Sci. Part A* **44**, 865–875 (2007).
 51. Chung, H.-J. & Liu, Q. Molecular structure and physicochemical properties of potato and bean starches as affected by gamma-irradiation. *Int. J. Biol. Macromol.* **47**, 214–222 (2010).
 52. Lotfy, S. Controlling degradation of low-molecular-weight natural polymer ‘dextrin’ using gamma irradiation. *Int. J. Biol. Macromol.* **44**, 57–63 (2009).
 53. Phillips, G. O., Moody, G. J. & Mattok, G. L. 710. Radiation chemistry of carbohydrates. Part I. Action of ionising radiation on aqueous solutions of D-glucose. *J. Chem. Soc.* 3522 (1958). doi:10.1039/jr9580003522
 54. Phillips, G. O. & Moody, G. J. 711. Radiation chemistry of carbohydrates. Part II. Irradiation of aqueous solutions of dextran with gamma radiation. *J. Chem. Soc.* 3534 (1958). doi:10.1039/jr9580003534
 55. Bisio, A. *et al.* Controlled γ -ray irradiation of heparin generates oligosaccharides enriched in highly sulfated sequences. *Carbohydr. Polym.* **55**, 101–112 (2004).
 56. Jeun, J.-P., Jeon, Y.-K., Nho, Y.-C. & Kang, P.-H. Effects of gamma irradiation on the thermal and mechanical properties of chitosan/PVA nanofibrous mats. *J. Ind. Eng. Chem.* **15**, 430–433 (2009).
 57. Wasikiewicz, J. M., Yoshii, F., Nagasawa, N., Wach, R. A. & Mitomo, H. Degradation of chitosan and sodium alginate by gamma radiation, sonochemical and ultraviolet methods. *Radiat. Phys. Chem.* **73**, 287–295 (2005).
 58. Nagasawa, N., Mitomo, H., Yoshii, F. & Kume, T. Radiation-induced degradation of sodium alginate. *Polym. Degrad. Stab.* **69**, 279–285 (2000).
 59. Relleve, L. *et al.* Degradation of carrageenan by radiation. *Polym. Degrad. Stab.* **87**, 403–410 (2005).
 60. Ulset, A.-S. T., Mori, H., Dalheim, M. Ø., Hara, M. & Christensen, B. E. Influence of Amino Acids, Buffers, and pH on the γ -Irradiation-Induced Degradation of Alginates. *Biomacromolecules* **15**, 4590–4597 (2014).
 61. Lee, D. W. *et al.* Effect of γ -Irradiation on Degradation of Alginate. *J. Agric. Food Chem.* **51**, 4819–4823 (2003).
 62. Şen, M., Rendeovski, S., Kavaklı, P. A. & Sepehrianazar, A. Effect of G/M ratio on the radiation-induced degradation of sodium alginate. *Radiat. Phys. Chem.* **79**, 279–282 (2010).
 63. Şen, M. & Atik, H. The antioxidant properties of oligo sodium alginates prepared by radiation-induced degradation in aqueous and hydrogen peroxide solutions. *Radiat. Phys. Chem.* **81**, 816–822 (2012).
 64. Bidzinska, E., Dyrek, K., Fortuna, T., Labanowska, M. & Pietrzyk, S. EPR Studies of Thermally Treated Oxidized Corn Starch. *Starch - Stärke* **56**, 461–468 (2004).

65. von Sonntag, C. & Schuchmann, H.-P. The Elucidation of Peroxyl Radical Reactions in Aqueous Solution with the Help of Radiation-Chemical Methods. *Angew. Chemie Int. Ed. English* **30**, 1229–1253 (1991).
66. Reis, A. *et al.* Electrospray tandem mass spectrometry of underivatized acetylated xylo-oligosaccharides. *Rapid Commun. Mass Spectrom.* **19**, 3589–99 (2005).
67. Moreira, A. S. P., Coimbra, M. A., Nunes, F. M., Simões, J. & Domingues, M. R. M. Evaluation of the Effect of Roasting on the Structure of Coffee Galactomannans Using Model Oligosaccharides. *J. Agric. Food Chem.* **59**, 10078–10087 (2011).
68. Moreira, A. S. P., Coimbra, M. A., Nunes, F. M. & Domingues, M. R. M. Roasting-induced changes in arabinotriose, a model of coffee arabinogalactan side chains. *Food Chem.* **138**, 2291–2299 (2013).
69. Hough, L., Taylor, T. J., Thomas, G. H. S. & Woods, B. M. 239. The oxidation of monosaccharides by periodate with reference to the formation of intermediary esters. *J. Chem. Soc.* 1212 (1958). doi:10.1039/jr9580001212
70. Halsall, T. G., Hirst, E. L. & Jones, J. K. N. 269. Oxidation of carbohydrates by the periodate ion. *J. Chem. Soc.* 1427 (1947). doi:10.1039/jr9470001427

CHAPTER 3

In vitro genotoxicity assessment of a dextrin-based hydrogel for biomedical applications



Hydrogels are three dimensional, crosslinked networks of hydrophilic polymers swollen with a large amount of water or biological fluids. Dextrin, a low-molecular-weight carbohydrate composed by glucose residues, has been used to develop an injectable hydrogel for biomedical applications. Dextrin was firstly oxidized (ODEX) to introduce aldehyde groups which then reticulate with adipic acid dihydrazide (ADH), forming the dextrin-based hydrogel (HG). Genotoxicity is an important endpoint in the safety assessment of polymeric-based medical devices. ISO 10993-3 recommends a battery of *in vitro* genotoxicity tests employing eukaryotic and prokaryotic models to determine the potential to induce gene mutations, changes in chromosome structure and number, and other DNA or gene abnormalities caused by the medical devices. Thus, in this study AMES, cytokinesis-block micronucleus (CBMN) and comet assays were used to assess the genotoxic potential of the HG and its isolated components (ODEX and ADH). The results revealed that HG, as well as, ODEX and ADH did not induce DNA and chromosomal damage, demonstrating the genocompatibility of the HG for biomedical applications. Further *in vivo* biocompatibility studies should be performed to confirm the safety of the HG for clinical use. To our best acknowledge, this is the first report with a detailed genotoxicity assessment of an aldehyde-modified polysaccharide/ADH hydrogel.

3.1 | Introduction

Hydrogels are three dimensional, crosslinked networks of hydrophilic polymers swollen with a large amount of water or biological fluids. They generally are biocompatible, biodegradable and mimic many of the properties of the native extracellular matrix, namely high-water content and viscoelastic mechanical properties, functional activity as provisional artificial support for cells and lack of mechanical strength. They display porosity and interconnectivity, enabling the transport of nutrients, gas diffusion, and removal of metabolic wastes, and they can also act as carriers of growth factors or cells and as drug delivery systems. Moreover, hydrogels can be injectable, enabling less invasive clinical procedures, and can conform to the shape of the surface to which they are applied. So that, hydrogels are used in clinical practice and experimental medicine in diverse applications, including tissue engineering and as drug delivery systems¹⁻³.

Dextrins are low-molecular-weight carbohydrates produced by partial hydrolysis of glycogen or starch obtained under acidic and/or enzymatic conditions⁴. They are composed by a linear ($\alpha 1 \rightarrow 4$)-D-glucose residues backbone, branched with ($\alpha 1 \rightarrow 4,6$)-linked-D-glucose residues. Some dextrins also present ($\alpha 1 \rightarrow 6$)-D-glucose residues in a small percentage^{5,6}.

Dextrin is a low cost, broadly available raw material, generally regarded as safe (GRAS), widely used in many industrial applications, such as adhesives, textiles, cosmetic and foods^{4,6}. Regarding biomedical applications, dextrin is still relatively unexplored, being clinically used as a peritoneal dialysis solution that can also perform as a drug delivery solution⁷⁻⁹, and as a wound dressing agent¹⁰. Although its limited number of current biomedical applications, dextrin displays a set of advantages that potentiates its use specifically in the biomaterials field. It is a biocompatible and non-immunogenic material, degradable *in vivo* by α -amylases and its molecular weight ensures renal elimination avoiding tissue accumulation upon repeated administration^{11,12}. During the last decade, due to its properties, which include the solubility in both water and DMSO, availability in medical grade, and availability of hydroxyl groups, dextrin has been explored for the design and fabrication of hydrogels suitable for controlled release applications and as tissue engineering scaffolds^{4,13}.

Dextrin has been used by our research group to develop a novel fully resorbable and injectable hydrogel. Dextrin was firstly oxidized (ODEX) with sodium periodate to produce dialdehydes, which in turn then reticulate with adipic acid dihydrazide (ADH), forming the hydrogel (HG) (**Figure 3.1**)¹⁴. The cross-linked ODEX is an *in situ* gelling hydrogel, which displays a three-dimensional network with interconnective pores, and is able to incorporate nanogels, cells and biomolecules for biomedical applications^{5,14,15}.

The development of biomaterials for medical applications includes extensive preclinical testing in order to demonstrate their safety and efficacy according to the regulatory agencies requirements. In this context, our group has already shown the *in vivo* biocompatibility of the HG after subcutaneous implantation in a rat model. In the same study, the HG was associated with granular ceramics, and was

able to stabilize the granules in the implant site, demonstrating its potential for the development of injectable bone substitutes¹⁵.

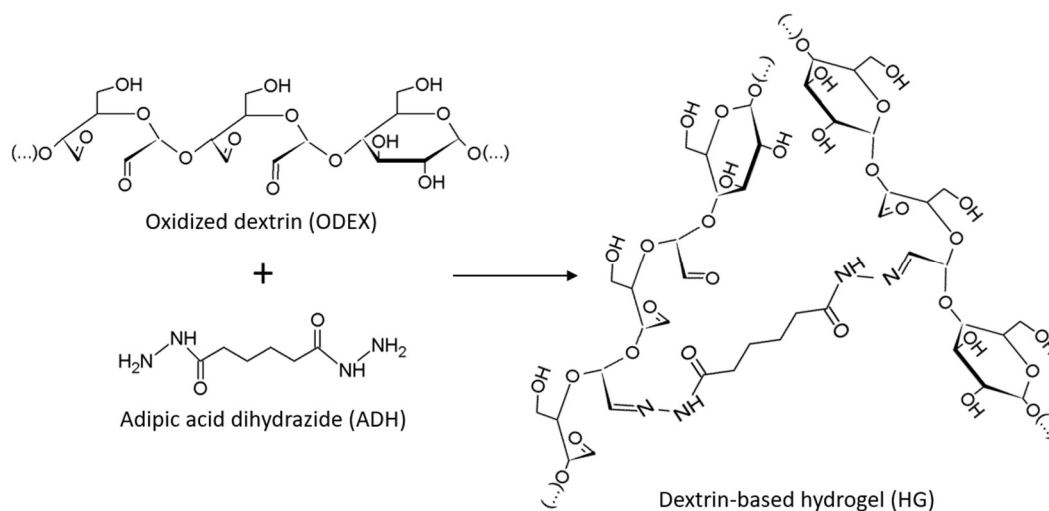


Figure 3.1: Chemical structures of oxidized dextrin (ODEX), adipic acid dihydrazide (ADH) and corresponding hydrogel (HG) formed after reticulation reaction between ODEX and ADH.

The systemic biocompatibility testing of materials includes genotoxicity assessment - evaluation of the presence of a DNA reactive component that may result in mutagenicity and carcinogenicity. The International Standard ISO 10993 on the biological evaluation of medical devices stipulates that implant devices, which are to be in contact with tissue/bone and blood for longer than 24 h must undergo genotoxicity assessment¹⁶. A battery of *in vitro* genotoxicity tests employing eukaryotic and prokaryotic models shall be used to determine the potential to induce gene mutations, changes in chromosome structure and number, and other DNA or gene abnormalities caused by the medical devices, materials and/or their extracts¹⁷. Thus, in the present work, the genotoxic potential of the dextrin-based hydrogel (HG) and its isolated components (ODEX and ADH) was assessed by the AMES test, micronucleus (MN) and comet assays.

3.2 | Experimental

3.2.1 | Chemicals

All chemicals used were of the highest purity or analytical grade available. Dextrin used in this work was Tackidex B 167 (batch E 1445), generously assigned by Roquette (Lestrem, France). Sodium *m*-periodate, diethylene glycol, adipic acid dihydrazide (ADH), 3-(4,5-dimethylthiazol-2-yl)-2,5-diphenyltetrazolium bromide (MTT), methyl methanesulfonate (MMS), dimethyl sulfoxide (DMSO), Triton X-100, low melting point (LMP) agarose and cytochalasin B (cytoB) were purchased from Sigma-Aldrich (St. Louis, MO, USA). Absolute ethanol, sodium hydroxide (NaOH), sodium chloride (NaCl), hydrochloric acid (HCl), acetic acid, Tris base and Giemsa's azur eosin methylene blue were obtained from Merck (Darmstadt, Germany). Mitomycin C (MMC) and molecular Probes® SYBR® Gold were

purchased from Thermo Fisher Scientific (Waltham, MA, USA), while ethylenediaminetetraacetic acid disodium salt (Na₂EDTA) was obtained from Prolab (Quebec, Canada). Phosphate-buffered saline (PBS) and normal melting point (NMP) agarose were supplied by Lonza (Basel, Swiss), while methanol was purchased from VWR (Radnor, PA, USA).

3.2.2 | Material preparation

3.2.2.1 | Dextrin oxidation

Dextrin oxidation was performed as described by Pereira *et al.*¹⁸. Briefly, aqueous solutions of Dextrin (2% w/v) were oxidized with sodium *m*-periodate, to yield the theoretical degree of oxidation of 40%, at room temperature, with stirring, and in the dark. After 20 h, the oxidation reaction was stopped by dropwise addition of an equimolar amount of diethylene glycol to reduce any unreacted periodate. Sodium *m*-periodate and diethylene glycol were removed by ultrafiltration, using a membrane with a molecular weight cut-off 1000 Da (Merck Millipore, Billerica, MA, USA), and then lyophilized.

3.2.2.2 | Preparation of the dextrin-based hydrogel

Oxidized dextrin (ODEX) was dissolved in PBS solution (30% w/v) and the solution was sterilized by gamma irradiation, using a ⁶⁰Co source, at 20 kGy (2 kGy/h), at room temperature. Adipic acid dihydrazide (ADH) was also dissolved in PBS solution (3.76% w/v) and sterilized by filtration, using a 0.22 μm pore filter (Pall Corporation, MI, USA). For the crosslinking reaction, ODEX and ADH solutions were mixed in a 7:3 volume ratio, respectively.

3.2.3 | Cell culture

The human lymphoblastoid TK6 cell line (ATCC®CRL8015™) was used for the cyto- and genotoxicity testing. The cells were maintained in RPMI-1640 medium (Thermo Fisher Scientific, Waltham, MA, USA) with 2 mM glutamine (Merck, Darmstadt, Germany) supplemented with 10% heat-inactivated fetal bovine serum (FBS; Thermo Fisher Scientific, Waltham, MA, USA), 100 units/mL of penicillin, 100 μg/mL of streptomycin and 0.25 μg/mL of amphotericin (Thermo Fisher Scientific, Waltham, MA, USA). Cells were maintained in a humidified atmosphere with 5% CO₂ at 37 °C.

3.2.4 | Cell exposure conditions

For cyto- and genotoxicity testing, the HG was tested by indirect method: as HG is not pipettable, it was diluted (HG_{dil}) in culture medium and different concentrations were prepared and tested (**Table 3.1**). The HG constituents (ODEX and ADH), which are two of the degradation products from the HG, were also tested separately, using the same concentrations used for the assessment of the HG_{dil} tested (**Table 3.1**). Thus, for the MTT reduction and cytokinesis-block micronucleus (CBMN) assays, 6 concentrations of the HG_{dil} (C1 to C6) were tested in parallel with its individual components (ODEX and ADH) (**Table 3.1**).

For the comet assay, 3 non-cytotoxic concentrations were tested (C1 to C3). In the AMES test, only six different concentrations of HG_{dil} were tested (C1 to C6). For all the experiments, a negative control (NC) and an appropriate positive control (PC) were used.

Table 3.1: Concentrations of the dilute dextrin-based hydrogel (HG_{dil}), oxidized dextrin (ODEX) and adipic acid dihydrazide (ADH) used in the cyto- and genotoxicity testing.

	HG _{dil}	ODEX	ADH
	(mg/mL)		
NC	0.000	0.000	0.000
C1	0.124	0.118	0.006
C2	0.248	0.235	0.013
C3	0.491	0.466	0.034
C4	0.965	0.916	0.049
C5	1.865	1.770	0.095
C6	3.494	3.316	0.178

3.2.5 | Assessment of the cellular viability

The effect of the HG, ODEX and ADH on cell viability was evaluated by the MTT reduction assay. To carry out the experiment, 1.7×10^5 cells/mL were seeded in 96-well round bottom plates. After 24 h, cells were incubated with different concentrations of HG_{dil}, ODEX and ADH, negative control (culture medium) or a positive control (DMSO). At the end of the exposure period (24 h), the test agents were removed by centrifugation ($130 \times g$, 2 min) and 100 μ L of MTT solution (1 mg/mL in serum-free medium) were added to each well and incubated for 3 h at 37 °C in the dark. For MTT removal, plates were centrifuged ($300 \times g$, 10 min), and the produced formazan was solubilized with 200 μ L DMSO. Thereafter, 150 μ L of the supernatant were transferred to a 96-well flat bottom plate and the absorbance was measured at 570 and 690 nm (reference wavelength), using a Cambrex ELx808 microplate reader (BioTek Winooski, VT, USA). Two independent experiments were performed, each in triplicate.

3.2.6 | Assessment of the DNA damage

The comet assay, also known as single-cell gel electrophoresis (SCGE) assay, was performed to evaluate the DNA damage induced by the HG and its components. For that purpose, TK6 cells were seeded into 24-well plates at a density of 1.7×10^5 cells/mL. After 24 h, cells were treated with non-toxic concentrations of HG_{dil}, ODEX and ADH (C1 to C3), selected based on the cellular viability data. Cells incubated with culture medium and the DNA alkylating agent MMS (40 μ g/mL; 1 h) served as NC and PC, respectively. At the end of the exposure period (24 h), incubation media was removed and cells washed with PBS pH 7.4. The comet assay was performed in alkaline conditions (pH>13) as previously described

by Mesquita *et al.*¹⁹, with minor modifications. All the steps described were conducted under a reduced light level to prevent additional DNA damage. Briefly, aliquots of 1×10^5 cells in PBS were centrifuged at $400 \times g$ for 3 min. The cell pellets were resuspended in 100 μ L 1% LMP agarose and 5 μ L of each cell suspension layered onto dry microscope slides (VWR, Darmstadt, Germany) pre-coated with 1% NMP agarose. After gel solidification at 4 °C, slides were placed in a Coplin jar and immersed in ice-cold lysis solution (2.5 M NaCl, 100 mM Na₂EDTA, 10 mM Tris-base, 10 M NaOH, pH 10, supplemented with 1% Triton-X 100) for 1.5 h at 4 °C (protected from light), to lyse the cells and separate DNA from histones. For DNA unwinding, all slides were immersed in freshly prepared electrophoresis buffer (200 mM Na₂EDTA, 0.3 M NaOH pH>13) in the electrophoresis unit for 40 min at 4 °C, followed by electrophoresis for 20 min at 30 V and 300 mA. Then, the gels were then washed with H₂O and fixed with ethanol 70% and 96% for 15 min each, at room temperature. After air-drying the slides overnight, DNA was stained with a 0.07 % SYBR Gold solution. The slides were coded and one scorer performed the comet analysis using a fluorescence microscope (Nikon Eclipse E400 microscope attached to an epifluorescence illuminator Nikon C-SHG1) with a 400x magnification and the image analysis software Comet Assay IV (Perceptive Instruments, Suffolk, UK). The % DNA in the comet tail (tail intensity) and the olive tail moment were used as a measure of the amount of DNA damage. At least 100 cells were scored (50 for each replicate gel) and three independent experiments were performed, each in triplicate.

3.2.7 | Assessment of the chromosomal damage

The Micronucleus (MN) assay was performed to evaluate the potential chromosome damage induced by the HG, ODEX and ADH in TK6 cells, according to the OECD test guideline (TG) 487²⁰, in the presence of cytoB, an actin polymerisation inhibitor. To carry out the experiment, 1.7×10^5 cells/mL were seeded in 12-well plates, and treated for 24 h with different concentrations of HG_{dil}, ODEX and ADH, with 0.04 μ g/mL MMC as positive control, and with culture medium (NC). At the end of the exposure period, cells were centrifuged ($100 \times g$, 7 min; Sigma 302k), resuspended in fresh culture medium, and transferred to a new 12-well plate. The culture medium was then supplemented with cytoB at a final concentration of 4 μ g/mL. After 30 h (recovery time), cells were transferred into 15 mL conical tubes, centrifuged ($100 \times g$, 7 min), and the supernatant discarded by inverting the tube. The residual supernatant was resuspended by gentle agitation of tubes. Then, cells were incubated in 5 mL of a hypotonic 0.075 M KCl solution for 4 min followed by addition of 400 μ L of an ice-cold methanol:acetic acid pre-fixing solution (3:5 v/v) under gentle agitation. Samples were centrifuged again, and resuspended in 5 mL of ice-cold fixing solution (methanol:acetic acid, 5:1 v/v), and then centrifuged ($100 \times g$, 10 min). The supernatant was decanted, the cell pellets were resuspended in the residual supernatant and dropped onto clean glass slides and air-dried. The slides were stained with 3% Giemsa and analysed using a light microscope (Nikon E400 Eclipse) under a high magnification (400-1000x). For this test, two independent experiments were performed, each in duplicate. For scoring, MN frequencies were analysed in at least 2000

binucleate cells per concentration and control, equally divided among the replicates. The criteria for MN and binucleate cells scoring were in accordance with the principles described by Fenech ²¹. Only the concentrations whose cytotoxicity was below $55 \pm 5 \%$ were scored for MN. The cytotoxicity was measured in accordance with the OECD TG 487 ²⁰, by using the cytokinesis-block proliferation index (CBPI), which indicates the average number of cell cycles per cell during the period of exposure to cytoB, and may be used to calculate cell proliferation, as follow:

$$\% \text{ Cytostasis} = 100 - 100[(CBPI_T - 1) \div (CBPI_C - 1)], T = \text{Test and } C = \text{Control}$$

Where:

CBPI

$$= \frac{(\text{No. mononucleate cells}) + (2 \times \text{No. binucleate cells}) + (3 \times \text{No. multinucleate cells})}{(\text{Total number of cells})}$$

For its determination at least 500 cells per slide were counted.

3.2.8 | Assessment of mutagenicity

The mutagenic potential of the HG was assessed by the AMES test, using the kit Ames MPF™ Penta I (Xenometrix AG, Allschwil, Switzerland), which follows the OECD TG 471 ²². Histidine-dependent auxotrophic mutants of *Salmonella typhimurium* (strains TA98, TA100, TA1535 and TA1537) and tryptophan-dependent auxotrophic mutants of *Escherichia coli* (strains WP2 uvrA and WP2 [pKM101]) were used and two sets of experiments were performed: in the presence and absence of Aroclor 1254-induced rat liver (S9). The test procedure was provided by the kit manufacturer. Briefly, the tested strains (the two *E. coli* strains that were grown separately overnight were mixed and renamed *E. coli Combo* mix were exposed to different concentrations of the HG_{dil}, as well as to a positive and a negative control (PBS), all in triplicate, for 90 min (*E. coli* +S9: 20 min), at 37 °C, under agitation in liquid minimal histidine (*Salmonella* strains) or tryptophan (*E. coli*) exposure media. After exposure, the cultures were diluted in pH indicator medium lacking histidine or tryptophan and aliquoted into 48 wells of a 384-well plate. The 384-well plates were incubated at 37 °C for 48 h. The bromocresol purple in the indicator medium turns yellow as the pH drops as a result of the catabolic activity of revertant bacteria that grow in the absence of the required amino acid. The number of positive (yellow) wells out of 48 wells per replicate and concentration was counted and compared with the number of spontaneous revertants obtained with the NC. The PC used in absence of S9 were: 2 µg/ml 2-nitrofluorene for TA98; 0.1 and 2 µg/ml 4-nitroquinoline-N-oxide for TA100 and *E. coli Combo* mix, respectively; 100 µg/ml N⁴-aminocytidine for TA1535; and 15 µg/ml 9-aminoacridine for TA1537. The PC used in the presence of S9 were: 1 and 50 µg/ml 2-aminoanthracene for TA98 and *E. coli Combo* mix, respectively, and 2.5 µg/ml 2-aminoanthracene for TA100, TA1535 and TA1537. Evaluation and interpretation of the results were

performed according to Xenometrix criteria: the fold increase over the baseline, which is the ratio of the mean number of positive wells for the dose concentration divided by the baseline, was determined for each concentration. The baseline was obtained by adding one standard deviation to the mean number of positive wells of the NC. If the baseline was below 1, it was set to 1. A test compound that showed a clear dose response and/or yields multiple fold increase greater than 2.0, was classified as a mutagen.

3.2.9 | Statistical analysis

Experimental data were presented as mean \pm standard deviation (SD). Statistical analysis and graphs were performed using the Prism[®] version 6.1 (GraphPad Software Inc., La Jolla, CA, USA). Statistical analyses of the MTT and comet assays data were performed by one-way analysis of variance (ANOVA) followed by the Dunnett post-test. For the MN assay data, a chi-square test was performed to determine a statistically significant difference of the MN frequency between exposed and control cells. Significance was accepted at a p -value < 0.05 .

3.3 | Results

3.3.1 | Cellular viability

The cytotoxicity of the HG was evaluated by the MTT reduction assay in TK6 cells following 24 h of exposure. As shown in **Figure 3.2**, the viability of the cells after exposure to the HG_{dil} decreased in a concentration-dependent manner. Regarding the effects of the isolated components of the HG upon cell viability, it was observed that ADH did not induce cytotoxicity at the tested concentrations, while ODEX significantly decreased the viability of the cells, also in a concentration-dependent manner, suggesting that HG_{dil}'s cytotoxicity is due to ODEX. When the HG_{dil} was compared with ODEX, it was observed that ODEX presented an increased cytotoxic effect alone than in the HG_{dil} at concentrations greater than 0.916 mg/mL ($p < 0.001$).

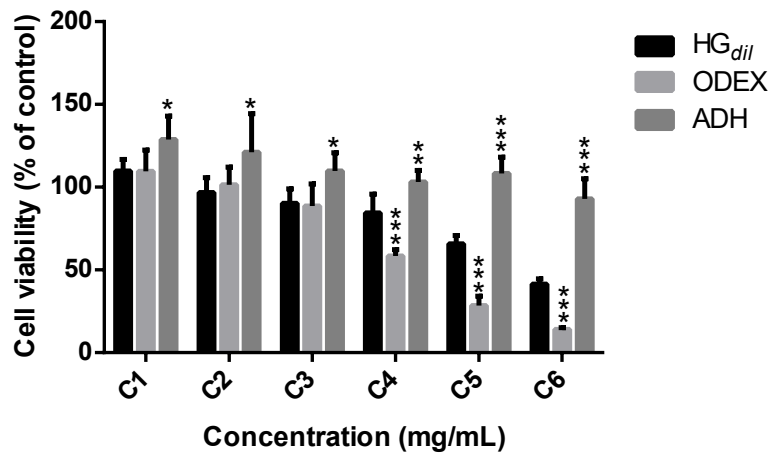


Figure 3.2: Effect of the different concentrations of the dilute hydrogel (HG_{dil}) and its isolated components – oxidized dextrin (ODEX) and adipic acid dihydrazide (ADH) – on TK6 cell viability as assessed by the MTT reduction assay. Cells were exposed to different concentrations (C1-C6) of the test agents for 24 h. Results were calculated as percentage of negative control (NC) and data are presented as mean \pm SD of two independent experiments (n = 3 replicates per group). Data were analyzed by one-way ANOVA analysis followed by Dunnett’s post hoc test: * $p < 0.05$, ** $p < 0.01$ and *** $p < 0.001$ versus HG_{dil}.

3.3.2 | DNA damage

Three non-cytotoxic concentrations of the HG_{dil}, according to the MTT results (C1 to C3), and the same concentrations of the hydrogel isolated components (ODEX and ADH) were assessed for DNA damage by the comet assay, after 24 h of exposure in TK6 cells. The results are represented in **Table 3.2**. Cells treated with different concentrations of HG_{dil}, ODEX and ADH displayed a predominant round-shaped nucleus (**Figure 3.3**) like untreated cells (NC), while positive control-treated cells (MMS) exhibited a typical comet tail indicative of DNA damage. As outlined in **Table 3.2**, no significant differences in tail intensity (%) and olive tail moment values of the cells exposed to the different concentrations of HG_{dil} and its isolated components were observed compared to untreated cells, indicating that HG_{dil} did not induce DNA damage in TK6 cells after 24 h of exposure. On the other hand, in positive control-treated cells it was observed a significant increase in tail intensity (%) and olive tail moment ($p < 0.001$).

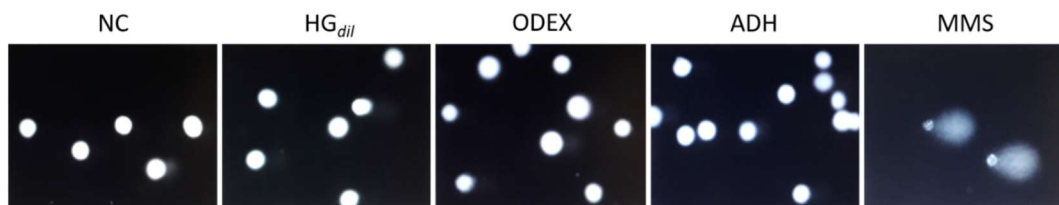


Figure 3.3: Representative images (400x magnification) of the comet assay in TK6 cells after 24 h of exposure to negative control (NC) and to the highest concentration (C3) of the dilute hydrogel (HG_{dil}), oxidized dextrin (ODEX) and adipic acid dihydrazide (ADH) used. Methyl methanesulfonate (MMS, 40 μ g/mL, 1 h) was used as positive control.

Table 3.2: Comet assay analysis of DNA damage in TK6 cells exposed to different concentrations of the dilute hydrogel (HG_{dil}) and its isolated components – oxidized dextrin (ODEX) and adipic acid dihydrazide (ADH) – for 24 h.

	Tail intensity (%)	Olive tail moment
NC	7.02 ± 1.38	0.92 ± 0.26
HG _{dil}		
C1	7.13 ± 0.87	0.93 ± 0.32
C2	7.60 ± 1.47	0.98 ± 0.41
C3	7.84 ± 1.57	1.08 ± 0.36
ODEX		
C1	7.15 ± 1.54	0.99 ± 0.40
C2	7.60 ± 1.49	1.11 ± 0.41
C3	8.58 ± 1.41	1.30 ± 0.39
ADH		
C1	6.93 ± 1.06	0.88 ± 0.32
C2	7.17 ± 1.51	0.89 ± 0.27
C3	6.37 ± 1.48	0.82 ± 0.33
MMS	73.98 ± 8.67*	22.92 ± 6.99*

Methyl methanesulfonate (MMS, 40 µg/mL, 1 h) was used as positive control. Results are presented as mean ± SD of three independent experiments ($n = 3$ replicates per group). Data were analysed by one-way ANOVA analysis followed by Dunnett's post hoc test: * $p < 0.001$ versus negative control (NC).

3.3.3 | Chromosomal damage

The MN scoring was only performed in concentrations of HG_{dil}, ODEX and ADH inducing cytotoxicity levels below $55 \pm 5\%$, since cell death can confound the interpretation of the CBMN assay data. The results relative to MN frequency (% MN) in binucleate cells exposed to HG, ODEX and ADH and its respective cytotoxicity are presented in **Figure 3.4**.

In agreement with the MTT assay data, the HG_{dil} and ODEX induced a concentration-dependent increase in cytotoxicity, greater in ODEX-exposed cells, while ADH did not display cytotoxicity. TK6 cells treated with the HG concentration C6 (3.494 mg/mL) exhibited a cytotoxicity of $89.99 \pm 2.26\%$, and accordingly were not scored for MN frequency. Regarding ODEX, cells incubated with the concentration C5 (1.770 mg/mL) displayed a cytotoxicity about $89.28 \pm 1.27\%$, so that, only four concentrations of ODEX were scored for MN. Since ADH was not cytotoxic, all concentrations were used for MN scoring. After 24 h of TK6 cells incubation with the tested concentrations of HG_{dil}, ODEX and ADH no significant MN induction was observed, while MMC (with a cytotoxicity about $37.46 \pm 1.37\%$) significantly increased the number of binucleate cells with MN ($p < 0.001$) compared to control cells. These results indicate that HG does not induce chromosome damage on TK6 cells under our experimental conditions.

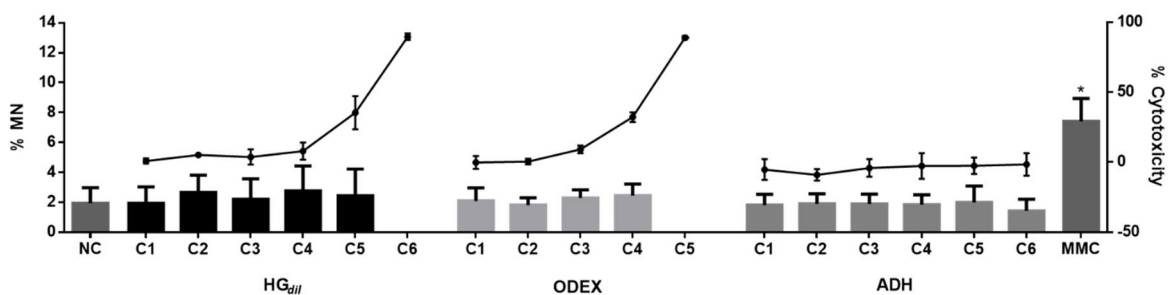


Figure 3.4: CBMN assay in TK6 cells exposed to different concentrations of the dilute hydrogel (HG_{dil}) and its isolated components – oxidized dextrin (ODEX) and adipic acid dihydrazide (ADH) – for 24 h. Mitomycin C (MMC, 0.04 µg/mL) was used as positive control. Columns: percentage of micronucleus (% MN) in binucleate cells; lines: % cytotoxicity. Results are presented as mean ± SD of two independent experiments (n = 2 replicates per group). Data were analysed by chi-square test: * $p < 0.001$ versus negative control (NC).

3.3.4 | AMES test for mutagenicity

Data obtained in the AMES test for mutagenicity, in the presence and in the absence of human S9 fraction are presented in **Tables 3.3** and **3.4**, respectively. Results showed that HG_{dil} did not induce a twofold increase in the number of positive wells compared to the NC at any of the concentrations tested, either in the presence or absence of S9. Additionally, it was not observed a clear dose-dependent increase in the number of positive wells. On the other hand, all the mutagenic PC tested produced more than a threefold increase in the number of revertant colonies compared to the negative control. Taking together, the above described results indicated that HG was not mutagenic in any of the tested concentrations.

3.4 | Discussion

In the present work, a combination of different genotoxicity assays was used to assess the genotoxic potential of the HG and its isolated components (ODEX and ADH), which were performed in mammalian cell line and prokaryotic models.

The mammalian cell line used was TK6 human lymphoblastoid cells. These cells have a wild-type p53 gene, are karyotypically stable, display DNA repair capacity and stable spontaneous mutation frequencies^{23–26}. According with the 5th International Workshop on Genotoxicity Testing (IWGT) guidelines, p53-competent, preferably human, are preferable to p53-compromised cells for the evaluation of the MN induction for human risk assessment²⁶, because of “false” positive results obtained in the p53-compromised rodent cell lines (e.g. V79, CHL and CHO cells)²⁷. In this way and due to inherent characteristics, TK6 cell line is already suggested in the OECD test guideline for the MN²⁰, being even one of the most used for such assay²⁴. Another advantage of using TK6 cells is that it is a well-studied human cell line, ease of culturing, and its use eliminates the donor to donor variability observed with primary human lymphocytes²⁸. Consequently, TK6 cell line may be deemed appropriate for performing

in vitro genotoxicity assessment of medical devices for tissue regeneration purposes to be applied in tissues highly vascularized, like bone.

In order to avoid misleading positive results in the comet and CBMN assays, the different concentrations of HG_{dil}, ODEX and ADH were firstly evaluated for their cytotoxicity. The results from MTT and CBMN (using CBPI method) showed that HG_{dil} is cytotoxic in a concentration-dependent manner. By analysing the effect of the isolated components of HG, ADH component showed to be non-cytotoxic. It's important to note that, ADH is a minor component of the HG (~5 % w/w), thus lower concentrations were tested. Silva *et al.* evaluated and compared the cytotoxicity of ADH with glutaraldehyde⁵. The later is a widely used crosslinker, often considered cytotoxic^{29,30}, but still used for reticulation of biomedical products³¹. Silva *et al.* showed that glutaraldehyde caused a much higher cytotoxicity than ADH: dihydrazide-induced cell death occurred only at concentrations 300 times higher than those of glutaraldehyde⁵. In contrast, ODEX induced cytotoxicity in a concentration-dependent manner. These results suggest that the cytotoxic effect of the HG_{dil} was most likely due to the presence of free aldehydes from ODEX. The formation of the HG depends on the reaction of aldehydes present in ODEX with free amines provided by ADH, producing hydrazone bonds, and the degradation of HG is caused by the hydrolysis of the hydrazone bonds, yielding again the original free ODEX and ADH components¹⁴. Therefore, biological reactivity presumably depends on the presence of excess aldehyde groups, those not involved in hydrazone bond formation. This can also explain the stronger concentration-dependent cytotoxic effect of ODEX in comparison to the HG at higher concentrations (C4, C5 and C6): when ODEX is used alone, all aldehydes groups are free, while when ADH is added to cells together with ODEX (originating the HG), aldehydes can react with ADH, reducing the number of free aldehydes. Toxicity of other types of aldehyde-modified polysaccharides has been already reported for other cell types, such as human and murine fibroblasts³²⁻³⁵, macrophage cells (THP-1 and RAW 264.7)^{33,36}, epidermal keratinocytes, endothelial cells³² and nasopharyngeal epithelial cells³³. The cytotoxic effect of aldehydes is most likely due to their reaction with amino acids of the culture medium and free amines in the cell, causing a negative effect on cellular growth^{34,35}. When the excess of aldehyde groups is reduced to a primary alcohol^{34,36} or the degree of oxidation of the backbone is reduced³⁷, the biocompatibility is highly improved. Although the aldehyde-modified polysaccharides derivatives showed some degree of cytotoxicity *in vitro*, several studies have shown biocompatibility, safety and good performance *in vivo* in diverse biomedical applications, such as hydrogels for prevention of post-operative adhesions³⁸⁻⁴⁰, surgical haemostatics⁴¹, bioadhesives and sealants^{42,43}. As a matter of fact, in our experience, the HG presented excellent *in vivo* biocompatibility in subcutaneous implantation assay¹⁵. This may partially be explained by the slow degradation of the HG *in vivo* and dilution/excretion of the solubilized products, which most likely never reach the concentrations observed to be cytotoxic in this work.

Table 3.3: Mutagenic potential of the different concentrations of the dilute hydrogel (HG_{dil}) assessed by the AMES test using different strains of *Salmonella typhimurium* and a combination of two *Escherichia coli* strains (*E. coli* combo mix), in absence of a metabolic activator (human S9 mix).

	TA98		TA100		TA1535		TA1537		E. coli Combo mix	
	Positive wells	Fold increase	Positive wells	Fold increase	Positive wells	Fold increase	Positive wells	Fold increase	Positive wells	Fold increase
NC	7.00 ± 4.36		10.33 ± 2.89		1.33 ± 0.58		9.00 ± 1.73		8.67 ± 2.52	
C1	12.33 ± 3.21	1.09	9.33 ± 2.08	0.71	1.67 ± 1.15	0.87	8.00 ± 3.61	0.75	4.33 ± 0.58	0.39
C2	10.33 ± 1.53	0.91	12.76 ± 3.51	0.96	3.00 ± 1.00	1.57	9.67 ± 2.31	0.90	6.67 ± 2.31	0.60
C3	10.33 ± 0.58	0.91	13.00 ± 4.00	0.98	0.67 ± 0.58	0.35	11.67 ± 3.06	1.09	4.00 ± 2.65	0.36
C4	12.00 ± 4.00	1.06	12.00 ± 2.00	0.91	1.67 ± 1.15	0.87	6.00 ± 1.00	0.56	2.67 ± 1.53	0.24
C5	11.00 ± 2.00	0.97	15.33 ± 4.16	1.16	3.00 ± 0.00	1.57	7.00 ± 2.65	0.65	5.00 ± 1.00	0.45
C6	11.00 ± 2.65	0.97	16.67 ± 4.62	1.26	1.67 ± 2.08	0.87	5.67 ± 1.15	0.53	3.33 ± 2.08	0.30
PC	48.00 ± 0.00	4.23*	46.67 ± 0.58	3.53*	48.00 ± 0.00	25.12*	48.00 ± 0.00	4.47*	41.67 ± 2.08	3.73

Results are presented as mean ± SD. The test compound with a clear dose response and/or yields multiple fold increase greater than 2.0, was classified as a mutagen, which was assigned with *. Positive controls (PC) were as follows: 2 µg/ml 2-nitrofluorene for TA98; 0.1 and 2 µg/ml 4-nitroquinoline-N-oxide for TA100 and *E. coli Combo* mix, respectively; 100 µg/ml N⁴-aminocytidine for TA1535; and 15 µg/ml 9-aminoacridine for TA1537.

Table 3.4: Mutagenic potential of the different concentrations of the dilute hydrogel (HG_{dil}) assessed by the AMES test using different strains of *Salmonella typhimurium* and a combination of two *Escherichia coli* strains (*E. coli* combo mix), in presence of a metabolic activator (human S9 mix).

	TA98		TA100		TA1535		TA1537		<i>E. coli</i> Combo mix	
	Positive wells	Fold increase	Positive wells	Fold increase	Positive wells	Fold increase	Positive wells	Fold increase	Positive wells	Fold increase
NC	3.67 ± 2.08		6.33 ± 2.52		1.33 ± 0.58		3.33 ± 1.53		4.00 ± 1.73	
C1	1.33 ± 1.53	0.23	7.00 ± 2.00	0.79	0.67 ± 1.15	0.35	3.00 ± 1.73	0.62	6.00 ± 1.73	1.05
C2	2.00 ± 1.00	0.35	7.33 ± 1.53	0.83	0.33 ± 0.58	0.17	1.67 ± 0.58	0.34	2.33 ± 1.53	0.41
C3	1.67 ± 0.58	0.29	8.67 ± 2.52	0.98	0.67 ± 0.58	0.35	4.00 ± 2.00	0.82	3.67 ± 2.89	0.64
C4	3.00 ± 1.00	0.52	5.33 ± 0.58	0.60	1.00 ± 1.73	0.52	2.00 ± 0.00	0.41	2.67 ± 2.08	0.47
C5	2.33 ± 2.52	0.41	5.67 ± 1.53	0.64	0.67 ± 0.58	0.35	2.33 ± 2.08	0.48	4.67 ± 1.15	0.81
C6	2.00 ± 1.00	0.35	10.00 ± 0.00	1.13	1.67 ± 1.15	0.87	3.00 ± 1.73	0.62	3.33 ± 1.53	0.58
PC	48 ± 0.00	8.35*	47.67 ± 0.58	5.39*	27.67 ± 7.57	14.48*	48.00 ± 0.00	9.87*	32.00 ± 2.00	5.58*

Results are presented as mean ± SD. According to the manufacturer's criteria, a test compound with a clear dose-response and/or yields multiple fold increase greater than 2.0, was classified as a mutagen, which was assigned with *. Positive controls (PC) were as follows: 1 and 50 µg/ml 2-aminoanthracene for TA98 and *E. coli* Combo mix, respectively, and 2.5 µg/ml 2-aminoanthracene for TA100, TA1535 and TA1537.

Despite extensive research on cytotoxicity (effects on cell proliferation/viability) of aldehyde-modified polysaccharides and ADH, genotoxicity studies are still scarce, in particular, on ADH-reticulated polyaldehyde-based hydrogels^{44–48}. Genotoxicity is an important endpoint of the safety assessment of regulated products, but no single test is available to detect all types of genotoxicity. Therefore, a battery of standard genotoxicity assays is recommended by ISO 10993-3¹⁷ for screening of potential genotoxicants. In this study, a detailed genotoxicity assessment of dextrin-based hydrogel and its isolated components to be used in medical devices for bone regeneration was performed, using the CBMN, comet and the Ames assays. Among these tests, CBMN and AMES are set out in ISO 10993-3 guideline¹⁷.

The CBMN assay is a sensitive method, which detects chromosomal damage in cells that have undergone cell division during or after test exposure to a test agent, through the observation of a MN. The MN results from chromosomal loss or fragmentation, where this damaged genetic material lags behind during chromosome segregation and is not included in either of the resulting daughter nuclei²¹. Our data showed that the HG, as well as its individual components, did not induced an increase of MN frequency in binucleate cells, suggesting that this dextrin-based hydrogel does not promote chromosomal mutations.

The comet assay is a versatile, sensitive and rapid method for measuring DNA single- and double-strand breaks at the level of individual cells⁴⁹. It has been assigned as a valuable addition to the MN assay due to its independence from cell proliferation and coverage of a wider spectrum of DNA damage²⁶: the stranded breaks can be resulting, for example, from direct interactions with DNA, alkali labile sites or as a consequence of transient DNA strand breaks resulting from DNA excision repair. These strand breaks may be repaired, resulting in no persistent effect, may be lethal to the cell, or may be fixed into a mutation resulting in a permanent viable change. They may also lead to chromosomal damage, which is also associated with many human diseases, including cancer²¹. In this test, the length and fluorescence intensity of the comet tail is directly proportional to the amount of DNA damage⁴⁹. In our study, the basal damage observed in TK6 cells were comparable to that reported by others^{50,51}. The results of the % tail intensity and olive tail moment of HG_{dii}, ODEX and ADH were similar to the control, indicating that none of them promoted DNA damage.

The AMES test is the most classic test to evaluate the mutagenic potential of chemicals. It is commonly employed as an initial screening for genotoxic activity and, in particular, for point mutation-inducing activity. Point mutations are the cause of many human genetic diseases and there is substantial evidence that point mutations in oncogenes and tumour suppressor genes of somatic cells are involved in tumour formation in humans⁵². The low number of positive wells and the lack of a dose-response, either in presence or absence of S9 fractions suggest that the HG lacks mutagenic activity at the concentrations tested. Negative mutagenicity results have been also reported for a hydrogel composed by succinyl chitosan and aldehyde dextran (0.5 – 8 mg/mL) as assessed by the Ames test³³.

3.5 | Conclusions

An oxidized dextrin-based hydrogel reticulated with ADH, previously developed by our group, aiming to perform as an injectable carrier of hydroxyapatite granules for bone tissue engineering and as a drug delivery system has been characterized for cyto- and genotoxicity. Genotoxicity is an important endpoint in the safety assessment of medical devices but many times undervalued by polymeric biomaterial's researchers in the biomedical field. In this work, a battery of *in vitro* genotoxicity assays was performed, and the obtained results indicate that HG is non-genotoxic and non-mutagenic under the experimental conditions tested, confirming the huge potential of this HG for biomedical applications. Future *in vivo* studies will be conducted in order to confirm the potential and safety of the HG for such applicability. To our best acknowledge, this is the first report with a detailed genotoxicity assessment of an aldehyde-modified polysaccharide/ADH hydrogel.

3.6 | References

1. Drury, J. L. & Mooney, D. J. Hydrogels for tissue engineering: Scaffold design variables and applications. *Biomaterials* **24**, 4337–4351 (2003).
2. Geckil, H., Xu, F., Zhang, X., Moon, S. & Demirci, U. Engineering hydrogels as extracellular matrix mimics. *Nanomedicine* **5**, 469–484 (2010).
3. Hoare, T. R. & Kohane, D. S. Hydrogels in drug delivery: Progress and challenges. *Polymer (Guildf)*. **49**, 1993–2007 (2008).
4. Gonçalves, C., Moreira, S. M., Carvalho, V., Silva, D. M. & Gama, M. in *Encyclopedia of Biomedical Polymers and Polymeric Biomaterials* (ed. Mishra, M.) 2634–2649 (Taylor & Francis, 2016).
5. Silva, D. M. *et al.* Structural analysis of dextrans and characterization of dextrin-based biomedical hydrogels. *Carbohydr. Polym.* **114**, 458–466 (2014).
6. Tomasiak, P., Wijek, S. & Pałasiński, M. in *Advances in Carbohydrate Chemistry and Biochemistry* **47**, 279–343 (1989).
7. Peers, E. & Gokal, R. Icodextrin provides long dwell peritoneal dialysis and maintenance of intraperitoneal volume. *Artif. Organs* **22**, 8–12 (1998).
8. Takatori, Y. *et al.* Icodextrin technique survival rate in peritoneal dialysis patients with diabetic nephropathy by improving body fluid management: a randomized controlled trial. *Clin. J. Am. Soc. Nephrol.* **6**, 1337–1344 (2011).
9. Treetharnmathurot, B. *et al.* Dextrin–trypsin and ST-HPMA–trypsin conjugates: Enzyme activity, autolysis and thermal stability. *Int. J. Pharm.* **373**, 68–76 (2009).
10. DeBusk, A. O. V. & Alleman, T. Method for preparing medical dressings. (2006).
11. Hreczuk-Hirst, D., Chicco, D., German, L. & Duncan, R. Dextrans as potential carriers for drug targeting: tailored rates of dextrin degradation by introduction of pendant groups. *Int. J. Pharm.* **230**, 57–66 (2001).
12. Moreira, S. *et al.* In Vivo Biocompatibility and Biodegradability of Dextrin-based Hydrogels. *J. Bioact. Compat. Polym.* **25**, 141–153 (2010).
13. Das, D. & Pal, S. Modified biopolymer-dextrin based crosslinked hydrogels: application in controlled drug delivery. *RSC Adv.* **5**, 25014–25050 (2015).
14. Molinos, M., Carvalho, V., Silva, D. M. & Gama, F. M. Development of a Hybrid Dextrin Hydrogel Encapsulating Dextrin Nanogel As Protein Delivery System. *Biomacromolecules* **13**, 517–527 (2012).
15. Silva, D. M. *et al.* Inflammatory response to dextrin-based hydrogel associated with human

- mesenchymal stem cells, urinary bladder matrix and Bonelike[®] granules in rat subcutaneous implants. *Biomed. Mater.* **11**, 065004 (2016).
16. ISO 10993-1. *Biological evaluation of medical devices - Part 1: Evaluation and testing within a risk management process.* (2009). at <<https://www.iso.org/standard/44908.html>>
 17. ISO 10993-3. *Biological evaluation of medical devices - Part 3: Tests for genotoxicity, carcinogenicity and reproductive toxicity.* (2014). at <<https://www.iso.org/standard/55614.html>>
 18. Pereira, I. *et al.* Effects of gamma irradiation and periodate oxidation on the structure of dextrin assessed by mass spectrometry. *Eur. Polym. J.* **103**, 158–169 (2018).
 19. Mesquita, B. *et al.* Gold nanorods induce early embryonic developmental delay and lethality in zebrafish (*Danio rerio*). *J. Toxicol. Environ. Heal. Part A* **80**, 672–687 (2017).
 20. OECD. *Test No. 487: In Vitro Mammalian Cell Micronucleus Test.* (OECD Publishing, 2016). doi:10.1787/9789264264861-en
 21. Fenech, M. Cytokinesis-block micronucleus cytochrome assay. *Nat. Protoc.* **2**, 1084–1104 (2007).
 22. OECD. *Test No. 471: Bacterial Reverse Mutation Test.* (OECD Publishing, 1997). doi:10.1787/9789264071247-en
 23. Zhang, L.-S. *et al.* A comparative study of TK6 human lymphoblastoid and L5178Y mouse lymphoma cell lines in the in vitro micronucleus test. *Mutat. Res. Lett.* **347**, 105–115 (1995).
 24. Lorge, E. *et al.* Standardized cell sources and recommendations for good cell culture practices in genotoxicity testing. *Mutat. Res. Toxicol. Environ. Mutagen.* **809**, 1–15 (2016).
 25. Islaih, M. *et al.* Relationships between genomic, cell cycle, and mutagenic responses of TK6 cells exposed to DNA damaging chemicals. *Mutat. Res. Mol. Mech. Mutagen.* **578**, 100–116 (2005).
 26. Pfuhrer, S. *et al.* In vitro genotoxicity test approaches with better predictivity: Summary of an IWGT workshop. *Mutat. Res. Toxicol. Environ. Mutagen.* **723**, 101–107 (2011).
 27. Fowler, P. *et al.* Reduction of misleading (“false”) positive results in mammalian cell genotoxicity assays. I. Choice of cell type. *Mutat. Res. Toxicol. Environ. Mutagen.* **742**, 11–25 (2012).
 28. Sobol, Z. *et al.* Development and validation of an in vitro micronucleus assay platform in TK6 cells. *Mutat. Res. Toxicol. Environ. Mutagen.* **746**, 29–34 (2012).
 29. Huang-Lee, L. L. H., Cheung, D. T. & Nimni, M. E. Biochemical changes and cytotoxicity associated with the degradation of polymeric glutaraldehyde derived crosslinks. *J. Biomed. Mater. Res.* **24**, 1185–1201 (1990).
 30. McPherson, J. M., Sawamura, S. & Armstrong, R. An examination of the biologic response to injectable, glutaraldehyde cross-linked collagen implants. *J. Biomed. Mater. Res.* **20**, 93–107 (1986).
 31. Fürst, W. & Banerjee, A. Release of Glutaraldehyde From an Albumin-Glutaraldehyde Tissue Adhesive Causes Significant In Vitro and In Vivo Toxicity. *Ann. Thorac. Surg.* **79**, 1522–1528 (2005).
 32. Draye, J.-P. *et al.* In vitro and in vivo biocompatibility of dextran dialdehyde cross-linked gelatin hydrogel films. *Biomaterials* **19**, 1677–1687 (1998).
 33. Aziz, M. A. *et al.* In vitro biocompatibility and cellular interactions of a chitosan/dextran-based hydrogel for postsurgical adhesion prevention. *J. Biomed. Mater. Res. Part B Appl. Biomater.* **103**, 332–341 (2015).
 34. Rousseau, C. F. & Gagnieu, C. H. In vitro cytocompatibility of porcine type I atelocollagen crosslinked by oxidized glycogen. *Biomaterials* **23**, 1503–1510 (2002).
 35. Hyon, S.-H., Nakajima, N., Sugai, H. & Matsumura, K. Low cytotoxic tissue adhesive based on oxidized dextran and epsilon-poly-L-lysine. *J. Biomed. Mater. Res. Part A* **102**, 2511–2520 (2014).
 36. Sokolsky-Papkov, M., Domb, A. J. & Golenser, J. Impact of Aldehyde Content on Amphotericin B-Dextran Imine Conjugate Toxicity. *Biomacromolecules* **7**, 1529–1535 (2006).
 37. Chan, M., Brooks, H., Moratti, S., Hanton, L. & Cabral, J. Reducing the Oxidation Level of Dextran Aldehyde in a Chitosan/Dextran-Based Surgical Hydrogel Increases Biocompatibility and

- Decreases Antimicrobial Efficacy. *Int. J. Mol. Sci.* **16**, 13798–13814 (2015).
38. Ito, T. *et al.* The prevention of peritoneal adhesions by in situ cross-linking hydrogels of hyaluronic acid and cellulose derivatives. *Biomaterials* **28**, 975–983 (2007).
 39. Athanasiadis, T. *et al.* Effects of a Novel Chitosan Gel on Mucosal Wound Healing Following Endoscopic Sinus Surgery in a Sheep Model of Chronic Rhinosinusitis. *Laryngoscope* **118**, 1088–1094 (2008).
 40. Lauder, C. I. W., Strickland, A. & Maddern, G. J. Use of a Modified Chitosan–Dextran Gel to Prevent Peritoneal Adhesions in a Porcine Hemicolectomy Model. *J. Surg. Res.* **176**, 448–454 (2012).
 41. Rajiv, S. *et al.* The efficacy and safety of chitosan dextran gel in a burr hole neurosurgical sheep model. *Acta Neurochir. (Wien)*. **155**, 1361–1366 (2013).
 42. Artzi, N., Shazly, T., Baker, A. B., Bon, A. & Edelman, E. R. Aldehyde-Amine Chemistry Enables Modulated Biosealants with Tissue-Specific Adhesion. *Adv. Mater.* **21**, 3399–3403 (2009).
 43. Hoffmann, B. *et al.* Characterisation of a new bioadhesive system based on polysaccharides with the potential to be used as bone glue. *J. Mater. Sci. Mater. Med.* **20**, 2001–2009 (2009).
 44. Maia, J. *et al.* Ocular injectable formulation assessment for oxidized dextran-based hydrogels. *Acta Biomater.* **5**, 1948–1955 (2009).
 45. Su, W.-Y., Chen, Y.-C. & Lin, F.-H. Injectable oxidized hyaluronic acid/adipic acid dihydrazide hydrogel for nucleus pulposus regeneration. *Acta Biomater.* **6**, 3044–3055 (2010).
 46. Hu, M. *et al.* In situ forming oxidised hyaluronic acid/adipic acid dihydrazide hydrogel for prevention of epidural fibrosis after laminectomy. *Eur. Cells Mater.* 307–320 (2017). doi:10.22203/eCM.v034a19
 47. Schramm, C. *et al.* The Cross-linked Biopolymer Hyaluronic Acid as an Artificial Vitreous Substitute. *Investig. Ophthalmology Vis. Sci.* **53**, 613 (2012).
 48. Bouhadir, K. H., Hausman, D. S. & Mooney, D. J. Synthesis of cross-linked poly(aldehyde guluronate) hydrogels. *Polymer (Guildf)*. **40**, 3575–3584 (1999).
 49. Tice, R. R. *et al.* Single cell gel/comet assay: Guidelines for in vitro and in vivo genetic toxicology testing. *Environ. Mol. Mutagen.* **35**, 206–221 (2000).
 50. Sharma, A. *et al.* Different DNA damage response of cis and trans isomers of commonly used UV filter after the exposure on adult human liver stem cells and human lymphoblastoid cells. *Sci. Total Environ.* **593–594**, 18–26 (2017).
 51. Sotiriou, G. A. *et al.* Engineering safer-by-design silica-coated ZnO nanorods with reduced DNA damage potential. *Environ. Sci. Nano* **1**, 144 (2014).
 52. Tubbs, A. & Nussenzweig, A. Endogenous DNA damage as a source of genomic instability in cancer. *Cell* **168**, 644–656 (2017).

CHAPTER 4

In vivo systemic toxicity assessment of a dextrin-based hydrogel and its effectiveness as a carrier and stabilizer of granular synthetic bone substitutes



The worldwide incidence of bone disorders is increasing, mainly due to ageing population. As a result, the use of bone graft substitutes has dramatically increased in the last decade. The lack of effective treatments is pushing the development of synthetic bone substitutes (SBSs). Most ceramic-based SBS commercially available display limited handling properties. Attempting to improve the handling properties and the acceptance of these formulations, granular ceramics have been associated with hydrogels to produce injectable/mouldable SBSs. Dextrin, a low-molecular-weight carbohydrate, was used to develop a fully resorbable and injectable hydrogel. Dextrin was firstly oxidized with sodium periodate and then cross-linked with adipic acid dihydrazide. The *in vivo* biocompatibility and safety of the dextrin-based hydrogel (HG) was assessed by subacute systemic toxicity and skin sensitization tests, using rodent models. The results showed that the HG did not induce any systemic toxic effect or skin reaction, neither impaired the bone repair/regeneration process. Then, the HG was successfully combined with granular ceramics (250-500 μm) to obtain a mouldable/injectable SBS, which was implanted in tibial fractures in goats for 3 and 6 weeks. The results showed that HG allowed the stabilization of the granules into the defect, ensuring effective handling and moulding properties of the formulation, as well as, an efficient cohesion of the granules.

4.1 | Introduction

Bone is a dynamic and highly vascularized tissue with a unique capacity to heal and regenerate itself throughout the lifetime of an individual. However, in some situations where the template for an orchestrated regeneration fails, clinical procedures are needed¹. Currently, the standard procedure to treat bone defects is the autograft, which consists in harvesting a small amount of bone tissue from the patient and its transplantation to the defect site. Despite this procedure has the best clinical outcome, explant site pain and morbidity and limited availability represent main limitations. Allografts (bone tissue from other individuals or corpses) or xenografts (bone tissue from other species) can overcome these issues, but the risk of immune reactions, transmission of diseases and low availability of tissue banks limit their utilization^{1,2}. In this respect and considering that the worldwide incidence of bone disorders and conditions has trended steeply upward, mainly due to ageing population, alloplastic biomaterials, such as synthetic bone substitutes (SBSs) have appeared as a valid alternative to tissue transplants^{1,3}.

Ceramic-based SBSs are widely used as bone substitutes in the clinical practice⁴. Many of these commercially available products are presented in granular form¹. They are difficult to handle and to fit into the defects, namely in irregular defects and the granules can be washed out from the implanted site by body fluids and, consequently, migration of granular particles to the surrounding tissues occurs, which can cause adverse or unexpected events^{3,5,6}. Moreover, the micromovements of the granules within the defect can affect the formation of new bone tissue.

In order to potentiate the clinical application of the granular SBSs, they have been combined with hydrogels⁷⁻⁹. Hydrogels can ensure granules cohesiveness/stabilization into the bone defect. They can also serve as space-holders to prevent granule packing and allow easier bone ingrowth^{10,11}, and provide mouldable properties, allowing the clinicians to handle and shape the formulations into the bone defects without leakage of the granules. Moreover, the combination of bioactive properties of granular ceramics with the elastomeric properties of hydrogels, results in composites with better mechanical properties, such as higher extensibilities¹²⁻¹⁸. One of the major advantages in using hydrogels is the possibility to develop injectable formulations of bone substitutes. From a clinical point of view, injectability of biomaterials for the regeneration of bone defects offers several clinical and economic advantages as compared to solid, prefabricated implants. Using these flowable materials, complete filling of the defect site can be established by means of minimally invasive techniques^{3,8,9,19}. In particular, stimuli-responsive hydrogels have been appointed as the best candidates to achieve this goal. Their ability to gel *in situ* in response to external physical or chemical stimuli - as temperature, pH or UV light - allow hydrogels mixed with ceramics to be administered as flowable viscous liquids (sol state) into the bone defect, then turning into standing hydrogels (gel state)⁹.

Our research group has been developing and characterizing a fully resorbable and injectable dextrin-based hydrogel (HG) which was intended to perform as a multifunctional platform, enabling the combination with stem cells and other bioactive agents, during clinical procedures²⁰⁻²³. To obtain the

HG, dextrin was firstly oxidized with sodium periodate to produce dialdehydes, which then reticulate with adipic acid dihydrazide²⁰. We proposed that *in situ* forming dextrin-based hydrogel would be a suitable carrier for ceramic granules in clinical applications.

The development of biomaterials for medical applications includes extensive preclinical testing in order to demonstrate their safety and efficacy according to the regulatory agencies requirements²⁴. Thus, in the present study, the systemic toxicity of the HG was assessed, as well as the bone histocompatibility and skin sensitization, using rodent models. Then, the HG was associated with granular ceramics (250-500 μm) for the development of a mouldable and injectable bone substitute, and the effectiveness of the HG to stabilise the granules into the defect was evaluated in a goat tibial fracture.

4.2 | Experimental

4.2.1 | Chemicals

Dextrin used in this work was Tackidex B 167 (Batch E 1445), generously provided by Roquette (Lestrem, France). All chemicals used were of highest purity or analytical grade available. Sodium *m*-periodate, diethylene glycol, adipic acid dihydrazide (ADH), Triton X-100, low melting point (LMP) agarose, Tris base, Freund's complete adjuvant (FCA) and sodium dodecyl sulphate (SDS), sodium carbonate (Na_2CO_3), calcium hydrogenphosphate (CaHPO_4), calcium fluoride (CaF_2), di-phosphorus penta-oxide (P_2O_5) and polyvinyl alcohol (PVA), formaldehyde were purchased from Sigma-Aldrich (St. Louis, MO, USA). Absolute ethanol, sodium hydroxide (NaOH), sodium chloride (NaCl), hydrochloric acid (HCl), Tris base, Giemsa's azur eosin methylene blue, ethylenediaminetetraacetic acid disodium salt (Na_2EDTA) and hydrogen peroxide solution (H_2O_2) were obtained from Merck (Darmstadt, Germany). Invitrogen® SYBR® Gold was purchased from Thermo Fisher Scientific (Waltham, MA, USA). Sterile phosphate-buffered saline (PBS) solution without calcium and magnesium was purchased to Biochrom GmbH (Berlin, Germany), normal melting point (NMP) agarose was supplied by Bionline (London, UK) and Lymphoprep™ was obtained from STEMCELL Technologies (Vancouver, Canada).

4.2.2 | Material preparation

4.2.2.1 | Dextrin oxidation

Dextrin oxidation was performed as previously described by Pereira et al.²⁵. Briefly, aqueous solutions of Dextrin (2% w/v) were oxidized with sodium *m*-periodate, to yield the theoretical degree of oxidation of 40%, at room temperature, with stirring, in the dark. After 20 h, the oxidation reaction was stopped by adding drop wise an equimolar amount of diethylene glycol, to reduce any unreacted periodate. Sodium *m*-periodate and diethylene glycol were removed by ultrafiltration, using a membrane with a molecular weight cut-off 1000 Da (Merck Millipore, Billerica, MA, USA), and then lyophilized.

4.2.2.2 | Preparation of dextrin-based hydrogel

Oxidized dextrin (ODEX) was dissolved in PBS buffer (phosphate buffered saline) (30% w/v) and the solution was sterilized by gamma irradiation, using a ^{60}Co source, at 20 kGy (2 kGy/h), at room temperature, by IONISOS (Dagneux, France). Adipic acid dihydrazide (ADH) was dissolved also in PBS buffer (3.76% w/v) and sterilized by filtration, using filters with pore 0.22 μm (Pall Corporation, MI, USA). For crosslinking reaction, ODEX and ADH solutions were mixed with volume ratio 7:3.

4.2.2.3 | Preparation of Bonelike[®] granules

Ceramic powder was synthesized according to the method described elsewhere^{26,27}. Briefly, P_2O_5 -CaO based glass with the chemical composition of 65 P_2O_5 -15CaO-10CaF₂-10Na₂O (mol %) was prepared by mixing the appropriate quantities of Na_2CO_3 , CaHPO_4 , CaF_2 , and P_2O_5 in a platinum crucible, and then heating it at 1450 °C for 90 min in a glass furnace. The prepared glass was crushed in an agate mortar and sieved to a granule size below 50 μm . Bonelike[®] was obtained by adding 2.5 % wt. of bioglass to the previous prepared hydroxyapatite (HAP). The Bonelike[®] powder was mixed with the microcrystalline cellulose and PVA and the resulting suspension was poured into Alumina (Al_2O_3) plates, dried in a woven at 60 °C for two days and then the samples were sintered at 1300 °C using a heating rate of 4 °C/min, followed by natural cooling inside the furnace. Finally, using standard milling and sieving techniques, Bonelike[®] granules with particle size between 250-500 μm were obtained. Throughout this work, Bonelike[®] will be abbreviated to BL.

4.2.2.4 | Association of Bonelike[®] granules to dextrin-based hydrogel

In order to set the higher concentration of BL granules which can be loaded into the HG without compromising the extrusion process and granules' stability and mouldability, different concentrations of BL were tested (30, 40 and 60% ($w_{\text{BL}}/v_{\text{HG}}$) of granules). For each formulation, all components (BL, ODEX and ADH) were mixed, transferred into 2 mL syringes and incubated for 30 min. To evaluate the injectability of the formulations, the syringe was fixed vertically on the texture analyzer TA-XT2i (Stable Mycro Systems, UK). During the test, while using a load cell of 5 kgf, the syringe piston was pushed at a velocity of 1 mm/s, through a distance of 10 mm and the extrusion force was measured. The test was performed in triplicate.

4.2.3 | Animals

All the animal testing procedures were in conformity with the European norms for animal welfare (European Directive 2010/63/EU) and with the approval of the Portuguese Veterinary Authorities (*Direção-Geral de Alimentação e Veterinária*), in accordance with the Portuguese legislation (Portaria 1005/92) and European Communities Council Directive of November 1986 (86/609/EEC). Humane endpoints were followed in accordance to the OECD Guidance Document on the Recognition,

Assessment and Use of Clinical Signs as Humane Endpoints for Experimental Animals Used in Safety Evaluation ²⁸. Adequate measures were taken to minimize pain and discomfort, considering humane endpoints for animal suffering and distress.

4.2.4 | Subacute systemic toxicity test

The potential of the HG to cause adverse systemic reactions was evaluated in Wistar rats (Charles River Laboratories Inc, USA) for 3 weeks, and was performed according to requirements and guidances described by ISO 10993-11 ²⁹. Twenty rats of both genders, 8 to 9-week-old, were randomly divided in test group (HG) and control group (PBS). One femoral defect was induced per animal, and HG (test group) or PBS (control group) were then injected. For the creation of the femoral defect, the pelvic limb from the lumbar midline to the knee was shaved and aseptically prepared with gluconate chlorhexidine. A longitudinal skin incision beginning over greater trochanter extending down the lateral side was made, exposing the tensor fascia lata, which was then dissected. A deep dissection was performed splitting vastus lateralis. Retractors were placed at the proximal femur and then bone surface was exposed with subperiosteal dissection. A lateral unicortical 3 mm circular defect was drilled under irrigation using a round diamond turbine bur (iM3, Republic of Ireland), and then the materials (PBS or HG) were placed and fitted in the defects. After, the surgical wound was closed in two layers using a 4-0 glyconate reabsorbable suture (Monosyn; BBraun, Portugal) for muscle and for the skin. Animals received analgesic medication for 5 days and antibiotic treatment for 6 days. After 3 weeks of implantation surgery, the animals were anaesthetized and then euthanized with an intraperitoneal injection of sodium pentobarbital (Eutasil; CEVA, Portugal).

During the experimental period of 3 weeks, mortality, body weight, and clinical signs (respiratory, motor activities, convulsion, reflexes, ocular and cardiovascular signs, salivation, piloerection, analgesia, muscle tone, gastrointestinal and skin signs) were observed and recorded. Immediately before sacrificing the animals, the blood samples were collected for haematological and biochemical parameters determination and genotoxicity assessment. After sacrifice, all animals were subjected to a necropsy examination and the adrenals, brain, epididymides, heart, kidneys, liver, ovaries, spleen, testes, thymus and uterus were collected and weighed. Spleen, liver, kidneys, lungs, pancreas and femur were fixed in 10% neutral-buffered formalin for further histopathological examination.

4.2.4.1 | Genotoxicity assay

Comet assay, also known as the single-cell gel electrophoresis (SCGE) assay was performed in rat whole-blood and isolated peripheral blood mononuclear cells (PBMC) to evaluate the DNA damage. For whole-blood, 5 and 10 μL of blood (duplicates) were suspended in 995 and 990 μL of PBS, respectively, and then centrifuged at 400 $\times g$ for 3 min. The obtained pellets were mixed in 100 μL 1% (w/v) LMP agarose and layered onto dry microscope slides (VWR, Darmstadt, Germany) pre-coated with 1% (w/v)

NMP agarose. For PBMC, 100 μ L of venous blood sample (duplicates) were suspended in 100 μ L of PBS, and gently layered over 150 μ L of Lymphoprep™. Then, samples were centrifuged at 400 $\times g$ for 5 min, the PBMC layer was retrieved, resuspended in PBS up to 1 mL, and centrifuged at 400 $\times g$ for 3 min. The obtained pellets were mixed in 100 μ L 1% (w/v) LMP agarose and layered onto dry microscope slides (VWR, Darmstadt, Germany) pre-coated with 1% (w/v) NMP agarose. After gel solidification, rat whole-blood and PBMC slides immersed in 200 μ M H₂O₂ (20 min) and 25 μ M H₂O₂ (3 min), respectively, protected from light and kept in the refrigerator, served as positive controls. All the slides were then placed in a Coplin jar and immersed in ice-cold lysis solution (2.5 M NaCl, 100 mM Na₂EDTA, 10 mM Tris base, 10 M NaOH, pH 10, supplemented with 1% Triton-X 100) for 1.5 h at 4 °C, protected from light to lyse the cells and separate DNA from histones. For unwinding of the DNA, all slides were immersed in freshly prepared electrophoresis buffer (200 mM Na₂EDTA, 0.3 M NaOH pH>13) in the electrophoresis unit for 40 min at 4 °C, followed by electrophoresis for 20 min at 30 V and 300 mA. Then, the gels were washed with H₂O, fixed with ethanol 70% and 96% for 15 min, each at room temperature. After air-drying the slides overnight, DNA was stained with a 0.07 % SYBR Gold solution. The slides were coded, and one scorer performed the comet analysis using a fluorescence microscope (Nikon Eclipse E400 microscope attached to an epifluorescence illuminator Nikon C-SHG1) with 400x magnification and the image analysis software Comet Assay IV (Perceptive Instruments, Suffolk, UK). The % DNA in the comet tail (tail intensity) and the olive tail moment were used as a measure of the amount of DNA damage. At least 200 cells, per animal, were scored (50 for each replicate gel).

4.2.4.2 | Histological processing

Spleen, liver, kidneys, lungs, pancreas and femur from Wistar rats were routinely processed, dehydrated and embedded in paraffin wax, in a Shandon® automatic tissue processor Hypercenter XP. Consecutive 3 μ m sections were cut and stained with haematoxylin and eosin (HE) and kept for histopathological analysis. Prior to tissue processing, femurs were decalcified with Surgipath decalcifier II Leica®, for 48 h. Images were acquired using a Nikon VR microscope connected to a Nikon VR digital camera DXM1200.

4.2.5 | Skin sensitization test

The maximization sensitization test was performed to determine the potential of the HG to produce skin sensitization in guinea pigs, according to ISO 10993-10³⁰ and OECD 406³¹ guidelines. Fifteen Dunkin Hartley guinea pigs (seven males and eight females) (Charles River Laboratories Inc, USA) were used for the experiment, with ten animals in the test group and five in the control group. The test consisted of three phases: intradermal induction phase, topical induction phase and challenge phase. The pelage of guinea median back region (for the intradermal or topical application) and flank region (for the challenge dose) was shaved. Then (intradermal induction phase), three pairs of intradermal injections of 100 μ L

were given in the median back region: i) PBS mixed with FCA (1:1 v/v), ii) HG and iii) HG mixed with FCA (1:1 v/v); in the control group, HG was substituted by PBS (vehicle). Six days later, all animals received a topical application of 10% SDS, in the injection area, in order to create a local irritation. In the next day, a gauze fully-loaded with 2.5-fold diluted HG (for test group) and PBS (for control group) was applied in the same area, and held in contact by an occlusive dressing for 48 h. The challenge phase was conducted 14 days after the topical application, in which the diluted HG was applied in right flank region of all animals, using a loaded gauze (1 x 1 cm) and covered with an occlusive dressing. The dressings were removed after 24 h. The appearance of the challenge skin areas of the animals was observed 24 h and 48 h after removal of the dressings. The description and grade of the skin reactions for erythema and oedema was done according to the Magnusson and Kligman grading scale³⁰.

4.2.6| Application of the Bonelike® granules combined to dextrin-based hydrogel in bone defects

The assessment of the effectiveness of the dextrin-based hydrogel to mould and stabilise Bonelike® granules in bone defects was performed in a tibia fracture on a goat model. For this purpose, adult goats (n = 24) were used and randomly divided into 2 groups: control (empty defect) and test (HG + BL). The surgical steps for the creation of the segmental defect in the diaphysis of the right tibia are represented in **Figure 4.1**. Briefly, the periosteum was elevated on the medial tibial shaft and the eight-hole stainless-steel dynamic compression plate was fixed in the distal segment in order to perform the holes to insert the 4.5 mm screws in the distal segment. Then, the plate was removed, and the transverse osteotomy of the tibia was performed using a high-speed oscillating saw. After that, a width 4 mm metallic spacer was inserted between the two segments of the tibia to create a uniform defect. Then, the plate was screwed first to the distal segment and then the holes were drilled, and the fixation was done in the proximal segment. The spacer was removed, and the defect was filled with HG + BL. The soft tissues were closed in two layers with resorbable sutures. After surgery, X-rays images were obtained. The goats were set free in a 25 m² open space and allowed to move without restriction after surgery and received analgesic medication for 4 days and antibiotic treatment for 7 days. The goats were randomly sacrificed 3 and 6 weeks (n = 6) after surgery with a lethal intravenous injection of 40% sodium pentobarbital (Euthasol®, Esteve, Spain). The tibia was then harvested and fixed in 4% formaldehyde solution for further analysis.

4.2.6.1| Micro-computed tomography analysis

Micro-computed tomography (microCT) scans were taken for qualitative evaluation of the new bone formed in tibial defects, using the microCT 100 scanner (SCANCO Medical AG, Brüttisellen, Switzerland), which operated with a cone beam originating from a 5 µm focal-spot X-ray tube. The photons were detected by a CCD-based area detector and the projection data were computer-reconstructed into a

2058 x 2058 image matrix. A 0.5 mm aluminium filter was used for taking optimized images. For each sample at least 1500 projections/180° of X-rays (90 kVp, 155 μ A, integration time 300 ms, scanning time 56 min) were acquired.

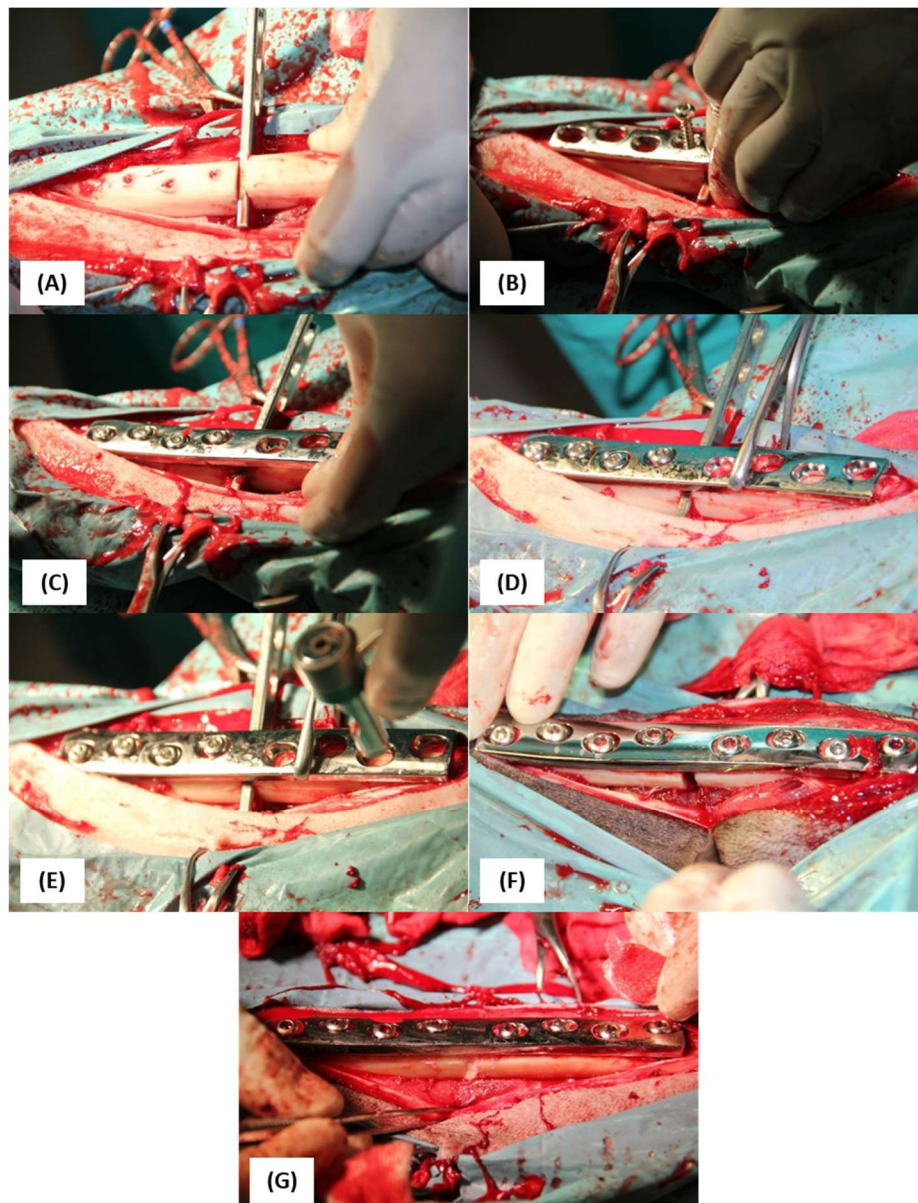


Figure 4.1: Steps for creation of the bone defect in the diaphysis of the right tibia: **(A)** the holes were performed for inserting screws in the distal segment and placement of the 4 mm spacer, **(B)** fixation of the plate in the distal segment, **(C)** adjustment of the plate to the proximal side, **(D)** temporary fixation with forceps of the proximal segment, **(E)** the holes were performed in the proximal segment, **(F)** Bone defect realized and fixed with plate and screws, and **(G)** Filling of the bone defect with the HG + BL formulation.

4.2.7 | Statistical analysis

Experimental data were presented as mean \pm standard deviation (SD). Statistical analysis and graphs were performed using the Prism® version 6.1 (GraphPad Software Inc., La Jolla, CA, USA). Statistical analysis of data was performed by two-tailed *t*-test. Significance was accepted at a *p*-value < 0.05.

4.3 | Results and discussion

4.3.1 | Subacute systemic toxicity assessment

Following implantation of biomaterials, leachates or degradation products may be released and spread all over the body. Therefore, the systemic toxicity assessment is of great importance to demonstrate the safety of such biomaterials. The dextrin-based hydrogel is composed by ODEX and ADH linked by hydrazine bonds, which are susceptible to hydrolysis under aqueous environment²⁰. In a previous study, the *in vivo* biocompatibility of the HG after subcutaneous implantation in a rat model was assessed. It was verified that after 15 days small amount of HG residues were still present in the implant sites²². In the present work, the systemic toxicity of the HG after implantation in a bone defect was evaluated over a period of 3 weeks. During this experiment, no animal mortalities were observed for any of the test or control groups, all presenting normal vital parameters and behaviour. The body weight of animals of both genders in the test groups did not vary significantly from the respective control group (**Table 4.1**). The gain in body weight in all the test groups was comparable to that of the control group. Thus, no HG-related effects were observed in relation to mortality, clinical signs and body weight changes.

Table 4.1: Body weight, in grams, of female and male rats exposed to the hydrogel (test group) and PBS (control group), at the beginning (0th week) and 1st and 3rd weeks after surgery.

	Female		Male	
	Control	Test	Control	Test
0 th week	175.80 ± 12.19	168.60 ± 7.13	268.20 ± 8.44	276.00 ± 8.43
1 st week	188.80 ± 6.98	196.20 ± 7.66	294.60 ± 10.81	305.00 ± 6.56
3 rd week	212.40 ± 6.35	224.00 ± 13.02	346.00 ± 26.53	351.40 ± 25.23

Results are presented as mean ± SD ($n = 5$ replicates per group). Data were analysed by two-tailed *t*-test. No statistical significant differences from the respective control group were found.

Haematology and biochemical analyses were also performed to all animals to investigate toxic effects in tissues, organs and other systems. The biochemical profile (**Table 4.2**) revealed no significant changes in the various biochemical parameters. These results corroborated well with the haematological profiles of animals in the test group of both genders compared with the control group (**Table 4.3**). Despite a significant reduction in the eosinophils levels ($p < 0.01$) observed in females of the test group, the values are within the normal range³².

Systemic effects were also evaluated in the animals during the necropsy, where careful macroscopic assessment of the internal organs was carried out in order to confirm the clinical observations performed during the study period. The internal organs of the animals from test groups presented normal topography and morphological features, without any signs of necrosis, congestion, and abnormal accumulations. The determination of organ coefficient ($\% w_{organ}/w_{body}$) confirmed that HG did not

promote any toxicity in vital organs, since no statistical difference to the control group was observed (**Figure 4.2**). Additionally, careful histopathological analysis was performed for kidneys, liver, lungs, pancreas and spleen, which did not exhibit any alteration in the normal cellular architecture of the organs of both male and female animals (**Figure 4.3**).

Table 4.2: Biochemical parameters in female and male rats treated with hydrogel (test group) and PBS (control group), at 3 weeks after surgery.

Parameter (Unit)	Female		Male	
	Control	Test	Control	Test
Albumin (g/L)	15.91± 1.73	15.98 ± 1.79	12.08 ± 0.65	12.12 ± 0.70
ALP (U/L)	111.80 ± 11.95	106.90 ± 23.72	163.80 ± 35.95	151.60 ± 18.04
ALT (U/L)	39.20 ± 10.85	31.30 ± 6.89	32.40 ± 10.21	41.80 ± 20.22
AST (U/L)	241.60 ± 76.32	146.70 ± 68.66	123.60 ± 72.76	154.80 ± 119.48
Total Protein (g/L)	63.50 ± 5.57	64.00 ± 6.04	56.00 ± 2.74	55.00 ± 1.58
Total Bilirubin (mg/dL)	0.04 ± 0.05	0.02 ± 0.04	0.02 ± 0.04	0.00 ± 0.00
Cholesterol (mg/dL)	52.90 ± 10.80	50.50 ± 6.91	35.60 ± 7.09	39.40 ± 3.97
Creatinine (mg/dL)	0.40 ± 0.00	0.40 ± 0.00	0.42 ± 0.04	0.44 ± 0.09
Glucose (mg/dL)	341.20 ± 89.97	341.90 ± 75.21	448.20 ± 91.95	470.80 ± 94.62
Triglycerides (mg/dL)	182.60 ± 85.57	163.50 ± 61.76	113.60 ± 41.94	146.80 ± 32.20
Urea (mg/dL)	36.30 ± 3.93	39.90 ± 2.92	37.40 ± 3.36	37.60 ± 2.30
Calcium (mg/dL)	11.88 ± 1.20	12.04 ± 0.93	11.64 ± 0.42	11.44 ± 0.49
Sodium (mol/L)	140.84 ± 2.18	141.85 ± 1.30	138.24 ± 1.77	138.62 ± 1.11
Potassium (mol/L)	7.28 ± 0.72	6.38 ± 1.06	7.17 ± 0.45	6.76 ± 0.89
Chloride (mol/L)	100.96 ± 3.55	101.52 ± 2.46	99.24 ± 1.75	99.12 ± 1.80
Phosphorus (mg/dL)	12.77 ± 2.14	11.13 ± 1.82	10.26 ± 0.33	10.40 ± 1.16

Abbreviations: ALP - Alkaline phosphatase; ALT - Alanine aminotransferase; AST - Aspartate aminotransferase. Results are presented as mean ± SD ($n = 5$ replicates per group). Data were analysed by two-tailed t -test. No statistical significant difference from the respective control group was found.

Table 4.3: Haematological parameters in female and male rats treated with hydrogel (test group) and PBS (control group), at 3 weeks after surgery.

Parameter (Unit)	Female		Male	
	Control	Test	Control	Test
White Blood Cells ($10^9/L$)	3.15 ± 0.83	2.07 ± 0.87	3.78 ± 2.25	3.22 ± 2.59
Red Blood Cells ($10^{12}/L$)	8.79 ± 0.15	8.31 ± 0.72	7.54 ± 1.45	8.43 ± 0.82
Hemoglobin (g/L)	164.40 ± 5.55	154.80 ± 13.01	138.80 ± 23.97	156.00 ± 15.28
Hematocrit (%)	48.38 ± 2.72	45.08 ± 3.05	44.50 ± 8.83	47.34 ± 2.84
MCV (fL)	54.96 ± 2.15	54.30 ± 1.33	56.90 ± 2.19	56.32 ± 2.71
MCH (pg)	18.72 ± 0.34	18.64 ± 0.38	18.50 ± 0.60	18.52 ± 0.41
MCHC (g/L)	340.00 ± 8.94	343.20 ± 6.30	324.80 ± 5.36	329.00 ± 13.11
Platelets ($10^9/L$)	834.00 ± 62.13	798.00 ± 103.67	786.00 ± 115.87	729.20 ± 133.33
Neutrophils ($10^9/L$)	0.37 ± 0.17	0.22 ± 0.05	0.40 ± 0.30	0.47 ± 0.45
Lymphocytes ($10^9/L$)	2.72 ± 0.72	1.83 ± 0.84	2.88 ± 1.37	2.70 ± 2.38
Monocytes ($10^9/L$)	0.04 ± 0.07	0.02 ± 0.03	0.06 ± 0.05	0.08 ± 0.13
Eosinophils ($10^9/L$)	0.02 ± 0.01	$0.01 \pm 0.01^*$	0.01 ± 0.01	0.02 ± 0.03
Basophils ($10^9/L$)	0.00 ± 0.00	0.00 ± 0.00	0.01 ± 0.01	0.00 ± 0.01

Results are presented as mean \pm SD ($n = 5$ replicates per group). Data were analysed by two-tailed t -test: * $p < 0.01$ versus control group.

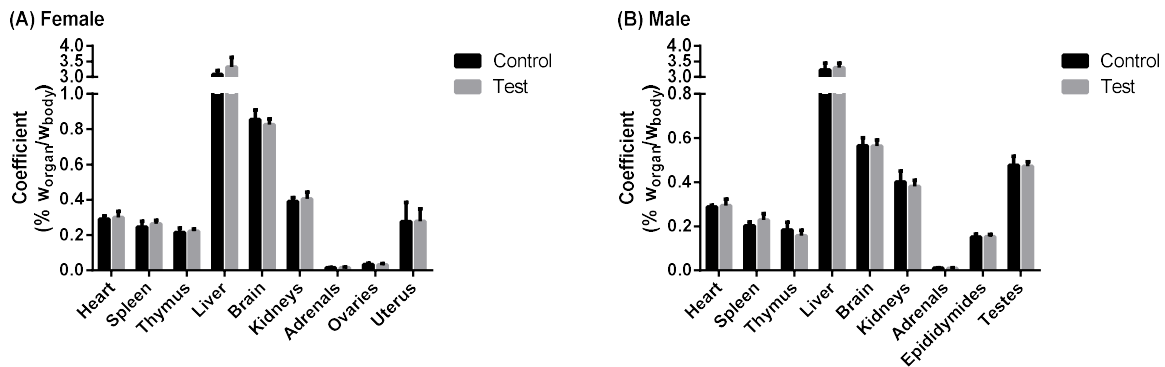


Figure 4.2: Coefficients of organs in female (A) and male (B) rats treated with hydrogel (test group) and PBS (control group), at 3 weeks after surgery. Results are presented as mean \pm SD ($n = 5$ replicates per group). Data were analysed by two-tailed t -test. No statistical significant difference from the respective control group was found.

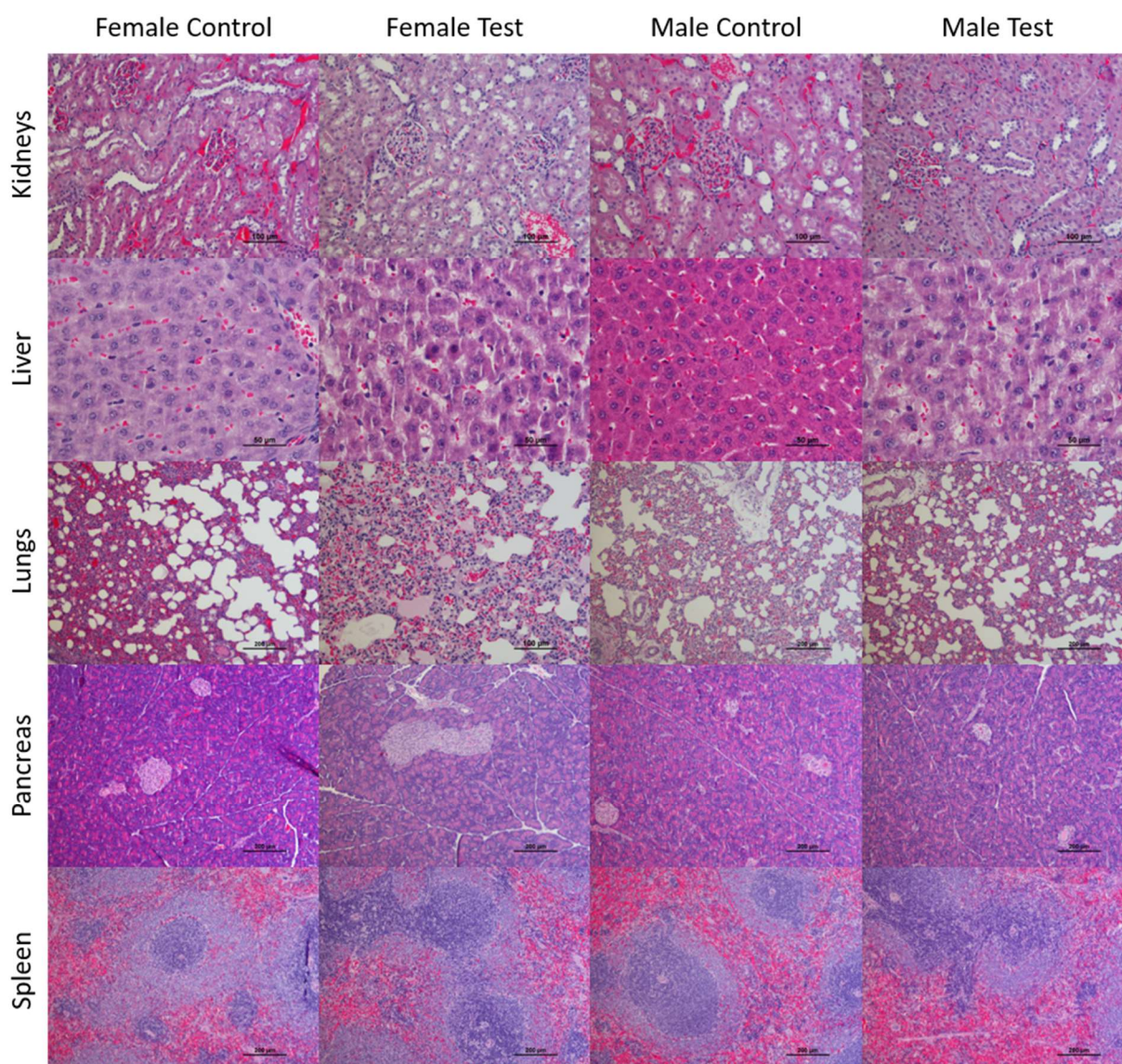


Figure 4.3: Representative photographs of histopathologic examination, after haematoxylin and eosin staining, of kidneys, liver, lungs, pancreas and spleen of control and test groups of both genders, after 3 weeks after surgery.

Dextrin is a biocompatible, nonimmunogenic polysaccharide and biodegradable by alpha-amylases. Furthermore, the molecular weight of dextrin is appropriate to ensure renal elimination, thus excludes the threat of progressive accumulation after repeated administration^{33,34}. However, dextrin is still relatively unexplored in biomedical field, being clinically used as a peritoneal dialysis solution^{35–37} and as wound dressing agent³⁸. Dextrin displays important chemical features, such as solubility in both water and DMSO, and availability of hydroxyl groups, allowing an easy chemical modification of its backbone^{39,40}. It is known that dextrin backbone modification and/or the degree of such modifications can affect the biodegradability of the dextrin^{34,41,42}. During last years, few researchers have successfully developed and characterized dextrin-based hydrogels^{20,43–48} and nanogels^{33,49–54} for drug delivery and tissue engineering applications. However, *in vivo* toxicity studies are scarce and focus mainly local degradation and inflammatory response in subcutaneous assays^{22,41}, or *in vivo* drug release studies for nanogels^{51,55}. Das and colleagues⁴⁵ synthesized and characterized a biodegradable crosslinked hydrogel, consisting of

polylactic acid (PLA) and dextrin in presence of crosslinker *N,N*-methylene bisacrylamide - Dxt-g-PLA hydrogel. The acute toxicity of the Dxt-g-PLA hydrogel was assessed in mice after a single orally administered dose of hydrogel (2000 mg/kg body weight), and no mortality was observed within 12 weeks⁴⁵. Relating to dextrin-based nanogels, Gonçalves *et al.*⁴⁹ have developed self-assembling nanogels of dextrin - Dextrin-VA-SC16 (VA: vinyl acrylate, SC16: alkyl chain) and studied their organ biodistribution after intravenous administration in rodent models⁵⁶. The radioactivity of the Dextrin-VA-SC16 nanogels were mainly located in the organs of the Mononuclear Phagocytic System (liver and spleen) and kidneys. The reduction of the radioactivity levels observed after 2 h suggested that the material does not accumulate in the organs, presumably being metabolized and excreted. Indeed, some renal uptake of the nanogels, and excretion in the urine was detected⁵⁶. The results obtained in the present study clearly demonstrated that the oxidized dextrin-based hydrogel did not promote any metabolic abnormalities and no toxic effects on vital organs, like liver or kidney, after its implantation in bone defects, demonstrating its safety.

4.3.2 | Genotoxicity assessment

Increased levels of DNA damage and ineffective repair mechanisms are the underlying biomolecular events in the pathogenesis of most of the life-threatening diseases, like cancer and degenerative diseases⁵⁷. It is generally accepted that DNA damage in blood cells can reflect the level of oxidative stress in the body, albeit not always is clear whether this damage could be either the cause or the effect of diseases⁵⁸. Accordingly, genotoxicity assessment in parallel with systemic toxicity evaluation may add more information about the HG safety.

The comet assay is a versatile, sensitive and rapid method for measuring DNA strand breaks at the level of individual cells⁵⁹. Both whole-blood cells and PBMC were evaluated and the results are presented in **Table 4.4**. Tail intensity (%) and olive tail moment values of whole-blood cells and PBMC from the animals treated with HG were not significantly different in relation to the respective control group, in animals of both genders, suggesting that HG did not induce DNA damage. On the other hand, cells exposed to a H₂O₂ solution (positive control) displayed a significant increase in tail intensity (%) and olive tail moment ($p < 0.001$). The results herein obtained with blood cells are in agreement with *in vitro* findings in human lymphoblastoid TK6 cells exposed to different concentrations of the HG that revealed no DNA and chromosomal damage, as assessed by the micronucleus and comet assays²³, supporting the view that the HG is genocompatible.

Although the use of isolated PBMC for DNA damage analysis by the comet assay has been well established, the advantage of using whole-blood for *in vivo* studies is here highlighted, mainly in situations where time is a limiting factor as more samples can be handled in a short period of time, since no cell separation procedures are necessary^{58,60}. This option is also advantageous when sample volume is critical, for instance, when younger rats or mice (e.g. C57BL/6) are used and/or when many different

analyses should be performed with blood. In this study, it was demonstrated that only a few microliters of whole-blood (5 μL) could be used directly for comet assay analysis, much less than it is required for isolation of PBMC (100 μL). It was also demonstrated that whole-blood approach provides reliable results for genotoxicity biomonitoring in rodent models, since the conclusions resulting from PBMC do not differ from those derived from whole-blood cells, as previously reported by Chuang and Hu⁶⁰.

Table 4.4: Comet assay analysis of DNA damage in whole-blood cells and PBMC of female and male rats exposed to hydrogel (test group) and PBS (control group), 3 weeks after surgery.

	Whole-Blood		PBMC	
	Tail intensity (%)	Olive tail moment	Tail intensity (%)	Olive tail moment
Female Control	10.72 \pm 3.66	1.14 \pm 0.43	8.29 \pm 1.87	0.86 \pm 0.22
Female Test	9.32 \pm 0.99	0.99 \pm 0.15	6.21 \pm 0.60	0.55 \pm 0.11
Male Control	10.18 \pm 2.25	1.11 \pm 0.33	7.72 \pm 1.88	0.73 \pm 0.18
Male Test	10.55 \pm 0.33	1.07 \pm 0.03	8.36 \pm 2.90	0.83 \pm 0.37
Positive Control	27.72 \pm 3.12*	4.70 \pm 1.37*	40.00 \pm 7.81*	7.53 \pm 2.66*

H₂O₂ (200 μM and 25 μM for whole-blood cells and PBMC, respectively) was used as positive control. Results are presented as mean \pm SD ($n = 5$ replicates per group). Data were analysed by two-tailed t -test: * $p < 0.001$ versus control group.

4.3.3 | Assessment of implanted site

The local effects were evaluated through macroscopic observation of the femurs and histological analysis to the implanted site. Macroscopic observation was conclusive for the absence of abnormalities, necrosis, infection or changes in the normal structure of the femurs. Histological analysis was performed in order to assess the bone tissue response to injectable HG. Representative histological images stained with HE are presented in **Figure 4.4**. No HG was found in the defect site. The histological appearance of the HG-treated defects from both genders was identical to the defects in the control group. The defects were occupied by connective tissue with variable neovascularization, containing active osteoblasts at the margins of the defect. The presence of inflammatory cells was not observed in any sample, nor necrosis or fatty infiltrate. The performed defect was non-critical, which means that it will heal spontaneously over the time. The results demonstrated that HG does not affect the bone healing process, displaying a good histocompatibility.

In a previous study, the HG was evaluated for inflammatory response, using subcutaneous implants in rats²². In that study, histological analysis after 3 and 15 days showed typical acute and chronic inflammatory responses, respectively. HG was scored as slightly irritant after 3 days of implantation and as non-irritant after 15 days. Several studies on hydrogels containing aldehyde-modified polysaccharides have shown biocompatibility, safety and good performance *in vivo* in diverse biomedical applications, such as hydrogels for prevention of post-operative adhesions^{61–63}, surgical haemostatics⁶⁴, bioadhesives

and sealants^{65,66}. In this study, the bone biocompatibility of the oxidized dextrin-based hydrogel has been demonstrated, which supports its use as a safe candidate for the development of injectable bone substitute.

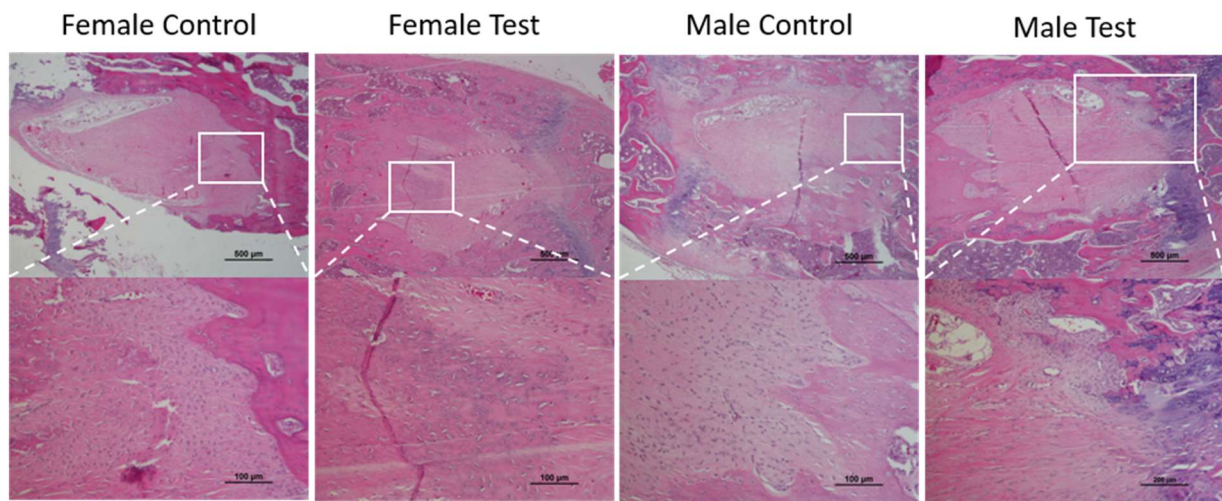


Figure 4.4: Representative photographs of histologic images, after hematoxylin and eosin staining, from femur defect site of animal from control and test groups of both genders, after 3 weeks after surgery.

4.3.4 | Skin sensitization assessment

The guinea pig has been the animal of choice for the detection of sensitizing activity of chemicals and medical devices for several decades. Among the guinea pig assays recommended by ISO 10993-10, the Guinea Pig Maximization Test (GPMT) is the most sensitive one^{30,31}. In this test, the guinea pigs (both in test and control groups) did not show signs of erythema and oedema, or any adverse skin response in the challenge skin areas at 24 and 48 h after removal of the dressings. The numerical grading for erythema and oedema was zero. These results indicate that HG did not induce any allergic reactions and corroborate the results obtained in the systemic toxicity assay.

Polymeric glucose-based pharmaceutical products have been reported to induce allergic reactions, including anaphylaxis. This is the case of dextran⁶⁷⁻⁶⁹ and hydroxyethyl starch (HES)⁷⁰⁻⁷², both used as plasma volume expanders. Concerning to dextrin, it is being clinically used as a peritoneal dialysis (PD) solution (icodextrin)^{35,36,73}. It is generally safe and well tolerated by PD patients, but there are few reports of acute self-limiting allergic hypersensitivity reaction to icodextrin, such as skin rashes⁷⁴⁻⁷⁶. Our hydrogel is composed mainly by dextrin ($\approx 95\%$), containing about 40% of residues with dialdehydes²⁵. The obtained results suggest that such modification did not promote any skin sensitization.

4.3.5 | Association of Bonelike® granules to dextrin-based hydrogel

Dextrin-based hydrogel was conceived as a multifunctional and injectable matrix able to carry and stabilize other materials and/or cells in medical procedures²⁰⁻²². Specifically, in bone regeneration procedures where synthetic bone grafts are used, an injectable carrier and/or granules stabilizer matrix

may ease the clinical application/handling of grafts or drugs, promoting a suitable environment for regeneration⁹. In this work, HG was combined with glass-reinforced HAP particles (250-500 μm), registered as Bonelike[®]⁷⁷. BL is a three-phase material, consisting of α - and β -TCP phases homogeneously dispersed in the HAP matrix, resulting in improved mechanical properties and enhanced bioactivity, compared to the commercial HAP^{77,78}. Furthermore, the presence of glass in this formulation allows the introduction of several ions into BL composition, such as magnesium, fluoride and sodium, making it possible to achieve a chemical composition closer to the mineral phase of the bone⁷⁹. Clinical trials revealed its remarkable potential of osteoconductivity and osseointegration on orthopedic and dental applications⁸⁰⁻⁸³. However, clinical applications were often performed using autologous blood as a carrier for the granules, which raises the need for a more adequate and less invasive vehicle to better stabilize the granules in large defects or unstable sites, avoiding dispersion or medullar infiltration. Moreover, the development of a mouldable/injectable formulation will increase the diversity of clinical cases in which BL can be applied.

HG was associated to different loads of BL, as to determine the higher amount that may be used without compromising the extrusion process, the granules' stability and the handling/moulding of the final formulation. The **Figure 4.5 (A)** displays the appearance of the formulations after complete gelation of the HG when combined with different concentrations of BL (30, 40 and 60 % w/v). The HG was able to envelop and aggregate the granules well. The formulation containing 60% of BL presents a perfect cohesion, the granules being homogeneously distributed over the HG, contrary to what was verified with lower concentrations (30 and 40%, whose granules started to settle at the bottom of the syringe, during the gelation time process, resulting in a more heterogeneous formulation. For superior concentrations, the HG was unable to aggregate/stabilize all the granules. Moreover, with 60 % of BL, the resulted formulation displayed suitable malleability and handling properties after the gelation process, allowing the surgeon to manipulate/shape it, without dispersing the granules or breaking the HG.

In an injectable system it is essential to study the extrusion force required to inject the material. The injectability curves of the formulations with different concentrations of BL are shown in **Figure 4.5 (B)**. The three formulations presented similar extrusion profiles. Initially, a drastic rise in the force required was observed, which corresponds to the beginning of the extrusion, followed by the *plateau* which corresponds to the continuous and uniform flow of the material. The formulation containing 30, 40 and 60% of BL displayed maximum extrusion forces of 5.89, 5.83 and 7.13 N, respectively. There was a slight increase in the extrusion force when using 60% of BL, since a greater force is required to extrude a larger quantity of granules.

Thus, the formulation containing 60% of BL was chosen to be tested in *in vivo* studies, since it was found i) to be injectable, ii) to envelop and aggregate the BL granules well and uniformly distributed, iii) and able to maintain a whole and mouldable structure during and after the injection.

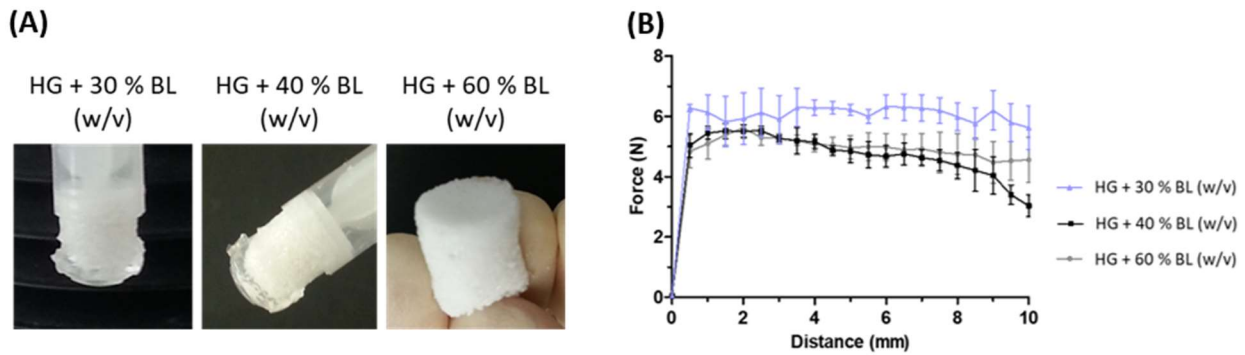


Figure 4.5: Preparation of the injectable bone substitute: macroscopic evaluation of dextrin-based hydrogel (HG) with different concentrations of Bonelike® (BL) granules, after completely gelation reaction **(A)** and the results of the injectability test **(B)**.

4.3.6 | Assessment of the effectiveness of the dextrin-based hydrogel to mould and stabilize Bonelike® granules in bone defects

The surgical procedure was simple, fast and well tolerated by the animals. Immediately after recover from surgery, the animals were able to walk and support weight in the treated limb. The surgeon prepared himself the formulation and controlled the gelling process and was able to implant easily and quickly the formulation. As the defect displayed only two vertical walls (**Figure 4.1 (B)**), the formulation was implanted during the final phase of the gelation process, when it displayed as a “mouldable paste”, by using a surgical spatula. The formulation was well shaped to the defects and allowed the complete filling of the bone gap, without leakage of the granules. It’s important to note that the main goal of this defect model was to evaluate the capability of the HG to stabilise BL granules into the bone defect, as well as the mouldable properties of the final formulation.

During the post-surgery period, no complications were observed, such as infections, abscesses and allergic reactions and the surgical skin incision healed normally. X-rays images were obtained after surgery (**Figure 4.6 (A)**), while microCT images were acquired after animal sacrifice at 3 and 6 weeks) (**Figure 4.6 (B)**). The radiographic images of the control group presented a radio-transparent gap in the defect site after surgery, which remained after 3 weeks and 6 weeks, as can be seen in microCT reconstruction images (**Figure 4.6 (B)**), indicating that the bone healing process was not complete. Regarding the test group, the radiographic images taken post-surgery presented a radio-opacity in the defect site, corresponding to BL granules. After 3 and 6 weeks (**Figure 4.6 (B)**) BL granules are still in place and did not fall down to the medullar cavity. The microCT images of treated animals (**Figure 4.6 (B)**) also allowed to observe the presence of BL granules uniformly distributed within the gap region after 3 and 6 weeks. This result demonstrated the capability of the hydrogel to maintain the granules’ cohesion and stabilise them within the defect. During the sample collection after sacrificing the animals, no macroscopic evidence of adverse tissue reaction was observed, demonstrating again the biocompatibility of the formulation HG + BL.

It's important to note that BL granules were not designed to withstand load-bearing bone defects and the tibial fracture was used in this work as an extreme model to demonstrate the ability of the HG on the BL granules' stability and cohesion within the gap region.

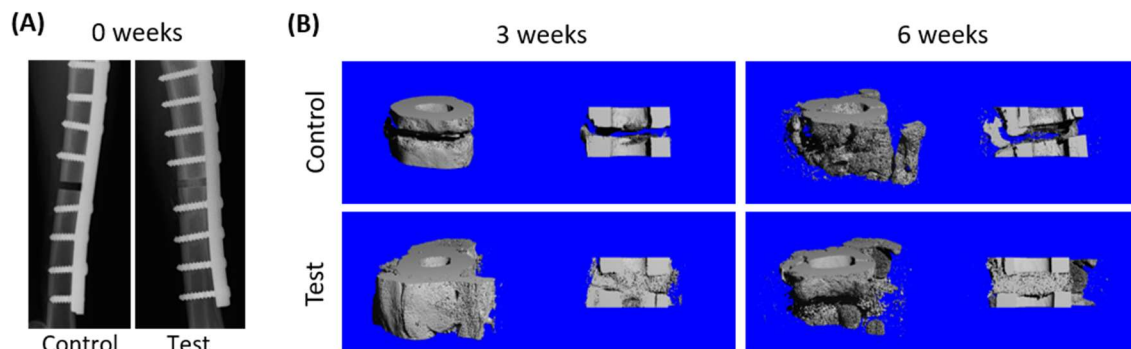


Figure 4.6: Representative radiographic and microCT images of tibial fracture from control and test groups: **(A)** radiographic images of tibia after surgery (0 weeks) from control and test groups and **(B)** microCT images of tibia after 3 and 6 weeks, showing the whole sample and the hollow cylindrical region of interest within the whole sample.

Covalently and ionically crosslinked hydrogels are generally composed by two components (polymer and crosslinking agent, or polymers modified with chemically complementary groups) which can easily be mixed by the surgeon under aseptic conditions and injected/implanted⁹. One advantage of these systems in relation to others (e.g. sensitive to temperature, UV crosslinked) is the ability of the surgeons to follow gelation process: after mixing the formulation, the crosslinking process starts, the mixed solution becomes more viscous over time as it gels. During this process, the surgeon can choose the best moment in which the formulation can be implanted into the defect, since depending on defects type and size very mouldable/viscous solutions or liquid ones may be preferable. Many authors have reported gelling times from seconds to several minutes for this kind of injectable bone substitutes^{14,84–87}. Surgeons generally advise 5–30 min as a suitable gelation time⁸⁶. Our formulation takes about 10-15 min to gel. Another advantage consists in the ability to add bioactive agents, such as proteins, cells, at the time the formulation are being prepared, to improve the bone healing process^{13,16,17,84,85,88–90}. The results showed that the HG is an effective matrix to carrier, featuring good handling and stabilization of the granular-based SBSs.

4.4 | Conclusions

In the present study it was demonstrated that the oxidized dextrin-based hydrogel did not induce any systemic toxic effect, neither impaired the bone repair/regeneration process. The HG was successfully combined with BL granules to obtain a mouldable/injectable bone substitute. The tibial fracture results showed that the HG allowed the stabilization of the BL granules into the defect, ensuring effective handling properties of the HG+BL formulation, as well as, an efficient cohesion of the granules. Thus, this

work addressed technical requirements of IBS currently unmet and requiring further research and development. Other studies have been performed to better characterize the bone healing process of HG+BL formulations in critical-sized defects.

4.5 | References

1. Stevens, M. M. Biomaterials for bone tissue engineering. *Mater. Today* **11**, 18–25 (2008).
2. Amini, A. A. & Nair, L. S. Injectable hydrogels for bone and cartilage repair. *Biomed. Mater.* **7**, 024105 (2012).
3. Bohner, M. Resorbable biomaterials as bone graft substitutes. *Materials Today* **13**, 24–30 (2010).
4. Campana, V. *et al.* Bone substitutes in orthopaedic surgery: from basic science to clinical practice. *J. Mater. Sci. Mater. Med.* **25**, 2445–2461 (2014).
5. Bongio, M., van den Beucken, J. J. J. P., Leeuwenburgh, S. C. G. & Jansen, J. A. Development of bone substitute materials: from ‘biocompatible’ to ‘instructive’. *J. Mater. Chem.* **20**, 8747 (2010).
6. Navarro, M., Michiardi, A., Castaño, O. & Planell, J. A. Biomaterials in orthopaedics. *J. R. Soc. Interface* **5**, 1137–1158 (2008).
7. D’Este, M. & Eglin, D. Hydrogels in calcium phosphate mouldable and injectable bone substitutes: Sticky excipients or advanced 3-D carriers? *Acta Biomater.* **9**, 5421–5430 (2013).
8. Utech, S. & Boccaccini, A. R. A review of hydrogel-based composites for biomedical applications: enhancement of hydrogel properties by addition of rigid inorganic fillers. *J. Mater. Sci.* **51**, 271–310 (2016).
9. Pereira, I., Rodrigues, C., Rodrigues, A., Oliveira, M. & Gama, M. in *Bioinspired Materials for Medical Applications* (eds. Rodrigues, L. & Mota, M.) 241–271 (Elsevier, 2017). doi:10.1016/B978-0-08-100741-9.00009-7
10. Fellah, B. H. *et al.* Bone repair using a new injectable self-crosslinkable bone substitute. *J. Orthop. Res. Off. Publ. Orthop. Res. Soc.* **24**, 628–35 (2006).
11. Trojani, C. *et al.* Ectopic bone formation using an injectable biphasic calcium phosphate/Si-HPMC hydrogel composite loaded with undifferentiated bone marrow stromal cells. *Biomaterials* **27**, 3256–3264 (2006).
12. Gaharwar, A. K., Dammu, S. A., Canter, J. M., Wu, C.-J. & Schmidt, G. Highly Extensible, Tough, and Elastomeric Nanocomposite Hydrogels from Poly(ethylene glycol) and Hydroxyapatite Nanoparticles. *Biomacromolecules* **12**, 1641–1650 (2011).
13. Gao, C., Cai, Y., Kong, X., Han, G. & Yao, J. Development and characterization of injectable chitosan-based hydrogels containing dexamethasone/rhBMP-2 loaded hydroxyapatite nanoparticles. *Mater. Lett.* **93**, 312–315 (2013).
14. Han, Y., Zeng, Q., Li, H. & Chang, J. The calcium silicate/alginate composite: preparation and evaluation of its behavior as bioactive injectable hydrogels. *Acta Biomater.* **9**, 9107–17 (2013).
15. Killion, J. A. *et al.* Hydrogel/bioactive glass composites for bone regeneration applications: synthesis and characterisation. *Mater. Sci. Eng. C. Mater. Biol. Appl.* **33**, 4203–12 (2013).
16. Killion, J. A., Geever, L. M., Devine, D. M., Farrell, H. & Higginbotham, C. L. Compressive Strength and Bioactivity Properties of Photopolymerizable Hybrid Composite Hydrogels for Bone Tissue Engineering. *Int. J. Polym. Mater. Polym. Biomater.* **63**, 641–650 (2014).
17. Killion, J. A., Geever, L. M., Devine, D. M. & Higginbotham, C. L. Fabrication and in vitro biological evaluation of photopolymerisable hydroxyapatite hydrogel composites for bone regeneration. *J. Biomater. Appl.* **28**, 1274–83 (2014).
18. Nguyen, T. P., Doan, B. H. P., Dang, D. V., Nguyen, C. K. & Tran, N. Q. Enzyme-mediated in situ preparation of biocompatible hydrogel composites from chitosan derivative and biphasic calcium phosphate nanoparticles for bone regeneration. *Adv. Nat. Sci. Nanosci. Nanotechnol.* **5**, 015012

- (2014).
19. Bongio, M. *et al.* Subcutaneous tissue response and osteogenic performance of calcium phosphate nanoparticle-enriched hydrogels in the tibial medullary cavity of guinea pigs. *Acta Biomater.* **9**, 5464–5474 (2013).
 20. Molinos, M., Carvalho, V., Silva, D. M. & Gama, F. M. Development of a Hybrid Dextrin Hydrogel Encapsulating Dextrin Nanogel As Protein Delivery System. *Biomacromolecules* **13**, 517–527 (2012).
 21. Silva, D. M. *et al.* Structural analysis of dextrans and characterization of dextrin-based biomedical hydrogels. *Carbohydr. Polym.* **114**, 458–466 (2014).
 22. Silva, D. M. *et al.* Inflammatory response to dextrin-based hydrogel associated with human mesenchymal stem cells, urinary bladder matrix and Bonelike[®] granules in rat subcutaneous implants. *Biomed. Mater.* **11**, 065004 (2016).
 23. Pereira, I., Fraga, S., Silva, S., Teixeira, J. P. & Gama, M. In vitro genotoxicity assessment of an oxidized dextrin-based hydrogel for biomedical applications. *J. Appl. Toxicol.* (2018). doi:10.1002/jat.3754
 24. ISO 10993-1. *Biological evaluation of medical devices - Part 1: Evaluation and testing within a risk management process.* (2009). at <<https://www.iso.org/standard/44908.html>>
 25. Pereira, I. *et al.* Effects of gamma irradiation and periodate oxidation on the structure of dextrin assessed by mass spectrometry. *Eur. Polym. J.* **103**, 158–169 (2018).
 26. Cortez, P. P. *et al.* Characterization and preliminary in vivo evaluation of a novel modified hydroxyapatite produced by extrusion and spheronization techniques. *J. Biomed. Mater. Res. Part B Appl. Biomater.* **99B**, 170–179 (2011).
 27. Santos, J. D., Lopes, M. A. & Silva, M. A. Hydroxyapatite and bioglass-based pellets, production process and applications of thereof. (2010). at <<https://patents.google.com/patent/WO2010021559A1/en>>
 28. OECD. *Guidance Document on the Recognition, Assessment and Use of Clinical Signs as Human Endpoints for Experimental Animals Used in Safety Evaluation.* (OECD Publishing, 2002). doi:10.1787/9789264078376-en
 29. ISO 10993-11. *Biological evaluation of medical devices -- Part 11: Tests for systemic toxicity.* (2006). at <<https://www.iso.org/standard/35977.html>>
 30. ISO 10993-10. *Biological evaluation of medical devices -- Part 10: Tests for irritation and skin sensitization.* (2010). at <<https://www.iso.org/standard/40884.html>>
 31. OECD. *Test No. 406: Skin Sensitisation.* (OECD Publishing, 1992). doi:10.1787/9789264070660-en
 32. Giknis, M. L. A. & Clifford, C. B. Clinical laboratory parameters for Crl:WI(Han). *Charles River Lab.* (2008).
 33. Carvalho, V. *et al.* Biological activity of heterologous murine interleukin-10 and preliminary studies on the use of a dextrin nanogel as a delivery system. *Int. J. Pharm.* **400**, 234–242 (2010).
 34. Hreczuk-Hirst, D., Chicco, D., German, L. & Duncan, R. Dextrins as potential carriers for drug targeting: tailored rates of dextrin degradation by introduction of pendant groups. *Int. J. Pharm.* **230**, 57–66 (2001).
 35. Peers, E. & Gokal, R. Icodextrin provides long dwell peritoneal dialysis and maintenance of intraperitoneal volume. *Artif. Organs* **22**, 8–12 (1998).
 36. Takatori, Y. *et al.* Icodextrin technique survival rate in peritoneal dialysis patients with diabetic nephropathy by improving body fluid management: a randomized controlled trial. *Clin. J. Am. Soc. Nephrol.* **6**, 1337–1344 (2011).
 37. Treetharnmathurot, B. *et al.* Dextrin–trypsin and ST-HPMA–trypsin conjugates: Enzyme activity, autolysis and thermal stability. *Int. J. Pharm.* **373**, 68–76 (2009).
 38. DeBusk, A. O. V. & Alleman, T. Method for preparing medical dressings. (2005). at <<https://patents.google.com/patent/WO2004002460A1/en>>

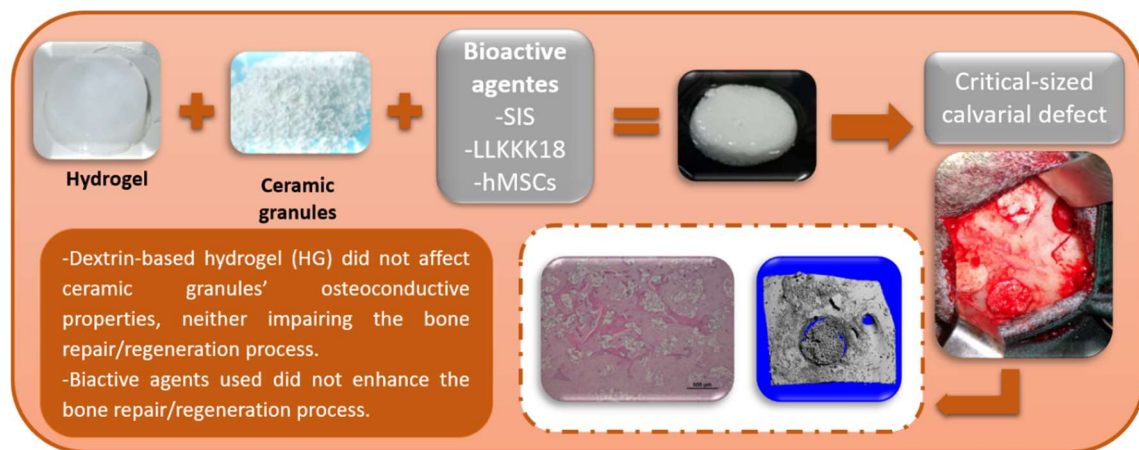
39. Das, D. & Pal, S. Modified biopolymer-dextrin based crosslinked hydrogels: application in controlled drug delivery. *RSC Adv.* **5**, 25014–25050 (2015).
40. Gonçalves, C., Moreira, S. M., Carvalho, V., Silva, D. M. & Gama, M. in *Encyclopedia of Biomedical Polymers and Polymeric Biomaterials* (ed. Mishra, M.) 2634–2649 (Taylor & Francis, 2016).
41. Moreira, S. *et al.* In Vivo Biocompatibility and Biodegradability of Dextrin-based Hydrogels. *J. Bioact. Compat. Polym.* **25**, 141–153 (2010).
42. Gonçalves, C. *et al.* Dextrin nanoparticles: Studies on the interaction with murine macrophages and blood clearance. *Colloids Surfaces B Biointerfaces* **75**, 483–489 (2010).
43. Carvalho, J., Gonçalves, C., Gil, A. M. & Gama, F. M. Production and characterization of a new dextrin based hydrogel. *Eur. Polym. J.* **43**, 3050–3059 (2007).
44. Carvalho, J., Moreira, S., Maia, J. & Gama, F. M. Characterization of dextrin-based hydrogels: Rheology, biocompatibility, and degradation. *J. Biomed. Mater. Res. Part A* **9999A**, 398–399 (2009).
45. Das, D., Das, R., Mandal, J., Ghosh, A. & Pal, S. Dextrin crosslinked with poly(lactic acid): A novel hydrogel for controlled drug release application. *J. Appl. Polym. Sci.* **131**, 40039 (2014).
46. Das, D. & Pal, S. Dextrin/poly (HEMA): pH responsive porous hydrogel for controlled release of ciprofloxacin. *Int. J. Biol. Macromol.* **72**, 171–178 (2015).
47. Das, D. *et al.* Synthesis and characterization of biodegradable copolymer derived from dextrin and poly(vinyl acetate) via atom transfer radical polymerization. *RSC Adv.* **6**, 9352–9359 (2016).
48. Roy, A., Maity, P. P., Dhara, S. & Pal, S. Biocompatible, stimuli-responsive hydrogel of chemically crosslinked β -cyclodextrin as amoxicillin carrier. *J. Appl. Polym. Sci.* **135**, 45939 (2018).
49. Gonçalves, C. & José A. Martins, F. M. G. Self-Assembled Nanoparticles of Dextrin Substituted with Hexadecanethiol. *Biomacromolecules* **8**, 392–398 (2007).
50. Manchun, S., Dass, C. R. & Sriamornsak, P. Designing nanoemulsion templates for fabrication of dextrin nanoparticles via emulsion cross-linking technique. *Carbohydr. Polym.* **101**, 650–655 (2014).
51. Manchun, S., Dass, C. R., Cheewatanakornkool, K. & Sriamornsak, P. Enhanced anti-tumor effect of pH-responsive dextrin nanogels delivering doxorubicin on colorectal cancer. *Carbohydr. Polym.* **126**, 222–230 (2015).
52. Das, D. *et al.* Dextrin and poly(lactide)-based biocompatible and biodegradable nanogel for cancer targeted delivery of doxorubicin hydrochloride. *Polym. Chem.* **7**, 2965–2975 (2016).
53. Das, D. *et al.* Biocompatible nanogel derived from functionalized dextrin for targeted delivery of doxorubicin hydrochloride to MG 63 cancer cells. *Carbohydr. Polym.* **171**, 27–38 (2017).
54. Das, D. *et al.* Biocompatible amphiphilic microgel derived from dextrin and poly(methyl methacrylate) for dual drugs carrier. *Polymer (Guildf)*. **107**, 282–291 (2016).
55. Carvalho, V. *et al.* Self-assembled dextrin nanogel as protein carrier: Controlled release and biological activity of IL-10. *Biotechnol. Bioeng.* **108**, 1977–1986 (2011).
56. Gonçalves, C. *et al.* Studies on the biodistribution of dextrin nanoparticles. *Nanotechnology* **21**, 295103 (2010).
57. Gunasekarana, V. A comprehensive review on clinical applications of comet assay. *J. Clin. diagnostic Res.* **9**, GE01-5 (2015).
58. Giovannelli, L., Pitozzi, V., Riolo, S. & Dolara, P. Measurement of DNA breaks and oxidative damage in polymorphonuclear and mononuclear white blood cells: a novel approach using the comet assay. *Mutat. Res. Toxicol. Environ. Mutagen.* **538**, 71–80 (2003).
59. Tice, R. R. *et al.* Single cell gel/comet assay: Guidelines for in vitro and in vivo genetic toxicology testing. *Environ. Mol. Mutagen.* **35**, 206–221 (2000).
60. Chuang, C.-H. & Hu, M.-L. Use of whole blood directly for single-cell gel electrophoresis (comet) assay in vivo and white blood cells for in vitro assay. *Mutat. Res. Toxicol. Environ. Mutagen.* **564**, 75–82 (2004).

61. Athanasiadis, T. *et al.* Effects of a Novel Chitosan Gel on Mucosal Wound Healing Following Endoscopic Sinus Surgery in a Sheep Model of Chronic Rhinosinusitis. *Laryngoscope* **118**, 1088–1094 (2008).
62. Ito, T. *et al.* The prevention of peritoneal adhesions by in situ cross-linking hydrogels of hyaluronic acid and cellulose derivatives. *Biomaterials* **28**, 975–983 (2007).
63. Lauder, C. I. W., Strickland, A. & Maddern, G. J. Use of a Modified Chitosan–Dextran Gel to Prevent Peritoneal Adhesions in a Porcine Hemicolectomy Model. *J. Surg. Res.* **176**, 448–454 (2012).
64. Rajiv, S. *et al.* The efficacy and safety of chitosan dextran gel in a burr hole neurosurgical sheep model. *Acta Neurochir. (Wien)*. **155**, 1361–1366 (2013).
65. Artzi, N., Shazly, T., Baker, A. B., Bon, A. & Edelman, E. R. Aldehyde-Amine Chemistry Enables Modulated Biosealants with Tissue-Specific Adhesion. *Adv. Mater.* **21**, 3399–3403 (2009).
66. Hoffmann, B. *et al.* Characterisation of a new bioadhesive system based on polysaccharides with the potential to be used as bone glue. *J. Mater. Sci. Mater. Med.* **20**, 2001–2009 (2009).
67. Shiratori, T., Sato, A., Fukuzawa, M., Kondo, N. & Tanno, S. Severe Dextran-induced anaphylactic shock during induction of hypertension-hypervolemia-hemodilution therapy following subarachnoid hemorrhage. *Case Reports Crit. Care* **2015**, 1–5 (2015).
68. Zinderman, C. E., Landow, L. & Wise, R. P. Anaphylactoid reactions to Dextran 40 and 70: reports to the United States Food and Drug Administration, 1969 to 2004. *J. Vasc. Surg.* **43**, 1004–1009 (2006).
69. Zanoni, G. *et al.* Dextran-specific IgG response in hypersensitivity reactions to measles-mumps-rubella vaccine. *J. Allergy Clin. Immunol.* **122**, 1233–1235 (2008).
70. Ebo, D. G., Schuerwegh, A. & Stevens, W. J. Anaphylaxis to starch. *Allergy* **55**, 1098–1099 (2000).
71. Boldt, J. Modern rapidly degradable hydroxyethyl starches: current concepts. *Anesth. Analg.* **108**, 1574–1582 (2009).
72. Kim, H. J., Kim, S. Y., Oh, M. J. & Kim, J. M. Anaphylaxis induced by hydroxyethyl starch during general anesthesia: a case report. *Korean J. Anesthesiol.* **63**, 260 (2012).
73. McIntyre, C. W. Update on peritoneal dialysis solutions. *Kidney Int.* **71**, 486–490 (2007).
74. Köksal Cevher, Ş., Ozkayar, N. & Dede, F. A case report on allergic rash caused by Icodextrin. *Case Reports Nephrol. Dial.* **5**, 26–29 (2014).
75. Goldsmith, D., Jayawardene, S., Sabharwal, N. & Cooney, K. Allergic reactions to the polymeric glucose-based peritoneal dialysis fluid icodextrin in patients with renal failure. *Lancet* **355**, 897 (2000).
76. Ankur, G. & Mohan, B. Icodextrin and skin rash: Unusual presentation. *Indian J. Nephrol.* **22**, 62 (2012).
77. Atayde, L. M. *et al.* Morphology effect of bioglass-reinforced hydroxyapatite (Bonelike®) on osteoregeneration. *J. Biomed. Mater. Res. Part B Appl. Biomater.* **103**, 292–304 (2015).
78. Lopes, M. ., Knowles, J. ., Santos, J. ., Monteiro, F. . & Olsen, I. Direct and indirect effects of P205 glass reinforced-hydroxyapatite composites on the growth and function of osteoblast-like cells. *Biomaterials* **21**, 1165–1172 (2000).
79. Cortez, P. P. *et al.* A glass-reinforced hydroxyapatite and surgical-grade calcium sulfate for bone regeneration: In vivo biological behavior in a sheep model. *J. Biomater. Appl.* **27**, 201–217 (2012).
80. Gutierrez, M. *et al.* Biological behaviour of Bonelike® graft implanted in the tibia of humans. *Key Eng. Mater.* **284–286**, 1041–1044 (2005).
81. Gutierrez, M. *et al.* Histological and scanning electron microscopy analyses of bone/implant interface using the novel Bonelike® synthetic bone graft. *J. Orthop. Res.* **24**, 953–958 (2006).
82. Sousa, R. C. *et al.* A clinical report of bone regeneration in maxillofacial surgery using Bonelike® synthetic bone graft. *J. Biomater. Appl.* **22**, 373–385 (2008).
83. Lobato, J. V. *et al.* Titanium dental implants coated with Bonelike®: Clinical case report. *Thin Solid Films* **515**, 279–284 (2006).

84. Martínez-Sanz, E. *et al.* Minimally invasive mandibular bone augmentation using injectable hydrogels. *J. Tissue Eng. Regen. Med.* **6 Suppl 3**, s15-23 (2012).
85. Martínez-Álvarez, C. *et al.* Injection and adhesion palatoplasty: a preliminary study in a canine model. *J. Surg. Res.* **183**, 654–62 (2013).
86. Tan, R., Niu, X., Gan, S. & Feng, Q. Preparation and characterization of an injectable composite. *J. Mater. Sci. Mater. Med.* **20**, 1245–53 (2009).
87. Cardoso, D. A. *et al.* Gelation and biocompatibility of injectable alginate-calcium phosphate gels for bone regeneration. *J. Biomed. Mater. Res. Part A* **102**, 808–817 (2014).
88. Trojani, C. *et al.* Ectopic bone formation using an injectable biphasic calcium phosphate/Si-HPMC hydrogel composite loaded with undifferentiated bone marrow stromal cells. *Biomaterials* **27**, 3256–3264 (2006).
89. Fu, S. *et al.* Injectable and thermo-sensitive PEG-PCL-PEG copolymer/collagen/n-HA hydrogel composite for guided bone regeneration. *Biomaterials* **33**, 4801–4809 (2012).
90. Hulsart-Billström, G. *et al.* Calcium phosphates compounds in conjunction with hydrogel as carrier for BMP-2: A study on ectopic bone formation in rats. *Acta Biomater.* **7**, 3042–3049 (2011).

CHAPTER 5

The effect of the dextrin-based hydrogel associated with granular synthetic bone substitute and other bioactive agents in the regeneration of critical-sized defects, using a goat model



The development of injectable bone substitutes (IBS) have garnered great importance in the bone regeneration field, as a strategy to reach areas of the body using minimally invasive procedures and showing the ability of perfect fitting according to irregularities of bone tissue defects. In this context, the combination of injectable hydrogels and ceramic granules is emerging as a well-established trend. Particularly, *in situ* forming hydrogels have arisen as a new IBS generation. An *in situ* forming and injectable dextrin-based hydrogel (HG) was developed, aiming to act as a carrier for bone graft granules and bioactive agents. In this work, the HG was combined with granular bone substitute, registered as Bonelike® (BL, 250-500 μm) and the final formulation was implanted in a goat critical-sized calvarial defects (14 mm) for 3, 6 and 12 weeks. The obtained results showed that HG improved the handling properties of the BL granules and did not affect the BL granules' osteoconductive properties, neither impairing the bone repair/regeneration process. Peptides resulted from hydrolysis of extracellular matrix from small intestinal submucosa (SIS) and LLKKK18, a pro-angiogenic peptide, as well as, human mesenchymal stem cells (hMSCs) from umbilical cord were also combined with the IBS to improve the bioactivity of the formulations. The agents did not enhance the bone regeneration process.

5.1 | Introduction

Increasing life expectancy and population ageing has raised the incidence of bone fractures as well as the interest in bone regeneration research ¹. Conventional treatments (auto-, allo- and xenograft) present drawbacks such as limited supply, adverse immunological responses, disease transmission and morbidity ^{1,2}. The lack of a simultaneously effective and safe treatment is pushing the development of synthetic bone substitutes (SBSs) ^{1,3}. Glass-reinforced hydroxyapatite (HAP) composites are calcium phosphate-based substitutes able to chemically mimic the bone inorganic structure composition. Its osteoconductive behavior creates an ideal environment for cell adhesion and proliferation, thus promoting bone regeneration ⁴⁻⁶. However, many commercially accessible SBSs are available in granular form ¹, and so, may be difficult to handle and to fit in irregularly shaped defects. Also, granules can be washed out from the implanted site and, consequently, migration into the surrounding tissues with adverse or unexpected events ^{3,7,8}. Moreover, the micromovements of the granules within the defect can affect the formation of new bone tissue.

Attempting to solve these issues and improve their applicability in the surgical theatre, granular ceramics have been associated with hydrogels to achieve injectable/mouldable SBSs, that are able to ensure granules cohesiveness, site retention and adaptability to the defect area ⁹⁻¹¹. In addition, injectable bone substitutes (IBSs) may be advantageous in some clinical applications where the access to the bone defects is restricted, such as the spine injuries and maxillofacial defects ¹². The hydrogel can also improve the osteoconductive properties of the SBS and grant them osteoinductive and osteogenic properties, among others, by the incorporation of bioactive molecules or cellular systems within the hydrogel matrix ^{9,11}. In particular, *in situ* gelation hydrogels has the advantage to improve the bioactivity of the IBSs, since they enable the homogeneous dispersion of the cellular systems and bioactive molecules, immediately before the crosslinking reaction and gelation. These systems also allows the *in situ* tailoring of the formulation, by the incorporation of specific therapeutics according to the needs of each clinical case ¹¹.

In this context, our research group has been developing and characterizing a fully resorbable and injectable dextrin-based hydrogel (HG) which was intended to perform as a multifunctional platform, enabling the combination with stem cells and other bioactive agents, during clinical procedures ¹³⁻¹⁶. In previous chapter, it was demonstrated the ability of the *in situ* forming dextrin-based hydrogel to carry and stabilize ceramic granules in clinical applications.

The extracellular matrix (ECM) comprehends a collection of structural and functional molecules secreted by the resident cells, that are responsible for the intrinsic biochemical and mechanical cues that regulate cell behavior and function, as well as homeostasis and response to injury ¹⁷. For these reasons, ECM has been applied as biological scaffolds for tissue engineering applications ¹⁸. *In vitro* studies have shown that the degradation products of ECM (obtained through chemical, enzymatic and heat treatment) display chemotactic and mitogenic activity on stem and progenitor cells ¹⁹⁻²⁵, as well as

antimicrobial activity^{26,27}. We hypothesize that the incorporation of ECM degradation products in the HG could improve the bioactivity of the IBS systems.

Vascularization is a crucial process in the bone regeneration process and a limiting step in the healing of large bone defects^{28,29}. In this scenario, we hypothesized that the inclusion of angiogenic factors within the IBS systems can facilitate and enhance bone regeneration. LL37 is an antimicrobial peptide with 37 amino acid residues belonging to the family of cathelicidins³⁰. LL37, in addition to its antimicrobial activity, has been reported to be involved in mast cells and leukocytes chemotaxis, angiogenesis and in wound healing promotion³⁰⁻³². Recent studies have demonstrated that LL37 can accelerate the bone regeneration process by promoting angiogenesis and subsequent recruitment of Mesenchymal stem cells (MSCs) into the bone defect³³, as well as inhibition of osteoclastogenesis³⁴. LL37 derivatives have been engineered to enhance its antimicrobial properties and to decrease its cytotoxicity for human cells and binding to plasma protein^{35,36}. One of them, LLKKK18, presents higher chemoattractant activity³⁵, and preserved the ability to improve skin wound healing³⁷. However, to date no significant data is available regarding LLKKK18 effect on bone regeneration.

MSCs are an important tool in regenerative medicine due to their intrinsic characteristics, such as, chemotactic, multilineage differentiation and immunogenic and inflammatory modulation capacities³⁸. Human MSCs have been defined by the International Society for Cellular Therapy ISCT³⁹ as being plastic adherent in standard culture conditions expressing specific cluster of differentiation (CD) 105⁺, 73⁺, 90⁺ and lacking expression of hematopoietic markers: CD45⁺, CD34, CD14 or CD11b, CD79 α or CD19 and HLA-DR surface molecules. The lack of expression of HLA-DR surface molecules enables the xenogeneic application of hMSCs, without the risks of immunogenic reactions. MSCs derived from the umbilical cord tissue represent a potent MSC source due to their youth, as they derive from a tissue collected at birth, in an easy and non-invasive procedure. Also, the quality and availability of cryopreserved tissue in private and public cryopreservation banks represents an advantage regarding the application of this cell source. Several studies have reported the beneficial properties of MSCs in bone tissue regeneration, not only through their differentiation potential but more importantly due to paracrine secretion of cytokines and growth factors modulating tissue repair process⁴⁰⁻⁴³.

The main aims of this work were i) to evaluate the association of the dextrin-based hydrogel with granular ceramics (250-500 μm) on the regeneration of calvarial critical-sized defects, using a goat model and ii) to assess the effect of porcine small intestinal submucosa (SIS) enzymatic degradation products, LLKKK18 and umbilical cord derived hMSCs on bone regeneration, when combined with the dextrin-based IBS system.

5.2 | Experimental

5.2.1 | Chemicals

Dextrin used in this work was Tackidex B 167 (Batch E 1445), generous gift from Roquette (Lestrem, France). Extracellular matrix (ECM) from porcine small intestinal submucosa (SIS) was a gift from Cook Biotech Inc (West Lafayette, Indiana, USA). Custom synthesis of LLKKK18 (KEFKRIVKRIKKFLRKLKLV) was obtained from Schafer-N (Copenhagen, Denmark). All reagents used were of highest purity or analytical grade available. Sodium *m*-periodate, diethylene glycol, adipic acid dihydrazide (ADH), silver nitrate, Sodium thiosulfate, dexamethasone, ascorbic acid-2-phosphate, β -glycerphosphate, Alcian Blue, acetic acid, sodium carbonate (Na_2CO_3), calcium hydrogenphosphate (CaHPO_4), calcium fluoride (CaF_2), diphosphorus penta-oxide (P_2O_5) and polyvinyl alcohol (PVA), formaldehyde, pepsin and chloridric acid (HCl) were purchased from Sigma-Aldrich (St. Louis, MO, USA). DMEM (with GlutaMAX™, without nucleosides), fetal bovine serum (FBS), penicillin, streptomycin, amphotericin B, HEPES Buffer solution, StemPro® Adipogenesis Differentiation kit, StemPro® Chondrogenesis Differentiation kit were obtained from Gibco®. Accutase™ Cell detachment solution, Stain Buffer and CD90, CD105, CD44, CD34, CD11b, CD19, CD45, MHC class II antibodies were obtained from BD Biosciences®.

5.2.2 | Dextrin oxidation

Dextrin oxidation was performed as described by Pereira et al.¹⁶. Briefly, aqueous solutions of Dextrin (2% w/v) were oxidized with sodium *m*-periodate, to yield the theoretical degree of oxidation of 40%, at room temperature, with stirring, in the dark. After 20 h, the oxidation reaction was stopped by adding drop wise an equimolar amount of diethylene glycol, to reduce any unreacted periodate. Sodium *m*-periodate and diethylene glycol were removed by ultrafiltration, using a membrane with a molecular weight cut-off 1000 Da (Merk Millipore, Billerica, MA, USA), and then lyophilized.

5.2.3 | Preparation of dextrin-based hydrogel

Oxidized dextrin (ODEX) was dissolved in PBS buffer (phosphate buffered saline) (30% w/v) and the solution was sterilized by gamma irradiation, using a ⁶⁰Co source, at 20 kGy (2 kGy/h), at room temperature, by IONISOS (Dagneux, France). Adipic acid dihydrazide (ADH) was dissolved also in PBS buffer (3.76% w/v) and sterilized by filtration, using filters with pore 0.22 μm (Pall Corporation, MI, USA). For crosslinking reaction, ODEX and ADH solutions were mixed in a volume ratio of 7:3, before implantation in calvarial critical-sized defects.

5.2.4 | Preparation of Bonelike® granules

Ceramic powder was synthesized according to the method described elsewhere^{44,45}. Briefly, P_2O_5 -CaO based glass with the chemical composition of 65 P_2O_5 -15CaO-10CaF₂-10Na₂O (mol %) was prepared

by mixing the appropriate quantities of Na_2CO_3 , CaHPO_4 , CaF_2 , and P_2O_5 in a platinum crucible, and then heating it at 1450 °C for 90 min in a furnace. The prepared glass was crushed in an agate mortar and sieved to a granule size below 50 μm . Bonelike[®] was obtained by adding 2.5 % wt. of bioglass to the previous prepared hydroxyapatite (HAP). The Bonelike[®] powder was mixed with the microcrystalline cellulose and PVA and the resulting suspension was poured into Alumina (Al_2O_3) plates, dried in a oven at 60 °C for two days and then the samples were sintered at 1300 °C using a heating rate of 4 °C/min, followed by natural cooling inside the furnace. Finally, using standard milling and sieving techniques, Bonelike[®] granules with particle size between 250-500 μm were obtained, displaying interconnective macroporosity. Throughout this work, Bonelike[®] will be abbreviated to BL.

5.2.5 | Enzymatic hydrolysis of small intestinal submucosa matrix

This procedure was carried out as reported before¹⁴. Briefly, 150 mg of powdered SIS was hydrolysed with 15 mg of pepsin in 15 mL of 0.01 M HCl solution, during 48 h, at 37 °C, under stirring. After the pepsin inactivation, the hydrolysates were lyophilized.

5.2.6 | Human mesenchymal stem cells culture and characterization

Human MSCs from the umbilical cord stroma were obtained from PromoCell. Cells were thawed and expanded *in vitro* using standard protocols. hMSCs were maintained in DMEM, with GlutaMAX™, without nucleosides supplemented with 10% (v/v) FBS, 100 IU/ml penicillin, 0.1 mg/ml streptomycin, 2.05 $\mu\text{g}/\text{ml}$ amphotericin B and 10 mM HEPES Buffer solution, at 37°C and in a 95% humidified atmosphere with 5% CO_2 .

hMSCs identity was confirmed by flow cytometry and trilineage differentiation. Briefly, for flow cytometry, cells were cultured for 5 days, as described previously³⁸, harvested using Accutase™ Cell detachment solution, counted and resuspended in Stain Buffer. Passage 5 cultures (P5) were incubated with anti-positive (CD90, CD105, CD44) and anti-negative marker (CD34, CD11b, CD19, CD45, MHC class II) antibodies (Human MSC Analysis Kit). Analysis was performed using a BD FACSCalibur™ 3 CA Becton Dickinson, and acquired data was processed using FlowJo Engine X10.4 (v3.05478, LLC).

For trilineage differentiation, hMSCs were plated onto 24-well plates (8.000 viable cells/ cm^2) and expanded to a confluency of 70-80% of culture surface. Cells were transitioned onto specific differentiation media for adipogenesis (StemPro[®] Adipogenesis Differentiation kit) and osteogenesis (standard culture medium supplemented with 5nM Dexamethasone, 250 μM ascorbic acid-2-phosphate (AsA2-P) and 10mM β -glycerphosphate (β -GP)). Undifferentiated controls were maintained in standard media. Every 3 days, differentiation and standard media was refreshed. After 14 days, adipogenic differentiation cells were stained with Oil Red O (ORO), for lipid droplet detection. Von Kossa staining was employed to visualize mineral extracellular deposition. Cells were fixated and dehydrated with increasing ethanol concentrations. Then, cells were rehydrated and incubated with 2% Silver nitrate

solution, under Ultra-violet light and sodium thiosulfate 5% for 3 minutes. Wells were rinsed, and photographic record obtained. For chondrogenic differentiation, hDPSCs were plated at a concentration of 2×10^4 viable cells/well onto a 96-well plate. After 48 hours, cells were transferred to chondrogenic culture medium (StemPro® Chondrogenesis Differentiation kit) while control wells remained in standard supplementation. Media were renewed each 2 days, for 14 days. After that time, proteoglycan's synthesis by differentiated chondrocytes was assessed through Alcian Blue staining. Cells were fixated with 4% formaldehyde and stained with Alcian Blue solution. After removal of the staining solution, cells were rinsed with acetic acid at 3% (v/v). Acidity was neutralized with distilled water. Differentiated cells were observed under inverted microscope.

5.2.7 | Preparation of dextrin-based formulations

SIS and LLKKK18 were incorporated in ADH solution before crosslinking. For the HG + SIS and HG + BL + SIS formulations, SIS was previously sterilized by gamma irradiation (20 kGy, 2 kGy/h, at room temperature) and dissolved in sterile ADH solution, in order to obtain hydrogels with 4 mg/mL SIS. For HG + LLKKK18 and HG + BL + LLKKK18 formulations, the peptide was dissolved together with ADH, then the solution was sterilized using filters with pore 0.22 μm (Pall Corporation, MI, USA). The final concentration of LLKKK18 in the HG was 1 mg/mL. For formulations with BL (HG + BL), BL granules were previously sterilized by autoclaving and mixed in ODEX solution to humidify the granules and to allow the ODEX entering into the granules' pores. The final concentration of BL in hydrogel was about 60% ($w_{\text{BL}}/v_{\text{HG}}$). For formulations containing hMSCs, 4×10^4 cell were added to ODEX solutions immediately before reticulation.

5.2.8 | Surgical procedure

All procedures were in conformity with the European norms for animal welfare (European Directive 2010/63/EU) and with the approval of the Portuguese Veterinary Authorities (*Direção-Geral de Alimentação e Veterinária*), in accordance with the Portuguese legislation (Portaria 1005/92) and European Communities Council Directive of November 1986 (86/609/EEC). Humane endpoints were followed in accordance to the OECD Guidance Document on the Recognition, Assessment and Use of Clinical Signs as Humane Endpoints for Experimental Animals Used in Safety Evaluation⁴⁶. Adequate measures were taken to minimize pain and discomfort, considering humane endpoints for animal suffering and distress.

Surgeries were conducted under general anaesthesia using intravenous injection of a combination of drugs consisting in ketamine (5 mg/kg), diazepam (0.25mg/kg) and propofol (4mg/kg). During the surgery, the maintenance of general anaesthesia was performed with isoflurane, after endotracheal intubation. After preparation and antisepsis with chlorhexidine 4% of the calvarial skin, an incision was made along the sagittal plan from the base of the horns until the middle of the nasal bone. The

periosteum was elevated and four full thickness calvarial critical-sized defects were drilled with a cylindrical trephine with 14 mm of diameter, while irrigating with saline solution. For each goat, one defect was used as control (non-treated defect) and the other ones were randomly filled with the formulations HG, HG + SIS, HG + LLKKK18, BL, HG + BL, HG + BL + SIS, HG + BL + LLKKK18 and HG + BL + hMSCs (**Figure 5.1**). The soft tissues were closed in layers with resorbable sutures in a continuous pattern and the skin with an intradermic suture. The goats were set free and received analgesic medication for 4 days with flunixin meglumine and antibiotic treatment for 7 days with amoxicilin. The goats were randomly sacrificed 3, 6 and 12 weeks ($n = 5$) after surgery with a lethal intravenous injection of 40% sodium pentobarbital (euthasol®). The frontal bones were harvested and fixed in 4% formaldehyde solution, and X-rays images were obtained. After proper fixation of the tissues, each calvarial defect was individualized using an oscillating saw for sectioning the frontal bone. Each sample was maintained in formaldehyde for further analysis.

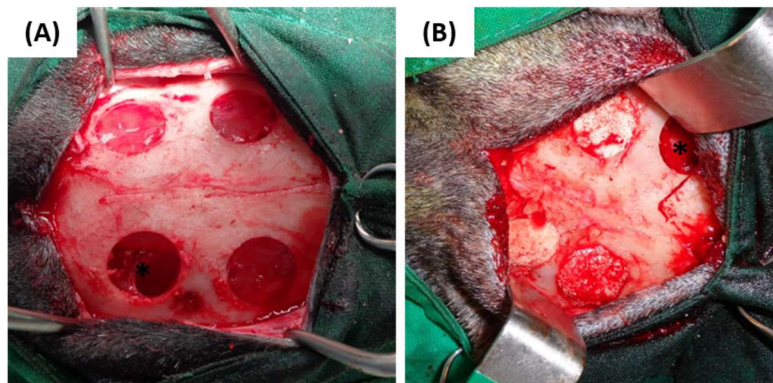


Figure 5.1: Calvarial critical-sized defects performed in the animals filled with the dextrin-based hydrogel formulations without Bonelike® granules **(A)** or in presence of them **(B)**. In each goat was performed a control defect (non-treated defect) marked with an asterisk.

5.2.9 | Micro-computed tomography analysis

Micro-computed tomography (microCT) scans were taken for quantitative and qualitative evaluation of new bone formed in calvarial critical-sized defects with different formulations of HG, using the μ CT 100 scanner (SCANCO Medical AG, Brüttisellen, Switzerland), which operated with a cone beam originating from a 5 μ m focal-spot X-ray tube. The photons were detected by a CCD-based area detector and the projection data were computer-reconstructed into a 3072 x 3072 image matrix. A 0.5 mm aluminium filter was used for taking optimized images. For each sample at least 1500 projections/180° of X-rays (90 kVp, 200 μ A, integration time 275 ms, scanning time at least 39 minutes) were acquired. The sample was segmented based on its gray scale values in the CT slices. The volume of interest was defined by a cylindrical contour, diameter was defined by the diameter of the drill hole (14 mm) and the height was defined by chosen the same number of slices for every sample (300 slices, 7.35 mm). The

evaluation was done twice, firstly with a threshold of 250 to segment the BL granules only and secondly with a lower threshold of 150 to segment the new bone and the BL granules.

5.2.10 | Histological processing

After microCT analyses, samples were histologically analysed. Samples were decalcified with Surgipath decalcifier II Leica®, for 48 h, dehydrated and embedded in paraffin wax, in a Shandon® automatic tissue processor Hypercenter XP. Consecutive 3 µm sections were cut and stained with haematoxylin and eosin (HE). Images were acquired using a Nikon VR microscope connected to a Nikon VR digital camera DXM1200.

5.2.11 | Statistical analysis

Experimental data were presented as mean ± standard deviation (SD). Statistical analysis and graphs were performed using the Prism® version 6.1 (GraphPad Software Inc., La Jolla, CA, USA). Statistical analysis of data was performed by one-way analysis of variance (ANOVA) followed by the by Bonferroni's post-test. Significance was accepted at a *p*-value < 0.05.

5.3 | Results

5.3.1 | Mesenchymal stem cells characterization

Human MSCs (**Figure 5.2 (A)**) demonstrated to be plastic adherent and to present characteristic surface markers, as assessed through flow cytometry. Results showed that 92% of the population was positive for CD90, CD105 and CD44, while ≤2% were negative for CD34, CD11b, CD19, CD45 and MHC II.

Trilineage differentiation through ORO, ARS and Von Kossa protocols, were used to evaluate adipogenic, osteogenic and chondrogenic differentiation, respectively. Results demonstrated successful differentiation towards the three lineages, with significant differences from undifferentiated controls (**Figure 5.2 (B)**).

5.3.2 | Surgical and post-surgical observations

The surgical procedure was simple, fast and well tolerated by the animals. The hydrogel formulations (HG, HG + SIS and HG + LLKKK18) were perfectly well-shaped to the defects. All BL containing formulations (HG + BL, HG + BL + SIS, HG + BL + LLKKK18, HG + BL + hMSCs) were easy to handle and shape into the defects, allowing the complete filling up to the periosteum level without leakage of the granules. The HG matrix facilitated the handling of the BL granules, as well as, their cohesiveness and stability within the defect. Oppositely, the BL only was more difficult to handle. The surgeon implanted the granules mixed with blood with a surgical spoon, compressing gently the granules against each other's and against the walls of the defect to prevent their leakage of the defect. The addition of SIS and

LLKKK18 did not affect the handling of the HG + BL formulations, as well as, the cohesiveness and stability of the BL granules within the defect.

During the post-surgery period, it was not observed any surgical complications, such as infections, abscesses and allergic reactions and the surgical skin incision healed without any complication. During the sample collection, skulls revealed no evidence of adverse tissue reaction.

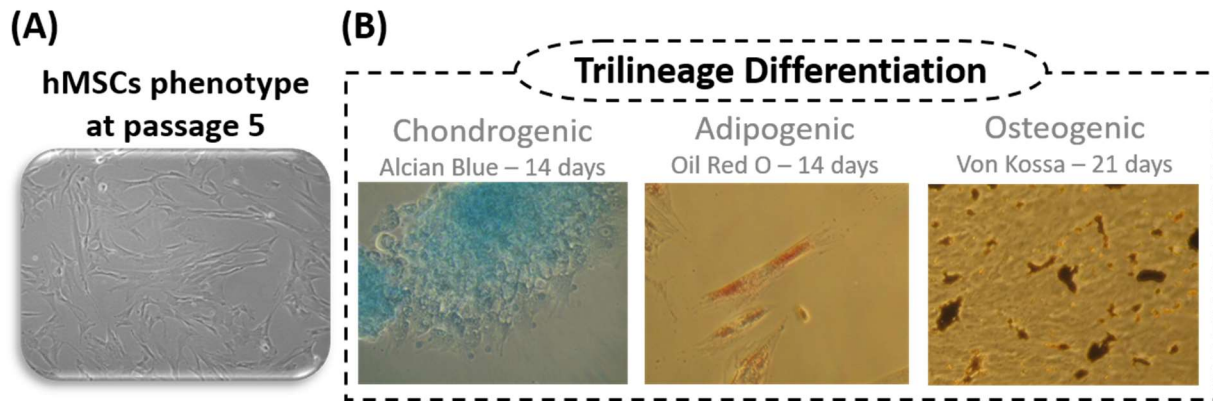


Figure 5.2: Human umbilical cord Mesenchymal stem cells (hMSCs) characterization: **(A)** hMSCs from umbilical cord at passage 5 in standard culture conditions. **(B)** Chondrogenic, adipogenic and osteogenic, and differentiation visualized through Alcian Blue, Oil Red O, and Von Kossa and histochemical staining.

5.3.3 | Performance of the dextrin-based hydrogel in bone regeneration of calvarial critical-sized defects

5.3.3.1 | Micro-computed tomography analysis

MicroCT reconstruction was performed for the calvarial bone samples at each time point to provide a comprehensive visualization of the whole bone region where the defect was created, as shown in **Figure 5.3**. The images allowed to verify that non-treated defects (control) did not heal over time, only a small amount of bone formation being observed in the periphery of the defect (**Figure 5.3 (A)**). The same was observed for the HG treated defects (**Figure 5.3 (A)**). The addition of osteoconductive BL granules promoted new bone formation over time; at 12 weeks post-surgery, it is no longer possible to identify the initial defect, being observed a complete osseointegration (**Figure 5.3 (B)**). In defects treated with HG + BL formulation an empty space in peripheral areas of the defects was observed, which decreased over time. A progressive osseointegration of the formulation occurred over time, although slower than in defects treated with BL granules only (**Figure 5.3 (B)**). These results suggest that HG delayed the onset of the bone tissue ingrowth process, not preventing however the formation of new bone, neither affecting the BL granules' osteoconductivity.

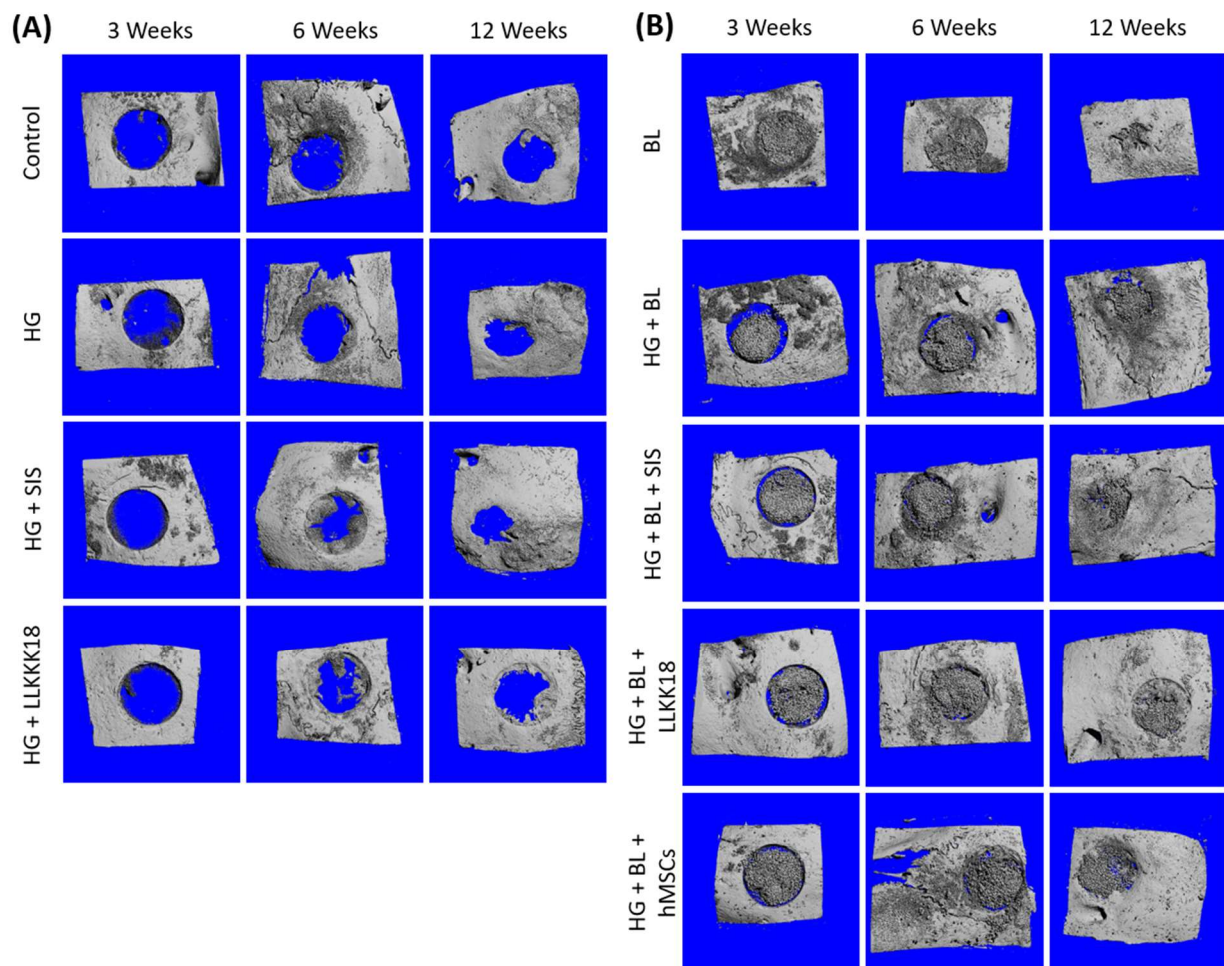


Figure 5.3: Representative microCT reconstruction images of calvarial critical-sized defects, after 3, 6 and 12 weeks, for the different dextrans-based hydrogel (HG) formulations without Bonelike® (BL) granules **(A)** or in presence of them **(B)**.

The microCT bone quantification (**Figure 5.4 (A)**) confirmed that in the non-treated defects and in those treated with HG only, little amount of bone was formed, being the bone volume similar over time in both defects. In relation to BL and HG + BL treated defects, the granules volume and the total bone volume were quantified, allowing the calculation of the new bone volume. At 3 weeks, the mean value of total bone volume in the HG + BL group was 35 % lower ($p < 0.01$) than observed in the BL group. The values obtained in the two groups converging overtime to similar mean values (**Figure 5.4 (B)**). In the case of BL treated defects, the total bone volume was almost constant over time. Relating to the volume of BL granules, the same amount of BL granules was applied in defects treated with only BL (with autologous blood) and HG+BL. The amount of BL was practically the same over time (**Figure 5.4 (C)**) in each group, BL and HG+BL. However, the microCT quantification revealed that the volume of granules in defects treated with HG + BL was significantly lower ($42.8 \% \pm 3.6$) at all time points ($p < 0.05$). Considering the new bone volume (**Figure 5.4 (D)**), it was similar over time in BL treated defects. In the case of the HG + BL treated ones, less new bone volume (about 37 %) was observed at 3 weeks, in comparison to the BL group ($p < 0.01$), but a significant deposition of new bone occurred over time ($p <$

0.05) and at 12 weeks more new bone (14 %) was observed in the HG + BL treated defects than in BL counterpart.

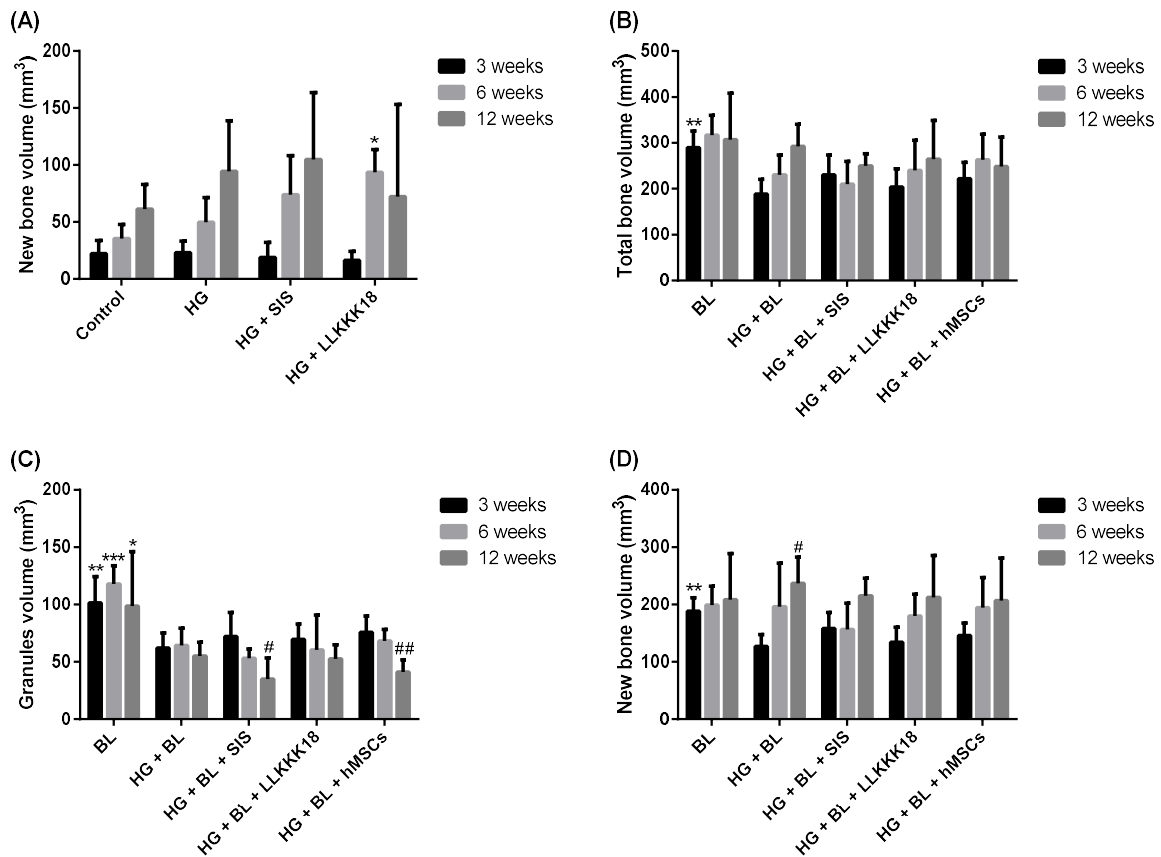


Figure 5.4: Results of microCT analysis for critical-sized calvarial defects, after 3, 6 and 12 weeks: quantification of the new bone volume formed in the defects treated with the dextrin-based hydrogel (HG) alone and loaded with 4 mg/ml of SIS (HG + SIS) or with 1 mg/mL of LLKKK18 (HG + LLKKK18) and the non-treated defect (control) **(A)**; quantification of the total bone volume (new bone and granules volume) **(B)**, the granules volume **(C)** and the new bone volume **(D)** in the defects treated with Bonelike (BL) granules alone or incorporated into HG matrix (HG + BL) and its combination with 4 mg/ml of SIS (HG + BL + SIS), 1 mg/mL of LLKKK18 (HG + BL + LLKKK18) or hMSCs (HG + BL + hMSCs). Data are presented as mean \pm SD ($n = 5$ replicates per group) and were analysed by one-way ANOVA followed by Bonferroni's post hoc test: * $p < 0.05$, ** $p < 0.01$ and *** $p < 0.001$ vs HG + BL treatment, # $p < 0.05$ and ## $p < 0.01$ vs 3 weeks (intra group).

5.3.2.2 | Histological analysis

To further complement the above findings of microCT, histological analysis of decalcified tissue sections HE staining (**Figure 5.5**) was conducted at each time-point.

Histological images showed that the non-treated defects (control) were mainly occupied by dense fibrous tissue with residual bone formation at the margins of the defect, at all tested times. From 6 weeks post-surgery, remodeled bone was also observed in the edges of the defect.

For the defects treated with the HG, at 3 weeks no traces of HG were observed within the defects, and no signs of inflammatory response, nor bone necrosis or fatty infiltrate were observed. The defects

were mainly occupied by dense fibrous tissue with residual bone formation at the margins of the defect, in all tested times, as observed in non-treated defects.

The defects treated with BL granules only revealed a growing increase of newly formed bone in the entire defect between the granules, over time, accompanied by a decrease in fibrous tissue. At 3 weeks, osteoid formation in the intergranular space was found, and in some spots mineralized matrix was also observed. Intragranular spaces were colonized by fibrous tissue. At 6 and 12 weeks, the new bone matrix was mineralized almost in the entire defect.

The defects treated with HG + BL revealed a delay in the deposition and formation of new bone, in comparison to BL treated counterpart. At 3 weeks, the intergranular space was composed mostly by fibrous tissue. Osteogenic cells around and/or inside the granules were also observed, as well as new vessels. At 6 weeks, the entire defect is still composed mostly by fibrous tissue. At 12 weeks, some spots of bone matrix were observed, most of them composed by unmineralized matrix. Many new vessels could be observed, close to the BL granules.

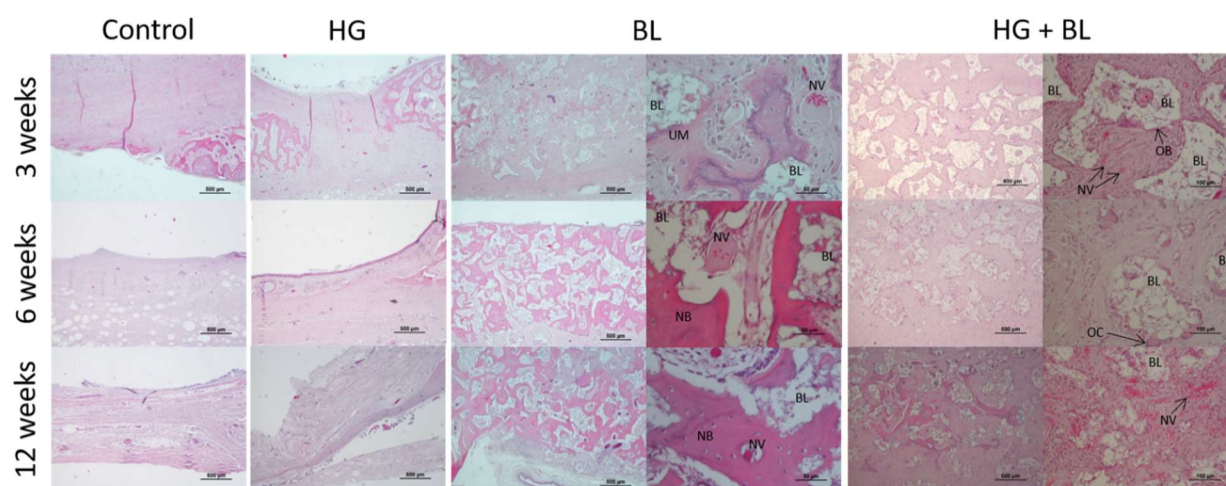


Figure 5.5: Haematoxylin and eosin stained histological sections from calvarial critical-sized defects of decalcified samples. BL, Bonelike® granules; NB, new bone; NV, new vessels; OB, osteoblasts; OC, osteoclasts; UM, unmineralized bone.

5.3.4| The effect of SIS, LLKKK18 and hMSCs on the performance of the hydrogel-based formulations in the regeneration of the calvarial critical-sized defects

5.3.4.1| Micro-computed tomography analysis

MicroCT reconstruction was performed for the calvarial bone samples at each time point as shown in **Figure 5.3 (A)**. The images allowed to verify that the defects treated with HG + SIS and HG + LLKKK18 did not heal over time, presenting only a little formed bone localized in the periphery of the defect, as observed in HG group. The addition of SIS and LLKKK18 to the HG seemed display better bone formation tendency on the periphery of the defects than the control and HG alone treated defects, mainly after 6 weeks. However, the void still clearly remains 12 weeks after post-surgery in these cases. For the BL complemented counterparts, as well as for HG + BL + hMSCs, it is possible to observe an empty space in

peripheral areas of the defects, which decreased over time, concomitant with a progressive osseointegration of the formulation (**Figure 5.3 (B)**), as observed in HG + BL treated defects.

The microCT quantification results (**Figure 5.4 (A)**) demonstrated that SIS and LLKKK18 complemented HG formulations displayed more new bone volume than defects treated with HG alone, in all time points, except for HG + LLKKK18 group at 12 weeks. However, no statistical difference was observed, except for HG + LLKKK18 group at 6 weeks. The obtained microCT results indicate that the combination of 4 mg/mL of SIS and 1 mg/mL of LLKKK18 to the HG was not capable to promote the full-regeneration of critical-sized calvarial defects. The microCT quantification results (**Figure 5.4**) also showed that the new bone and granules volumes obtained with HG + BL + (SIS, LLKKK18 or hMSCs) was statistically indistinguishable from those observed with HG + BL, for each time point. These results suggest that SIS, LLKKK18 and hMSCs did not significantly enhance the new bone formation.

5.3.4.2| Histological analysis

To further complement the above findings of microCT, histological analysis of decalcified tissue sections HE staining (**Figure 5.6**) was conducted at each time-point.

The results revealed that the defects treated with HG + SIS and HG + LLKKK18 are composed mainly by fibrous tissue, in all time points, containing remodelled and new formed bone only in the edges of the defect. In comparison to HG treated defects, the addition of SIS and LLKKK18 resulted in a higher number of new vessels in earlier times. However, such vascularization did not result in an increased new bone formation.

For HG + BL formulations, the histological images revealed that the addition of SIS, LLKKK18 and hMSCs induced a little more neovascularization, the new bone formation profile observed, being similar cases. Again, these results suggest that SIS, LLKKK18 and hMSCs did not accelerated the new bone formation in HG + BL formulations, under the conditions tested.

5.4| Discussion

Despite the high innate regenerative capacity of bone, critical-sized defects fail to heal and remain a clinical challenge, both in orthopedics and maxillo-facial fields. Healing such defects requires the formation of large amounts of bone in an environment often rendered hostile to osteogenesis by damage to the surrounding soft tissues and vasculature⁴⁷. In this work, full-thickness craniotomies with 14 mm diameter were created in goats, to obtain critical-sized defects, which means that they do not heal spontaneously. Indeed, the non-treated defects (control) only displayed little new formed bone at periphery of the defects for 12 weeks, and it is expected that they will not heal in the long run.

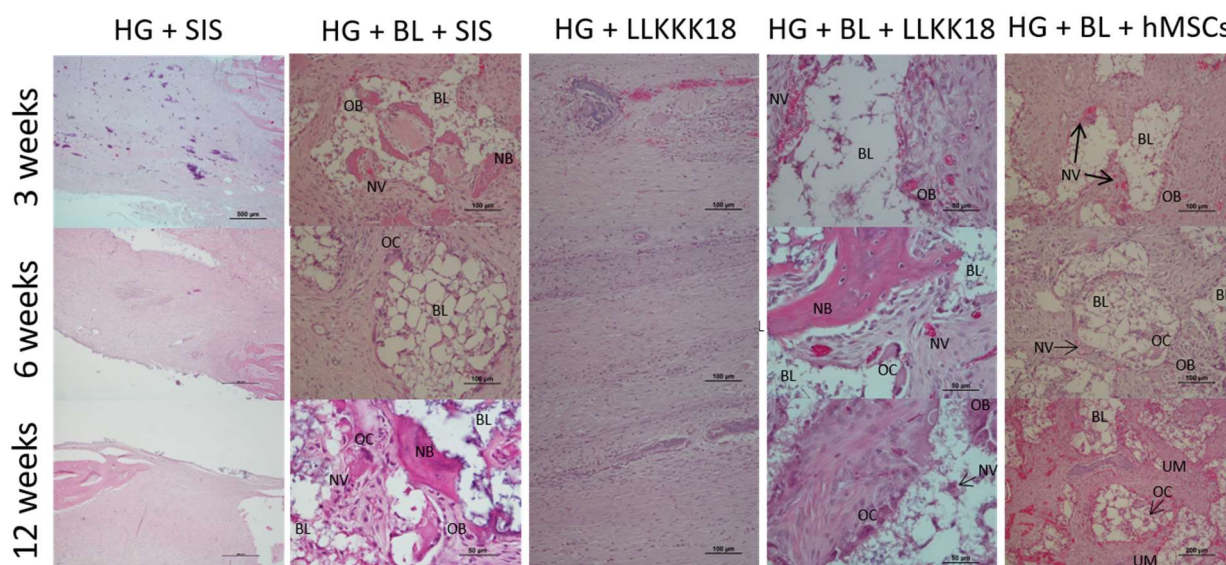


Figure 5.6: Haematoxylin and eosin stained histological sections from calvarial critical-sized defects of decalcified samples. BL, Bonelike® granules; NB, new bone; NV, new vessels; OB, osteoblasts; OC, osteoclasts; UM, unmineralized bone.

Bonelike® is a synthetic bone substitute that has been commercially available (Bioskin S.A.) and is composed of modified calcium phosphate and controlled proportions of hydroxyapatite (HAP), tricalcium phosphate (TCP) and ionic species, mimicking the chemical and structural composition of human bone^{4,48}. Several studies on orthopedics, maxillofacial and dental applications, performed in humans and animals, have reported the BL osteoconductive properties^{6,48-52}. Moreover, such studies have shown that BL is rapidly osteointegrated after implantation and displays a sustained controlled resorption, while new bone formation occurs. The results obtained in this study confirmed the remarkable potential of osteoconductivity and osseointegration of BL, since the granules and empty spaces were quickly colonized and osteointegrated in bone tissue, being able to regenerate critical-sized defects. At 3 weeks, the empty inter- and intra-granular spaces were filled with new bone, the formation of additional new bone being henceforward dependent of granules' resorption. The clinical applications use autologous blood as a carrier for the granules, which is not satisfactory. A more adequate and less invasive vehicle to improve the per-operative handling properties, stabilizing the granules in large defects or unstable sites, and avoiding the migration of particles from the site of implantation is required. For that, we proposed the use of a dextrin-based hydrogel as a carrier and stabilizer of BL granules¹⁵.

In this study, it was demonstrated that HG, alone, did not stimulate the bone healing process of critical-sized defects. Also, it was also not harmful to the native bone, since no inflammatory reaction or necrotic tissue were observed. Furthermore, according to surgeons, the combination of HG and BL granules improved the handling properties of the granules, as well as its application in the defects. Concerning to the bone healing process, such combination resulted in a short delay in bone tissue ingrowth. This delay can be explained by the considerable decrease of BL granules volume observed in HG + BL formulations compared to treatment with BL alone. Before the preparation of the final

formulation to be implanted, the BL granules were mixed in ODEX solution as to wetting the granules and to allow the ODEX permeating into the granules' pores. As the ODEX solution is acidic, such acidity resulted in an acceleration of the initial resorption of the BL minerals, mainly of TCP phase, which is more soluble than HAP³. Other studies reported the enhanced degradation of calcium phosphate-derived granules induced by polymeric solutions/hydrogels⁵³⁻⁵⁵. Daculsi *et al.* studied specifically the biphasic calcium phosphate (BCP) granules' surface interactions with hydroxypropyl methyl cellulose (HPMC) by high-resolution transmission electron microscopy⁵⁶. In this study, evidence of β -TCP crystals dissolution and HAP crystals hydrolysis via precipitation was shown, but only from the surface to a depth of ~13 nm into the crystals. The hydrolysis of the HAP surface and/or the dissolution of the β -TCP surface remained unchanged after a short incubation with HPMC (1 week) up to 1 year. Further experiments are required to determine the BL surface interactions with the HG, mainly with ODEX component, at the unit cell crystal level. Attending that the BL supports the bone healing by means of osteoconduction, a decreasing in granules volume in earlier times resulted in a reduction of new bone deposition at 3 weeks. However, at 6 and 12 weeks a recover of new bone formation was verified. This evidence suggests that HG did not impaired the formation of new bone over time, neither affected the BL granules' osteoconductivity.

When the BL granules were implanted into the bone defect the inter- and intragranular spaces were immediately colonized by cells. However, when BL was combined with HG, the matrix had to be firstly degrade from granules' surface for cells to be able to adhere to osteoconductive granules, proliferate, differentiate and deposit new bone. This could also contribute for the short delay in bone tissue ingrowth observed in the defects treated with HG + BL at 3 weeks, when compared to the defects treated only with BL. A delay in bone tissue ingrowth have also been described with fibrin glue⁵⁷ and HPMC-Si hydrogel^{53,58} with BCP granules. Additionally, in the HG + BL formulations, the HG moved towards the periphery of the defects in the earlier times, creating a gap between the defect wall and the BL granules. But after hydrogel's reabsorption, bone regeneration proceeded normally over time, simultaneously with the osseointegration process.

Besides allowing to obtain mouldable and injectable bone substitutes and granules' cohesiveness, hydrogels can also modulate cell colonization, as well as the bone healing process, since these systems allow the incorporation of several bioactive agents able to improve cell adhesion, osteoinductivity and osteointegration of the IBSs^{9,11}. Different approaches have been reported to improve the bioactivity of the IBSs-based hydrogels. Some authors have added ECM components into the hydrogel matrix, such as collagen^{59,60}, hyaluronic acid⁶¹, immobilized covalently RGD peptides on hydrogel⁶² or even used peptide- and hyaluronic acid-based hydrogels^{54,63} to improve cell adhesion and hence to modulate cell events (cell proliferation, migration and differentiation). Others have included bone morphogenetic protein-2 (BMP-2)⁶³⁻⁶⁷ or dexamethasone^{67,68} to obtain osteoinductive IBSs. IBSs with antimicrobial features have also been reported^{61,68,69}. In this study, several approaches were tested to improve the performance of the HG and HG + BL formulations on the regeneration of critical-sized bone defects. Such

approaches included the incorporation of MEC-based signals (degradation products from MEC-SIS), angiogenic factors (LLKKK18) and stem cell therapy (hMSCs). However, no significant differences in new bone formation process were observed when compared with HG or HG + BL groups.

With regard to MSCs, in a recent study (unpublished data) on a non-critical sized defect in ovine model, where the same cells were combined with BL granules, the obtained results demonstrated that the addition of hMSCs resulted in an improved bone regeneration, compared with BL alone, at 120 d of the healing period. It is also possible that the benefits associated with the hMSCs, SIS and LLKKK18 appear downstream. Thus, a long-term experiment should be performed to better assess the effect of SIS, LLKKK18 and hMSCs on bone regeneration. Indeed, neovascularization was improved using SIS and LLKKK18, being conceivable that this may improve the healing process in the long run.

5.5 | Conclusions

In conclusion, the HG allowed to improve the handling properties of granular ceramics. It did not affect Bonelike® granules' osteoconductive properties neither impaired the bone repair/regeneration process of critical-sized defects, demonstrating the HG's ability to act as a biocompatible mouldable carrier. The HG also allowed the incorporation and delivery of diverse bioactive agents, including short half-life agents. However, the association of the tested agents did not improve the bone regeneration process over 12 weeks. Long-term experiments should be performed for better assess the effect of SIS, LLKKK18 and hMSCs.

5.6 | References

1. Stevens, M. M. Biomaterials for bone tissue engineering. *Mater. Today* **11**, 18–25 (2008).
2. Amini, A. A. & Nair, L. S. Injectable hydrogels for bone and cartilage repair. *Biomed. Mater.* **7**, 024105 (2012).
3. Bohner, M. Resorbable biomaterials as bone graft substitutes. *Materials Today* **13**, 24–30 (2010).
4. Lopes, M. ., Knowles, J. ., Santos, J. ., Monteiro, F. . & Olsen, I. Direct and indirect effects of P2O5 glass reinforced-hydroxyapatite composites on the growth and function of osteoblast-like cells. *Biomaterials* **21**, 1165–1172 (2000).
5. Lopes, M. ., Knowles, J. . & Santos, J. . Structural insights of glass-reinforced hydroxyapatite composites by Rietveld refinement. *Biomaterials* **21**, 1905–1910 (2000).
6. Gutierrez, M. *et al.* Bone ingrowth in macroporous Bonelike® for orthopaedic applications. *Acta Biomater.* **4**, 370–377 (2008).
7. Bongio, M., van den Beucken, J. J. J. P., Leeuwenburgh, S. C. G. & Jansen, J. A. Development of bone substitute materials: from 'biocompatible' to 'instructive'. *J. Mater. Chem.* **20**, 8747 (2010).
8. Navarro, M., Michiardi, A., Castaño, O. & Planell, J. A. Biomaterials in orthopaedics. *J. R. Soc. Interface* **5**, 1137–1158 (2008).
9. D'Este, M. & Eglin, D. Hydrogels in calcium phosphate mouldable and injectable bone substitutes: Sticky excipients or advanced 3-D carriers? *Acta Biomater.* **9**, 5421–5430 (2013).
10. Utech, S. & Boccaccini, A. R. A review of hydrogel-based composites for biomedical applications: enhancement of hydrogel properties by addition of rigid inorganic fillers. *J. Mater. Sci.* **51**, 271–310 (2016).

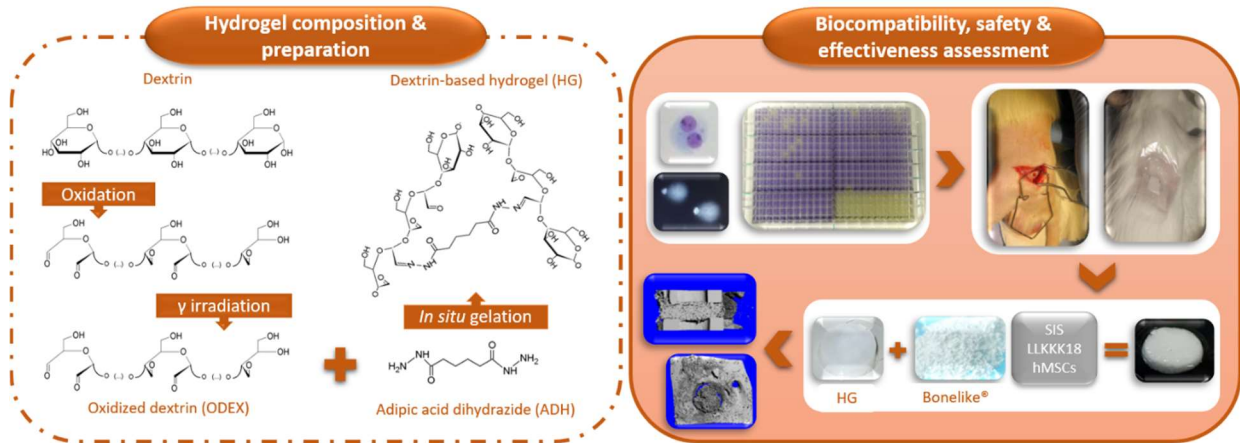
11. Pereira, I., Rodrigues, C., Rodrigues, A., Oliveira, M. & Gama, M. in *Bioinspired Materials for Medical Applications* (eds. Rodrigues, L. & Mota, M.) 241–271 (Elsevier, 2017). doi:10.1016/B978-0-08-100741-9.00009-7
12. Drury, J. L. & Mooney, D. J. Hydrogels for tissue engineering: Scaffold design variables and applications. *Biomaterials* **24**, 4337–4351 (2003).
13. Molinos, M., Carvalho, V., Silva, D. M. & Gama, F. M. Development of a Hybrid Dextrin Hydrogel Encapsulating Dextrin Nanogel As Protein Delivery System. *Biomacromolecules* **13**, 517–527 (2012).
14. Silva, D. M. *et al.* Structural analysis of dextrans and characterization of dextrin-based biomedical hydrogels. *Carbohydr. Polym.* **114**, 458–466 (2014).
15. Silva, D. M. *et al.* Inflammatory response to dextrin-based hydrogel associated with human mesenchymal stem cells, urinary bladder matrix and Bonelike[®] granules in rat subcutaneous implants. *Biomed. Mater.* **11**, 065004 (2016).
16. Pereira, I. *et al.* Effects of gamma irradiation and periodate oxidation on the structure of dextrin assessed by mass spectrometry. *Eur. Polym. J.* **103**, 158–169 (2018).
17. Saldin, L. T., Cramer, M. C., Velankar, S. S., White, L. J. & Badylak, S. F. Extracellular matrix hydrogels from decellularized tissues: Structure and function. *Acta Biomater.* **49**, 1–15 (2017).
18. Badylak, S. F. Xenogeneic extracellular matrix as a scaffold for tissue reconstruction. *Transpl. Immunol.* **12**, 367–377 (2004).
19. Agrawal, V. *et al.* Epimorphic regeneration approach to tissue replacement in adult mammals. *Proc. Natl. Acad. Sci.* **107**, 3351–3355 (2010).
20. Brennan, E. P., Tang, X.-H., Stewart-Akers, A. M., Gudas, L. J. & Badylak, S. F. Chemoattractant activity of degradation products of fetal and adult skin extracellular matrix for keratinocyte progenitor cells. *J. Tissue Eng. Regen. Med.* **2**, 491–498 (2008).
21. Li, F. *et al.* Low-Molecular-Weight Peptides Derived from Extracellular Matrix as Chemoattractants for Primary Endothelial Cells. *Endothelium* **11**, 199–206 (2004).
22. Reing, J. E. *et al.* Degradation Products of Extracellular Matrix Affect Cell Migration and Proliferation. *Tissue Eng. Part A* **15**, 605–614 (2009).
23. Tottey, S. *et al.* Extracellular Matrix Degradation Products and Low-Oxygen Conditions Enhance the Regenerative Potential of Perivascular Stem Cells. *Tissue Eng. Part A* **17**, 37–44 (2011).
24. Tottey, S. *et al.* The effect of source animal age upon extracellular matrix scaffold properties. *Biomaterials* **32**, 128–136 (2011).
25. Vorotnikova, E. *et al.* Extracellular matrix-derived products modulate endothelial and progenitor cell migration and proliferation in vitro and stimulate regenerative healing in vivo. *Matrix Biol.* **29**, 690–700 (2010).
26. Brennan, E. P. *et al.* Antibacterial Activity within Degradation Products of Biological Scaffolds Composed of Extracellular Matrix. *Tissue Eng.* **12**, 2949–2955 (2006).
27. Sarikaya, A. *et al.* Antimicrobial Activity Associated with Extracellular Matrices. *Tissue Eng.* **8**, 63–71 (2002).
28. Santos, M. I. & Reis, R. L. Vascularization in Bone Tissue Engineering: Physiology, Current Strategies, Major Hurdles and Future Challenges. *Macromol. Biosci.* **10**, 12–27 (2010).
29. Grellier, M., Bordenave, L. & Amédée, J. Cell-to-cell communication between osteogenic and endothelial lineages: implications for tissue engineering. *Trends Biotechnol.* **27**, 562–571 (2009).
30. Suttichai Krisanaprakornkit. An Emerging Role of Cathelicidin Antimicrobial Peptides in Bone Biology. *J. Dent. Assoc. Thai.* **64**, 192–209 (2014).
31. Dürr, U. H. N., Sudheendra, U. S. & Ramamoorthy, A. LL-37, the only human member of the cathelicidin family of antimicrobial peptides. *Biochim. Biophys. Acta - Biomembr.* **1758**, 1408–1425 (2006).
32. Ramos, R. *et al.* Wound healing activity of the human antimicrobial peptide LL37. *Peptides* **32**,

- 1469–1476 (2011).
33. Kittaka, M. *et al.* The antimicrobial peptide LL37 promotes bone regeneration in a rat calvarial bone defect. *Peptides* **46**, 136–142 (2013).
 34. Nakamichi, Y., Horibe, K., Takahashi, N. & Udagawa, N. Roles of cathelicidins in inflammation and bone loss. *Odontology* **102**, 137–146 (2014).
 35. Ciornei, C. D., Sigurdardottir, T., Schmidtchen, A. & Bodelsson, M. Antimicrobial and Chemoattractant Activity, Lipopolysaccharide Neutralization, Cytotoxicity, and Inhibition by Serum of Analogs of Human Cathelicidin LL-37. *Antimicrob. Agents Chemother.* **49**, 2845–2850 (2005).
 36. Nagaoka, I. *et al.* Augmentation of the Lipopolysaccharide-Neutralizing Activities of Human Cathelicidin CAP18/LL-37-Derived Antimicrobial Peptides by Replacement with Hydrophobic and Cationic Amino Acid Residues. *Clin. Vaccine Immunol.* **9**, 972–982 (2002).
 37. Silva, J. P. *et al.* Improved burn wound healing by the antimicrobial peptide LLKKK18 released from conjugates with dextrin embedded in a carbopol gel. *Acta Biomater.* **26**, 249–262 (2015).
 38. Caseiro, A. R. *et al.* Human umbilical cord blood plasma as an alternative to animal sera for mesenchymal stromal cells in vitro expansion – A multicomponent metabolomic analysis. *PLoS One* **13**, e0203936 (2018).
 39. Dominici, M. *et al.* Minimal criteria for defining multipotent mesenchymal stromal cells. The International Society for Cellular Therapy position statement. *Cytotherapy* **8**, 315–317 (2006).
 40. Pereira, T. *et al.* MSCs Conditioned Media and Umbilical Cord Blood Plasma Metabolomics and Composition. *PLoS One* **9**, e113769 (2014).
 41. Parekkadan, B. & Milwid, J. M. Mesenchymal Stem Cells as Therapeutics. *Annu. Rev. Biomed. Eng.* **12**, 87–117 (2010).
 42. Baraniak, P. R. & McDevitt, T. C. Stem cell paracrine actions and tissue regeneration. *Regen. Med.* **5**, 121–143 (2010).
 43. Rita Caseiro, A. *et al.* in *Frontiers in Stem Cell and Regenerative Medicine Research* (eds. Atta-Ur-Rahman & Anjum, S.) 21–70 (Bentham Science Publishers, 2017). doi:10.2174/9781681084770117060004
 44. Cortez, P. P. *et al.* Characterization and preliminary in vivo evaluation of a novel modified hydroxyapatite produced by extrusion and spheronization techniques. *J. Biomed. Mater. Res. Part B Appl. Biomater.* **99B**, 170–179 (2011).
 45. Santos, J. D., Lopes, M. A. & Silva, M. A. Hydroxyapatite and bioglass-based pellets, production process and applications of thereof. (2010). at <<https://patents.google.com/patent/WO2010021559A1/en>>
 46. OECD. *Guidance Document on the Recognition, Assessment and Use of Clinical Signs as Human Endpoints for Experimental Animals Used in Safety Evaluation.* (OECD Publishing, 2002). doi:10.1787/9789264078376-en
 47. S Verrier, M Alini, E Alsberg, SR Buchman, D Kelly, MW Laschke, MD Menger, WL Murphy, JP Stegemann, M Schütz, T Miclau, MJ Stoddart, C. E. Tissue engineering and regenerative approaches to improving the healing of large bone defects. *Eur. Cells Mater.* **32**, 87–110 (2016).
 48. Atayde, L. M. *et al.* Morphology effect of bioglass-reinforced hydroxyapatite (Bonelike®) on osteoregeneration. *J. Biomed. Mater. Res. Part B Appl. Biomater.* **103**, 292–304 (2015).
 49. Gutierrez, M. *et al.* Histological and scanning electron microscopy analyses of bone/implant interface using the novel Bonelike® synthetic bone graft. *J. Orthop. Res.* **24**, 953–958 (2006).
 50. Gutierrez, M. *et al.* Biological behaviour of Bonelike® graft implanted in the tibia of humans. *Key Eng. Mater.* **284–286**, 1041–1044 (2005).
 51. Sousa, R. C. *et al.* A clinical report of bone regeneration in maxillofacial surgery using Bonelike® synthetic bone graft. *J. Biomater. Appl.* **22**, 373–385 (2008).
 52. Cortez, P. P. *et al.* A glass-reinforced hydroxyapatite and surgical-grade calcium sulfate for bone

- regeneration: In vivo biological behavior in a sheep model. *J. Biomater. Appl.* **27**, 201–217 (2012).
53. Daculsi, G., Uzel, A. P., Weiss, P., Goyenvalle, E. & Aguado, E. Developments in injectable multiphasic biomaterials. The performance of microporous biphasic calcium phosphate granules and hydrogels. *J. Mater. Sci. Mater. Med.* **21**, 855–61 (2010).
 54. Amosi, N. *et al.* Acidic peptide hydrogel scaffolds enhance calcium phosphate mineral turnover into bone tissue. *Acta Biomater.* **8**, 2466–2475 (2012).
 55. Bohner, M. Design of ceramic-based cements and putties for bone graft substitution. *Eur. Cells Mater.* **20**, 1–12 (2010).
 56. Daculsi, G., Rohanizadeh, R., Weiss, P. & Bouler, J. M. Crystal polymer interaction with new injectable bone substitute; SEM and Hr TEM study. *J. Biomed. Mater. Res.* **50**, 1–7 (2000).
 57. Le Guéhennec, L., Layrolle, P. & Daculsi, G. A review of bioceramics and fibrin sealant. *Eur. Cells Mater.* **8**, 1–11 (2004).
 58. Daculsi, G., Uzel, A. P., Cursolle, J. C., Goyenvalle, E. & Aguado, E. Scaffold effects of microporous biphasic calcium phosphate granules and role of HPMC hydrogels in injectable multiphasic bone substitute developments. *Bioceram. Dev. Appl.* **1**, 1–4 (2011).
 59. Moreira, C. D. F., Carvalho, S. M., Mansur, H. S. & Pereira, M. M. Thermogelling chitosan-collagen-bioactive glass nanoparticle hybrids as potential injectable systems for tissue engineering. *Mater. Sci. Eng. C. Mater. Biol. Appl.* **58**, 1207–16 (2016).
 60. Fu, S. *et al.* Injectable and thermo-sensitive PEG-PCL-PEG copolymer/collagen/n-HA hydrogel composite for guided bone regeneration. *Biomaterials* **33**, 4801–4809 (2012).
 61. Morais, D. S. *et al.* Biological evaluation of alginate-based hydrogels, with antimicrobial features by Ce(III) incorporation, as vehicles for a bone substitute. *J. Mater. Sci. Mater. Med.* **24**, 2145–2155 (2013).
 62. Bongio, M. *et al.* Biomimetic modification of synthetic hydrogels by incorporation of adhesive peptides and calcium phosphate nanoparticles: In vitro evaluation of cell behavior. *Eur. Cells Mater.* **22**, 359–376 (2011).
 63. Martínez-Sanz, E. *et al.* Minimally invasive mandibular bone augmentation using injectable hydrogels. *J. Tissue Eng. Regen. Med.* **6 Suppl 3**, s15-23 (2012).
 64. Hulsart-Billström, G. *et al.* Calcium phosphates compounds in conjunction with hydrogel as carrier for BMP-2: A study on ectopic bone formation in rats. *Acta Biomater.* **7**, 3042–3049 (2011).
 65. Stenfelt, S. *et al.* Pre-incubation of chemically crosslinked hyaluronan-based hydrogels, loaded with BMP-2 and hydroxyapatite, and its effect on ectopic bone formation. *J. Mater. Sci. Mater. Med.* **25**, 1013–23 (2014).
 66. Martínez-Álvarez, C. *et al.* Injection and adhesion palatoplasty: a preliminary study in a canine model. *J. Surg. Res.* **183**, 654–62 (2013).
 67. Gao, C., Cai, Y., Kong, X., Han, G. & Yao, J. Development and characterization of injectable chitosan-based hydrogels containing dexamethasone/rhBMP-2 loaded hydroxyapatite nanoparticles. *Mater. Lett.* **93**, 312–315 (2013).
 68. Killion, J. A., Geever, L. M., Devine, D. M. & Higginbotham, C. L. Fabrication and in vitro biological evaluation of photopolymerisable hydroxyapatite hydrogel composites for bone regeneration. *J. Biomater. Appl.* **28**, 1274–83 (2014).
 69. Killion, J. A., Geever, L. M., Devine, D. M., Farrell, H. & Higginbotham, C. L. Compressive Strength and Bioactivity Properties of Photopolymerizable Hybrid Composite Hydrogels for Bone Tissue Engineering. *Int. J. Polym. Mater. Polym. Biomater.* **63**, 641–650 (2014).

CHAPTER 6

Final remarks



In this final chapter, an overview of this work is presented along with the main conclusions that resulted from this PhD. Finally, and considering the results obtained in this thesis, the suggestions for future work are also proposed.

6.1 | General conclusions

Synthetic bone substitutes (SBSs) are widely used in clinical practice, however they display limited handling properties and are difficult to apply in defects with complex geometry. This is a major shortcoming, critical concerning commercial success. The combination of injectable hydrogels and granular ceramic-based SBSs is emerging as a well-established trend for the development of injectable bone substitutes (IBSs). Besides acting as binders and stabilisers for ceramic granules and improve handling properties, hydrogels display mechanical and structural properties that resembles extracellular matrix and can modulate the bone healing process. Hydrogels can also be valuable to stimulate the healing process, through their capability to deliver drugs and cells, particularly, the *in situ* gelling hydrogels.

Within this scope, this PhD work focused on the study of the biocompatibility, safety and effectiveness of a dextrin-based hydrogel (HG) for the development of an IBS. The HG is composed by two components: oxidized dextrin (ODEX) and adipic acid dihydrazide (ADH). Dextrin is firstly oxidized (ODEX) with sodium periodate and then cross-linked with ADH, a non-toxic cross-linking agent. The cross-linked ODEX is an *in situ* gelling hydrogel, and is completely reabsorbed by the organism.

One key aspect when developing a biomaterial for clinical use is its susceptibility to sterilization. In the case of bone substitutes composed by different components (e.g. organic and inorganic materials) different sterilization processes may be necessary. In that cases, products with each component individually packaged are preferred. ADH is easily sterilized by filtration, while the ODEX sterilization treatment by gamma irradiation (20 kGy, 2 kGy/h) was investigated. Gamma irradiation was able to sterilize the ODEX solutions and did not compromise the HG formation after cross-linking with ADH. Moreover, sugars and glycosidic-linkage, as well as MS-based analysis showed that sterilizing gamma irradiation did not promote changes on the chemical structure of ODEX, showing that it can be used as suitable terminal sterilization method for ODEX solutions.

In vitro biocompatibility assessment of the HG and its individual components (ODEX and ADH) revealed that HG displayed concentration dependent cytotoxicity, due to ODEX, but did not promote DNA and chromosomal damage. When implanted in the human body, biomaterials, their lixivates or degradation products may be reabsorbed and spread systemically. Hence, *in vivo* biocompatibility and safety must be also assessed. For that, subacute systemic toxicity and skin sensitization tests were performed, using rodent models. These experiments showed that the HG did not induce any metabolic abnormalities, toxic effects on vital organs or skin reaction. Subacute systemic toxicity test was also used to access the geno- and bone histocompatibility of the HG. The results showed that HG did not induced DNA damage in blood cells, neither compromise the bone repair/regeneration process.

A new IBS based on dextrin hydrogel was successfully developed, using glass-reinforced HAP granules (250-500 μm), registered as Bonelike[®] (BL), and tested for the regeneration of tibia fractures for 3 and 6 weeks and critical-sized calvarial defects for 3, 6 and 12 weeks, in goats. The formulation containing 60%

(w_{BL}/v_{HG}) of BL displayed a homogeneous distribution of granules over the HG. The tibial fracture results showed that the HG allowed the stabilization of the BL granules into the defect, ensuring effective handling and moulding properties of the HG+BL formulation, as well as, an efficient cohesion of the granules. In calvarial defects study, it was confirmed that the HG did not affect the BL granules' osteoconductive properties, neither impairing the bone repair/regeneration process. Overall, the obtained results demonstrated that the HG is biocompatible and gather promising features for the development of novel IBS.

Peptides obtained by hydrolysis of extracellular matrix from small intestinal submucosa (SIS), LLKKK18, a pro-angiogenic peptide and human mesenchymal stem cells (hMSCs) from umbilical cord were also combined with the IBS to improve the bioactivity of the formulations. However, up 12 weeks post-implantation, no beneficial effects of these agents were observed in the regeneration process' improvement.

6.2 | Suggestions for future work

In this PhD work, the biocompatibility and great potential of the dextrin-based hydrogel as an injectable/mouldable carrier for granular ceramic-based SBSs was validated using, for that, a combination of *in vitro* and *in vivo* approaches, many of them in compliance with international standard guidelines (ISO and OECD). However, for its clinical use further investigation should be performed beyond this work.

The following goals are proposed for future work:

- i) Development/customization of suitable syringes, taking into consideration that mixture of different components should be easily done by the surgeon under aseptic conditions prior to administration.
- ii) Performing pre-clinical trials in different kinds of fracture, e.g. non-unions.
- iii) Conducting clinical trials, for instance, in dentistry and maxillofacial applications.
- iv) Different kinds of bone fracture and disease require different mechanical and biological properties. In order to satisfy the growing demand of products tailored for specific therapeutics, future research should explore the association and controlled release of anti-tumor, pro-angiogenic, anti-osteoporotic and analgesic drugs, as well as, alternatives to BMP-2. The development of formulations for osteomyelitis (bone infections) should be also considered.